Functional Properties and Pharmacological Regulation of Two-Pore Domain Potassium Channels Associated with Pulmonary Disorders

Kevin Peter Cunningham

A thesis submitted in partial fulfilment of the requirements of the University of Kent and the University of Greenwich for the Degree of Doctor of Philosophy

September 2018

DECLARATION

I certify that this work has not been accepted in substance for any degree, and is not concurrently being submitted for any degree other than that of the Doctor of Philosophy being studied at the Universities of Greenwich and Kent. I also declare that this work is the result of my own investigations except where otherwise identified by references and that I have not plagiarised the work of others.

Candidate

Signed: Kevin Peter Cunningham

Date: September 2018

“Anything’s possible if you’ve got enough nerve.”

J.K. Rowling

Acknowledgements

Firstly, thank you to my two supervisors, Professor Alistair Mathie and Dr Emma Veale, as without you both this work would not have been possible. I am grateful for the guidance and numerous opportunities you have provided me with throughout my PhD, I could not have asked for better supervisors. Alistair, it has been a privilege to be part of your research group and to benefit from your vast knowledge and advice. Emma, I will be forever grateful for the help and supervision you have given me. The time you have dedicated and invested in me is certainly not underappreciated!

I owe a lot of thanks to my lab group, Dr Mustafa Hassan for introducing me to the patch clamp technique and advising me during the early stages of my PhD. Dr Yvonne Walsh, I am grateful for the many exchanges of ideas and help with problems in the lab, particularly with the random noise on the rig! Robyn (Big Rob), thank you for all the hours spent on the confocal and taking one for the team with the ‘bad bear’ when we needed something, and for the coffee and gossip that was always a welcome break.

To my fellow PhD students, for all the conversations, lunches and drinks, the support and friendships has made the PhD process extremely enjoyable. I would also like to thank all the staff at the Medway School of Pharmacy for providing me with such an enjoyable PhD experience.

To my Mum and Dad, you have supported me to the fullest in all my endeavours, despite not knowing what I do, you have always provided me, Tom and Bob with everything we have ever needed and more, thank you for everything.

Abstract

Potassium (K^+) channels have been found to regulate the background 'leak' current maintaining resting membrane potential and therefore controlling the excitability of mammalian cells. The two-pore domain K^+ channel (K2P) family has been suggested to underlie the K^+ channels responsible for this leak current and can be regulated by a variety of stimuli. This study investigated multiple K2P channels and their role within pulmonary disorders using a combination of electrophysiological, imaging and biochemical approaches.

Carotid bodies are responsible for oxygen sensing within the carotid artery. TASK channels (TASK-1 and TASK-3) are highly expressed in the carotid body and are sensitive to changes in the chemical composition of the blood, stimulating ventilatory responses. This study shows that doxapram, a ventilatory stimulant, is a highly potent inhibitor of both human TASK-1 and TASK-3 channels, despite being a more selective inhibitor of rodent TASK-1 channels. I provide further evidence of the importance of key amino acids, previously identified in rodents, involved in the effect of doxapram on TASK-3. I also show that the M1P1 loop of the channel is important for doxapram inhibition.

TASK-1 channels have been implicated in pulmonary arterial hypertension (PAH). I characterised homozygous mutations of TASK-1, G106R and L214R, found in patients diagnosed with an aggressive form of PAH. I show that whilst the mutated TASK-1 channels are expressed and trafficked to the membrane, they appear to be non-functional. Riociguat and sildenafil, used in the treatment of PAH, enhanced current through WT TASK-1 channels but were unable to restore function through the mutated TASK-1 channels.

TREK-1 and TREK-2 channels have been shown to play a role in neuronal pain signalling. The majority of patients undergoing treprostinil therapy, as part of their treatment, experience severe pain at the site of infusion. This study shows that treprostinil rapidly inhibits TREK-1 and TREK-2 channels, suggesting they may play a role in the site pain experienced by patients. I also show that the N-terminus of TREK-1 is not important for treprostinil effect.

K2P channels play a key role within the pulmonary system and their ability to be regulated by a variety of stimuli makes them a key therapeutic target when treating pulmonary disorders.

Table of Contents

List of Figures

Chapter 1: Introduction

Chapter 2: Materials and Methods

Chapter 3: Doxapram Inhibition of TASK-3 K2P Channels

Chapter 6: Appendix

Abbreviations

AA	Arachidonic Acid
AC	Adenylyl Cyclase
AF	Atrial Fibrillation
Ag	Silver
ATI	Alternative Translation Initiation
BEN	Balkan Endemic Nephropathy
BMPR2	Bone Morphogenetic Protein Receptor Type 2
Ca^{2+}	Calcium
cAMP	Cyclic Adenosine Monophosphate
Ca_v	Voltage-Gated Calcium Channel
cGMP	Cyclic Guanosine Monophosphate
Cl^-	Chloride
CNS	Central Nervous System
COPI	Coat Protein 1
COX	Cyclooxygenase
DAG	Diacylglycerol
DMSO	Dimethyl Sulfoxide
DP_2	Prostaglandin DP_2 Receptor
E.coli	*Escherichia coli*
ECG	Electrocardiogram
ECM	Extracellular Matrix
EDTA	Ethylenediaminetetraacetic Acid
EGTA	Ethylene Glycol-bis(β-aminoethyl ether)-N,N,N',N'-Tetraacetic Acid
EP_2	Prostaglandin EP_2 Receptor
ERA	Endothelin Receptor Antagonist
ET	Endothelin
FDA	United States Food and Drug Administration
FFA	Flufenamic Acid
GAL-053	Negative Enantiomer of Doxapram
GAL-054	Positive Enantiomer of Doxapram
GC	Guanylyl Cyclase
GFP	Green Fluorescent Protein
GHK	Goldman-Hodgkin-Katz
GIRKs	G Protein-Gated Inward-Rectifier Potassium Channel

GPCRs	G Protein-Coupled Receptors
HA	Hemagglutinin
HEK	Human Embryonic Kidney
HEPES	(4-(2-hydroxyethyl)-1-piperazineethanesulfonic Acid
HERG	Human *Ether-à-Go-Go*-Related *Gene*
HIFBS	Heat-Inactivated Foetal Bovine Serum
hPAH	Heritable Pulmonary Arterial Hypertension
HUGO	Human Genome Organisation
IBMX	3 -isobutyl-1-methylxanthine
IP	Prostaglandin IP Receptor
IP_3	Inositol 1,4,5-triphosphate
iPAH	Idiopathic Pulmonary Arterial Hypertension
IUPHAR	The International Union of Basic and Clinical Pharmacology
K^+	Potassium
K2P	Two-Pore Domain Potassium Channel
K_{ATP}	ATP-Sensitive Potassium Channel
K_{Ca}	Ca^{2+}-Activated Potassium Channel
K_{ir}	Inward-Rectifier Potassium Channel
K_{Na}	Sodium-Activated Potassium Channel
K_v	Voltage-Gated Potassium Channel
MLC	Myosin Light Chain
Na^+	Sodium
nAChR	Nicotinic Acetylcholine Receptor
Na_v	Voltage-Gated Sodium Channel
NO	Nitric Oxide
NOTCH3	Neurogenic locus Notch Homolog Protein 3
p	Probability Level
PAH	Pulmonary Arterial Hypertension
PASMCs	Pulmonary Arterial Smooth Muscle Cells
PBS	Phosphate Buffered Saline
PCC	Pearson’s Correlation Coefficient
PDE	Phosphodiesterase
PDL	Poly-D-Lysine
PFA	Paraformaldehyde
PGI_2	Prostacyclin
PH	Pulmonary Hypertension
PIP	Phosphatidylinositol 4,5-biphosphate

PKA	Protein Kinase A
PKC	Protein Kinase C
PKG	Protein Kinase G
PLA_2	Phospholipase A_2
PLC	Phospholipase C
PUFA	Polyunsaturated Fatty Acids
RHC	Right Heart Catheterisation
ROI	Region of Interest
R_s	Series Resistance
SEM	Standard Error Of The Mean
SMAD1	Mothers Against Decapentaplegic homologue 1
SNPs	Single Nucleotide Polymorphisms
SSRIs	Serotonin-Selective Reuptake Inhibitors
TALK	Twik-Related Alkaline pH-Activated Potassium Channel
TASK	Twik-Related Acid-Sensitive Potassium Channel
TBST	Tween-20 Phosphate Buffered Saline
THIK	Twik-Related Halothane-Inhibited Potassium Channel
TM	Transmembrane
TP	Thromboxane Receptors
TREK	Twik-Related Potassium Channel
TRESK	Twik-Related Spinal Cord Potassium Channel
TRP	Transient Receptor Potential Channel
TTE	Transthoracic Echocardiogram
TWIK	Tandem Pore Weak Inward Rectifier Potassium Channel
UV	Ultraviolet
V	Voltage
WHO	World Health Organisation
WT	Wildtype

1. INTRODUCTION

1.1 Background

In the 1780s, the studies of Luigi Galvani, observed contractions upon frog nerve preparations stimulated by electricity, which he coined “animal electricity” (Piccolino, 2008). The phenomenon that animals contained the “powers” of electricity was widely contested by an opposing theory from Alessandro Volta that Galvani’s findings, were a result of the apparatus used and not the frog preparation (Pera, 1992). This dispute was resolved by the work of Emil du Bois-Reymond, in the 1840s, who detected what we now know as action potentials, within frog muscles (Finkelstein, 2015). du Bois-Reymond developed the concept that biological tissue has constituents capable of electrical activity and the practice of electrophysiology was born.

It was then Sydney Ringer, who was first responsible for revealing the importance of ions in electrophysiological process with a series of papers in the 1880s (Ringer, 1882a, 1882b, 1883a, 1883b, 1884, 1885, 1887). In these papers, Ringer highlighted the importance of the concentration of calcium (Ca^{2+}), potassium (K^{+}) and sodium (Na^{+}) for the contraction of a frog’s heart. Following on from this in 1902 (and the following years), Julius Bernstein, correctly developed his “membrane hypothesis” which stated that cells have negative resting potentials due to the membrane being selectively permeable to K^{+} ions and upon excitation the membrane becomes permeable to other ions (Bernstein, 1902a, 1902b, 1912). Bernstein adopted the work of a physical chemist, Walther Nernst, and applied his formula known as the Nernst equation (Figure 1.1) to physiological conditions. The Nernst equation calculates the membrane potential (V) in which there is no net flow of a specific ion across a membrane.

$$\sum_{ion} = \frac{RT}{zF} \ln \frac{[extracellular\ ion]}{[intracellular\ ion]}$$

Figure 1.1 – Nernst Equation

Nernst equation, where Σ_{ion} is the ion reversal potential (V), R is the universal gas constant (8.314 J K^{-1} mol^{-1}), T is the temperature (K), z is the electron charge of the ion, F is Faraday’s constant (C mol^{-1}).

A series of papers by Cole & Curtis (1939, 1949), Hodgkin & Huxley (1939, 1945, 1952) and Hodgkin & Katz (1949), interrupted by the 2nd World War, provided an understanding of the critical role Na^+ plays in the generation of action potentials, as well as the ion channel kinetics involved in calculating the membrane potential. It should be noted that Huxley stated (Huxley, 2002) that these findings would have been made much earlier had they have known of the work by Charles Ernest Overton (1902). Hodgkin & Huxley went on to be awarded the Nobel Prize for Physiology and Medicine in 1963. One of the most important outcomes from their work was the Goldman-Hodgkin-Katz (GHK) voltage equation (Figure 1.2). The GHK equation enables the calculation of the reversal potential of the membrane in regards to the concentration of ions on each side of the membrane. This built upon the Nernst equation significantly, as where the Nernst equation only factored in a single permeable ion, the GHK equation allows calculation of the reversal potential of a membrane that is permeable to multiple ions.

$$V_m = \frac{RT}{F}\ln\left(\frac{P_{Cl}[Cl^-]_i + P_K[K^+]_o + P_{Na}[Na^+]_o}{P_{Cl}[Cl^-]_o + P_K[K^+]_i + P_{Na}[Na^+]_i}\right)$$

Figure 1.2 – Goldman-Hodgkin-Katz voltage equation

Goldman-Hodgkin-Katz voltage equation use for the calculation of membrane reversal potential which accounts for the difference in ion concentrations either side of the membrane. V_m is the membrane potential (V), R is the universal gas constant (8.314 J K^{-1} mol^{-1}), T is the temperature (K), F is Faraday's constant (C mol^{-1}), P_{ion} is the permeability of that ion (m/s), $[ion]_i$ is the intracellular concentration of that ion, $[ion]_o$ is the extracellular concentration of that ion.

The next major leap in electrophysiology occurred 20 years later when, in 1976, Erwin Neher and Bert Sakmann first demonstrated the patch-clamp technique which allowed the recording of current through a single ion channel (Neher and Sakmann, 1976). In 1991 Neher and Sakmann were award the Nobel Prize for Physiology and Medicine and revolutionised the field of electrophysiology and the study of ion channels. To accompany this, the

development of recombinant DNA techniques enabled the ability to clone and sequence the (primary) structure of the nicotinic acetylcholine receptor (nAChR) from an electric ray (Noda, 1982). The same group then, this time from an electric eel, published the sequence of a voltage-gated sodium channel (Noda, 1984). These two discoveries led to the initial classification of the first two ion channel families: voltage-gated ion channels and ligand-gated ion channels.

1.2 Ion channels

Ion channels, or pores, are integral membrane proteins that allow the passage of ions across the membrane (either plasma membranes or membranes of intracellular organelles; Hille, 2001). Ion channels have three key properties which are critical to homeostatic processes in cells: rapid ion conduction; selective ion conduction; and regulation in response to stimuli (MacKinnon, 2004).

There are over 400 different genes already identified in the human genome that encode for ion channel proteins and their alternatively spliced variants (Alexander *et al*., 2015). These channels differ in their localisation, mechanism of gating, ionic selectivity, modulation by accessory subunits and signalling molecules, all of which contribute to the heterogeneity and many physiological roles of ion channels.

The diversity of ion channels allows the cellular response to multiple stimuli including changes in pH, temperature, voltage, ligands and many more (Hille, 2001). The selectivity of ion channels to permit access of specific ions through the channel has been researched for decades, but due to ion channels containing many hydrophobic transmembrane domains, they have been very difficult to study (Rasband, 2010). One aspect of ion selectivity that has been uncovered is the selectivity filter which contains conserved amino acid sequences across ion channels. For example, K^+ channels contain a ‘TVGYG’ conserved sequence. As this sequence becomes less conserved the ion selectivity of the channel is reduced, with an eight amino acid sequence

'XXTTXGXG' required for the channel to be potassium selective (MacKinnon, 2004).

A comparison of the amino acid sequence relationship of the minimal pore regions of known ion channels, results in structurally related channels being separated into seven groups (Figure 1.3).

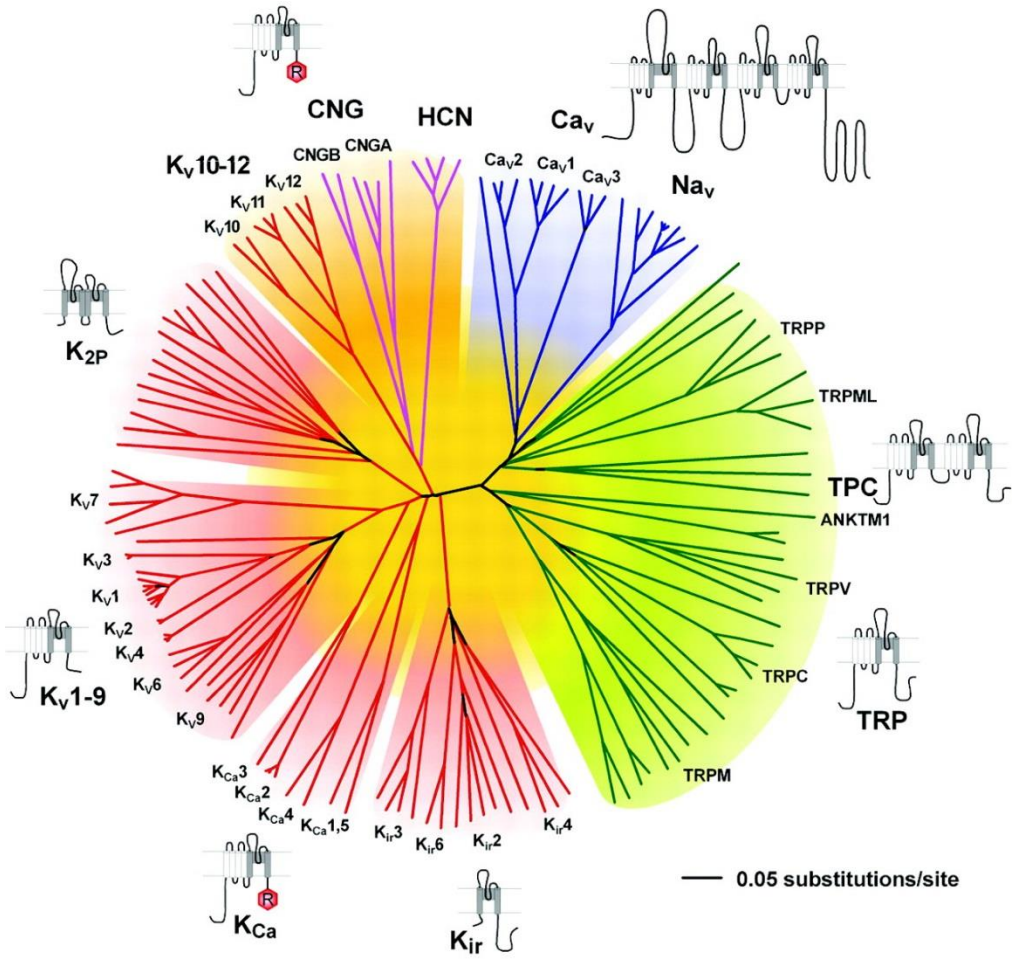

Figure 1.3 – Phylogenetic tree of ion channels

Amino acid sequence relationship of the minimal pore regions. 143 structurally related channels are separated into 7 groups, with the four-domain voltage-gated calcium (Ca_v) and voltage-gated sodium channels (Na_v) represented as blue branches. Transient receptor potential channels (TRP) and related channels are shown as green branches, potassium selective channels are shown as red branches and cyclic nucleotide-gated channels shown as magenta branches. (Reproduced from Yu and Catterall, 2004).

1.3 Potassium Channels

In humans, K^+ channels represent the largest family of ion channels with >78 mammalian α-subunit and 13 β-subunit genes identified to date. However, the diversity of these channels far exceeds the 78 α-subunit genes identified, due to heteromeric assembly within subfamilies, association with auxiliary subunits, and channel susceptibility to alternative splicing.

Production of K^+ channel crystal structures identified that K^+ channels contain four subunits that help form the channel pore. These subunits are α helical loops, often named P loops, and are located between two transmembrane (TM) helices (Figure 1.4). It is a standard feature of K^+ channels to have a 2TM/P domain but different K^+ channels contain further structural differences. For example voltage-gate K^+ channels characteristically have 4 further TM domains (S1-4) that precede their 2TM/P domain, with S4 providing the channel with a voltage-sensing ability (Choe, 2002).

Based upon their structural and physiological characteristics these channels have been classified into 3 main subfamilies of K^+ channels classified by their TM/P structure and are 2TM/P channels which include inward-rectifier K^+ channels (K_{ir}), 4TM/2P channels which include two-pore domain K^+ channels (K2P), 6TM/P channels such as voltage-gated K^+ channels (K_V) and Ca^{2+}-activated K^+ channels (K_{Ca}).

1.3.1 Two Transmembrane domain K^+ Channels

The first family of K^+ channels are the 2TM/P domain channels, which as they have one P loop per subunit require tetrameric formation to generate a functioning channel (Figure 1.4). Inwardly rectifying potassium (K_{ir}) channels form the majority of 2TM/P channels, which are named justly as their inward current (negative current) is much larger than the outward current (positive current). K_{ir} channels can be further divided in to four subfamilies based on their properties: classical K_{ir} channels, ATP sensitive K^+ (K_{ATP}) channels, G protein-gated K_{ir} (GIRKs) channels and K^+ transport channels. K_{ir} channel gating is not dependent on the membrane voltage but the electrochemical

gradient of K^+ ions, resulting in the ability to regulate action potentials and maintain resting membrane potential through the blocking of the pore by Mg^{2+} and polyamines (Hibino *et al.,* 2010). K_{ir} channels are found in a diverse range of cells including but not limited to neurons, epithelial, cardiac myocytes and osteoclasts (Bal *et al.,* 2018; Bardou *et al.,* 2009; López-Izquierdo *et al.,* 2011; Wang *et al.,* 2012).

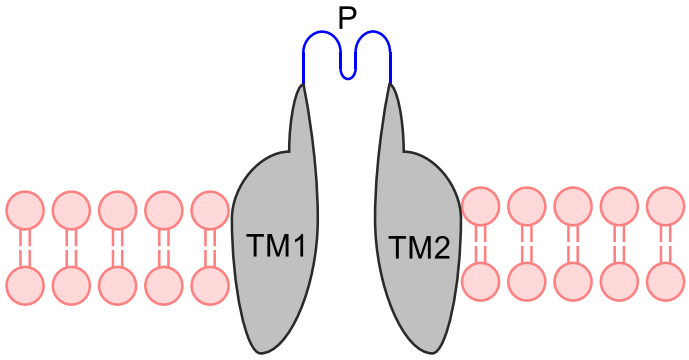

Figure 1.4 – Trademark structure of K^+ channels

Characteristic two transmembrane domain (TM) connected via an α helical loop (P loop) – 2TM/P. Four P loops are required to form a K^+ channel pore.

1.3.2 Six/Seven Transmembrane domain K^+ Channels

The next family of K^+ channels is the 6TM/P domain family, which have 6TM domains per pore domain (Figure 1.5). As with 2TM/P domain channels, these require tetrameric formation, for a functioning channel. The S4 TM domain is responsible for voltage-sensing within 6TM/P K^+ channels. The major role of 6TM/P channels is in regulating action potential duration, via membrane repolarisation, following the generation of an action potential (Labro and Snyders, 2012). The 6TM/P channel family consists of K_V, KCNQ, HERG-like K^+, Na^+-activated K^+ (K_{Na}) and K_{Ca} channels (BK, IK and SK). Each of these are regulated in a variety of ways. K_{Na} and K_{Ca} are regulated by cytoplasmic Na^+ and Ca^{2+} respectively, however some K_{Ca} channels are also voltage-dependent and contain an extra TM domain at the amino terminus (Miller, 2000). HERG-like K^+ channels, named after their conductance resemblance to the human *ether-à-go-go*-related gene product (HERG), are voltage-dependent K_V channels found mainly within neuron and cardiac cells (Wang

and MacKinnon, 2017). KCNQ channels are implicated in many pathways such as pain signalling and are inhibited by a variety of $G_{q/11}$-coupled neurotransmitter receptors (Hernandez *et al.,* 2008). K_V channels are voltage-dependent via the S4 TM domain. This domain has a unique feature within all K_V channels in that an arginine or lysine residue appears in every third or fourth position (Pongs *et al.,* 1988; Miller, 2000).

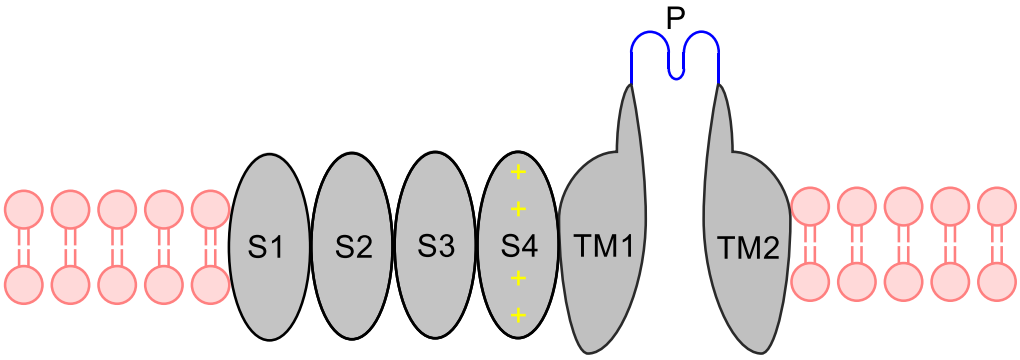

Figure 1.5 – Typical K_v Channel structure

Voltage-gated K^+ channel structure, each 2TM/P subunit is preceded by four transmembrane helices (S1-4) with S4 being responsible for voltage sensing as represented with plus signs.

1.3.3 Four Transmembrane domain K^+ Channels

The final superfamily of K^+ channels is the 4TM domain family. These K^+ channels differ from the others in that they have 2 pore-forming regions in one alpha subunit, which dimerises with another subunit to form a functioning channel, with a single pore (Lesage *et al.,* 1996a; Figure 1.6). The first P loop is situated between TM1 and TM2, whilst the second is between TM3 and TM4. As each subunit of this family contains two P loops they were named two-pore domain potassium (K2P) channels. The M1P1 loop in each K2P subunit is characteristically extended and thought to play a key role in dimerization. Initially it was proposed that a disulphide bridge was formed between the M1P1 loop of each subunit however in recent years, this has been shown to not be the case for all K2P channels e.g TASK-1 and TASK-3 (Niemeyer *et al.,* 2003).

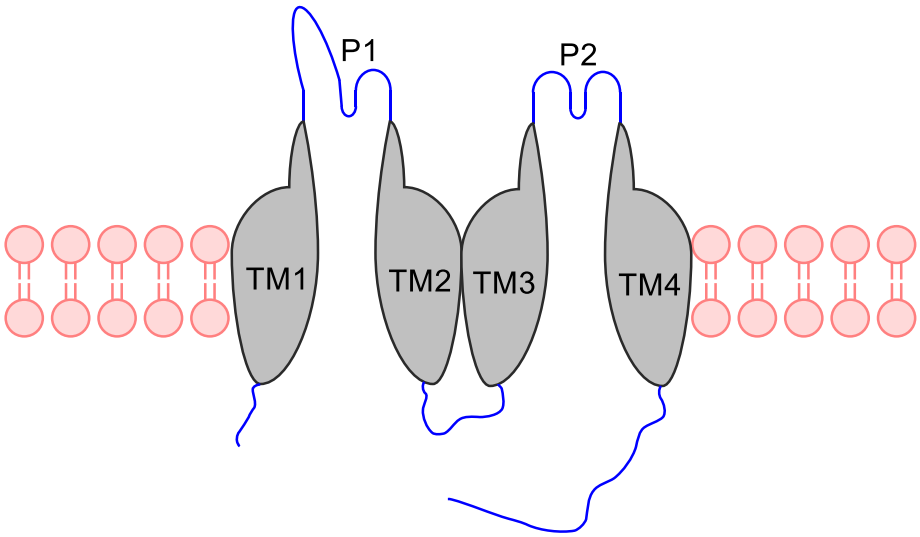

Figure 1.6 – Four transmembrane domain K^+ channel structure

Four transmembrane (TM) domain channel structure, each subunit contains four TM domains with two P loops contributing to the pore region. One functional channel requires the dimerization of two subunits.

The first ion channel crystal structure solved was a K^+ channel, KcsA, from *Streptomyces lividans* and was produced in 1998 (Doyle *et al.,* 1998). The generation of this crystal structure enabled the understanding of K^+ channels and the selectivity sequence 'TVGYG' conserved within K^+ channels. K^+ ions control the cellular osmolarity in respect to its environment, this is a vital role for life (Choe, 2002). This TVGYG sequence was shown to form an 'antiprism' of water molecules which displaces the water molecules surrounding the free flowing K^+ ion, whilst enabling them to pass through the channel pore and excluding alternative ions that are not energetically favourable to pass through the selectivity filter, such as Na^+ ions (Zhou *et al.,* 2001; Figure 1.7). The selectivity filter has also been shown to change conformation depending on the extracellular K^+ concentration. When internal K^+ concentrations are low (2 mM), the selectivity filter loses a dehydrated K^+ ion causing a non-conductive structural change (Zhou *et al.,* 2001). Concentrations of K^+ above 20 mM is enough to cause the selectivity filter to change from a non-conductive state to a conductive state, with the entry of a second K^+ ion into the selectivity filter.

The selectivity filter contains four K^+ ion binding sites, but experimental studies have shown that the selectivity filter has the ability to accommodate a maximum of two K^+ ions at a given time at positions 1 and 3 or 2 and 4 due to electrostatic repulsion between the two K^+ ions (Morais-Cabral *et al.,* 2001). This electrostatic repulsion between the two K^+ ions helps increase the K^+ ion conduction rate of the K^+ channel by reducing the K^+ binding affinity to the selectivity filter.

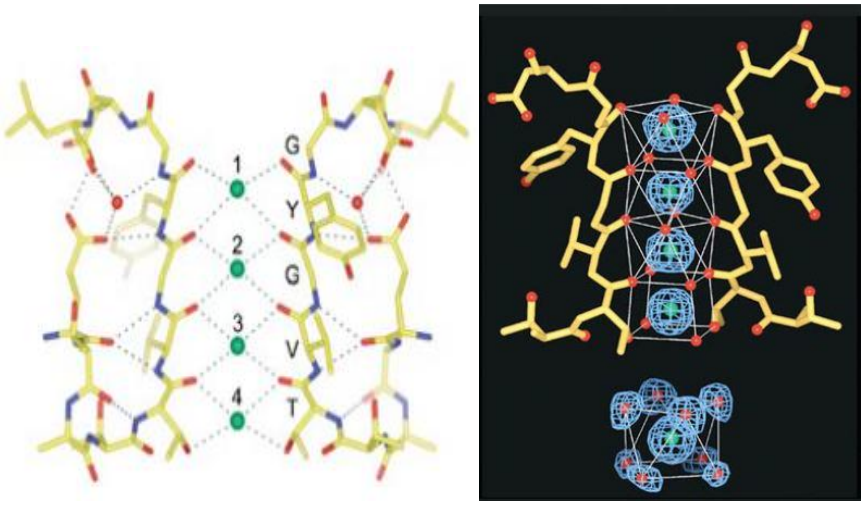

Figure 1.7 – Conserved amino acid region forming selectivity filter

Left) Structure of selectivity filter present in K^+ channels, two subunits shown. Conserved amino acid sequence indicated in single letter code, green spheres represent K^+ ions, red spheres represent oxygen and numbers correspond to K^+ ion binding site. Right) Representation of the antiprism formed by TVGYG selectivity sequence around K^+ ions and the similar environment water molecules created (reproduced from Zhou et al., 2001).

1.3.4 K^+ channel gating

K^+ channels must have the ability to open and close quickly for brief periods of time, due to the rapid speed of K^+ ion permeation through K^+ channels (in neuronal cells, rate is approximately 10^7 ions per second). If 10 K^+ channels were open for just one second then the cell would become depleted of K^+ ions. K^+ channels have acquired various gating and inactivation mechanisms to

prevent this (Choe, 2002). There are three confirmed methods of gating in K_V and K_{ir} channels, ball and chain inactivation by the amine terminal, activation gate conformational change and C-type inactivation. C-type inactivation is a slow mechanism of inactivation which involves a constriction at the selectivity filter (Kiss and Korn, 1998). In K2P channels, the gating mechanism is yet to be fully confirmed but C-type inactivation which occurs in and around the selectivity filter is currently proving to be the general consensus for K2P gating (Leuthy *et al.,* 2017). A reduced current is observed by protonation of a histidine residue at position 98 (H98) which is located next to the selectivity filter (Rajan *et al.,* 2000). Within the TWIK-related alkaline pH-activated (TALK) K^+ channel family, a key arginine residue, R224 has been shown to be critical for C-type gating of TASK-2 in a pH sensitive manner similar to that seen within TASK-3 and H98 (Niemeyer *et al.,* 2007). The M1P1 loop has also been implicated within TASK-3 channel gating and regulation, mutation of loop residues such as glutamate-70 (E70) and H98 can alter pH response as well as inhibition by Zinc (Clarke *et al.,* 2008). Another residue of TASK-3 shown to be involved in channel gating is E30, located at the end of the first TM domain (Veale *et al.,* 2005). The position of this glutamate residue at the end of the first TM domain is conserved throughout K2P channels and helps stabilise the channel in an open conformation. Mutation of this channel therefor reduces its ability to form an open conformation and reduces the whole-cell current recorded (Veale *et al.,* 2005; Mathie *et al.,* 2010a). Recent studies have proposed that the selectivity filter facilitates channel gating in response to stimuli, including stimuli that are detected at a distant location from the selectivity filter (Niemeyer *et al.,* 2016).

1.4 Two-Pore Domain K^+ (K2P) Channels

In the late 1990's, over four decades after leak current was first proposed by Hodgkin and Huxley it was finally pinpointed that the K2P channel family were responsible for this current (Hodgkin and Huxley, 1952; Ketchum *et al.,* 1995; Patel *et al.,* 1998). Previous to the attribution of K2P channels to the background leak current, this current was seen as insignificant (Niemeyer *et*

al., 2016). The first K2P channel to be discovered was TOK-1, which was found in yeast (Ketcum *et al.,* 1995). In more recent years, all identified mammalian K2P channels have contained 4TM domains rather than the 8TM domains found in TOK-1 (Ketchum *et al.,* 1995). Of the mammalian K2P channels there are 15 members that can be further subdivided into six distinct subfamilies, based on their structural and functional properties (Figure 1.8). Nomenclature for K2P channels is based on three main schemes, KCNKx, K_{2P} and a third acronym scheme. The KCNKx scheme is adopted by The Human Genome Organisation (HUGO) which uses the KCNK followed by a number (x) which denotes the order in which the gene was discovered. The K_{2P} nomenclature scheme adopted by The International Union of Basic and Clinical Pharmacology (IUPHAR), is similar to the KCNK scheme but the prefix is K_{2P} opposed to KCNK. The third scheme uses acronyms based on their functional and pharmacological properties: TWIK (**T**andem pore **W**eak **I**nward rectifier **K**$^+$ channel; Lesage *et al.,* 1996a), TREK (TWIK-related K+ channel), TASK (TWIK-related acid-sensitive K+ channel), TALK (TWIK-related alkaline pH-activated K+ channel), THIK (TWIK-related halothane-inhibited K+ channel) and TRESK (TWIK-related spinal cord K+ channel). As the first two methods of classifying K2P channels are non-informative and generally ignored by the K2P field, I will not use either the HUGO or IUPHAR classification, but instead continue with the original TWIK nomenclature to describe the K2P channels. This nomenclature is not without its problems, with channels such as TASK-2 and TASK-4 assigned to the TALK family, and not the TASK family, due to later information about the functional properties of these channels.

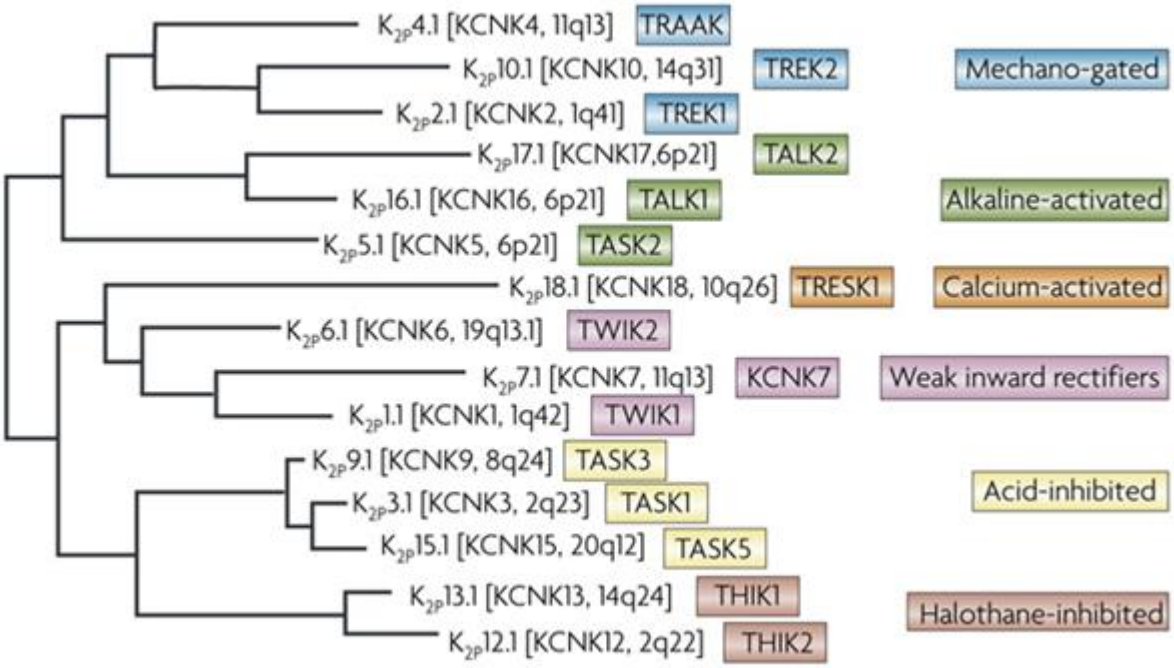

Figure 1.8 – Phylogenetic tree of the K2P family

Phylogenetic tree showing the 15 members of the K2P family. 6 subfamilies are present, divided on their functional properties: TWIK (Tandem pore Weak Inward rectifier K^+ channel), TREK (TWIK-related K+ channel), TASK (TWIK-related acid-sensitive K+ channel), TALK (TWIK-related alkaline pH-activated K+ channel), THIK (tandem pore halothane-inhibited K+ channel) and TRESK (TWIK-related spinal cord K+ channel). Reproduced from Honore, 2007.

Despite there being only 15 K2P mammalian members (around 50 for *C-elegans)*, these channels are further diversified due to heteromerisation, post-translational modifications and splicing (Feliciangeli *et al.,* 2015). The first K2P channels found to form heterodimers were TASK-1 and TASK-3. These heterodimer channels exhibited intermediate properties of the individual TASK-1 and TASK-3 channels, including sensitivity to pH. THIK1 and THIK2 as well as TREK-1, TREK-2 and TRAAK have since been shown to also form heterodimers (Czirjak and Enyedi, 2002; Enyedi and Czirjak, 2010; Levitz *et al.,* 2016; Blin *et al.,* 2016). In addition to this, TWIK-1 has been shown to form heterodimers with TASK-1 and TASK-3 channels (Plant *et al.,* 2012). An even further diversification of channel function and regulation occurs with auxiliary subunits such as coat protein 1 (COP-1 or COPI), 14-3-3, p11 and syntaxin-8

(Dedman *et al.,* 2009). 14-3-3 proteins have been shown to promote channel expression on the cell surface where as COPI binding has been shown to retain the channel within the endoplasmic reticulum (O'Kelly *et al.,* 2002).

1.4.1 TWIK subfamily

TWIK-1 (KCNK1) was the first mammalian K2P channel to be identified after cloning and subsequent full-length sequencing revealed a two-pore subunit of a weak inward rectifying K^+ channel (Lesage *et al.,* 1996b). TWIK-1 channels have been shown to be the only genuine "leak" K^+-selective K2P channel that follows GHK equation independently of voltage (Schewe *et al.,* 2016). Other K2P family members have been shown to act with a voltage-dependent behaviour as opposed to being simply "leaky". The ability for K2P channels to sense voltage changes has been attributed to an 'ion-flux-gating' mechanism. Ion-flux-gating has been coined to refer to the state of the selectivity filter of the K2P in response to both voltage and electrochemical K^+ gradients (Schewe *et al.,* 2016). Ion-flux-gated K2P channels such as the TREK family can be converted to 'leak' behaving channels with the application of certain molecules such as arachidonic acid (Schewe *et al.,* 2016). It has been proposed that TWIK-1 channels distinct selectivity filter is the reason behind its genuine GHK-leak behaviour, with changes to other K2P channels selectivity filter eradicating its ion-flux-gating ability and converting them to GHK-leak channels (Chen *et al.,* 2014). Other members of the TWIK family include TWIK-2 (KCNK6) and KCNK7, the latter appears to be non-functional and may not act as a K^+ channel as the conserved 'GYG' region of K^+ channels is 'GLE' within KCNK7 (Salinas *et al.,* 1999). Human TWIK channels are expressed in a variety of different tissues, TWIK-1 for example is expressed within the brain, kidney and lung (Arrighi *et al.,* 1998; Lesage *et al.,* 1996b).

Following the discovery of TWIK-1, 14 more K2P channels have been identified and named after TWIK-1 (T = TWIK-related). As mentioned earlier TWIK-1 was shown to be a voltage-independent K^+ channel, with a strong outward rectification due to the asymmetry of the K^+ gradient across the cell membrane that follows GHK equation (Lesage & Lazdunski, 2000a; Goldstein

et al., 2001). The latter 14 K2P channels were originally deemed to act in this manner however as mentioned previously they have been found to present time- and voltage-dependent conductance (Schewe *et al.,* 2016).

1.4.2 THIK subfamily

The THIK channel subfamily are classified based on their inhibition by the volatile anaesthetic, halothane, and encompass two channels, THIK-1 (KCNK13) and THIK-2 (KCNK12). THIK-2 appears to be non-functional as it is yet to be functionally expressed in its WT form however following the deletion of a 19 amino acid region (THIK-2Δ6-24) THIK-2 has been shown to be functionally expressed (Renigunta *et al.,* 2014a). Heterodimeric channels of THIK-1 and THIK-2 have been shown to be functionally expressed with intermediate properties of the WT channels (Blin *et al.,* 2014). THIK-1 may play a role within cerebellar Purkinje cells, as the K^+ current which is resistant to Tetraethylammonium (TEA) in these cells, shares properties that resemble THIK-1 channels (Rajan *et al.,* 2001; Bushell *et al.,* 2002).THIK-2 has been shown to be more widely expressed than THIK-1, with THIK-2 being widely expressed in the brain as well as kidney, liver and lungs and THIK-1 expression localised to areas in the brain such as granule cell layer of the olfactory bulb and hypothalamic and thalamic nuclei (Rajan *et al.,* 2001; Lazarenko *et al.,* 2010; Renigunta *et al.,* 2014a).

1.4.3 TRESK subfamily

The most recently discovered subfamily of K2P channels, is the TRESK subfamily which so far comprises only one channel, TRESK. A channel was identified as TRESK-2 however this was later proven to be just a species difference in mice (Kang *et al.,* 2004). TRESK channels were named as originally they were found to be only expressed within the spinal cord however more recent studies have identified expression within the brain and non-neuronal tissues such as liver, testis and lung (Sano *et al.,* 2003; Dobler *et al.,*

2007). Structurally TRESK is different to traditional K2P channels in that it has an additional extended intracellular loop between the M2 and M3 transmembrane domains (Enyedi *et al.,* 2012). Mutations of TRESK have been heavily linked to migraine with aura and TRESK agonists are a current therapeutic target for migraine therapy (Lafreniere *et al.,* 2010).

1.4.4 TALK subfamily

The TALK family were the second subfamily to be discovered and are termed due to their sensitivity to pH changes. The channels pH sensitivity is shifted to more alkaline pH resulting in larger currents through the channels at a higher pH range (Girard *et al.,* 2001). This subfamily is comprised of TALK-1, TALK-2, and TASK-2 (Girard *et al.,* 2001). TALK-2 was initially named TASK-4 in early studies (Decher *et al.,* 2001).TASK-2 was originally found within the kidney but mRNA expression has also been identified in the pancreas and liver (Reyes *et al.,* 1998; Decher *et al.,* 2001; Kang and Kim, 2004; Talley *et al.,* 2001). Interestingly, TALK-1 expression is localised to the pancreas and TALK-2 highest mRNA expression levels have been found in the pancreas but not limited to (Girard *et al.,* 2001; Enyedi and Czirjak, 2010). A mutation in TASK-2, TASK-2_T108P is prevalent in patients predisposed to Balkan endemic nephropathy (BEN) which is a renal disease that leads to chronic renal failure (Toncheva *et al.,* 2014; Veale and Mathie, 2016).

As the focus of my thesis is upon TASK and TREK channels associated with pulmonary disorders I will now describe them in greater detail than the other K2P families.

1.5 TWIK-related Acid-Sensitive K^+ (TASK) Channels

The fifth subfamily of K2P channels is the TASK subfamily which comprises of TASK-1, TASK-3 and TASK-5. TASK channels are assigned based on their sensitivity to extracellular pH within physiological ranges, TASK-1 and TASK-3 have pK values of approximately 7.5 and 6.8, respectively (Kemp *et al.,* 2004; Berg *et al.,* 2004). TASK-1 and TASK-3 are closely related sharing

approximately 60% identity in their amino acid sequence. They were also the first K2P channels seen to form functional heterodimers. This uncovered a new range of diversity within the K2P channels, as these heterodimers have intermediate properties to the homodimeric channels such as a pK value close to 7.3 (Cotton *et al.,* 2006; Czirjak and Enyedi, 2002; Berg *et al.,* 2004). A single histidine residue (H98) which is found within the M1P1 loop of TASK-1 and TASK-3 is responsible for the pH sensitivity of the channel. Mutation of this histidine abolishes the sensitivity to extracellular pH changes (Rajan *et al*., 2000).

1.5.1 TASK Channel Expression

TASK-5 has shown no functional expression to date, but has been placed in the TASK subfamily based on its structural properties (Enyedi and Czirjak, 2010). TASK channels have been shown to be expressed throughout the central nervous system (CNS), playing a crucial role in background currents. TASK-1 channels have been found to be highly expressed within the carotid bodies and pulmonary arterial smooth muscle cells (PASMCs; Yamamoto *et al.,* 2002; Gurney *et al.,* 2003). Like TASK-1, TASK-3 is widely expressed throughout the CNS (Talley *et al.,* 2001). TASK-3 is associated with a range of diseases such as cancer, hyperaldosteronism and cognitive impairments (Mu *et al.,* 2003; Davies *et al.,* 2008; Linden *et al.,* 2007).

1.5.2 Regulators of TASK Channels

Auxiliary subunits have been shown to regulate the expression of TASK channels on the cell surface. A short sequence within the C-terminus of TASK-1 and TASK-3 allows for coat protein complexes COPI to bind, binding of which has shown to retain TASK-1 and TASK-3 within the endoplasmic reticulum (Kilisch *et al.,* 2015). This COPI binding domain is overlapped with the binding domain for 14-3-3 proteins and binding of a 14-3-3 protein results in an increase in cell surface channel expression (Kilisch *et al.,* 2015). Serine residues in the C-terminus have been shown to be important in the binding of

14-3-3 proteins, phosphorylation of S373 in TASK-3 and S393 in TASK-1 have been shown to prevent COPI binding and as a result increase 14-3-3 protein binding which in turn increases channel expression at the cell surface (Kilisch *et al.,* 2016). In TASK-1, if S392 is phosphorylated following the phosphorylation of S393 it prevents 14-3-3 binding, further highlighting the dynamic regulation of TASK-1 trafficking by auxiliary subunits and kinases.

As well as 14-3-3 proteins and COPI, TASK-1 interacts with p11 (also known as S100A10) and syntaxin-8. p11 is a retention protein, highly expressed within the brain, that promotes TASK-1 localisation within the endoplasmic reticulum and deletion of its binding domain has shown to increase TASK-1 currents measured (Renigunta *et al.,* 2006). Syntaxin-8 is a SNARE protein that has been found to regulate the endocytosis of TASK-1, with co-expression of syntaxin-8 with TASK-1 can reduce current observed by fourfold (Renigunta *et al.,* 2014b; Kilisch *et al.,* 2015). TASK channels have also been shown to be silenced through sumoylation when expressed as heteromeric channels with TWIK-1 (Plant *et al.,* 2012).

1.5.3 Pharmacology of TASK Channels

TASK channels are not only regulated by pH but other chemical factors such as anaesthetics, hypoxia and signalling pathways. The biggest challenge faced when studying TASK channels is the lack of selective antagonists and agonists available (Bayliss and Barrett, 2008). Endocannabinoids such as anandamide and methanandamide have been found to significantly inhibit TASK current independent of cannabinoid receptors, which may account for adverse effects seen, such as hypokinesia and analgesia (Maingret *et al.,* 2001; Bayliss *et al.,* 2003).

Zinc selectively blocks TASK-3 but this inhibition can be abolished by the mutation of glutamate at position 70 (E70) or the H98, the pH sensor aforementioned, indicating a role of the M1P1 loop in TASK-3 channel activity regulation (Clarke *et al.,* 2008). As stated above, a key issue with TASK channels is the selectivity of compounds but techniques such as thallium flux assay have recently been used to identify more selective compounds, such as

terbinafine (Wright *et al.,* 2017). Terbinafine selectively activates TASK-3 with no effect upon TASK-1, as well as enhancing the mutated Birk-Barel TASK-3 channel. One compound with a mechanism of action disputed is doxapram, a ventilatory stimulant used primarily in the treatment for post-operative respiratory depression (Yost *et al.,* 2008). It has been debated as to whether doxapram is more effective against TASK-1 or TASK-3 in the carotid bodies (Buckler, 2015; Cotton *et al.,* 2006).

K_v1.5 channels have been implicated as a target in the treatment of obstructive sleep apnoea and atrial fibrillation. Known K_v1.5 blockers have been shown to have a higher affinity for TASK-1 channels (Kiper *et al.,* 2015). A293 and A1899 were found to be 43- and 68- fold more potent at blocking TASK-1 current than K_v1.5 current (Kiper *et al.,* 2015). AVE0118 another K_v1.5 blocker, has also shown a higher affinity to TASK-1 than K_v1.5 (IC_{50} values of 603 nM and 5.6 µM respectively), indicating TASK-1 may be the primary target of this compound in the atrium (Kiper *et al.,* 2015; Gögelein *et al.,* 2004). TASK-1 and TASK-3 inhibition within cerebellar granule neurons and sensory neurons by hydroxy-α-sanshool has been shown to underlie tingling and numbing feeling experienced after eating Szechuan peppercorns (Bautista *et al.,* 2008).

1.5.4 Regulation by Signalling Pathways

TASK-1 and TASK-3 channels are regulated by $G_{\alpha q}$-coupled receptors, however the signalling pathway through which this inhibition occurs is debated (Olschewski *et al.,* 2017). Earlier studies suggested a direct inhibitory effect of $G_{\alpha q}$ on the TASK-1 channel but more recent studies have indicated that phospholipase C (PLC) is essential for inhibition of the TASK-1 channel, with diacyleglycerol (DAG) shown to directly mediate TASK channels (Chen *et al.,* 2006; Schiekel *et al.,* 2013; Wilke *et al.,* 2014). $G_{\alpha s}$-proteins have been shown to increase TASK-1 and TASK-3 current through increased cell surface expression (Mant *et al.,* 2011). PKA phosphorylates the C-terminus of TASK-1 and TASK-3 restricting COPI binding and in turn retention within the endoplasmic reticulum (Mant *et al.,* 2011). $G_{\alpha i}$-proteins have also been shown

to be involved within TASK-1 current inhibition through PLC activity (Czirjak *et al.,* 2001).

1.5.5 Human Pathologies of TASK Channels

TASK channels have been implicated in a wide range of diseases. TASK-1 has been shown to play a pathophysiological role in pulmonary arterial hypertension (PAH), hyperaldosteronism and even obesity (Navas *et al.,* 2016; Antigny *et al.,* 2016; Heitzmann *et al.,* 2008; Chen *et al.,* 2017). In PAH, it is proposed that TASK-1 is downregulated and restoration of the channel current could provide a therapeutic benefit. Compounds such as the prostacyclin anaglogue, treprostinil, (acting through protein kinase A) and the phospholipase A2 inhibitor, ONO-RS-082 have been explored (Olschewski *et al.,* 2006; Ma *et al.,* 2013). Some patients with PAH have been shown to carry genetic mutations in their KCNK3 genes which produce non-functional or lower functioning channels (Ma *et al.,* 2013; Navas *et al.,* 2017). TASK-1 has also been indicated in the arrhythmogenesis of atrial fibrillation (AF) and heart failure, with mice models of both diseases showing atrial expression of TASK-1 was down-regulated compared to wild-type models (Weidmann *et al.,* 2018).

The gene for TASK-3, KCNK9, is maternally transmitted (with the paternal gene silenced) and a substitution of a glycine residue to an arginine at position 236 (G236R) and subsequent reduced outward current is seen in Birk-Barel syndrome (Barel *et al.,* 2008). Birk-Barel syndrome is a mental retardation dysmorphic syndrome that occurs due to dysfunctional TASK-3 channels, which in turn cause a migration defect of cortical neurons. Potential therapies have been suggested, such as the use of flufenamic acid (FFA) which has been shown to significantly enhance channel current (Bando *et al.,* 2014; Veale *et al.,* 2014a). TASK-3 has also be found to be over expressed within certain cancers such as breast cancer suggesting it plays an important role in oncogenesis (Mu *et al.,* 2003). Xenograft studies have shown that antibody targeting of TASK-3 looks a promising therapeutic strategy in the treatment of lung and breast cancer (Sun *et al.,* 2016).

TASK-3 has been found to be linked to menarche signals. Maternally inherited TASK-3 alleles have been found to increase age at menarche, whereas the

paternal allele has no significant effect (Perry *et al.,* 2014). Late menarche has been associated with lower body mass index values observed in adults, suggesting TASK-3 could have a role in obesity (Prentice and Viner, 2013). Further evidence for paternal TASK-3 in obesity has been investigated with single nucleotide polymorphisms (SNPs). SNPs on the paternal allele of TASK-3 increase BMI compared to SNPs on the maternal allele (Hoggart *et al.,* 2014). In addition to TASK-3, TASK-1 has also been linked to obesity, however TASK-1 knockout mice have shown resistance to hypothermia and obesity (Chen *et al.,* 2017).

1.6 TWIK-related K^+ (TREK) Channels

The TREK (Twik-related K^+ Channel) channel subfamily comprises of TREK-1, TREK-2 and TRAAK (Twik-Related arachidonic-acid-stimulated K^+ channel). TREK-1 was the second mammalian K2P channel to be identified and the first K2P channel to show evidence for existence within neurons (Fink *et al.*, 1996). TREK-1 shares 63% identity and 78% homology with TREK-2 (Noël *et al.,* 2011). TREK-1 and TREK-2 are outward rectifiers whereas TRAAK follows GHK rectification (Bayliss and Barrett, 2008).

1.6.1 Expression

TREK channels are expressed widely throughout the central nervous system such as hippocampus and cerebellum but are also expressed in high levels within nociceptors showing them to play a role in pain perception (Fink *et al.,* 1996; Marsh *et al.,* 2012; Alloui *et al.,* 2006). TREK-1 channels are expressed in dorsal root ganglion neurons often co-localised with excitatory channels such as TRPV1 (Talley *et al.,* 2001; Loucif *et al.,* 2018). TREK-1 channels have been found to be expressed within human myometrial smooth muscle cells and during labour they are down-regulated to enhance contraction (Buxton *et al.,* 2010).

1.6.2 Regulators of TREK channels

TREK channels are widely regulated, one key regulation pathway is due to TREK channels being mechanosensitive which means they are regulated by tension within the membrane. Stretching of the channel results in activation (Patel *et al.,* 1998). Membrane stretching alters the channel conformation between an “up” conformation during stretch and “down” when there is not sufficient membrane tension (Aryal *et al.,* 2017). TREK channels are also activated by temperature, maximum activation of TREK channels occurs at physiological temperature (between 30 ºC and 42 ºC) providing optimal control over membrane potential (Noël *et al.,* 2011). Polyunsaturated fatty acids (PUFA) such as arachidonic acid have been shown to directly regulate TREK channels. Arachidonic acid activates TREK channels in a reversible manner (Fink *et al.,* 1998). The neuroprotection observed within PUFA therapy has since been attributed to TREK channel mediation, highlighting a therapeutic target. Like TASK channels, TREK channels are regulated by pH, however TREK-1 and TREK-2 are differentially regulated. An extracellular pH change to pH 6.9 strongly inhibits TREK-1 current, however strongly activates TREK-2 (Sandoz *et al.,* 2009). The pH sensing effect is mediated through a conserved histidine residue, H126 in TREK-1 and H151 in TREK-2, therefore the differential effects of acidification must occur through alternative amino acid residues, the P2M4 loop has been implicated with this role (Sandoz *et al.,* 2009).

TREK channels are also affected by chaperone proteins such as AKAP150, which increases current by anchoring TREK-1 into a postsynaptic scaffold with G protein-coupled receptors (GPCRs) and altering its properties (Figure 1.9; Noël *et al.,* 2011; Mathie *et al.,* 2010b; Sandoz *et al.,* 2006). TREK-1 becomes a leak channel when co-expressed with AKAP150 and is inhibited by $G_{\alpha s}$-proteins at a faster rate. Interestingly, $G_{\alpha q}$-protein inhibition of TREK-1 is significantly reduced (Sandoz *et al.,* 2006). Another protein, Mtap2, has been shown to increase TREK-1 expression and trafficking to the postsynaptic membrane. Mtap2 and AKAP150 can both exert their actions simultaneously providing a cumulative activation in TREK-1 current density (Sandoz *et al.,* 2008).

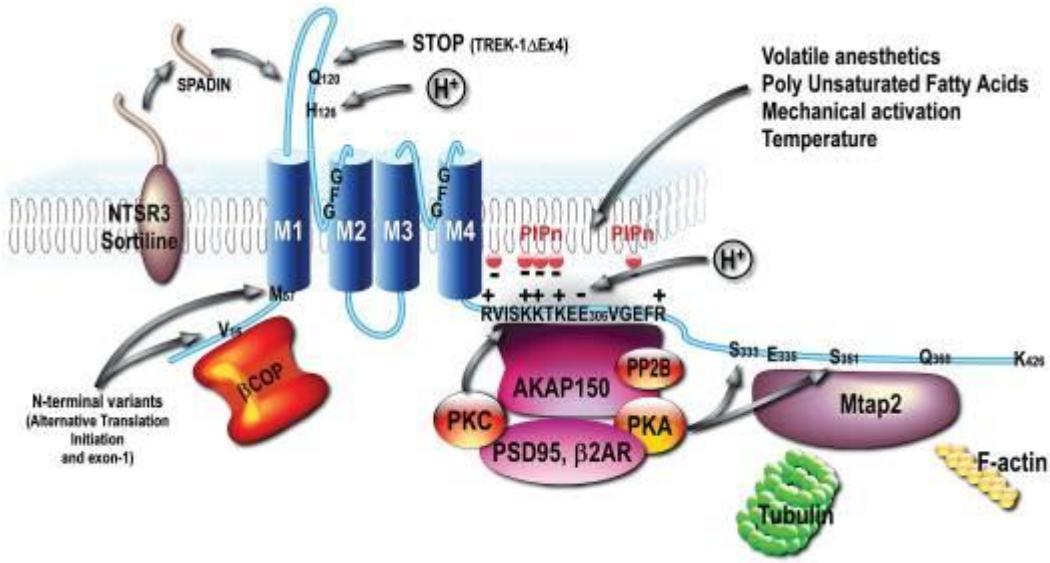

Figure 1.9 – Regulation and variants of TREK-1

Figure shows regulation of TREK-1 by anaesthetics, poly unsaturated fatty acids, stretch and temperature. Variants also indicated along channel. Channel activating proteins AKAP150 and Mtap2 shown. (Reproduced from Noël et al., 2011).

1.6.3 Functional Diversity of TREK channels

The TREK subfamily can be diversified with the formation of both homodimers and heterodimers between each of the family members (Blin *et al.*, 2016; Levitz *et al.*, 2016). The TREK subfamily can be further diversified by the generation of different isoforms of each channel. A process known as alternative translation initiation (ATI) can occur, creating different length isoforms of the TREK subfamily channels. ATI occurs when the ribosome skips the first translation initiation site due to a non-optimal starting sequence otherwise known as a Kozak sequence. After the ribosome has skipped this initiation site it will then proceed to start translation of the protein at the next optimal methionine (Kozak, 2005). For TREK-1 ATI creates two isoforms, a full length (426 amino acid) TREK-1 WT and a shorter form missing the first 56 residues, TREK-1 Δ1-56 (Thomas *et al.*, 2009). For TREK-2 there are three potential isoforms TREK-2 WT, TREK-2 Δ1-54 and TREK-2Δ1-66 (Simkin, Cavanaugh and Kim, 2008). TREK subfamily diversity can be increased

further by the process of alternative splicing (Noël, Sandoz and Lesage, 2011). Alternative splicing is the ability of one gene to produce multiple proteins by the inclusion or exclusion of different exons. As TREK channels have the same organisation of their respective 7 exons, each channel has similar spliced variants. Alternative splicing within the first exon produces channels with varying amino-termini (N-terminus) which creates two isoforms of TREK-1 and three variants of TREK-2 (Li *et al.*, 2006; Mirkovic and Wickman, 2011). The TREK-1 isoforms vary in length, one being 411 residues long and the other 426, but both exhibit identical functional properties (Li *et al.*, 2006). The TREK-2 isoforms are labelled TREK-2a, TREK-2b and TREK-2c, with TREK-2a being 538 residues and TREK-2b and -2c 508 residues long. These TREK-2 variants all appear to have similar channel properties, with the differing factor being their expression levels and locations (Noël, Sandoz and Lesage, 2011). The deletion of exon 4 creates two further isoforms TREK-1ΔEx4 and TRAAKt (TRAAK truncated), TREK-1ΔEx4 has no functional activity individually however it has been proposed to exert a dominant negative effect, affecting full length TREK-1 trafficking to the cell membrane and reducing overall whole cell current (Veale *et al.*, 2010). TRAAKt does not show any functional activity nor has it been shown to affect wild-type trafficking (Fink *et al.*, 1998). TRAAKt and TREK-1 ΔEx4 are 67 and 141 amino acid residues long respectively, with both containing the M1 and only part of the P1 loop. TREK subfamily channels are mechanosensitive meaning that tension on the cell membrane can have a direct effect upon channel activity, they are the only K2P channels that exhibit this property (Brohawn, Su and MacKinnon, 2014).

1.6.4 Signalling pathways

“Nociceptor” is the term used for the neurons that identify noxious stimuli. Nociceptors are widely populated within the skin and muscles through the peripheral axonal branch as well as the spinal cord through a central axonal branch. Cell bodies of nociceptors are found within dorsal root ganglia and trigeminal ganglia, it is from these locations that nociceptors span into the wider periphery. Nociceptors have the ability to selectively detect a wide range

of stimuli that have the potential to cause injury (Tsunozaki and Bautista, 2009). There are two major classes of nociceptor, Aδ fibres and C fibres. Aδ fibres are lightly myelinated and responsible for transmitting acute localised pain, C fibres however are unmyelinated and responsible for diffuse pain transmission (Plant, 2012). The ability for a fast response to damaging stimuli helps prevent injury and maintain homeostasis this occurs at Aδ fibres terminals, upon significant noxious stimuli (or potentially noxious), excitatory ion channels are opened which can result in action potential generation and pain signalling (Waxman and Zamponi, 2014). TRPV1, a thermosensitive channel, is an example of an excitatory ion channel that is opened within a sensory neuron terminal upon the presence of a stimulus such as heat. The opening of TRPV1 then results in the activation of Nav and Kv channels resulting in action potential generation (Woolf and Ma, 2007). The targeting of TRPV1 channels has provided therapeutic promise within recent years (Mathie, 2010). Studies have indicated a role for K2P channels within pain perception and as a result TREK-1, TREK-2 and TRESK have become a novel target for pain therapy (Mathie and Veale, 2015; Cohen *et al*., 2009; Acosta *et al*., 2014; Huang *et al*., 2008). TREK-1, TREK-2 and TRESK channels have been shown to be present in sensory neuron terminals and proposed to have an opposing effect to TRV1 channels, inhibition of these channels leads to the activation of Nav and Kv channels and the subsequent generation of an action potential. Activating TREK channels therefore provides a potential pain therapeutic avenue to explore, some clinically used drugs act upon TREK channels such as riluzole (Duprat *et al.,* 2000). TREK channels can be regulated by various stimuli, such as mechanosensitivity, heat, membrane depolarisation, G-proteins subunits, pH and arachidonic acid (Maingret *et al.,* 2000; Patel *et al*., 1998; Sandoz *et al*., 2009; Kang *et al*., 2006; Lesage *et al*., 2000). TREK-1 and TREK-2 channels have been shown to be regulated by multiple G proteins (Mathie, 2007). As seen in TASK-1 channels Gαq activation leads to PKC activation, whilst in TASK-1, DAG and IP3 manipulations play a role in channel inhibition it appears evidence for this in TREK channels is conflicted (Chemin *et al.,* 2005; Lopes *et al.,* 2005). PIP_2 has been shown to be a potent TREK-1 channel opener and hydrolysis of PIP_2 into DAG + IP3 has been shown to inhibit TREK-1 current (Chemin *et al.,* 2007;

Chemin *et al.,* 2005) There is a growing consensus that TREK-1 and TREK-2 inhibition through Gαq activation is due to PKC phosphorylation of the channel (Kang *et al*., 2006; Murbartian *et al*., 2005). Differentially to TASK-1, TREK channels have been shown to be down-regulated by Gαs and up-regulated by Gαi, in response to changes in intracellular cAMP levels (Lesage *et al.,* 2000). An increase in intracellular levels of cAMP leads to an inhibition of TREK channels through the phosphorylation of the C-terminus (Bockenhauer *et al.,* 2001). In TREK-1 Gαs-activated inhibition, the serine residue at position 333 (S333) is pivotal, providing alterations in the kinetic properties of the channel reducing the open-probability of the channel (Bockenhauer *et al.,* 2001). An increase in cAMP activates PKA leading to S333 phosphorylation and results in a reduction in open-probability of the channel. A further serine residue, S300, has also been indicated in phosphorylation-mediated inhibition with both cAMP and PKC inhibition of TREK-1 currents requires phosphorylation of S300 (Murbartian *et al.,* 2005).

1.6.5 Pharmacology of TREK channels

As with their regulation, TREK channels can be targeted by a range of pharmacological interventions. With their high importance in pain signalling, pharmaceutical development of a compound to selectively activate TREK channels has intensified. One class of compounds, fenamates, have been shown to enhance TREK-1 activity (Veale *et al.,* 2014b). Fenamate-like compounds are being used experimentally to generate more potent activators. BL-1249 has been shown to be 30 to 100 fold more potent than flufenamic acid on TREK-1 channels (Veale *et al.,* 2014b). One issue with fenamates is that they are not selective to TREK channels and regulate many other ion channel types (Mathie and Veale, 2015). More recently, rubidium-flux assays and electrophysiological experiments have shown GI-530139 to be a more selective activator than BL-1249 (Loucif *et al.,* 2018). GI-530139, selectively activates both TREK-1 and TREK-2 but not TRAAK or other K^+ channels (Loucif *et al.,* 2018). One selective TREK channel activator, ML67-33 has been

shown to act through a gate near the selectivity filter surmised in TREK channel activation (Bagriantsev *et al.,* 2013; Lolicato *et al.,* 2017).

1.6.6 Human Pathologies of TREK channels

In addition to pain signalling, TREK channels have been implicated in diseases including depression and blood-brain barrier dysfunction (Heurteaux *et al.,* 2006; Bittner *et al.,* 2013). Serotonin-selective reuptake inhibitors (SSRIs) were shown to inhibit TREK-1 and TREK-2 channels, this in combination with TREK knockout mice exhibiting depression resistant behaviour has led to the suggestion that TREK inhibition complements SSRI therapy (Heurteaux *et al.,* 2006; Enyedi and Czirjak, 2010). TREK-1 has been identified as a possible marker and target for prostate cancers due to its high expression that correlates with stage of the disease (Voloshyna *et al.,* 2008).

1.7 Objectives of the Study

The objectives of this research are to investigate the functional and pharmacological properties of TASK and TREK K2P channels. I will focus upon clarifying the mechanism of action of the ventilatory stimulant, doxapram, on TASK-3 channels (Chapter 3). I will then attempt to address the role of TASK-1 in pulmonary arterial hypertension and assess its pharmacological regulation by therapeutic compounds: ONO-RS-082 (Chapter 4.3); sildenafil (Chapter 4.4); riociguat (Chapter 4.4); and treprostinil (Chapter 4.5). Finally I will attempt to address the localised pain associated with treprostinil administration (Chapter 4.5). A more detailed description of the aims are given within each chapter.

2. Materials and Methods

2.1 Molecular Biology

pcDNA3.1 vector constructs (ThermoFisher Scientific, UK) cloned with the K2P channel gene of interest (hTASK-1, hTASK-3 and hTREK-1) were acquired as a gift from GlaxoSmithKline (UK). The pcDNA3.1 vector encoding hTREK-2 was obtained as a gift from Pfizer (UK). Full gene sequences of these channels are given in the appendix (6.1 – 6.4). The human prostaglandin receptors (DP_2, EP_2 and IP) were obtained from cDNA Resource Center (Pennsylvania, USA), catalogue numbers: PTGDR00000, PER0200000 and PTGIR00000, respectively. For confocal microscopy, a pAcGFP1-N1 vector (Clontech-Takara Bio Europe) encoding human wildtype or mutant human TASK-1 was used which tags a green fluorescent protein to the TASK-1 channel. For in-cell and on-cell western assays TASK-1 channel was tagged with hemagglutinin (HA) on the M1P1 loop between Alanine 50 (A50) and Arginine 51 (A51).

Mutated channels were created using a QuikChange kit (Stratagene, Amsterdam, The Netherlands). Short pairs (25-35 bases) complementary oligonucleotide primers, encoding the intended mutation, were synthesised (Eurofins MWG Operon, Ebersberg, Germany). The QuikChange kit is a site directed mutagenesis protocol which mutates the desired site using PCR by denaturing the plasmid template and annealing of primer containing the desired mutation. After annealing, dsDNA containing mutated site will be synthesised leaving both wildtype (WT) and mutated DNA. DPN-1 digestion then removes all WT DNA as WT DNA is produced in *Escherichia coli (E.coli)* it is DAM-methylated which can be digested by DPN-1 enzymes, *in vitro* production of DNA does not DAM-methylate DNA. Mutated DNA is then transformed into *E.coli.* The pcDNA 3.1 vector, contains an ampicillin resistance gene that can be cultured on ampicillin plates, allowing only bacteria containing the vector to grow. To extract the DNA from the *E.coli,* the bacteria are lysed and purified using appropriate kits for the needs of the experiments. Kits are based on the quantity of DNA required. For the work conducted in this thesis, minipreps or midipreps were used (Qiagen, The Netherlands). DNA concentrations of the preparations were determined using

a Nanodrop spectrophotometer (Implen, Germany). Mutant DNA constructs were sequenced (Eurofins MWG Operon) to confirm the introduction of the correct mutated bases.

2.2 Cell Culture

All cells were passaged within a HEPA filtered laminar flow hood (HeraSafe, Heraeus) using aseptic techniques. The hood was sterilised with 70% ethanol before and after use and all items introduced into the hood were sprayed with 70% ethanol. A lab coat and gloves were worn at all times throughout the cell culturing process and gloved hands were sprayed on every entry into the hood. All culture products were purchased from Sigma-Aldrich (Dorset, UK) unless otherwise stated.

2.2.1 Cell Line

The cell line used for all work conducted was tsA201 cells. A modified human embryonic kidney (HEK) 293 cell line. The tsA201 cells are stably transfected with the SV40 large T antigen and were obtained from the European Collection of Cell Cultures through Sigma-Aldrich. HEK293 cells are our cell line of choice as they have been shown to express high levels of recombinant protein (Thomas and Smart, 2005). HEK 293 cells express an epithelial morphology with a pyramidal or rhombic shape (Figure 2.1).

2.2.2 Cell Passage

tsA201 cells were grown in monolayers in 25 cm^2 or 75 cm^2 vented tissue culture flasks and were maintained in 88% (v/v) Dulbecco's modified Eagles media, 10% (v/v) heat-inactivated foetal bovine serum (HIFBS), 1% (v/v) non-essential amino acid solution, 2 mM L-Glutamine and 1% (v/v) penicillin (10,000 $U \cdot ml^{-1}$) and streptomycin (10 $mg \cdot ml^{-1}$). Cells were incubated with a humidified atmosphere of 95% oxygen and 5% carbon dioxide and at a temperature of 37 ºC. Cells were sub-cultured and plated when flasks reached 80% confluency. In order for the cells to be passaged the media was removed

and cells were dissociated from the bottom of the flask using trypsin-EDTA (10X, 0.5% trypsin, 0.2% EDTA). After 1 minute incubation at 37 ºC (2 minutes for 75 cm^2 flask) cells were removed from the bottom of the flask by agitating the flasks with several taps. Cells were then suspended in 5 ml of culture media to quench the action of trypsin and pipetted up and down repeatedly to disperse cell clumps. The cells were then centrifuged at 800 rpm for 3 minutes and the supernatant was removed. Cells were then further resuspended in 5 ml of culture media and 100 µL was taken for cell counting on a FastRead 102 slide. The appropriate amount of cell suspension was then taken and made up to 5 ml with culture media (20 ml for 75 cm^2 flasks) so that flasks were seeded at a density of 1.5 x 10^5 cells / ml. New flasks were then placed back into the incubator and sub-cultured when they reached 80% confluency. The remaining cell suspension was used for cryopreservation or to prepare plates for electrophysiological and imaging studies.

2.2.3 Cell Plating

For electrophysiological and imaging studies, cells were plated on 13 mm circular glass coverslips coated with poly-D-lysine hydrobromide (PDL) (0.5 mg / ml). Cells were plated at a density of 7 x 10^4 cells / ml to be transiently transfected the following day. Each well of the multidish contained 0.5 mls of cell suspension.

2.2.4 Transfection

For electrophysiological experiments transient transfection of K2P channel DNA and green fluorescent protein (GFP) DNA into the tsA201 cells was conducted using a modified calcium-phosphate protocol, described by Chen and Okayama (Chen and Okayama, 1987; Batard, Jordan and Wurm, 2001). Plated cells were transfected as follows. Eppendorf A contained 500 ng channel DNA, 500 ng GFP DNA and 5.6 µL $CaCl_2$ (2M) per well and was made up to 25 µL per well with ddH_2O for a final concentration of 225 mM $CaCl_2$ per well. Eppendorf B contained 25 µL of phosphate-free HEPES buffered saline,

(280 mM NaCl, 50 mM HEPES, pH to 6.95 using NaOH and 0.45 µL of phosphate buffer (100 mM Na_2HPO_4) per well was added.

The contents of eppendorf B was then added to the contents of eppendorf A via the drop-wise method and left to incubate at room temperature for 20 minutes allowing the formation of the $CaPO_4$/DNA complex. 50 µL of this solution was then pipetted into each well and the plate was gently rocked to ensure even distribution of the solution. The plates were then incubated for 4 – 6 hours after which the media was removed and washed twice with phosphate buffered saline (PBS), 1 ml per well and then 0.5 ml of fresh culture media was added to each well. The cells were then incubated over night at 37 ºC in 5% CO_2. The plates were utilised for electrophysiological or imaging studies the following day. For imaging experiments, transfection of DNA using TurboFect transfection reagent (ThermoFisher Scientific, UK) was conducted as per ThermoFisher Scientific protocol. The protocol involved mixing 0.5 µg of DNA (1 µg for pac gene vectors) with 100 µL per well followed by addition of 2 µL of TurboFect reagent and incubation for 15-20 minutes. 100 µL of mixture was then added to each plate well and incubated at 37 ºC in 5% CO_2 ready for electrophysiological or imaging studies after 24 – 48 hours.

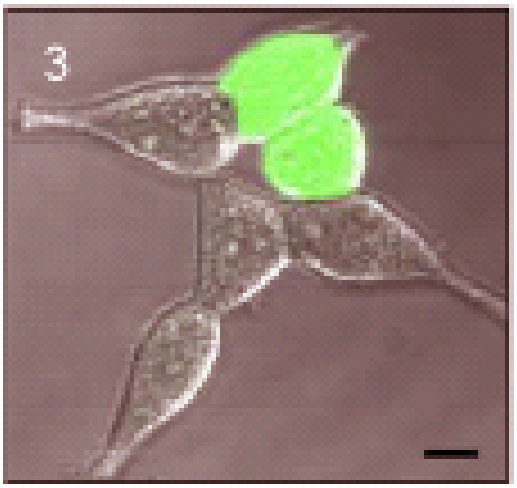

Figure 2.1 – Image of tsA201 cell transfected with GFP

Image shows tsA201 cell following calcium phosphate transfection with green fluorescent protein (GFP). Cells emitting green colour have been successfully transfected. Scale bar is equal to 10 µM (Reproduced from Thomas and Smart, 2005).

2.2.5 Cryopreservation

Over time tsA201 cells have been shown to lose efficiency in their ability to be transiently transfected. In order to combat this it is pivotal to keep a large stock of low passage number cells using cryogenic freezing. To begin, when the cells reached 80-90% confluency the culturing media was removed and cells were dissociated from the flask using 2 mL trypsin-EDTA and placed back into the incubator for 3-5 minutes. After this short incubation, the flasks were gently agitated to ensure all cells were dissociated from the flask. Cells were then suspended in 10 mL of culture media and pipetted up and down to ensure cells were isolated and not in clumps. Cells were centrifuged at 800 rpm for 3 minutes. The supernatant was then removed, cells were resuspended in 5 mL of fresh culture media and centrifuged again at 800 rpm for 3 minutes. The supernatant was again removed using a Pasteur pipette and the cells were resuspended in cryogenic media (90% HIFBS and 10% dimethyl sulfoxide, DMSO) so the cells were at a concentration of 2-4 x 10^6 cells per mL. The cell suspension was then aliquoted into 1 mL volumes per cryogenic vial. Vials were then labelled with the cell line, passage number and the date; and then placed into a Mr Frosty box (Sigma-Aldrich, UK) containing isopropyl alcohol within a -80 ºC freezer. The following day cells were moved to a liquid nitrogen storage vessel until required.

2.2.6 Resuscitation

To avoid the toxic effects of DMSO the thawing process must be undertaken quickly. Using a 70% ethanol soaked tissue the cap of the cryovial was opened a quarter turn to release any trapped liquid nitrogen. The vials were then swiftly transferred to a water bath at 37 ºC until no ice crystals remained within the vial. The contents of the vial were then transferred by pipetting to a 15 mL falcon that contained 5 mL of pre-warmed culturing media. The cells were then centrifuged at 800 rpm for 3 minutes and the supernatant was removed. Cells were then resuspended in 5 mL of culturing media and transferred to a 25 cm^2 filter capped culturing flask. The flask was then placed in an incubator overnight at 37 ºC with 5% CO_2 and assessed the following day to check whether the cells had adhered to the flask. The culturing media was then

poured away and 5 mL of fresh culturing media was added. Cells were then left to grow in the incubator until 70-80% confluent, at which point they were ready to be passaged as previously described.

2.3 Electrophysiology

Electrophysiological recordings of tsA201 cells and PASMCs were acquired using whole-cell patch-clamp method (Figure 2.2). Whole-cell patch clamping enables the measurement of ion movements across the membrane of the whole cell. The voltage-clamp configuration was adopted for these recordings. This involves holding the membrane potential at a constant level and then determining the flow of current required to maintain the voltage set. In reality the membrane current is not of interest, but it is membrane conductance that needs to be determined, as this represents the activity of the ion channel. However by creating a constant membrane potential it means that the current is linearly proportional to the voltage and therefore of interest to be studied (Guide, 2008).

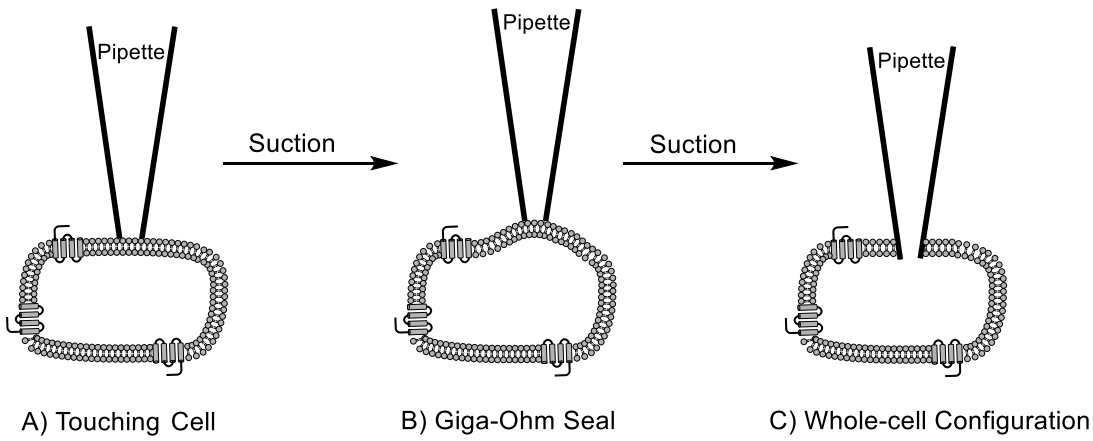

Figure 2.2 – Diagram of process to gain whole-cell configuration

A) Shows the pipette tip touching the cell membrane. B) After suction the formation of a seal between pipette tip and cell membrane with the resistance in the giga-ohm (GΩ) region, called giga-seal. C) Once a giga-seal has been achieved, further suction using the pulse technique removes the section of membrane within the pipette tip allows access to the interior of the cell.

2.3.1. Electrophysiological Rig Set-up

Electrophysiological studies were conducted using the rig set-up shown in figure 2.3. To isolate the set-up from external sources of vibration, which can affect recordings, the microscope, headstage and manipulator were placed on an air table (Technical Manufacturing Corporation). Recordings can be affected by interference from a wide range of electrical noise such as radio waves, therefore the set-up was encased in a Faraday cage. An additional reduction in electrical noise is taken with the grounding of the set-up to single point on the Faraday cage.

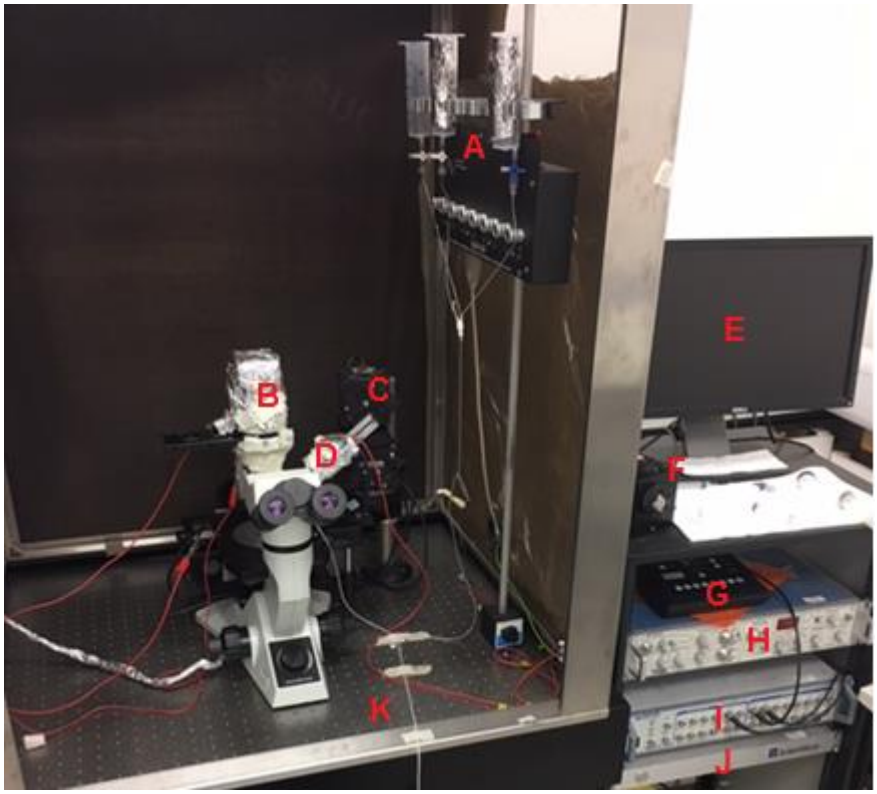

Figure 2.3 – Electrophysiological rig set-up

Layout of the electrophysiological rig set-up. A) Gravity feed perfusion system (ALA-VM8, ALA Scientific Instruments). B) Inverted microscope (Olympus CKX41). C) Amplifier headstage. D) Micro-manipulator (PatchStar, Scientifica). E) PC screen used as an oscilloscope (Dell). F) Micro-manipulator controller (Scientifca). G) Perfusion channel controller (ALA Scientific Instruments). H) Axopatch 200B amplifier

(Molecular Devices). I) Digidata 1440A digitizer (Molecular Devices). J) Micro-manipulator power source (Scientifica). K) Air table (Technical Manufacturing Corporation).

Coverslips prepared with cells grown on them, as previously described, were placed into a double-chambered Perspex bath (Figure 2.4). Cells were viewed upon an inverted, fixed stage microscope (Olympus CKX41) that has both a standard light source and a fluorescence illuminator (X-Cite 120Q, Excelitas technologies). Depending on the type of study, external solution (or containing the compound to be tested) was either continuously perfused across the chamber using the gravity-feed perfusion system or incubated with external solution (or compound to be tested) for 20 minutes prior to study and then placed in a bath of the same solution used for incubation. Surplus solution would flow through a narrow channel in the second chamber where the excess solution was removed using a MHRE 200 H.R. flow inducer (Watson-Marlow Ltd). The use of the second chamber enabled the reduction of noise to the recording system by separating the location of the suction and recording pipette. As the two chambers were connected through the narrow channel, the bath solution was grounded using a silver chloride pellet. Recordings were taken using the borosilicate micropipette encasing a silver wire coated with silver chloride. Micropipettes were manufactured using borosilicate glass capillaries (Harvard Apparatus, UK) with an outer diameter of 1.5 mm and internal diameter of 1.17 mm. The glass capillaries were placed into a vertical puller (PC-10, Narishige) generating two micropipettes with an average resistance of 5 – 10 MΩ and 1 – 2 µm tip diameter. The micropipette was positioned using a PatchStar Micromanipulator (Scientifca, UK) which was controlled from outside of the rig to remove any disruption to the set-up.

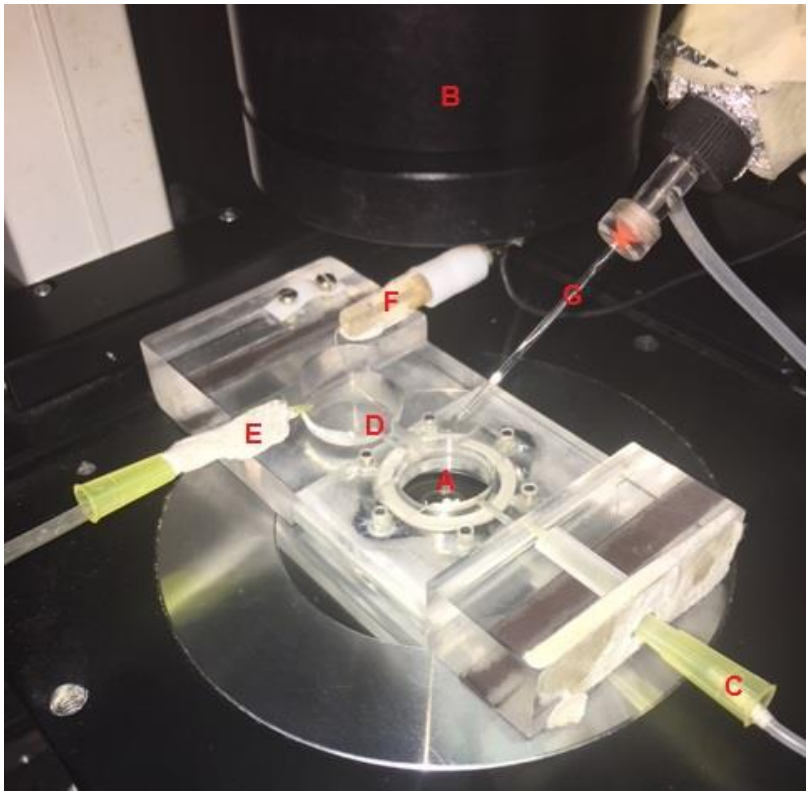

Figure 2.4 – Bath chamber arrangement

Layout of bath chamber. A) First chamber of the bath to which the coverslip is placed and cells are viewed using an inverted microscope (B), solution is perfused into this first chamber (C). Excess solution passes through a channel into the second chamber (D) where excess solution is suctioned out of the bath (E). The bath chamber is grounded using a silver chloride pellet (F) placed into the second chamber of the bath. Recordings were taken using borosilicate glass micropipettes (G) encasing a silver wire coated with silver chloride.

2.3.2 Signal acquisition

The coating of silver chloride on the silver wire creates a reversible reaction:

$$Ag + Cl^- \rightleftharpoons AgCl + e^-$$

This reaction enables the flow of ions to be converted to a flow of electrons within the silver wire which can then be measured. The micropipettes were connected to a headstage amplifier (CV 203BU, Axon Instruments) which in turn was linked to an Axopatch 200B amplifier (Axon Instruments). The headstage amplifier contained feedback circuitry capable of correcting for

series resistance of the micropipette (R_s) as in a model experiment the series resistance of the micropipette would be zero. R_s is calculated by the total of all resistance occurred between the headstage amplifier and the inside of the cell. In essence this equates to:

$$R_s = R_{access} + R_{pipette}$$

The micropipette (having correctly secured a 'patch') has its own potential (V_P) and transmits a current (I_P) to the inverting (current to voltage) input of the headstage amplifier (A_H). Meanwhile the chosen voltage for the micropipette to be clamped at (V_{CMD}) was also applied to A_H, however to the non-inverting input. This leads to the difference of the inputs ($V_{CMD} – V_P$) generating the output of A_H (V_1) which is a relative measurement of the membrane current flow. From V_1 a feedback resistor (R_F) applies a feedback current (I_F) to I_P which essentially eliminates I_P and results in V_P equalling V_{CMD}. This enables the ability to measure the current of the membrane whilst clamping the micropipette to the desired voltage.

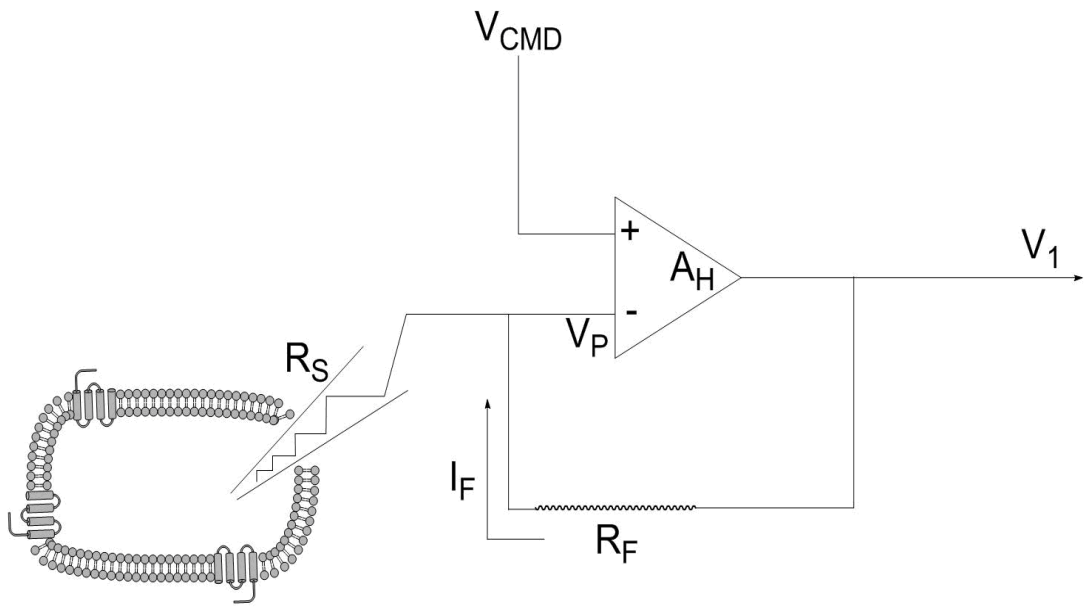

Figure 2.5 – Headstage series resistance correction

Diagram to represent the circuitry involved within the headstage of an electrophysiological set-up. The differential amplifier (A_H) calculates V_1, which is relative calculation of the membrane current flow, derived from the difference between voltage measured at the micropipette (V_P) and the desired voltage (V_{CMD}). A positive feedback loop through a feedback resistor (R_F) provides a current (I_F) that consequently leads to $V_P = V_{CMD}$, allowing the micropipette to be clamped at the desired voltage.

Once the recording reaches the whole cell configuration, the capacitance and the resistance of the cell membrane (C_m and R_m, respectively) can be calculated. Capacitance is defined as:

$$Cm = \frac{\varepsilon_0 \cdot A}{d}$$

Where, ε_0 represents the lipid property of the membrane, d the membrane thickness and A the surface area of the cell. As ε_0 and d remain relatively constant therefore C_m can be used as a measurement for the size of the cell. With a value of capacitance measured it is possible to normalise the current of cell to its size.

After the signal has been acquired by the headstage they are conveyed to the amplifier (Axopatch 200B, Axon Instruments) where it is filtered by the application of a 4-pole Bessel low-pass filter that was set at 5 KHz. This filtering enables all frequencies above 5 KHz (external noise) to be excluded from the final signal output. After being processed by the amplifier the signal is transmitted to the digitizer (Digidata 1440A, Axon Instruments) where the signal is converted from an analogue signal to a digital signal. From the digitizer the signal is passed onto an oscilloscope, in our case the computer. The computer using pCLAMP 10 software (Axon Instruments) to records and enables analysis of data.

2.3.3 Solutions and compounds

For electrophysiological experiments using tsA201 cells the external solution comprised of 145 mM NaCl, 2.5 mM KCl, 3 mM $MgCl_2$, 1 mM $CaCl_2$ and 10 mM HEPES with the pH being adjusted to pH 7.4 with the use of 1 M NaOH. External solution was then stored at 4 ºC and made fresh 1 – 2 times a week as necessary. For experiment using different pH ranges the external solution was made using the same composition just adjusted to the desired pH for the experiment using NaOH. The internal solution used for tsA201 cells comprised of 150 mM KCl, 3 mM $MgCl_2$, 5 mM EGTA and 10 mM HEPES. The pH of the internal solution was adjusted to pH 7.4 using 1 M KOH and filtered using 0.2 µm cellulose acetate filter (Sartorius). Internal solution was aliquoted into 1.5 ml Eppendorfs and stored at -20 ºC until required. pH 7.4 was selected as the pH to conduct experiments at because it represents physiological conditions. At this pH range TASK-1 is inhibited ~50% by protons whereas TASK-3 is ~10% (Bayliss *et al.,* 2015). All fine chemicals and compounds were purchased from Sigma-Aldrich unless otherwise stated.

Drug stock solutions were made up into mM concentrations using DMSO, ethanol or distilled water as required, aliquoted and then stored at -20 ºC to be defrosted and used when required. Aliquots of the drug stock were diluted in external solution as required for the desired experiment and used the same day. Any compounds with light sensitivity were maintained in the dark.

Compounds used were: Doxapram hydrochloride, Zinc chloride, Gal-054 (Galleon Pharmaceuticals Inc), ONO-RS-082 (Abcam), Treprostinil (gifted from Lucie Clapp at University College London), Riociguat (MedChem Express), Sildenafil citrate, IBMX, Forskolin (Abcam), and Pioglitazone (Abcam).

2.3.4 The whole-cell patch-clamp technique

To begin the cells are placed into the bath chamber immersed in external solution, when the micropipette, filled with internal solution, is submerged into the bath chamber the first stage of producing a recording occurs. A test pulse of –5 mV is applied and the current offset of the amplifier is adjusted to 0 allowing for the calculation of the micropipette resistance. Using Ohm's law the resistance for the micropipette is calculated, for example if the test pulse of –5 mV yields a response current of –750 pA then:

$$R_P = \frac{-5\ mV}{0.750\ nA} = 6.67\ M\Omega$$

Using the micromanipulator the micropipette is then manoeuvred into the field of view of the microscope. Selecting an appropriate cell to patch was the next stage of the process, cells chosen were preferably isolated and fluorescing green as the channel was co-transfected with GFP. To enable the viewing of GFP a fluorescence illuminator (X-Cite 120Q) was used which contained a mercury bulb and set at a wavelength of 395 nm. Once a cell has been selected the micropipette was lowered onto the cell membrane. The contact between the cell and micropipette can be identified by an increased in micropipette resistance shown on the PC screen. The application of negative pressure to the micropipette via a suction syringe generates a seal between micropipette and cell-membrane with a resistance in the GΩ region known as a giga-seal. From this position many different patch-clamp techniques can be implemented, for this study the whole-cell patch-clamp technique was adopted. To go from the giga-seal stage to whole-cell, the holding potential of the micropipette was adjusted to –60 mV and further negative pressure

‘pulses’ were applied. This further negative pressure breaks the membrane below the pipette tip creating low resistance entry to the entire interior of the cell. Access to the interior of the cell allows for current measurement of all open ion channels on the cell membrane (excluding the very small section broken as a result of going whole-cell). All electrophysiological experiments were conducted at room temperature (20 – 23 ºC).

2.3.5 Data Analysis

After the whole-cell patch clamp has been achieved, it is possible to make recordings using the PC and pCLAMP software. When recording, a protocol can be applied to evoke various characteristics of the ion channel that is being investigated and for this work the same protocol was used throughout (Figure 2.6). The protocol was termed a ‘step-ramp’ protocol as it consisted of both a voltage-step phase as well as a ramp. The ramp ensured that current-voltage (I – V) relationships could be assessed for the ion channel. The protocol was applied once every 5 seconds and a minimum of 5 sweeps were recorded and averaged for any given cell current value.

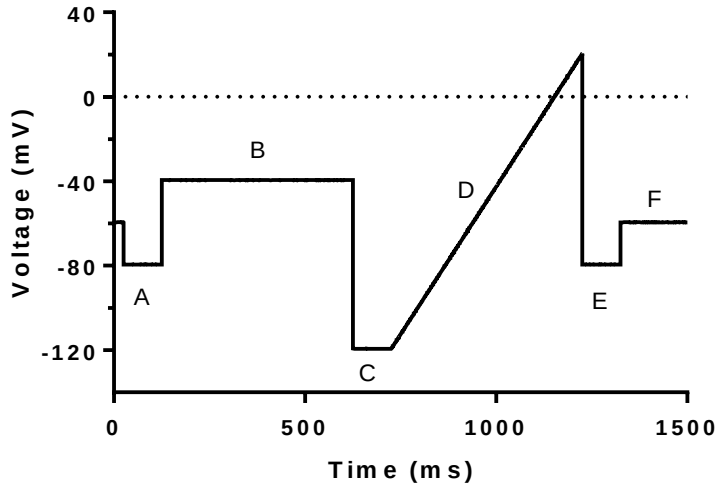

Figure 2.6 – Step-Ramp Voltage protocol

Step-ramp voltage protocol. A) Voltage step from –60 mV (holding potential) to –80 mV for 100 ms. B) Voltage step from –80 mV to –40 mV for 500 ms. C) Voltage step from –40 mV to –120 mV for 100 ms. D) Voltage ramp from –120 mV to +20 mV over

500 ms. E) Step from +20 mV to –80 mV for 100 ms. F) Step to holding potential –60 mV where it is held until protocol is applied again. Protocol was applied once every 5 seconds.

pClamp software combined with GraphPad Prism 7 (GraphPad Software Inc., CA) was then used to generate graphs. Graphs produced were time-course graphs (current vs time), average trace graphs, I – V graphs and current bar charts. Results were produced with an average current before and after drug application and percentage change, with error given as standard error of the mean (SEM). For electrophysiological data n = number of cells recorded. Currents for Chapter 3 were recorded as the difference in current between that recorded at -80 mV and that at -40 mV whereas for Chapter 4 currents were recorded at -40 mV only. Reasoning for this was due to previous data collected within the lab surrounding TASK-3 was analysed using this difference, and for chapter 4 TASK-1 currents are far smaller meaning the -80 mV current held a far larger influence on current size for these channels.

2.4 Imaging

To assess the location of channels within the cells confocal microscopy was used. This enabled the production of high resolution images to see whether different channels and their respective mutations used in electrophysiological studies varied in their cellular locations and quantities. Confocal microscopy is an advancement of fluorescence microscopy, which uses specific wavelengths of light to cause specific materials (in our case cellular components) to emit visible light. By labelling the specific components of the cell with selective fluorescent markers you are able to contrast the different components and analyse them visually. Confocal microscopy builds on this by the addition of a pinhole reduces background fluorescence producing a sharper, clearer image. This works as when focussing on a specific part of the slide, fluorescence from other areas of the slide not in the focal point still managed to be imaged by the objective lens but by applying a pinhole to the point of image made from the objective lens at that focal point it is able to block the majority of fluorescence generated outside of the focal point (Figure 2.7).

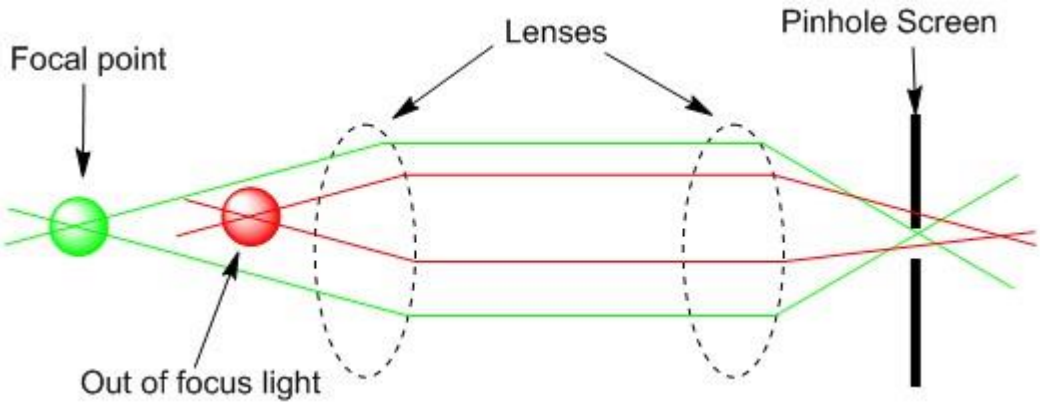

Figure 2.7 – Schematic of confocal microscopy background noise reduction

Diagram depicts how sources of light outside of the focal point may interfere with final image. The use of a pinhole screen used in confocal microscopy reduces this interference, note most of the light is removed from the final image but not all.

2.4.1 Sample preparation and cell fixation

Cells used for imaging studies were the same tsA-201 cells used in electrophysiological studies and prepared in the same way prior to transfection, on PDL-coated coverslips in 4 well dishes. DNA constructs used were the same sequences as used for electrophysiological studies however placed in a pAcGFP1-N1 vector (Clontech, USA). Cells were transfected with desired DNA using TurboFect transfection reagent (ThermoFisher Scientific, UK) described above. As the DNA constructs were expressed together with a pAcGFP, when expressed the cells fluoresced green. Prior to cell fixation if the cells were to have their membranes stained they would be treated with CellMask™ deep red plasma membrane stain (ThermoFisher Scientific) as per ThermoFisher Scientific protocol. Membrane staining involved incubating cells with CellMask™ deep red plasma membrane stain (1 mL of 1X solution per well) for 10 minutes at 37 ºC. For cell fixation cells were washed twice with room temperature PBS and then immersed in 1 mL of 2% paraformaldehyde (PFA) solution and placed in the fridge for 20 minutes. The cells were then further washed twice with PBS and if the nuclei were to be stained 500 µL of Hoechst solution (2 µL Hoechst 33258 [1 mg/mL in H_2O, Sigma-Aldrich] into 1 mL PBS) was added to each well and incubated at 37 ºC for 10 minutes. Cells were again washed twice with PBS and rinsed once with ddH_2O to remove salt crystals. The coverslips were then placed facedown onto slides containing a drop of Vectashield anti-fade mounting medium (Vector Laboratories, UK) and sealed.

2.4.2 Confocal microscopy

Once the slides had been prepared they were imaged using a Zeiss LSM 880 confocal microscope, placed upon an anti-vibration table, and analysed on a connected PC using Zen Black software (Zeiss). Cells were imaged using oil immersion under a Plan-Apochromat 63x/1.4 oil DIC M27 objective. The cells were excited with an argon laser at 561 nm, 488 nm and 405 nm for the CellMask™ deep red plasma membrane stain, pAcGFP-channel and Hoechst 33528, respectively, to elucidate fluorescence emission.

2.4.3 Co-localisation images

After images were generated and opened within Zen Black, the degree of co-localisation between the channel of interest and the membrane could be determined. It is key to note that of the images generated a region of interest (ROI) is selected so that values are conducted across only the cell (or cells) you wish to measure and eliminate unwanted measurements. First, control images for pAcGFP only and dsRed only cells were taken and used to set the crosshairs of the scatter plot, this ensures all pixels within the co-localised quadrant are not selected arbitrarily. After the controls have been imaged, ROI selected and the crosshairs set, an image from sample containing both pAcGFP and dsRed can be analysed. Zen Black generates multiple coefficients based on the scatterplot generated and for this study Pearson's Correlation Coefficient (PCC) was used. PCC values range from -1 to 1 and show the relationship between the structures, a value of 1 would indicate perfect correlation so for every pixel that contained dsRed it would also contain pAcGFP. For this study PCC values for each channel required a minimum of 6 cells over at least 3 days.

2.5 In-cell and on-cell assays

In cell and on cell assays were conducted in poly-D-lysine coated 96-well plates containing a cell density of 2 x 10^4 cells/well in a 100 µL of media. Cultures were incubated for 24 hours at 37 ºC in 5% CO_2 prior to transfection. Cells were transfected using TurboFect protocol, each well contained 200 ng of DNA and 0.4 µL of Turbofect and were incubated for 24 hours at 37 ºC in 5% CO_2. DNA contained each channel tagged with hemagglutinin (HA) on the M1P1 loop between Alanine 50 (A50) and Arginine 51 (A51), this area is extracellular so can be detected if the channel has reached the membrane. Media was then removed and cells were fixed with 40 µL PFA (2%) and incubated at room temperature for 20 minutes. Fixing solution was then removed and cells were washed with 1X PBS, PBS was then removed and the plate was patted dry. For on-cell (membrane staining) assay cells were washed with 40 µL (0.1%) Tween-20 PBS (TBST) and shaken on a rotor for 5 minutes and then TBST was removed, this step was repeated 5 times. For in-cell (whole cell staining) assay membranes were permeablised using 40 µL (0.1%) Triton X-100 (1 mL Triton in 10 mL PBS; Sigma Aldrich, UK), plates were then shook on a rotor for 5 minutes and then Triton was removed, this step was repeated 5 times. Cells were then incubated at room temperature with 100 µL blocking buffer, 2% bovine serum (Sigma Aldrich, UK) in 1X TBST for 60 minutes whilst on rotor, this prevents non-specific binding of primary antibody. Blocking buffer was then removed and cells were covered with 40 µL (2µg/µL) monoclonal anti-HA antibody (mouse; Sigma Aldrich, UK) in 2 mL blocking solution. Cells were incubated for 2 hours at room temperature with gentle rocking on the rotor. All cells (in-cell and on-cell) were then washed with 0.1% TBST and rocked for 5 minutes, this was repeat 5 times. Washing agent was removed and each well was then loaded with a mixture of secondary antibody, goat anti-mouse IRDye 800 CW (green; LI-COR, NE, USA) and DNA dye, DRAQ5 (5 mM, Abcam, UK) diluted in blocking buffer 1:1000 and 1:10,000, respectively. After 60 minutes incubation at room temperature and gentle rocking cells were washed for 5 minutes with 0.1% TBST and repeated 5 times. Cells were then dried and imaged. To image the plates they were scanned in a LI-COR plate reader at 700 nm and 800 nm (169 m resolution, 7

sensitivity, 3.2mm offset and medium quality). Integrated intensity values were then recorded and analysed.

2.6 Statistical Analysis

Statistical analysis were performed using GraphPad Prism 7 (GraphPad Software Inc., CA, USA). All values are expressed as mean ± standard error of the mean (SEM). For electrophysiological recordings n = number of individual cells recorded from. Statistical tests to determine significance between three or more groups used was one-way ANOVA followed by Dunnett's post-hoc test. Two-way ANOVA was used when there is more than one condition for two or more groups such as two different channels in control conditions and in presence of a drug. Student's t-test were used to analyse data from two cell populations, if the cell populations involved the same cells just in different conditions a paired Student's t-test was used however if the cell populations were not the same cells an unpaired Student's t-test was performed. Statistical significance was defined at a probability level (p) of < 0.05. Power calculations were performed using a calculation tool from The University of British Columbia which compared inference for means of two independent groups (https://www.stat.ubc.ca/~rollin/stats/ssize/n2.html). The calculator used the following formula:

$$n = 2\left(\frac{(Z_\alpha + Z_\beta)\sigma}{ES}\right)$$

Where n = required sample, Z_α = significance level based on normal distribution table, Z_β = power value required according to normal distribution table, σ = standard deviation of test sample and ES = difference in the mean between the two groups.

3. Doxapram Inhibition of TASK-3 K2P Channels

3.1 Introduction

Doxapram hydrochloride ($C_{24}H_{30}N_2O_2$, doxapram) is a central respiratory stimulant. Doxapram's analeptic respiratory action is characterised by an increase in tidal volume and a slight increase in respiratory rate, when administered intravenously. Sold under the name Dopram®, Stimulex and Respiram (Bedford Laboratories), doxapram is used clinically in the treatment of post-operative respiratory depression, acute respiratory failure, chronic obstructive pulmonary disorder and apnoea in premature infants (Lunsford *et al.,* 1964, Yost *et al.*, 2008). Doxapram's proposed mechanism of action is via the direct stimulation of peripheral chemoreceptors of type 1 cells within the carotid bodies and a subsequent release of catecholamines (Mitchell and Herbert, 1975; Nishino *et al*., 1982). These combined events result in the prevention or reversal of CNS depressant or narcotic-induced respiratory failure.

3.1.1 Arterial Chemoreceptors

Arterial chemoreceptors act as a feedback mechanism to inform cardiovascular and respiratory control centres in the brainstem of the chemical composition of arterial blood. They respond to low O_2 (hypoxia), high CO_2/H^+ (acid hypercapnia) and low glucose (hypoglycemia), in order to maintain oxygen delivery to the brain and vital organs (Gonzalez *et al.,* 1994, Peers and Buckler 1995). They are located in the vicinity of the carotid artery are the carotid bodies and the aortic bodies which make up the chemoreceptors (Figure 3.1, Nurse, 2014).

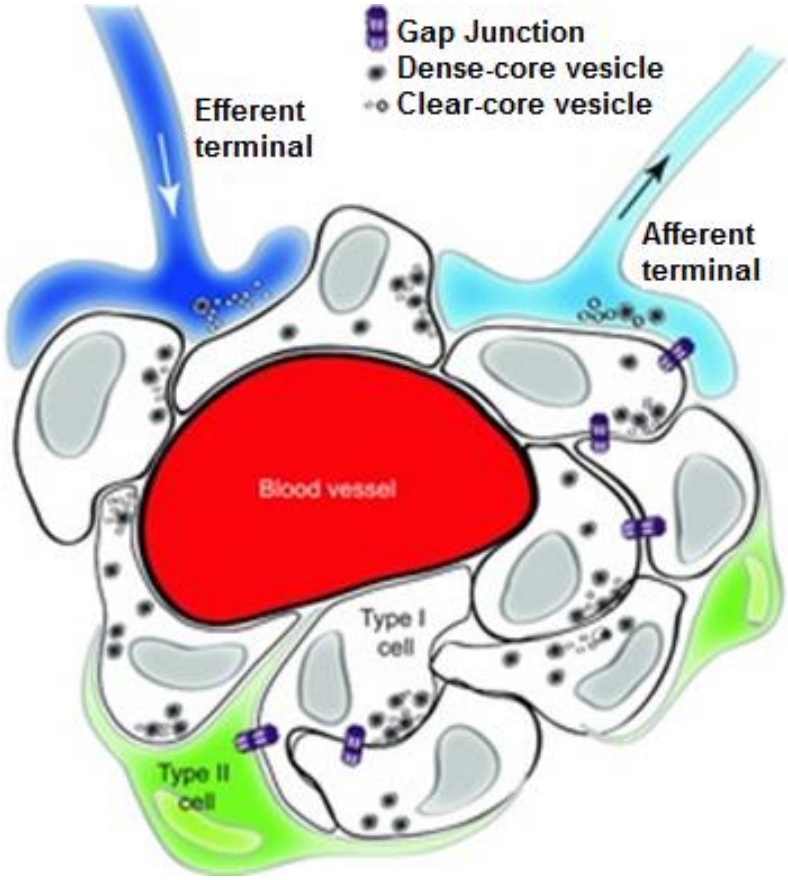

Figure 3.1: Cellular organization of the rat carotid body

Graphic representing the cluster of type I cells in close proximity with type II cells. Type I cells are innervated by afferent terminals. (Reproduced from Nurse, 2014).

3.1.2 Carotid Bodies

The carotid bodies are composed of type 1 (glomus) cells that are occasionally enveloped by glial-like type 2 (sustentacular) cells (Figure 3.1). Type 1 cells both chemically and electrically synapse with afferent nerve terminals of the carotid sinus nerve (McDonald, 1981; Eyzaguirre, 2007) and release a variety of neurotransmitters and neuromodulators. The carotid bodies are highly sensitive to changes in O_2, CO_2 and acidosis. They have also been found to be highly sensitive to mitochondrial poisons (Anichkov and Belen'kii, 1963; Mulligan and Lahiri 1981). In response to changes in arterial blood levels of chemicals, type 1 cells depolarize and release neurotransmitters such as ATP, dopamine, noradrenaline, acetylcholine etc (Nurse, 2005). These

neurotransmitters then excite afferent terminals of the carotid sinus nerve and afferent signals are relayed to the brainstem, which initiates respiratory and cardiovascular reflexes to restore blood homeostasis (Gonzalez *et al*., 1994).

Neurotransmitter release by the type 1 cells is thought to occur as a consequence of an increase in cytosolic calcium (Ca^{2+}) levels within the carotid body, in response to an electrical signal (Gonzalez *et al.,* 1992, Montoro *et al.,* 1996). The increase in Ca^{2+} is mediated by voltage-gated calcium channels (L- and P/Q type) that are highly expressed in type 1 cells (Rocher *et al.,* 2005). Activation of voltage-gated calcium channels and the subsequent increase in intracellular Ca^{2+} occurs as a consequence of membrane depolarization caused by the inhibition of a membrane potassium (K) conductance (Peers and Green, 1991; Anderson-Beck *et al.,* 1995; Peers and Kemp, 2001). Several K channels have been identified in carotid bodies, that can be modulated by chemoreceptive intracellular signaling pathways to invoke an electrical response that then results in voltage-gated calcium channel activation, extracellular Ca^{2+} influx and neurotransmitter release.

3.1.3 Role of Potassium Channels

Electrophysiological studies have identified a number of different potassium ion channels in type 1 cells, which includes delayed rectifier K^+-channels, calcium-activated K-channels (maxi K channels, BK_{Ca}), HERG channels, and TWIK-related acid-sensitive K^+-channels (López-Barneo *et al.,* 1988; Peers, 1990; Peers and O'Donnell, 1990; Buckler, 1997; Buckler *et al.,* 2000). Determining which of these K channels identified in the carotid bodies are sensitive to chemical changes in the arterial blood has resulted in a number of studies been conducted, many of them concluding that inhibition of various K channels, did not then lead to carotid body excitation (Doyle and Donnelly, 1994; Cheng and Donnelly, 1995; Gomez-Nino *et al.,* 2009; Buckler, 1997; Pardel *et al.,* 2000; Ortega-Saenz *et al.,* 2006). In 2000, Buckler and colleagues showed that the resting K conductance of carotid bodies was predominantly mediated by a TASK-like current which, when inhibited, results in an influx of Ca^{2+} ions and subsequent membrane depolarisation (Buckler,

2007; Buckler *et al.,* 2000 and Figure 3.2). Both TASK-1 and TASK-3 are expressed in the carotid body (Yamamoto *et al.,* 2002; Kim *et al.,* 2009).

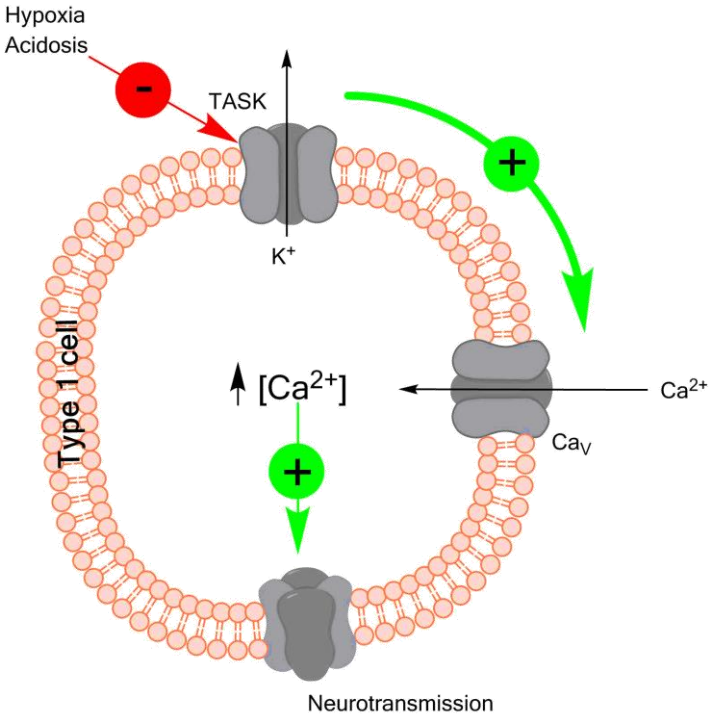

Figure 3.2 – Type 1 cell electrical excitation pathway

TASK channels, mainly TASK-1/TASK-3 heteromeric channels are responsible for the resting potential of the cells. Once a stimuli such as hypoxia or acidosis occurs this leads to the inhibition of TASK channels which depolarises the membrane activating voltage-gated calcium (Ca_v) channels. The activation of Ca_v channel leads to the increase of cytosolic Ca^{2+} levels which stimulates the release of neurotransmitters including dopamine, acetylcholine and ATP.

3.1.4 Role of TASK channels

Carotid bodies have been shown by single channel recordings to contain a mixture of homomeric and heteromeric TASK-1 and TASK-3 channels, with heteromeric channels being the predominant form (Kim *et al.,* 2009; Turner and Buckler, 2013).

TASK-1 and TASK-3 channels express structural amino acid similarity of approximately 60% and were the first K2P channels shown to form

heterodimers with intermediate functional properties of homomeric TASK-1 and TASK-3 (Chokshi *et al.,* 2015; Czirjak and Enyedi, 2002).

Stimulation of chemoreceptors by doxapram is thought to occur via inhibition of a TASK-like K channel (Cotton *et al.,* 2006; Buckler, 2015). However, doxapram's mechanism of action and the type of TASK channel that it inhibits is conflicting, depending upon which species is being studied. Early studies conducted using rat DNA showed doxapram selectivity favoured TASK-1, followed by TASK-1/TASK-3 heterodimeric channels and finally TASK-3 channels with EC_{50}'s of 410 nM, 9 µM and 37 µM respectively (Cotten *et al.*, 2006). This selective sensitivity was thought to reside at the carboxy intracellular terminal domains of the channels, where homology between TASK-1 and TASK-3 is the least (Cotton *et al.,* 2006). It is not clear if this differential sensitivity extends into human channels. Furthermore, TASK-1 expression has been shown to be different in human and pig hearts, when compared to rodents (Limberg *et al.,* 2011; Schmidt *et al.,* 2014). A concentration of 10 µM doxapram was selected for our experiments as blood plasma concentrations of doxapram have been identified at 4 µg/mL following intravenous administration and 3.78 µg/mL is equivalent to a 10 µM concentration (Robson and Prescott, 1978).

It would be advantageous for a compound like doxapram to selectively inhibit TASK-3 channels and not TASK-1 as an undesirable side effect of inhibiting TASK-1, is thought to be the development of hypertension. Hypertension is an adverse side effect commonly seen in patients on doxapram therapy (Vliegenthart *et al.,* 2017). Reduction in function or expression of TASK-1 has been heavily implicated within pulmonary arterial hypertension and is discussed in greater detail within Chapter 4 (Antigny *et al.,* 2016). Additionally another way to combat this adverse effect would be to combine doxapram therapy with a selective TASK-1 activator, although compounds that selectively activate K2P channels are scarce.

3.1.5 Putative Binding Site for Doxapram

Recent molecular modelling studies of TASK-1 and TASK-3 using inhibitory compounds such as A1899, PKTHPP and doxapram have suggested a

common intracellular binding site at the pore region of these channels (Streit *et al.,* 2011; Kiper *et al.,* 2015; Chokshi *et al.,* 2015). Specific amino acids in the pore Leucine (L) 122, Glycine (G) 236, L239 and Valine (V) 242, within rat TASK-3 channels (Figure 3.3) can considerably affect the efficacy of selective compounds (including doxapram), when mutated to aspartate (D), highlighting an important region of the K2P channels for the action of these compounds (Chokshi *et al.,* 2015). Interestingly, one of the amino acid sites is G236 is the same amino acid involved in Birk-Barel mental retardation syndrome.

A)

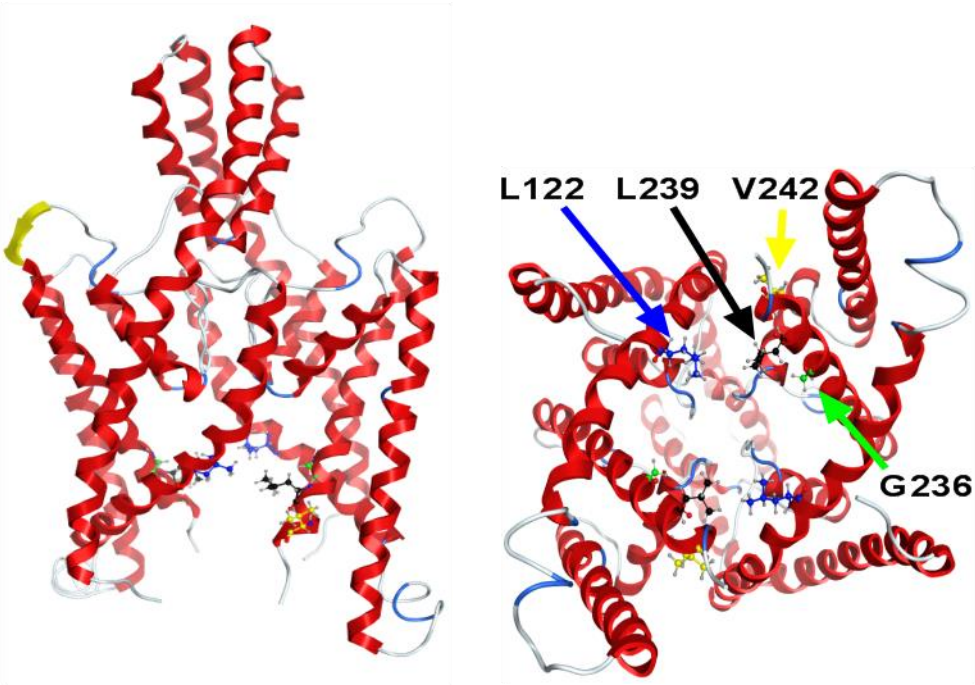

B)

```
TASK-1  120-LT-L-VMFQSLG--------230-TGLTVI-G-AF-L-NL-V-VLRFMTMNAEDEKRDAEH
TASK-3  120-LT-L-VMFQSLG--------230-VGLTVI-G-AF-L-NL-V-VLRFLTMNSEDERRDAEE
```

Figure 3.3 – Computer model of human TASK-3 channel with indicated putative binding site

A) Homology model of TASK-3 channel based upon TRAAK crystal structure (PDB ID 3UM7, Brohawn et al., 2012) depicting location of the four amino acids that form the putative site, L122, G236, L239 and V242. Left panel shows side view of the channel and right panel shows view from beneath the channel. B) Amino acid sequence alignment of TASK-1 and TASK-3, dashes represent gaps and numbers

represent the position of the amino acid where the sequence begins. The amino acids that form the putative site are highlighted by a box.

3.1.6 Doxapram

Doxapram is a racemic mixture of positive (GAL-054) and negative (GAL-053) enantiomers (Figure 3.4) and a study conducted by Galleon Pharmaceuticals Inc. showed that GAL-054 was the eutomer of doxapram whereas GAL-053 was the distomer (Golder *et al.,* 2012). The same study showed that the use of GAL-054 in isolation produced a greater efficacy than an equivalent dose of doxapram, as well as exhibiting fewer adverse side effects.

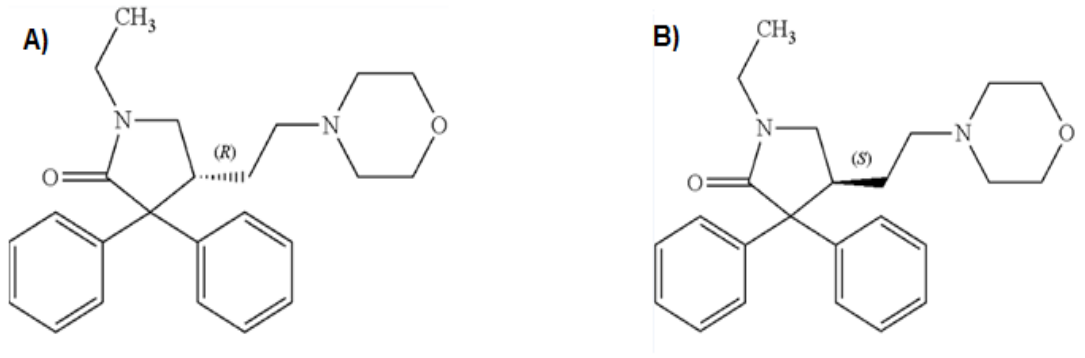

Figure 3.4 – Enantiomers of doxapram

A) Doxapram (+) enantiomer, known as GAL-054 to Galleon Pharmaceuticals Inc., PA, USA. B) Doxapram (-) enantiomer, known as GAL-053 to Galleon Pharmaceuticals Inc., PA, USA.

3.2 Objectives

Using an electrophysiological approach the first objective was to record currents through human TASK-3 channels and determine the effect of doxapram on the whole-cell current under physiological conditions.

The second objective was to determine whether the mutations identified in rat TASK-3 channels (L122D, G236D, L239D and V242D) that were shown to influence the effect of a selection of breathing stimulants (Chokshi *et al.,* 2015), had the same effect on human TASK-3 channels, using a site-directed mutagenesis and an electrophysiological approach.

As well as studying the effect of doxapram on these intracellular pore mutations, a well-known selective TASK-3 antagonist that acts extracellularly, zinc hydrochloride, was characterised.

I also investigated the effect of the different enantiomers of doxapram as identified by Galleon Pharmaceuticals on WT TASK-3 and a mutant channel.

Finally I investigated the role of the M1P1 loop of the TASK-3 channel, on doxapram regulation, using a chimera channel, with a substituted M1P1 loop from a TALK subfamily member, TASK-2.

3.3 Results

3.3.1 Electrophysiological properties of human TASK-3

Human TASK-3 (hTASK-3) wildtype (WT) DNA was transiently transfected in tsA201 cells and used for whole-cell patch-clamp recordings. The application of the step-ramp voltage protocol was used as previously described in the methods (Figure 2.6), to evoke hTASK-3 currents (Figure 3.5). hTASK-3_WT current was calculated as the difference between the current at -40 mV and -80 mV.

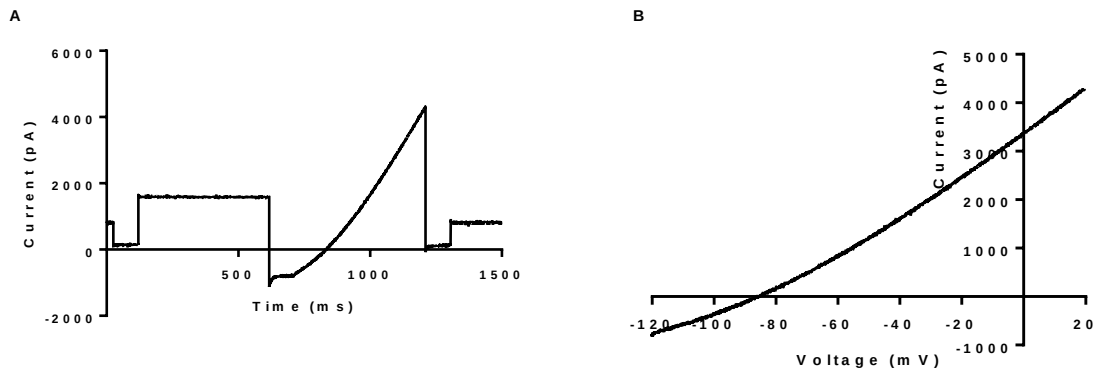

Figure 3.5 – hTASK-3_WT electrophysiological profile.

A) Representative trace for hTASK-3_WT channel in control conditions exposed to the step-ramp voltage protocol. B) Current-voltage representative graph for hTASK-3_WT in control conditions.

Expression of hTASK-3_WT produced an average current of 1178 ± 108 pA (n = 21) with an average reversal potential of -85 ± 1 mV (n = 21). The current-voltage graph (Figure 3.5B) shows the rectification of the current, whether the channel has any voltage-dependency as well as providing an approximation for the reversal potential of the current. hTASK-3_WT channels exhibited an outwardly rectifying current (Figure 3.5B).

3.3.2 Doxapram inhibition of TASK-3

Acute application of doxapram (10 µM) resulted in a significant inhibition ($p < 0.05$; paired t-test) of hTASK-3_WT current (Figure 3.6A) of 55 ± 2 % (n = 8) with an average current of 610 ± 66 pA (n = 8) in the presence of the drug. The perfusion of doxapram, represented with a solid black line, resulted in a partially reversible effect. The reversal potential of hTASK-3_WT was not significantly altered (Figure 3.6B) following acute application of doxapram (10 µM) with a value of -77 ± 3 mV (n = 8). Rectification of hTASK-3_WT remains unchanged (outward) in the presence of doxapram (10 µM).

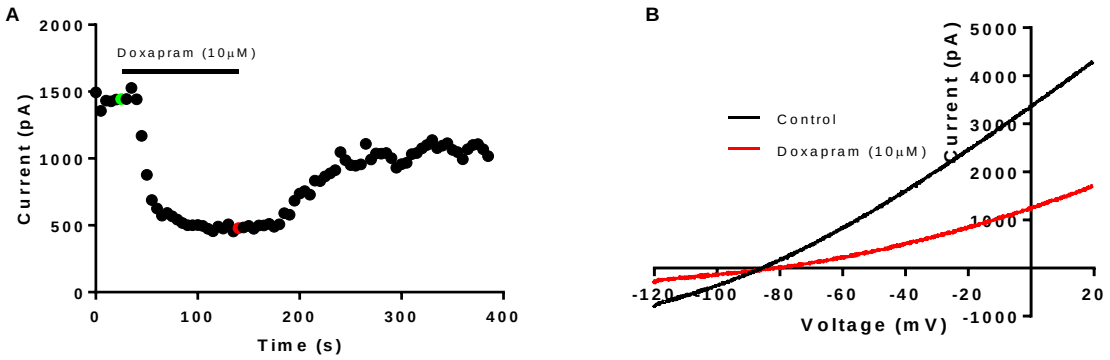

Figure 3.6 – Effect of doxapram (10 µM) on hTASK-3_WT

A) Time course graph showing the effect of doxapram (10 µM) on hTASK-3_WT current (pA) over time (s), doxapram perfusion represented by solid line, green starting point and red stopping point. B) Current-voltage graph shows the effect of doxapram (10 µM) on hTASK-3_WT current over different voltages. Current recorded in the presence of doxapram (10 µM) is shown in red.

3.3.3 Doxapram effect on TASK-3 containing mutations (L122D, G236D, L239D, V242D).

To test whether the putative doxapram binding site as suggested by Chokshi *et al.,* (2015) in rat, is critical to the observed doxapram effect on human TASK-3 channels, each amino acid was mutated individually by site-directed mutagenesis and assessed electrophysiologically.

3.3.3.1 hTASK-3_L122D

Whole-cell patch-clamping of hTASK-3_L122D yielded an average current (Figure 3.7A) of 1044 ± 130 pA (n = 18) with an average reversal potential (Figure 3.7B) equal to -83 ± 2 mV (n = 18), neither of which values were significantly different compared to hTASK-3_WT (Figure 3.11; $p > 0.05$; One-Way ANOVA with post-hoc Dunnett's test). However, unlike with hTASK-3_WT, acute application of doxapram (10 µM) did not significantly inhibit the current of hTASK-3_L122D (Figure 3.7C), with an average inhibition found to be 8 ± 2 % (n = 5; $p > 0.05$; paired t-test). Doxapram (10 µM) also did not affect the current of hTASK-3_L122D over the whole voltage range studied (Figure 3.7D).

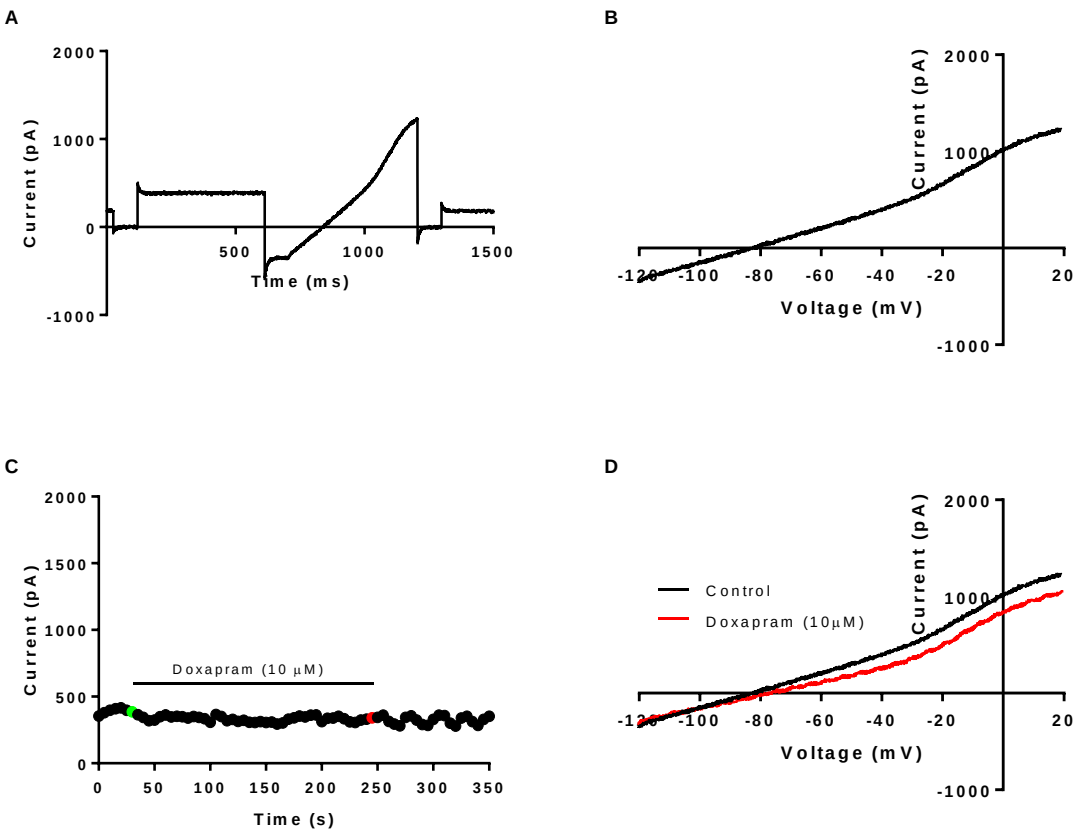

Figure 3.7 – hTASK-3_L122D electrophysiological profile and effect of Doxapram (10 µM)

A) Representative trace for hTASK-3_L122D channel in control conditions exposed to the step-ramp voltage protocol. B) Current-voltage graph for hTASK-3_L122D in control conditions. C) Time course graph showing the effect of doxapram (10 µM) on hTASK-3_L122D on current (pA) over time (s), doxapram perfusion represented by solid black line, green starting point and red stopping point. D) Typical current-voltage

graph showing the effect of doxapram (10 µM) on hTASK-3_L122D current over different voltages. Current recorded in the presence of doxapram (10 µM) is shown in red.

3.3.3.2 hTASK-3_G236D

The Birk-Barel mutation, G236R, has previously been shown to produce an inward rectifying current which is significantly reduced compared to the WT channel (Veale *et al.,* 2014a). However, the hTASK-3_G236D mutation produced an outward rectifying current at an average current of 1077 ± 141 pA (n = 16) in physiological conditions and an average reversal potential measured at -78 ± 2 mV (n = 16, Figure 3.8). Acute application of doxapram (10 µM) resulted in a 26 ± 5 % (n = 8) inhibition of the mutant channel, which was significantly reduced when compared to hTASK-3_WT ($p < 0.05$; paired t-test; Figure 3.8C). The average reversal potential was not affected by the application of doxapram (10 µM) measured at -77 ± 3 (n = 8; $p < 0.05$; paired t-test).

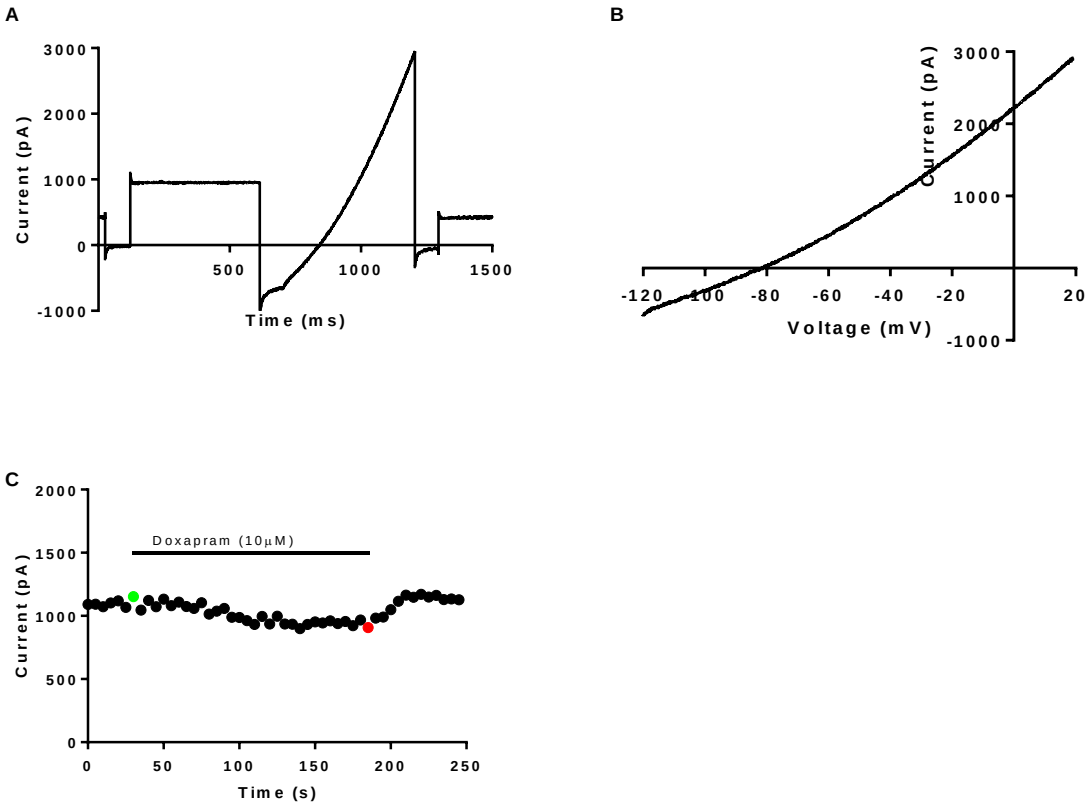

Figure 3.8 – hTASK-3_G236D electrophysiological profile and effect of Doxapram (10 µM).

A) Representative trace for hTASK-3_G236D channel in control conditions exposed to the step-ramp voltage protocol. B) Current-voltage graph for hTASK-3_G236D in control conditions. C) Time course graph showing the effect of doxapram (10 µM) on hTASK-3_G236D on current (pA) over time (s), doxapram perfusion represented by solid line, green starting point and red stopping point.

3.3.3.3 hTASK-3_L239D

The next mutation of hTASK-3 to be analysed was hTASK-3_L239D (Figure 3.9) which had an average current of 904 ± 105 pA (n = 13) and an average reversal potential of -82 ± 2 mV (n = 13) in control conditions (Figure 3.9A and B). The mutation of L239D in hTASK-3 resulted in the effect of doxapram being significantly reduced (Figure 3.12; $p < 0.05$ One-Way ANOVA with post-hoc Dunnett's test) with acute application of doxapram (10 µM) resulted in a significant, irreversible inhibition of 13 ± 3 % (n = 8; $p < 0.05$; paired t-test; Figure 3.9C) and an average reversal potential of -79 ± 6 mV (n = 8).

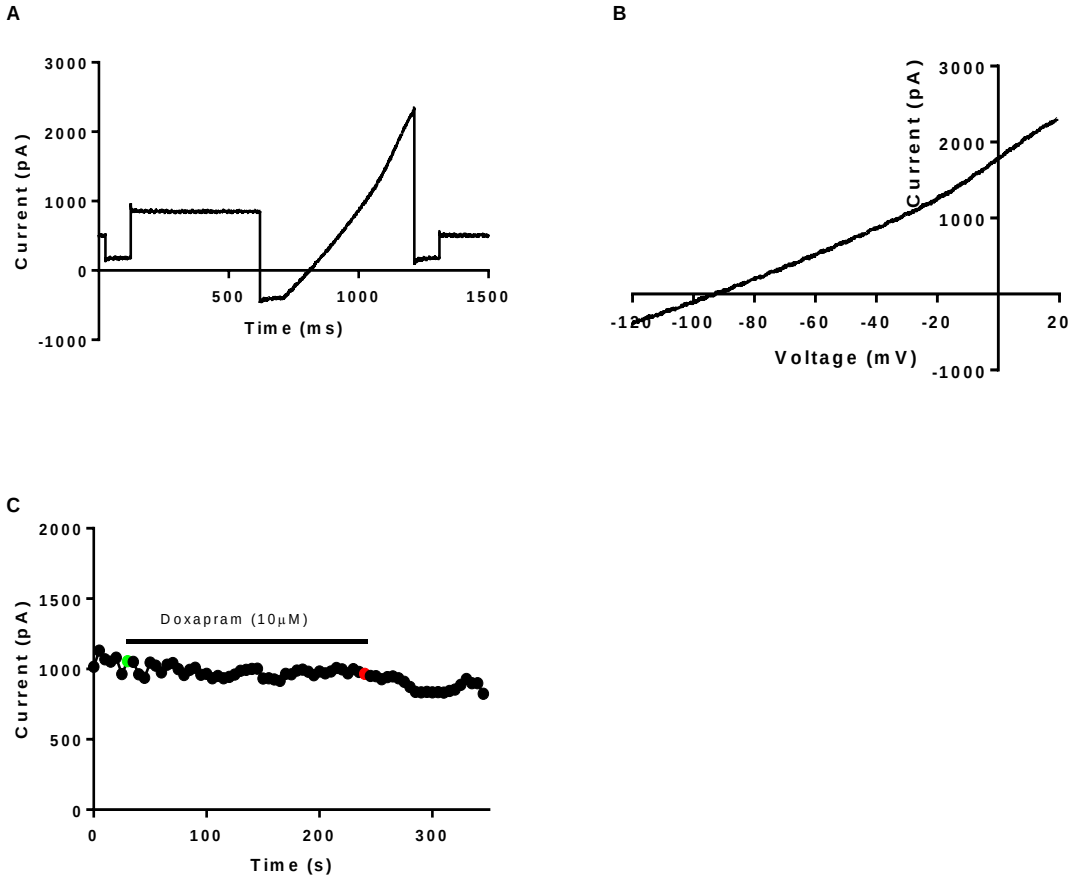

Figure 3.9 - hTASK-3_L239D electrophysiological profile and effect of Doxapram (10 µM).

A) Representative trace for hTASK-3_L239D channel in control conditions exposed to the step-ramp voltage protocol. B) Current-voltage graph for hTASK-3_L239D in control conditions. C) Time course graph showing the effect of doxapram (10 µM) on hTASK-3_L239D on current (pA) over time (s), doxapram perfusion represented by solid line, green starting point and red stopping point.

3.3.3.4 hTASK-3_V242D

The final mutation to be investigated was hTASK-3_V242D (Figure 3.10), which had an average current of 1133 ± 152 pA (n = 14) and an average reversal potential of -80 ± 2 mV (n = 14; Figure 3.10A and B). Acute application of doxapram (10 µM) resulted in a significant inhibition of current of 27 ± 5 % (n = 5; Figure 3.10C; $p < 0.05$; paired t-test), significantly lower than the effect

of doxapram (10 µM) on hTASK-3_WT ($p < 0.05$; Figure 3.12; One-Way ANOVA with post-hoc Dunnett's test).

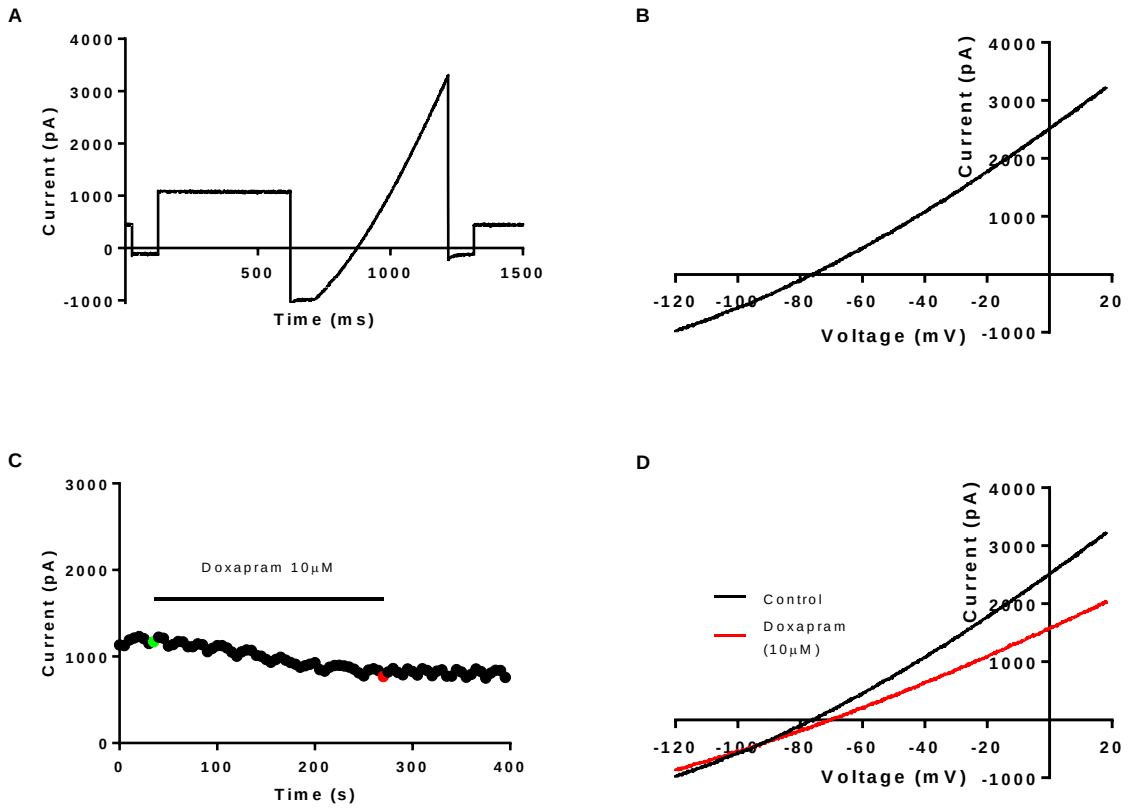

Figure 3.10 - hTASK-3_V242D electrophysiological profile and effect of Doxapram (10 µM).

A) Representative trace for hTASK-3_V242D channel in control conditions exposed to the step-ramp voltage protocol. B) Current-voltage graph for hTASK-3_V242D in control conditions. C) Time course graph showing the effect of doxapram (10 µM) on hTASK-3_V242D on current (pA) over time (s), doxapram perfusion represented by solid line, green starting point and red stopping point. D) Current-voltage graph shows the effect of doxapram (10 µM) on hTASK-3_V242D current over different voltages. Current recorded in the presence of doxapram (10 µM) is shown in red.

The average current recorded through mutant channels was not significantly different to that of hTASK-3_WT ($p > 0.05$; One-way ANOVA with post-hoc Dunnett's test; Figure 3.11).

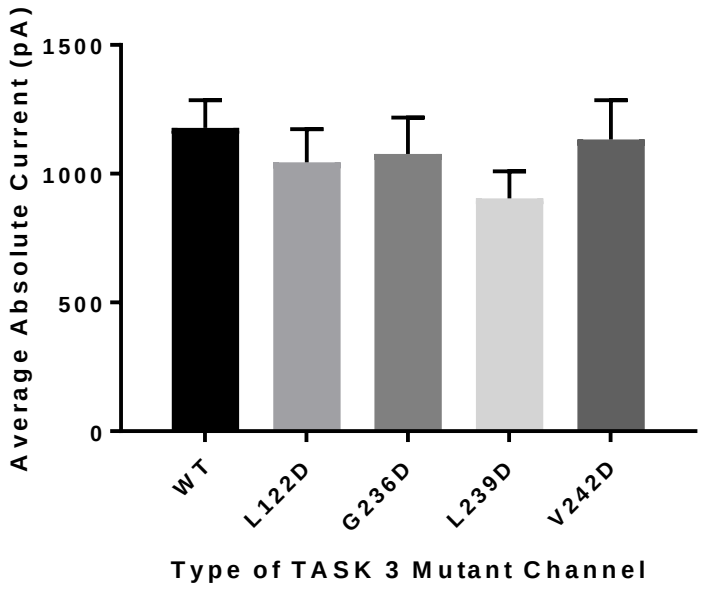

Figure 3.11 – Average absolute current (pA) of hTASK-3_WT and respective mutations.

When it came to the comparison of doxapram (10 µM) inhibition on hTASK-3_WT and the putative binding site mutations, all mutations resulted in a significant reduction in doxapram inhibition (Figure 3.12; $p < 0.05$; One-Way ANOVA with post-hoc Dunnett's test). Acute application of doxapram (10 µM) to hTASK-3_WT produced a 55 ± 2 % (n = 8) inhibition of current (Figure 3.12). The most significant reduction in doxapram inhibition was seen in the hTASK-3_L122D mutation which was recorded at 8 ± 2 %(n = 5). The inhibition of hTASK-3_L239D, hTASK-3_G236D and hTASK-3_V242D current by doxapram (10 µM) were also significantly reduced (13 ± 3 %, n = 8; 26 ± 5 %, n = 8; 27 ± 5, n = 5; respectively) compared to hTASK-3_WT ($p < 0.05$; One-Way ANOVA with post-hoc Dunnett's test).

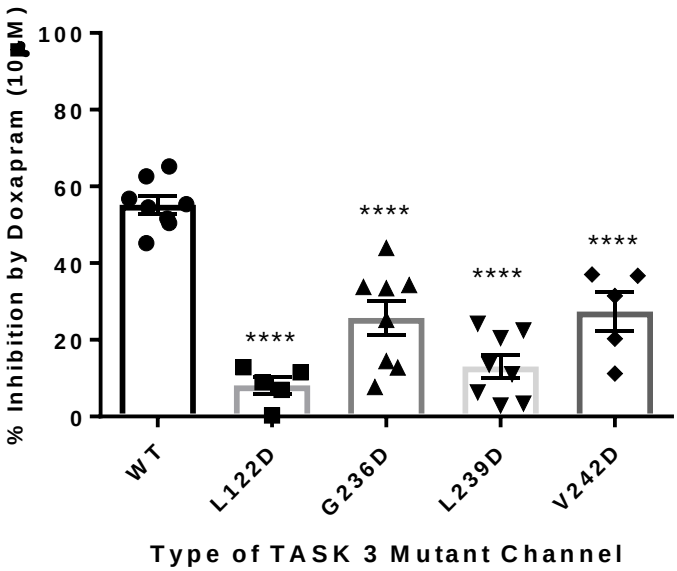

Figure 3.12 – Percentage inhibition by doxapram (10 μM) on hTASK-3_WT channel and respective mutations (*p < 0.05).

The results generated by the acute application of doxapram (10 μM) on the putative binding site suggests that the intracellular pore region of the channel may play a role in the binding of doxapram to hTASK-3 channels as well as rat channels (Chokshi *et al.,* 2015). The data suggests that hTASK-3_L122D and hTASK-3_L239D have the largest effect on doxapram inhibition. Whether these mutations directly prevent the binding of doxapram or have a secondary mechanism such as altering the gating of the channel is not yet confirmed.

To address this issue, I used another known TASK-3 inhibitor, zinc, which works extracellularly and at different amino acids, to determine whether the change seen in the inhibition by doxapram was a consequence of the above mutations, rather than a change in the gating of the channel, which could affect all inhibitors.

3.3.4 Effect of zinc on WT TASK-3 and TASK-3 mutants

Zinc (100 µM) acutely applied to hTASK-3_WT (Figure 3.13) produced a reversible effect (Figure 3.13C), with a maximal inhibition of 71 ± 6 % (n = 7). The average hTASK-3_WT current in the presence of zinc (100 µM) was 273 ± 57 pA (n = 7).

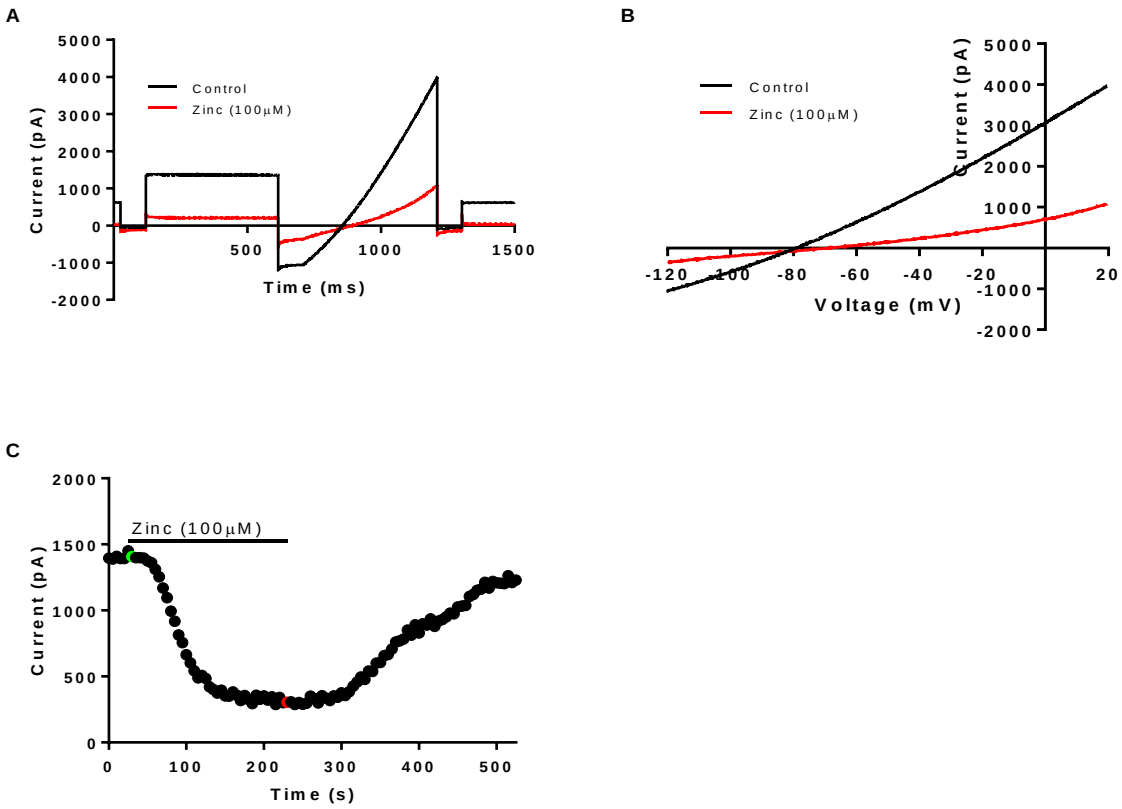

Figure 3.13 – Effect of zinc (100 µM) on hTASK-3_WT.

A) Representative trace for hTASK-3_WT channel in both control conditions and zinc (100 µM) when exposed to the step-ramp voltage protocol. B) Current-voltage graph shows the effect of zinc (100 µM) on hTASK-3_WT current over different voltages. Current recorded in the presence of zinc (100 µM) is shown in red. C) Time course graph showing the effect of zinc (100 µM) on hTASK-3_WT on current (pA) over time (s), zinc perfusion represented by solid black line, green starting point and red stopping point.

When zinc (100 µM) was acutely applied to hTASK-3_L122D it resulted in an inhibition of 55 ± 5 % (n = 8) with an average current of 414 ± 53 pA (n = 8; Figure 3.14). hTASK-3_L122D inhibition by zinc (100 µM) was reversible upon wash off.

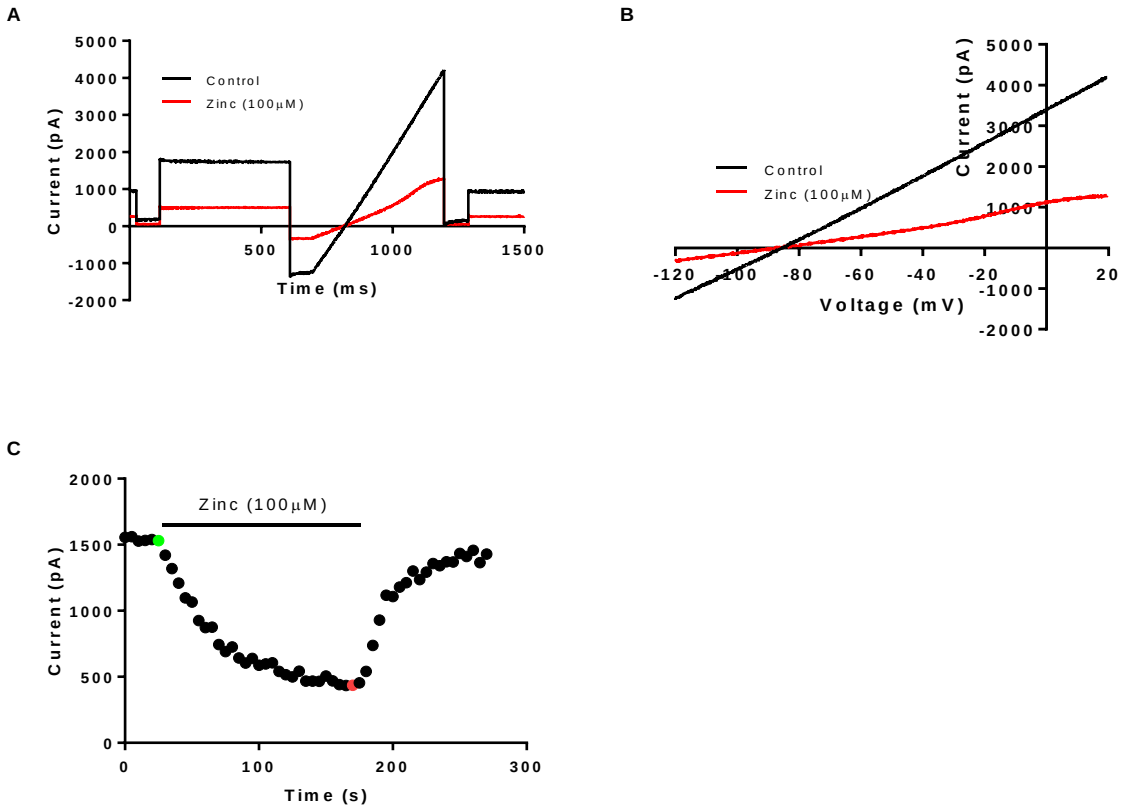

Figure 3.14 – Zinc inhibition of hTASK-3_L122D.

A) Representative trace for hTASK-3_L122D channel in both control conditions and zinc (100 µM) when exposed to the step-ramp voltage protocol. B) Current-voltage graph shows the effect of zinc (100 µM) on hTASK-3_L122D current over different voltages. Current recorded in the presence of zinc (100 µM) is shown in red. C) Time course graph showing the effect of zinc (100 µM) on hTASK-3_L122D on current (pA) over time (s), zinc perfusion represented by solid line, green starting point and red stopping point.

When zinc (100 µM) was applied to the remaining mutations (G236D, L239D and V242D) it produced current inhibition of 62 ± 4 % (n = 8), 70 ± 3 % (n = 5) and 56 ± 7 (n = 9), respectively (Figure 3.15). No mutation provided a significant change in the inhibition of zinc (100 µM) compared to hTASK-3_WT ($p > 0.05$; One-way ANOVA with post-hoc Dunnett's).

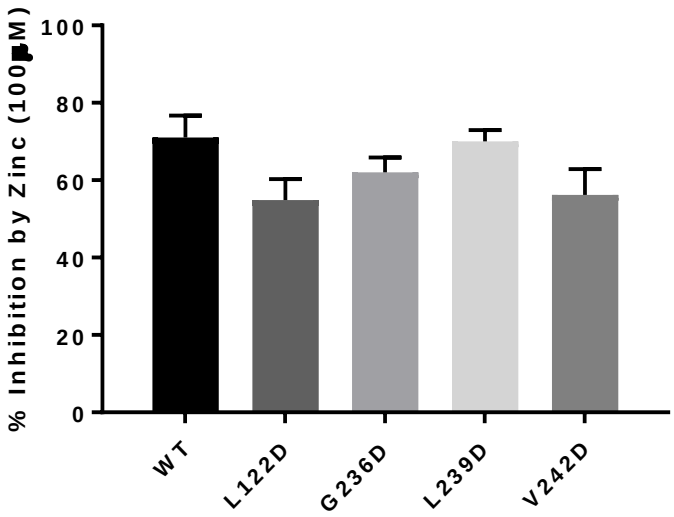

Figure 3.15 - Percentage inhibition by zinc (100 µM) on hTASK-3_WT channel and respective mutations.

Therefore as the mutations are not specific to all TASK-3 regulators, these mutations demonstrate specificity towards those compounds that act either in the pore region or intracellularly.

3.3.5 Investigation of Doxapram Enantiomer Gal-054 on hTASK-3_WT and hTASK-3_L122D mutant channel

Our results have shown that the amino acids identified by molecular docking and tested on rat TASK-3 channels, significantly reduces the effect of doxapram (10 µM) on the human mutant channel equivalents. As doxapram exists as a racemic mix of enantiomers, which have differing effects on WT channels (see Appendix 6.5 and 6.6), I felt it prudent to assess if this changes

the effect of what appears to be the active enantiomer (Gal-054) of doxapram. Gal-054 (10 µM) acutely applied to hTASK-3_WT, produced an average inhibition of 67 ± 4 % (n = 6) with an average current of 392 ± 116 pA (n = 6; Figure 3.16). The average reversal potential for hTASK-3_WT in the presence of Gal-054 (10 µM) was -78 ± 8 mV (n = 6). Inhibition of hTASK-3_WT current by GAL-054 (10 µM) was significantly more potent than inhibition by doxapram (10 µM; $p < 0.05$; unpaired t-test).

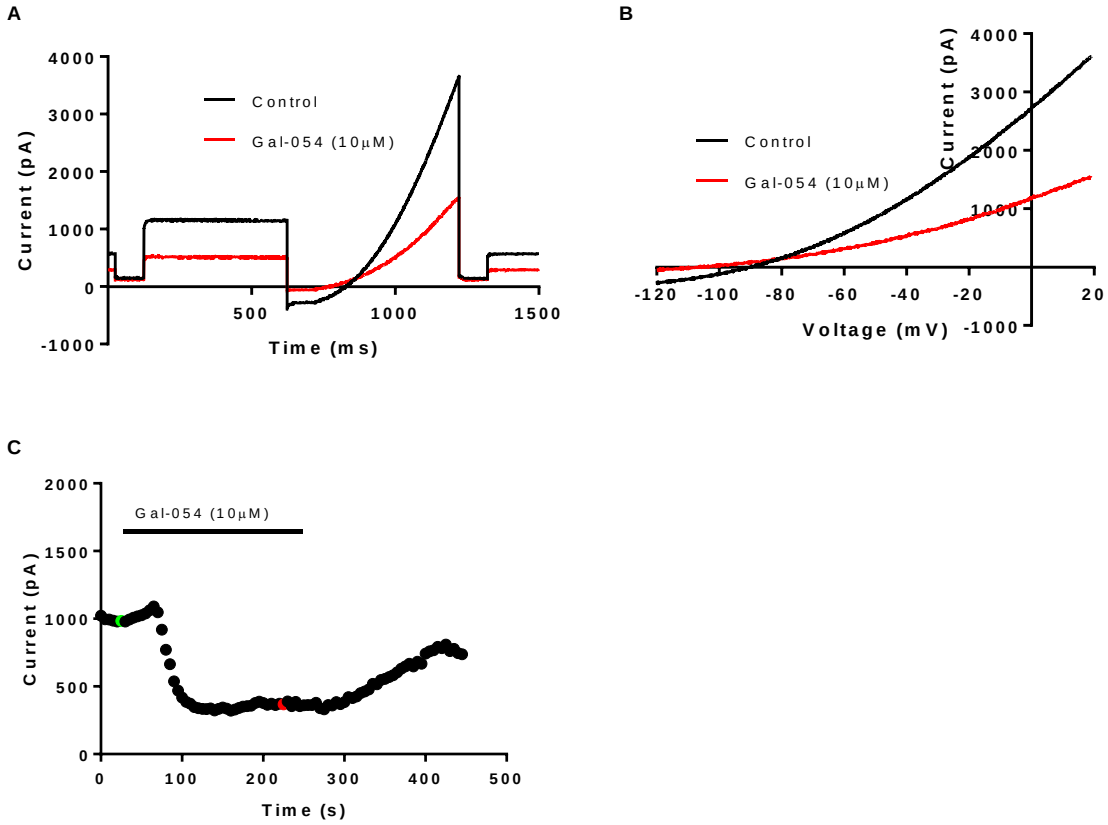

Figure 3.16 – Effect of Gal-054 on hTASK-3_WT

A) Representative trace for hTASK-3_WT channel in both control conditions and Gal-054 (10 µM) when exposed to the step-ramp voltage protocol. B) Current-voltage graph shows the effect of Gal-054 (10 µM) on hTASK-3_WT current over different voltages. Current recorded in the presence of Gal-054 (10 µM) is shown in red. C) Time course graph showing the effect of Gal-054 (10 µM) on hTASK-3_WT on current (pA) over time (s), Gal-054 perfusion represented by solid line, green starting point and red stopping point.

I went on to investigate the action of Gal-054 (10 µM) on the mutation, L122D, which attenuated the effect of doxapram the most. Acute application of Gal-054 (10 µM) on hTASK-3_L122D (Figure 3.17) resulted in a similar attenuated effect, as was observed with doxapram. Inhibition by GAL-054 was 8 ± 4 % (n = 5), with an average reversal potential of -84 ± 1 mV (n = 5).

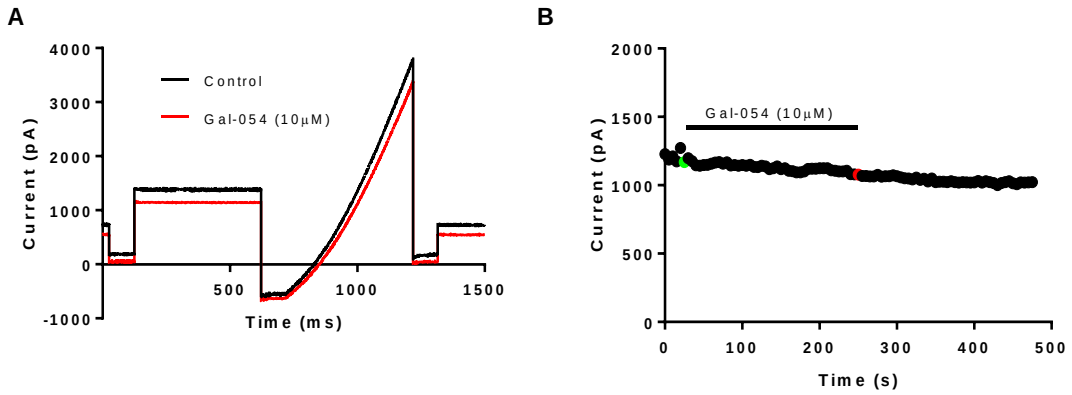

Figure 3.17 - Effect of Gal-054 on hTASK-3_L122D

A) Representative trace for hTASK-3_L122D channel in both control conditions and Gal-054 (10 µM) when exposed to the step-ramp voltage protocol. B) Time course graph showing the effect of Gal-054 (10 µM) on hTASK-3_L122D on current (pA) over time (s), Gal-054 perfusion represented by solid line, green starting point and red stopping point.

3.3.6 Investigating the role of the TASK-3 M1P1 loop on doxapram (10 µM) inhibition

The M1P1 loop has been shown to be a regulator of TASK channels as well as an essential component for the dimerization of the channels (Clarke *et al.,* 2008; Lesage *et al.,* 1996; Döring *et al.,* 2006). To investigate whether the M1P1 loop plays a role in the binding of doxapram to hTASK-3 channels we replaced the M1P1 loop of TASK-3 with that of hTASK-2_WT to form a chimeric channel, hTASK-3_{M1P1T2}. Despite its name, TASK-2 belongs to the TALK family of K2P channels and its pharmacological regulation and expression differs to that of TASK-1 and TASK-3. The effect of doxapram (10 µM) on hTASK-2_WT was conducted first (Figure 3.18). hTASK-2_WT had an average current of 969 ± 258 pA (n = 6) and an average reversal potential of

-82 ± 1 mV (n = 6; Figure 3.18A and B) in control conditions. After acutely applying doxapram (10 µM) to hTASK-2_WT the average current was reduced by 7 ± 5 % (n = 6) with an average reversal potential of -85 ± 2 (n = 6; Figure 3.18C and D).

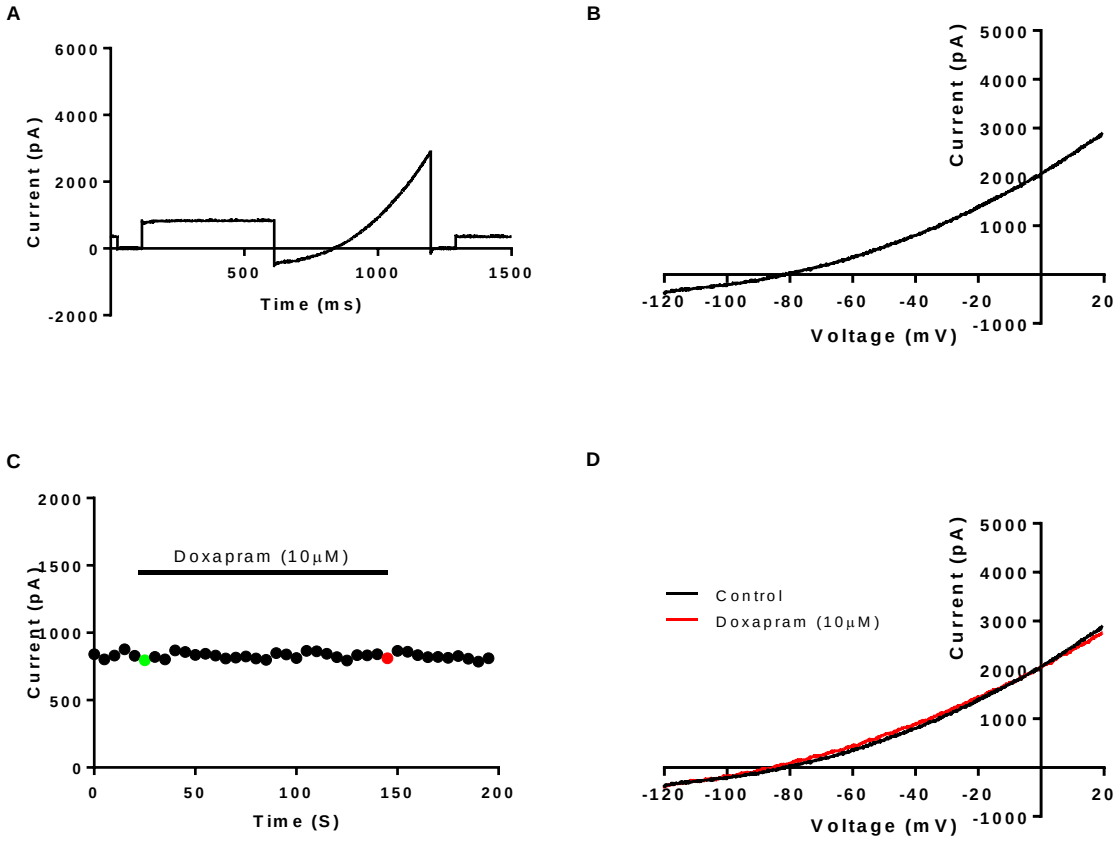

Figure 3.18 – Electrophysiological profile and effect of doxapram (10 µM) on hTASK-2_WT.

A) Representative trace for hTASK-2_WT channel in control conditions exposed to the step-ramp voltage protocol. B) Current-voltage graph for hTASK-2_WT in control conditions. C) Time course graph showing the effect of doxapram (10 µM) on hTASK-2_WT on current (pA) over time (s), doxapram perfusion represented by solid line, green starting point and red stopping point. D) Current-voltage graph shows the effect of doxapram (10 µM) on hTASK-2_WT current over different voltages. Current recorded in the presence of doxapram (10 µM) is shown in red.

As doxapram (10 µM) did not significantly inhibit the current of hTASK-2_WT I analysed the effect of doxapram upon hTASK-3$_{M1P1T2}$. The electrophysiological profile of hTASK-3$_{M1P1T2}$ showed an average current of 790 ± 223 pA (n = 8) and an average reversal potential of -88 ± 4 mV (n = 8; Figure 3.19A and B) in control conditions. The acute application of doxapram (10 µM) did not significantly alter the current of hTASK-3$_{M1P1T2}$ (Figure 3.19C and D) with an average inhibition of 8 ± 4 % (n = 8) and an average reversal potential of -87 ± 5 mV (n = 8).

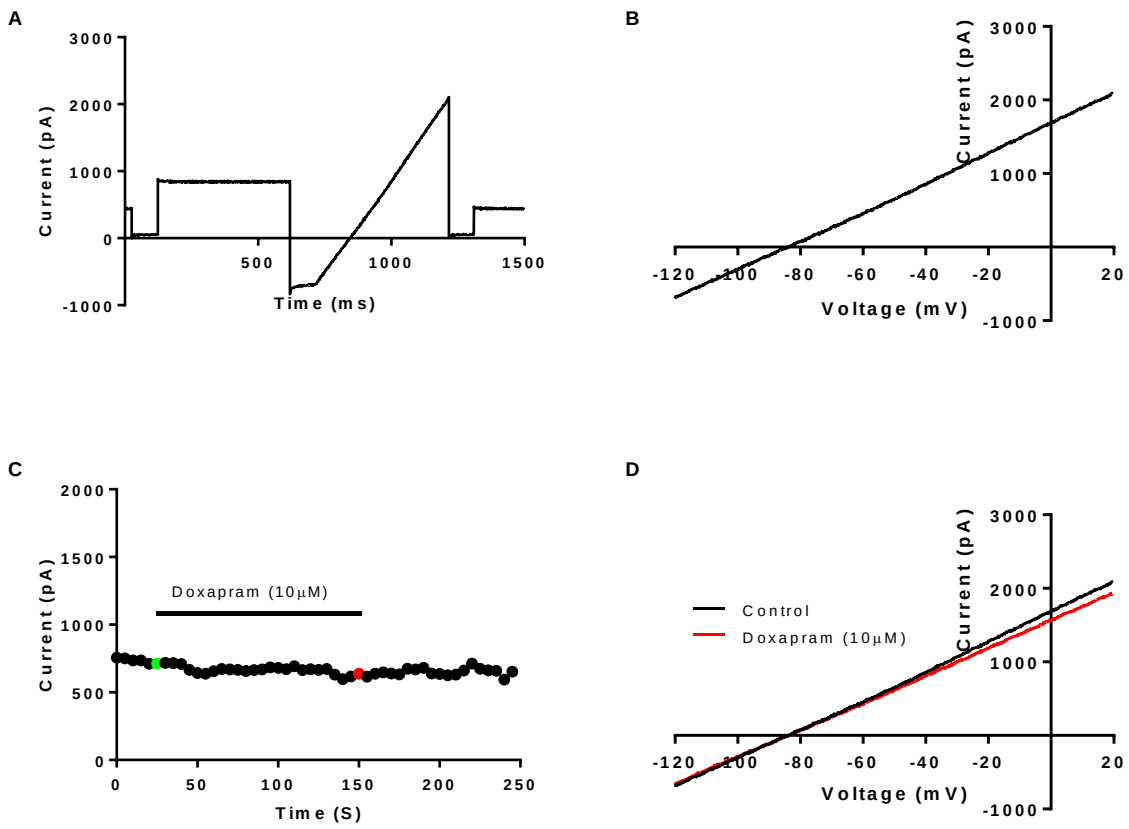

Figure 3.19 - Electrophysiological profile and effect of doxapram (10 µM) on hTASK-3$_{M1P1T2}$.

A) Representative trace for hTASK-3$_{M1P1T2}$ channel in control conditions exposed to the step-ramp voltage protocol. B) Current-voltage graph for hTASK-3$_{M1P1T2}$ in control conditions. C) Time course graph showing the effect of doxapram (10 µM) on hTASK-3$_{M1P1T2}$ on current (pA) over time (s), doxapram perfusion represented by solid line, green starting point and red stopping point. D) Current-voltage graph shows the effect of doxapram (10 µM) on hTASK-3$_{M1P1T2}$ current over different voltages. Current recorded in the presence of doxapram (10 µM) is shown in red.

Doxapram (10 µM) inhibition was significantly reduced in both hTASK-2_WT and hTASK-3_{M1P1T2} compared to hTASK-3_WT (Figure 3.20; $p < 0.05$; One-Way ANOVA with post-hoc Dunnett's test). Both hTASK-2_WT and hTASK-3_{M1P1T2} showed similar inhibition values strongly suggesting that the M1P1 loop of hTASK-3 may play a role in the effect of doxapram (10 µM).

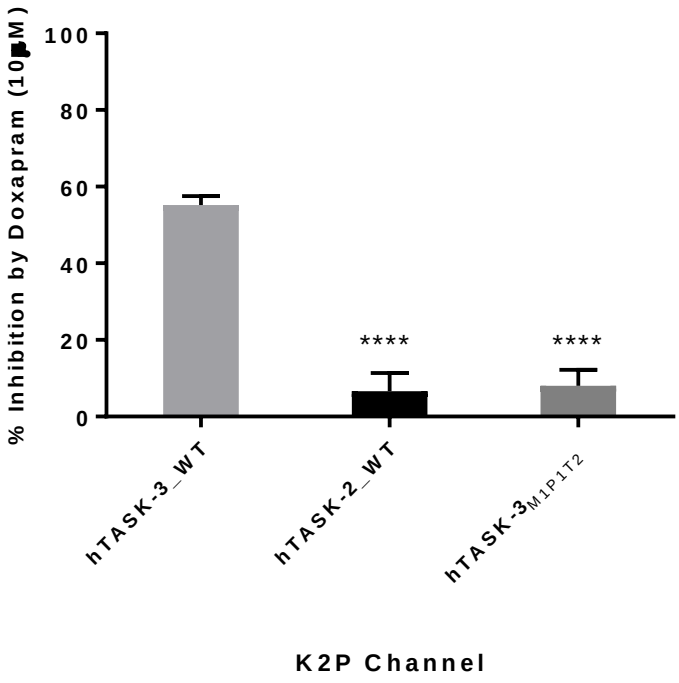

Figure 3.20 – Percentage inhibition by doxapram (10 µM) on selected K2P channels.

3.4 Discussion

In this study I have confirmed that the breathing stimulant doxapram, is a potent antagonist of the human TASK-3 channel when expressed in a heterologous expression system (55 ± 2 %, n = 8). Previous data from the lab, showed that doxapram was also a potent antagonist of human TASK-1 and TASK-3/TASK-1 heterodimeric channels, in identical experimental conditions (55 ± 4 %, n = 8 and 49 ± 4 %, n = 6; Appendix 6.5 and 6.7; Cunningham *et al.,* 2016). However, for mouse homologues it was found that doxapram was a more potent inhibitor of TASK-1 than TASK-3 (63 ± 5 %, n = 4 versus 22 ± 5 %, n = 4; Appendix 6.8; Cunningham *et al.,* 2016). The difference seen between the human and rodent channels, may explain the previous conflicting evidence from other studies (Cotton *et al.,* 2006; Cotton *et al.,* 2013). The equal potency of doxapram on human TASK channels, as has been identified here, is important when considering the compound therapeutically and the decline in its use due to the drugs side-effect profile and the availability of safer and shorter-acting agents. Inhibition or dysfunction of TASK-1 has been linked to the pathogenesis of multiple cardiovascular and pulmonary diseases such as pulmonary arterial hypertension, atrial fibrillation and dyspnoea (Golder *et al.,* 2013; Olschewski *et al.,* 2017).

3.4.1 Putative binding site for doxapram in the pore region

Previous work by Streit *et al.,* 2011 on TASK-1 showed that specific amino acids lining the intracellular pore vestibule of TASK-1 were involved in the inhibition by the breathing stimulant, A1899. Based upon molecular docking and homology modelling of TASK-3 by the group, Chokshi *et al.,* 2015 showed that specific amino acids (Leu-122, Gly-236, Leu-239) in the region highlighted by Streit *et al.,* 2011 on TASK-1, which are highly conserved in TASK-3, were also important for the effect of the same and other breathing stimulants. Their data suggested that the amino acids Leu-122, Leu-239 on both subunits of TASK-3, creates a hydrophobic narrowing of the pore, which affects the potency of three breathing stimulants (PKTHPP, A1899 and doxapram) with the effect on potency being the least for doxapram. Doxapram has been shown

in previous modelling studies to have a high molecular docking score, therefore affinity, towards a hydrophobic cleft in TM2 indicating further that within TASK channels doxapram will favour binding to the hydrophobic pore (Warner *et al.,* 2012).

By changing these amino acids to aspartate they suggested that this creates a hydrophilic (lipid-repelling) barrier in the pore which prevents the access of the breathing stimulants to hydrophobic residues deep in the pore. This is in part due to either an increase of water and potassium ion occupancy of the pore or this region acting as a fulcrum point for channel gating. Although they state that neither of these suggestions are mutually exclusive.

Previous work conducted on TASK-3_L122D has shown the mutation to play a vital role in TASK-3 gating (Luethy *et al.,* 2017). It has been proposed that binding of an anaesthetic to a specific pocket on either of the subunits of the TASK-3 channel produces a conformational change of the pore allowing the flow of ions and hence activation of the channel (Conway and Cotten, 2012). The previous work on L122D deduced that the mutation of a leucine to an aspartic acid at position 122 produces a fixed open conformation diminishing the effect of anaesthetics in producing a conformation change (Leuthy *et al.,* 2017).

Of the three breathing stimulant compounds tested by Choski *et al.,* 2015 the mutations affected the potency of doxapram the least. This they put down to doxapram being the smallest and least hydrophobic of the three compounds and because of its reduced potency on TASK-3 (Cotton *et al.,* 2006). As this work by Choski *et al.,* 2015 was performed on rat TASK-3 and as I have shown that for human channels, the effect of doxapram is different to that seen with rodent channels (i.e. more potent on human TASK-3), I wanted to determine whether these mutations affected the efficacy of doxapram to a higher extent than was observed with rat channel derivatives.

I looked at Leu-122, Gly-236, Leu-239 and Val-242 all of which were conserved between the two species. I found that all of the mutations significantly attenuated the effect of doxapram on the mutant channels when present on both subunits, with Leu-122 and Leu-239 having the biggest effect

on doxapram potency. I also looked at these mutations with a well characterised antagonist of TASK-3, zinc, which is proposed to exert its action at an extracellular site (Clarke *et al.,* 2004, Gonzalez *et al.*, 2013). None of these mutations were found to significantly alter the potency of zinc on TASK-3.

I have shown that L122D diminishes the effect of doxapram inhibition, but not that of zinc and agrees with the consensus that doxapram acts within the intracellular pore of TASK channels (Figure 3.21; Cotten *et al.,* 2015).

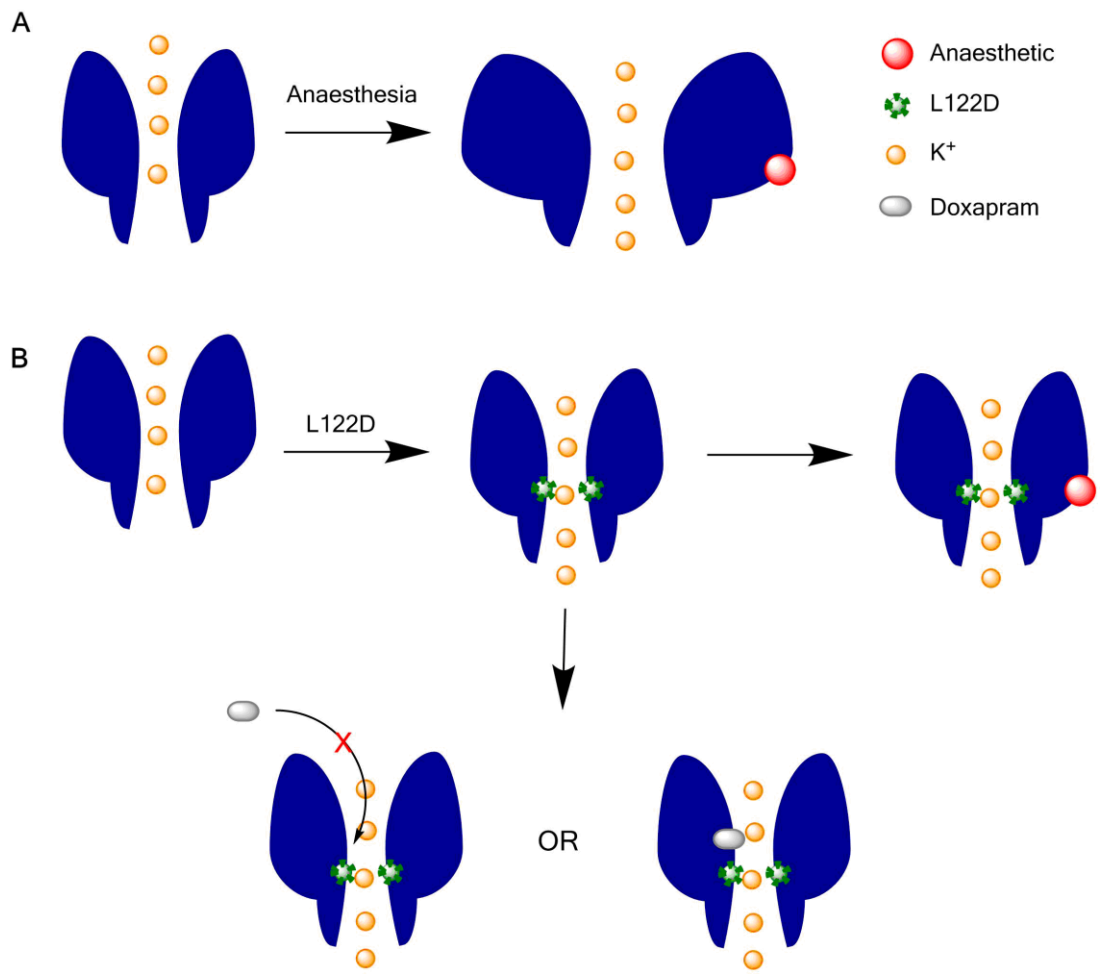

Figure 3.21 – Illustration of L122D mutation effect on TASK-3 channel gating.

A) TASK-3 activation by the binding of an anaesthetic to the binding pocket. B) Mutation of L122D causes conformational change within the intracellular pore leading to fixed open conformation of TASK-3. Use of anaesthetic on TASK-3_L122D fails enhance the current further. Proposed action of doxapram on TASK-3_L122D either the mutation prevents doxapram from binding to the intracellular pore or doxapram is able to bind but not sufficiently block K^+ ion flow.

3.4.2 Isolation of doxapram enantiomers

As previously mentioned doxapram is a racemic mixture of positive (GAL-054) and negative (GAL-053) enantiomers. It has been shown that the eutomer, GAL-054, has an improved therapeutic index compared to GAL-053 or doxapram, with GAL-053 showing little to no improvement in regards to respiratory stimulation, but retaining adverse effects such as dysrhythmias, seizures and death (Golder *et al.,* 2012). Therefore the use of GAL-054 holds potential to be a better therapy than the racemic mixture, doxapram, as a lower dose may be used with a reduction in adverse effects.

In my data I show that GAL-054 (10 µM) is a more potent antagonist on TASK-3_WT than doxapram is. Unpublished work undertaken in the lab has revealed that there is a significant difference in the effect of the two enantiomers, GAL-053 and GAL-054, on both wild-type TASK-1 and TASK-3 (Appendix 6.5 and 6.6). GAL-054 is significantly more potent than GAL-053 with the IC_{50} of GAL-053 being over 100-fold higher than the IC_{50} of GAL-054 for both TASK-1 and TASK-3. On human channels the potency of GAL-054 was the same for both TASK-1 and TASK-3 (75 ± 2 %, n = 6; 79 ± 2 %, n = 8; at 10 µM, respectively). These findings in combination with previous studies that show that adverse side effects are retained with GAL-053, but not GAL-054. This may suggest that clinical side-effects associated with the use of doxapram, which was attributed to the effects of the compound inhibiting TASK-1, may not actually be the case. Further studies will be needed with GAL-054 to fully assess its therapeutic profile as currently only a small number of rodent studies have been conducted. However, the use of the positive enantiomer in humans could be beneficial therapeutically.

3.4.3 The Role of Heterodimers

Both TASK-1 and TASK-3 have been shown to be highly expressed in the carotid bodies and the majority of these subunits are thought to form functional heterodimers of TASK-1 and TASK-3 (Kim *et al.,* 2009; Turner and Buckler, 2013). Previous studies and my own work has focused on homodimers of either TASK-1 or TASK-3. Unpublished work from the lab, using forced

concatamers of human TASK-1 and TASK-3, has shown that doxapram and GAL-054 are equally as potent on heterodimers, as homodimers. This is an important consideration when assessing the importance of particular amino acids, as this may alter the result when considering the combination of two α-subunits from different channel subtypes. Indeed forced homodimers of TASK-3, with only one subunit containing one of the outlined mutations, resulted in an intermediate effect between that observed for WT and a channel with both subunits mutated (see Choskhi *et al.,* 2015, Figure 5). Alignment of TASK-1 and TASK-3 channels, shows that sequences are nearly identical in the inner pore helix (Chokshi *et al.,* 2015, Figure 6), and as such a mutated heterodimer of these subunits would be expected to behave similarly to mutated homodimers in terms of hydrophobicity. Interestingly though, despite TASK-1 and TASK-3 have near identical homology for at least 60% of the protein, in rats, compounds such as doxapram are much more potent on TASK-1 channels, than TASK-3. Increased potency can be conferred to TASK-3 when the C-terminal is exchanged with that of TASK-1 (Cotten *et al.,* 2006). The C-terminus has little homology between the two channels and there is differing regulation between the two channel subtypes. Phosphorylation sites in the C termini of the two channels, for example, are different and thus the phosphorylation state of the channel may be an important consideration when considering pharmacological sensitivity and may again help explain differences seen between species.

3.4.4 M1P1 loop involvement in doxapram inhibition of TASK channels

K2P channels have an unusual feature in that they have a large pre-pore linker known as the M1P1 loop. The M1P1 loop has been identified to play a role in channel regulation and the formation of dimers (Clarke *et al.,* 2008; Döring *et al.,* 2006; Lesage *et al.,* 1996). The TASK-3 M1P1 loop linkers forms an extracellular cap, which plays a role in the regulation of ion entry to the pore. Whilst the cap obstructs the extracellular pathway to the selectivity filter it provides an extracellular ion pathway which are bilateral ‘tunnels’ leading to the selectivity filter (Figure 3.22; González *et al.,* 2013). These bilateral tunnels

have been shown to play a major role in TASK-3 gating, with the concentration of K ions within these tunnels being a key factor in pH sensitivity. As it only requires the protonation of one H-98 sensor to close the gating of the pore, it has been proposed that neutralisation of one H-98 sensor leads to an increased K^+ occupancy in the outermost region of the selectivity filter which in turn increases the probability of the second H-98 sensor becoming deprotonated and increasing the opening of the channel (González *et al.,* 2013).

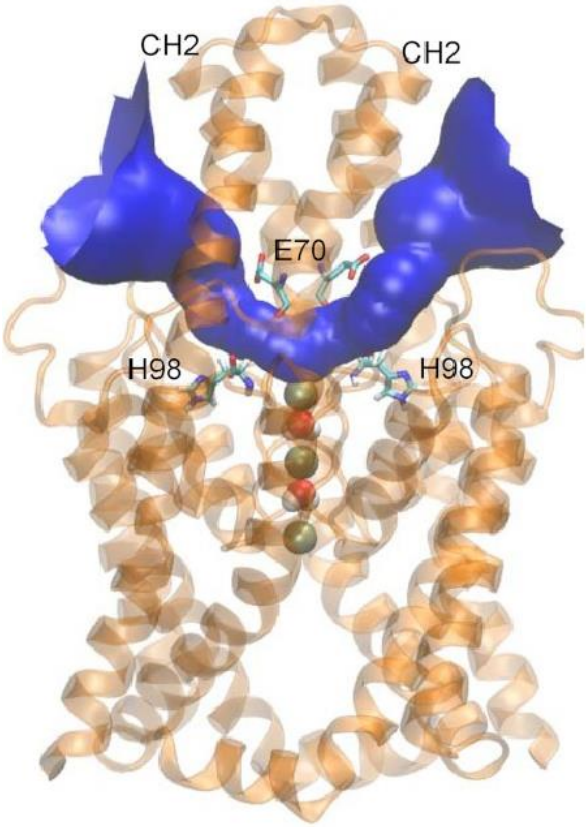

Figure 3.22 – Model of extracellular ion pathway in TASK-3

TASK-3 model showing extracellular pathway (blue tunnel) leading to selectivity filter. Sensing residues His-98 and Glu-70 also indicated (Reproduced from González et al., 2013).

I showed that the substitution of the TASK-3 channel M1P1 loop with that of TASK-2 resulted in the loss of effect of doxapram. TASK-2 is a member of the TALK subfamily, with the only similar characteristic towards the TASK subfamily is that it is acid-sensitive (hence why originally named in the TASK family) however the data shown here suggests the M1P1 loop plays a critical role in TASK channel inhibition by doxapram. The M1P1 loops of TASK-3 and TASK-2 differ considerably and this may alter the structure of the channel. It was a surprising result alone that channel activity occurred with the substitution in M1P1 loop due to the differences in M1P1. I postulate that changing the M1P1 loop affects the ability for doxapram to reach its intracellular binding site by forming a cap not conducive to doxapram entry.

3.4.5 Conclusion and further study

Here I have shown that doxapram and GAL-054 do not selectively favour TASK-1 or TASK-3 in humans suggesting TASK-1 may not be responsible for the adverse effects seen with doxapram thereapy. I also show GAL-054 to be a more potent inhibitor of TASK-3 than doxapram. In previous studies upon rodents it has been indicated that GAL-054 does not retain the adverse effects seen within doxapram therapy of humans (Golder *et al.,* 2012). Few studies have been conducted using GAL-054, none of which are in humans, so it is not possible to say if it is free from adverse side effects in people (Golder *et al,.* 2013). It may be that in targeting and inhibiting carotid body residing TASK channels, to treat ventilatory depression, this pathway generates the adverse effects seen and alternative therapy may be best to avoid these effects. Building upon this it would be important for further work looking into the enantiomers, particularly GAL-054. Further characterising its effects both with electrophysiological studies and within animal models. It should be noted that given the data shown here of a mouse species difference, it appears mice models would not be a suitable model of choice. This is seen with TASK-1 and pulmonary arterial hypertension, where the mouse model differs from rat and rabbit models (Manoury *et al.,* 2013).

The work in this study shows more evidence contributing to a binding site for doxapram on TASK-3 and TASK-1. Mutation of one of the sites, L122D, also further contributes to current studies suggesting it stabilises and fixes the pore in an open conformation attenuating the effects of anaesthetics and doxapram. Zinc inhibition was not affected by changes to this site, agreeing with current data for its inhibitory role being attributed to the selectivity filter. This study shows that the M1P1 loop is also vital to doxapram inhibition and further studies are required to pinpoint the exact mechanism of the loops role in doxapram's effect. To clarify doxapram's binding site, ideally, a crystallographic analysis of TASK-3 with doxapram bound, similarly to that with TREK-2 and Prozac, would clarify many of the issues including channel gating, doxapram binding and TASK involvement within the carotid bodies (Dong *et al.,* 2015). Hypothetically for the therapy to be most effective, it would be of importance to selectively target the heterodimer as those are the channels most abundant within the carotid bodies and if possible avoid inhibition of wild-type TASK-1 and TASK-3 (Kim *et al.,* 2009). It could be useful to assess the intermediate properties of the TASK-1/TASK-3 heterodimer such as hydrophobicity of the channel and try to develop a compound to favour these opposed to that of the homodimers, for this computer modelling may be the best initial approach using docking software and compound databases.

4. Action of Pulmonary Arterial Hypertension Therapeutic Agents on K2P channels

4.1 Introduction

Pulmonary hypertension encompasses a group of pulmonary vasculature diseases all with the common symptom of restricted blood flow. The World Health Organisation (WHO) divides pulmonary hypertension into five groups based on their pathological findings and similar characteristics. The five groups consist of pulmonary arterial hypertension (Group 1), pulmonary hypertension by left heart disease (Group 2), pulmonary hypertension due to chronic lung disease (Group 3), chronic thromboembolic pulmonary hypertension (Group 4) and pulmonary hypertension due to unclear mechanisms (Group 5; Simonneau *et al.,* 2013).

Pulmonary arterial hypertension (PAH, Group 1 pulmonary hypertension) has been defined as a progressive increase of pulmonary vascular resistance which leads to right ventricular failure and consequently premature death (Simonneau *et al.,* 2013). Over 20 years ago, idiopathic pulmonary arterial hypertension patients had an average life expectancy of 2.8 years yet even with greater focus on PAH research, the 5 year survival rate is at 34% (D'Alonzo *et al.,* 1991; Tang *et al.,* 2016). PAH can be defined by a mean pulmonary artery pressure greater than 25 mm Hg at rest measured by right heart catheterisation (Galie *et al.,* 2015a). Between 15 and 50 patients, per million, are affected by PAH with an average patient age of 50 years (Gailè *et al.,* 2010; Humbert *et al.,* 2014). A key factor associated with the poor survival rates of PAH patients is that it is often masked by co-morbidities and diagnosed at a late stage where the disease is more aggressive. In order to successfully diagnose PAH, guidelines state a lengthy algorithm process. Once pulmonary hypertension (PH) is suspected, the first test a patient will receive is a transthoracic echocardiogram (TTE; Barbera *et al.,* 2018). TTE are non-invasive and allow an assessment of the condition of the heart. If the assessment determines PH probability is intermediate or high, then left heart disease or respiratory disease will be considered. Further tests and considerations include risk factors, electrocardiogram (ECG), chest X-rays and high-resolution computed tomography. If left heart failure and respiratory disease are ruled out, the assessment of the circulation within the pulmonary

vasculature is conducted using V/Q scintigraphy, which involves using a radio-isotope aerosol. A PH specialist will then perform further tests to decide whether chronic thromboembolic PH is possible or PAH is more probable. These final examinations involve invasive techniques, such as right heart catheterisation (RHC), hence why they are used after other non-invasive tests have been utilised. During these final invasive tests, further vasoreactivity testing can be conducted to assess the response of the pulmonary vasculature to certain therapies such as calcium channel blockers.

After diagnosing PAH, determining the subgroup is necessary to outline a treatment plan. PAH can be divided into further subgroups based around its pathogenesis, these include idiopathic (iPAH), familial or heritable (hPAH), or associated with other conditions such as: drug/toxin-induced, HIV infection, schistosomiasis, congenital heart disease, connective tissue diseases and portal hypertension (Galiè *et al.,* 2015a; Ghofrani *et al.,* 2017). After diagnosis, it is important to determine the stage of the disease and how far it has progressed in order to tailor therapy. WHO categorise PH patients in to one of four classes based on the progression of their PH (Figure 4.1).

WHO CLASS	**Criteria**
I	Patients with PH, physical activity is not limited and does not cause dyspnoea, fatigue, chest pain or near fainting.
II	Patients with PH, physical activity slightly limited, comfortable when resting but does cause dyspnoea, fatigue, chest pain or near fainting
III	Patients with PH, physical activity is majorly limited, comfortable when resting, low level activity causes dyspnoea, fatigue, chest pain or near fainting
IV	Patients with PH, unable to perform any physical activity, symptoms of right-heart failure, possible dyspnoea or fatigue at rest.

Figure 4.1 – WHO Classification of Pulmonary Hypertension

WHO classification for PH patients based on their physical activity capabilities. Classification helps determine treatment plans in patients. (Adapted from Popa, 2002)

PAH is developed due to a reduction of the pulmonary arterial lumen through multiple factors such as inflammation, vasoconstriction, proliferation, remodelling and thrombosis, which leads to an increase in pulmonary arterial pressure (Galiè *et al.,* 2010). This continuous high pressure within the pulmonary artery leads to right ventricular overload which in turn develops hypertrophy and then right ventricular failure resulting in death if untreated.

4.1.1 Pulmonary Arterial Structure

Pulmonary arteries are responsible for carrying blood from the right hand side of the heart in to the lungs so it can be oxygenated. Pulmonary arteries are a three-layered structure, with each layer containing its own distinct individual characteristics (Figure 4.2). The three layers are named intima, media and adventitia. Each of these play a role in maintaining vascular homeostasis and respond to changes within the vessel (Stenmark *et al.,* 2011).

The intima layer comprises of a single layer of endothelial cells that line the lumen of the artery and extend into an internal elastic lamina. The intima can constitute up to 16% of total wall thickness (Townsley, 2013; Chazova *et al.,* 1995).

It is the composition of the media layer that defines the classification of the pulmonary artery. Two factors affect this classification, elastic lamina presence and muscularity. Pulmonary arteries can therefore be classified into five categories: muscular, partially muscular, non-muscular, elastic and transitional (containing both elastic and muscular arteries). The medial layer consists primarily of smooth muscle cells with the addition of collagen and elastin in varying quantities. Elastic arteries are categorised due to the high presence of elastin and low levels of smooth muscle fibres within the medial layer. In the main pulmonary artery, within human lungs, elastin constitutes for approximately a quarter of the wall area (Townsley, 2013). Muscular arteries contain high levels of smooth muscle cells in the medial layer, in a clearly distinct circular layer, with a single layer sheet of elastin found between the media and intima.

The final layer of the pulmonary artery wall is the adventitia, which has had the least research focus in regards to pulmonary hypertension, as its principle constituents are neither endothelial cells nor smooth muscle cells. However, an increase in focus within recent years has indicated it may play a critical role within vessel wall function (Stenmark *et al.,* 2011). The adventitia's principle cell type are fibroblasts, but also contain dendritic cells and progenitor cells, as well as being heavily influenced by the extra cellular matrix (ECM). Emerging concepts suggest that fibroblasts are the "sentinel cell" and the regulation of the pulmonary vascular occurs from the "outside in" as it has been shown within hypoxic models that pulmonary arterial fibroblasts are the first cell to increase in proliferation (Belknap *et al.,* 1997).

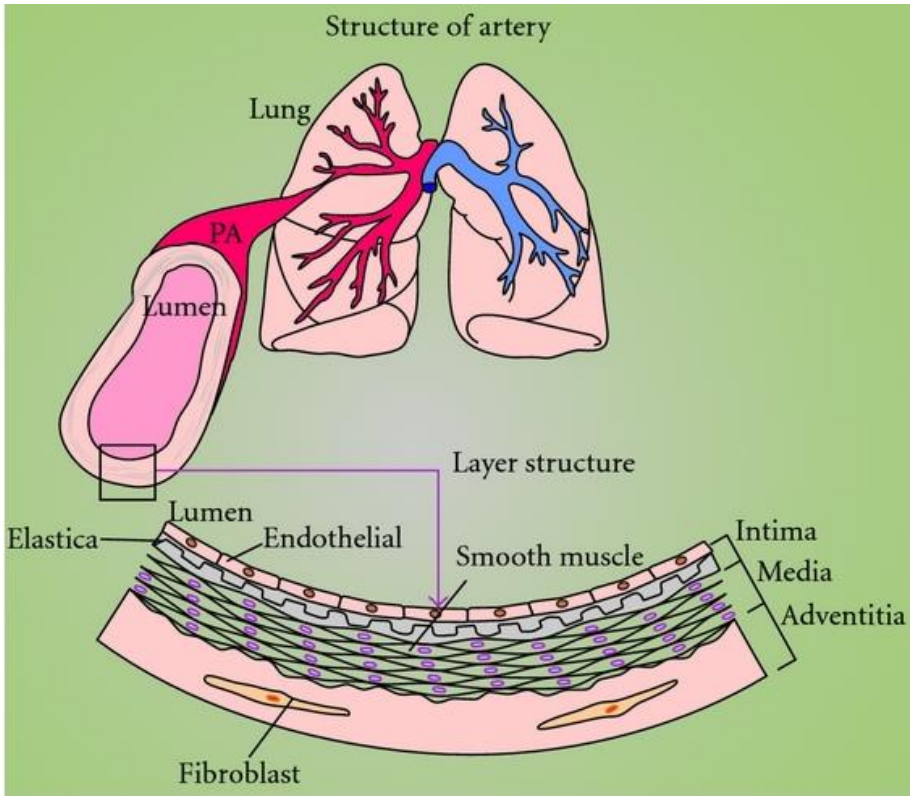

Figure 4.2 – Structure and composition of pulmonary artery

The structure and composition of layers of the pulmonary artery, highlights the three layers that form the pulmonary artery – Intima, Media and Adventitia. Key cells such as fibroblasts, smooth muscle cells and endothelial are also indicated along with their location within the artery. (Reproduced from Fernandez et al., 2012).

The initiation pathway of PAH is unknown, however it is widely surmised that PAH is commenced by initial damage to the endothelium with many studies suggesting a range of stimuli are responsible such as genetic predispositions, hypoxia and sheer stress upon the endothelium (Madonna *et al.,* 2015; Clapp and Gurung, 2015). A conception differing slightly from this, is that it is not the predisposition that initiates vascular injury and PAH, but a specific injury to the pulmonary arterial wall initiates PAH and the predisposition leaves the patient unable to counteract the cascade of events leading to PAH (Gailè *et al.,* 2010). The cascade of events that lead to an increase in vascular tone and cell proliferation is vast and these occur within a range of cell types including smooth muscle cells, endothelial cells and fibroblasts. In pulmonary arteries there are currently three known pathways that have been shown to contribute to vascular tone and proliferation, these are the endothelin (ET), nitric oxide (NO) and prostacyclin (prostaglandin I2; PGI_2) pathways (Hemnes and Humbert, 2017).

4.1.2 Pulmonary Arterial Regulatory Pathways

There are three key pathways that regulate pulmonary arterial tone, these pathways have been identified as most PAH patients show an imbalance of endogenous vasodilators and vasoconstrictors (summarised in Figure 4.3).

4.1.2.1 Endothelin Pathway

ET has three different isoforms (ET-1, 2 and 3) which are expressed within a variety of tissues and have different binding affinities to ET receptors, coupled with G-proteins (Galiè *et al.,* 2004). ET-1, is the most potent vasoconstrictor within the pulmonary circulation. The ET pathway within the pulmonary circulation consists of ET-1 and the G-protein coupled ET receptors, ET_A, ET_{B1} and ET_{B2} (Kedzierski and Yanagisawa, 2001). The ET_A receptors are located within the smooth muscle cells, whilst ET_{B1} and ET_{B2} can be found within the endothelium, as well as smooth muscle cells. The primary effect of ET-1 occurs within smooth muscle cells generating vasoconstriction and

proliferation (Sibton and Morell, 2012). Cross-talk between ET_A and ET_B has been shown to occur in ET-1 induced vasoconstriction (Sauvageau *et al.,* 2007). Conversely, within the endothelium, ET has been indicated to cause vasodilation through ET_B receptors by stimulating NO and PGI_2. However, under normal physiological conditions, ET_B receptors within the endothelium, do not significantly contribute to overall pulmonary arterial vascular tone (Chester and Yacoub, 2014; Dupuis and Hoeper, 2008; Dupuis *et al.,* 2000). A secondary action of ET-1 is on fibroblasts, where it has be shown to promote fibrosis, proliferation and contraction, which may give weight to the 'outside-in' theory (Stenmark *et al.,* 2012). The outside-in hypothesis is formed on the idea of initial damage or inflammation within the adventitia that over time progresses in towards the intima (Stenmark *et al.,* 2012).

Whilst ET receptors are widely distributed, the activity of the ET system has been shown to be that of a local autrocrine/paracrine signalling pathway. ET-1 is formed (by the conversion of big ET-1 [39 amino acid peptide] into ET-1 [21 amino acid peptide] by ET converting enzyme [ECE]) *in situ.* Circulating levels of ET-1 are below that required to induce vasoconstriction (Iglarz and Clozel, 2010; Sibton and Morrell, 2012). ET receptors ET_A and ET_B are coupled with $G_{\alpha q}$ receptors. The binding of ET-1 to these receptors leads to the activation of phospholipase C (PLC)-β, which in turn increases the production of intracellular messengers inositol 1,4,5-triphosphate (IP_3) and diacylglycerol (DAG) from phosphatidylinositol 4,5-biphosphate (PIP_2; Hisatsune *et al.,* 2005; Figure 4.3). The increase in IP_3 leads to the activation of ligand gated Ca^{2+} channels on the sarcoplasmic reticulum, which in turn increases intracellular Ca^{2+} levels promoting vasoconstriction. DAG however activates protein kinase C (PKC) which leads to a cascade of signalling protein activation, which ends in contraction either through inhibiting myosin light chain (MLC) phosphatases or enhancing actin polymerisation (Ward *et al.,* 2004).

4.1.2.2 Nitric Oxide Pathway

Within the pulmonary circulation NO is the principle vasodilator and is produced by nitric oxide synthases (NOS) within the endothelium. NO is

produced as a result of L-arginine being converted to L-citrulline and it acts upon smooth muscle cells. NO promotes vasodilation through the stimulation of soluble guanylate cyclase (sGC) which increases intracellular levels of cyclic guanine monophosphate (cGMP). The increase of intracellular cGMP activates protein kinase G (PKG) which in turn decreases Ca^{2+} release through an increase in sarcoplasmic Ca^{2+}-ATPase and MLC phosphatase promoting relaxation within the smooth muscle cell (Etter *et al.,* 2001; Jasińska-Stroschein and Orszulak-Michalak, 2014). In addition to this, PKG also phosphorylates RGS4, which inhibits $G_{\alpha q}$ proteins, thus reducing intracellular levels of IP_3 and DAG and promoting relaxation and vasodilation (Murthy, 2006; Figure 4.3).

4.1.2.3 Prostacyclin Pathway

The third pathway (Figure 4.3) within PAH pathogenesis is the PGI_2 pathway. PGI_2 is produced within the endothelium and the smooth muscle cells, through the oxidation of arachidonic acid by cyclooxygenase enzymes (Clapp and Gurung, 2015). The PGI_2 receptor, IP, is coupled to adenylyl cyclase (AC) via a G_s protein. Binding of this receptor increases the levels of intracellular cyclic adenosine monophosphate (cAMP). Increased levels of cAMP induces the activation of protein kinase A (PKA) and similarly to PKG, PKA inhibits sarcoplasmic Ca^{2+} release by phosphorylating RGS4, which in turn inhibits $G_{\alpha q}$.

PGI_2 does not only bind to IP receptors, but multiple prostanoid receptors, each with a different affinity. Different prostanoid receptors exert different actions. IP, EP_2 and DP_1 receptors have been shown to be vasodilatory receptors by increasing intracellular cAMP levels, through G_s protein coupling. EP_1 and EP_3 are vasoconstricting receptors coupled to $G_{\alpha q}$ and G_i proteins respectively however PGI_2 binds most potently to IP receptors, more than 5 fold more potently than it does to any other prostanoid receptor (Woodward *et al.,* 2011; Clapp and Gurung, 2015). With the discovery of PGI_2 and the prostanoid receptors, recent therapeutic strategies have been to selectively target the prostanoid receptors.

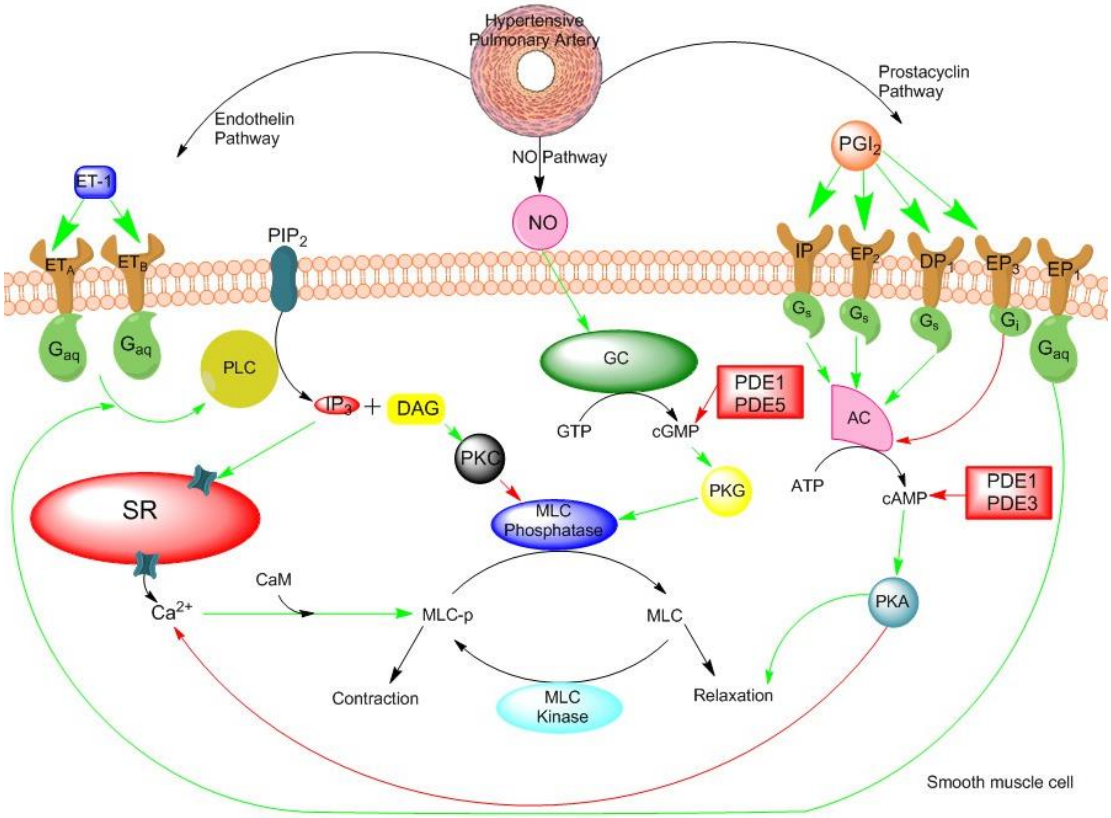

Figure 4.3 – Three Key Pathways in Pulmonary Arterial Hypertension Pathogenesis

The three key pathways established within PAH pathogenesis, endothelin, nitric oxide and prostacyclin. Figure indicates how the three pathways interact to regulate the arterial tone through contraction and relaxation. Endothelin pathway promotes vasoconstriction through increased levels of IP_3 and DAG. NO pathway stimulates vasodilation through increased levels of cGMP and MLC phosphatase activity. PGI_2 pathway can have altering effects depending on the receptors activated, IP, EP_2 and DP_1 promote vasodilation through increase cAMP levels whereas EP_3 reduces cAMP levels whilst EP_1 follows a similar path to ET by increasing IP_3 and DAG levels. Green lines represent stimulation, red lines represent inhibition. ET-1 represents endothelin-1; NO, nitric oxide; PGI_2, prostaglandin I2; PLC, Phospholipase C; SR, sarcoplasmic reticulum; CaM, calmodulin; MLC, myosin light chain; MLC-p, phosphorylated myosin light chain; PDE, phosphodiesterase; PKA, protein kinase A; PKC, protein kinase C; PKG, protein kinase G; AC, adenylyl cyclase and GC, guanylyl cyclase.

4.1.3 Pulmonary Arterial Hypertension Therapeutics

The foundation of PAH therapeutics is based upon the three key pathways. Different drugs have been developed or utilised for the treatment of PAH in order to promote vasodilation within the pulmonary arteries. Due to the complexity of PAH and the difficulty in measuring drug efficacy, there is no gold-standard treatment plan. Therapeutic response is measured by exercise capacity (usually a 6 minute walk test) and echocardiograms (Moonen *et al.,* 2017). Early strategies were to initiate treatment as a monotherapy and following an inadequate response combine with another drug or substitute for an alternative treatment. Less than two decades ago treatment was very primitive. Support therapy until patient deteriorates significantly and then provide IV epoprostenol, a synthetic salt analogue of PGI_2 (Hemnes, 2014). Differences in PAH subgroups and patient phenotypes creates differences in the response to therapies. For some patients monotherapies are adequate to see a response, whereas combinational approaches are needed in others (Humbert and Ghofrani, 2015). Since 1999, multiple drugs have been approved by the United States Food and Drug Administration (FDA) and trials at earlier interventions/combinations of drugs have been assessed, such as the ET receptor antagonist, bosentan (Galiè *et al.,* 2008). Conventional therapies used within PAH therapy are to encourage physical activity (but not to exertion), provide oxygen therapy (maintenance of PaO_2 over 60 mm Hg), diuretics to aid right ventricular preload and left ventricular filling. Some PAH patients also receive anticoagulation therapy with vitamin K antagonists and calcium channel blockers, such as nifedipine (Humbert *et al.,* 2014; Barbera *et al.,* 2018).

In recent years, tailored therapy has been designed, based on the three pathways of pathogenesis of PAH. The vast majority of approved and experimental compounds act as either ET receptor antagonists, stimulators of secondary messengers (cAMP and cGMP) or prostanoid receptor agonists/antagonists (receptor dependent, Figure 4.4).

4.1.3.1 Endothelin Receptor Antagonists

ET-1 receptor antagonists (ERAs) are used to bind and occupy ET-1 receptors (ET_A and ET_B) to prevent ET-1 exerting its vasoconstrictive effects. ERAs can be both selective (favouring either ET_A or ET_B) or dual acting. In theory, selective ERAs should be more therapeutically beneficial, as ET_B receptors have been shown to promote vasodilation. Some approved ERA drugs include the dual acting bosentan (marketed as Tracleer by Actelion Pharmaceuticals Ltd, Switzerland) and macitentan (marketed as Opsumit by Actelion Pharmaceuticals Ltd, Switzerland) and the selective ET_A receptor antagonist, ambrisentan (marketed in the EU as Volibris by GlaxoSmithKline, UK). Bosentan has been indicated for early use in PAH therapy, although it must be dosed appropriately, starting at a low dose and increased gradually, due to adverse effects of liver damage (Humbert *et al.,* 2007). In Europe, orally administered bosentan is used in the therapy of patients with WHO class II and III. Macitentan is also administered orally, but does not have the liver toxicity associated with bosentan. It does however appear to reduce haemoglobin levels (Pulido *et al.,* 2013). Like bosentan, macitentan is used for the long-term treatment of WHO class II and III PAH patients. Ambrisentan has been approved for use within WHO class II and III PAH patients and in theory, the selective ability of ambrisentan should provide a greater therapeutic effects than bosentan however, in trials bosentan appears more effective.

4.1.3.2 Secondary Messenger Modulators

As previously described, enhancing intracellular levels of the secondary messengers cAMP and cGMP can provide a vasodilatory effect within the pulmonary artery. To achieve this effect the pathway can be altered in a variety of ways including phosphodiesterase (PDE) inhibitors or (adenylyl or guanylate) cyclase stimulators. PDE’s degrade cAMP and cGMP by hydrolysing the phosphodiester bond forming AMP or GMP respectively. One therapeutic intervention has been to inhibit the action of PDE’s preventing the breakdown of secondary messengers and promoting vasodilation. PDE’s can

be selective or non-selective to the secondary messenger they degrade, PDE1, 2, 3, 10 and 11 act on both cAMP and cGMP whereas PDE4, 7 and 8 act only on cAMP, and PDE5, 6 and 9 act only on cGMP. One approved PDE inhibitor for PAH therapy is sildenafil citrate. Originally marketed under the name Viagra (Pfizer), it is used for patients within WHO class II and III. Sildenafil citrate is a selective PDE5 inhibitor, which enhances cGMP levels. It was originally designed to treat angina and hypertension yet after early clinical trials it was noted sildenafil had the ability to enhance erectile response in patients, that had previously experienced dysfunction (Boolell *et al.,* 1996). Between 2003 and 2017, Pfizer made almost $26.5 bn in revenue from Viagra sales alone (Statista, 2018). Long-term sildenafil citrate treatment (3 years) has been shown clinically to increase 6 minute walking distance in almost 50% of patients as well as stabilise or improve the WHO classification of the patients over that time period (Rubin *et al.,* 2011).

After the success of Viagra, many pharmaceutical companies developed PDE5 inhibitors to treat erectile dysfunction. One of those, tadalafil branded as Cialis (Eli Lilly and Co) is also approved for PAH therapy. Like sildenafil citrate, tadalafil is used to treat WHO class II and III PAH patients. Tadalafil and sildenafil citrate are both taken as oral tablets. Tadalafil has a longer half-life so is only required once daily, compared to three times with sildenafil.

Another approved PAH drug is riociguat. Marketed under the trade name Adempas (Bayer) it acts as a soluble guanylate cyclase (sGC) stimulator promoting intracellular levels of cGMP, independently of NO. Riociguat is used in PAH patients of WHO class II and III with an up dosing approach taken, until optimal dose is reached to prevent symptoms of hypertension. Combining riociguat therapy with sildenafil seems like an appropriate route of action in PAH therapy, as they both target separate areas of the pathway. However, a trial has shown unfavourable safety profiles of the combination, with no positive benefit to off-set the risk (Galiè *et al.,* 2015b).

4.1.3.3 Prostanoid Receptor Modulators

As previously mentioned different prostanoid receptors exert different signalling pathways within the cell. Prostanoid therapy for PAH must therefore selectively target and activate a prostanoid receptor that promotes vasodilation (IP, EP_2 and DP_1). An alternative option is to use an antagonist that selectively targets prostanoid receptors, which activates a vasoconstricting pathway. The first prostanoid therapy approved was epoprostenol. Its uses are held back for later stage PAH (WHO class III and IV), who have not had success with conventional therapy (Humbert and Ghofrani, 2016). Epoprostenol is administered intravenously and serious care must be taken with this drug as fatal adverse effects can occur through the central venous line, such as sepsis and thromboembolisms (Barst, 2010).

Another PGI_2 analogue is iloprost. Iloprost has an advantage over epoprostenol as it has a longer half-life (20 minutes compared to < 5 minutes) and can be administered through inhalation or intravenously. In Europe, only inhaled iloprost is approved for PAH patients (WHO class III). Disadvantages of inhaled iloprost is that it still requires frequent administration, between 6 and 9 times a day. In addition iloprost has poor selectivity on prostanoid receptors and is equally potent in the activation of IP and EP_1 receptors (Whittle *et al*., 2012; Clapp and Gurung, 2015). Activation of EP_1 receptors causes vasoconstriction via receptor-coupled $G_{\alpha q}$ proteins, which downstream increase intracellular IP_3 and DAG, as well as generating an increase in intracellular Ca^{2+} levels by upregulating PDE1 (Schermuly *et al.,* 2007).

Treprostinil is a PGI_2 analogue which can be administered orally, subcutaneously, intravenously and inhaled. Treprostinil has a great advantage in its mode of delivery, as subcutaneous therapy is approved in Europe for WHO class III PAH patients and reduces administration risk, when compared to epoprostenol. Treprostinil's half-life is considerably higher at 4 hours and is more stable at room temperature. One disadvantage to treprostinil is the severe site pain experienced in patients undergoing subcutaneous administration. One trial stated 85% of patients exhibited this pain (Simonneau *et al.,* 2002). Experiencing pain during drug administration could be a big factor

in patients wishing to discontinue therapy. 8% of patients, in the study that report pain, wished to be discontinued from treprostinil treatment (Simonneau *et al.,* 2002). Treprostinil favours the binding of the vasodilatory prostanoid receptors IP, DP_1 and EP_2 with binding affinity (K_i) values of 32 nM, 4.4 nM and 3.6 nM, respectively, compared to 212 nM and 2505 nM for EP_1 and EP_3, respectively (Clapp and Gurung, 2015). Improvements in patients six minute walking distance has been seen in multiple studies, with different delivery methods, indicating treprostinil therapy is a beneficial therapy (Simonneau *et al.,* 2002; McLaughlin *et al.,* 2010; Jing *et al.,* 2013).

4.1.3.4 Experimental Compounds

As PAH therapy is still inadequate, many compounds are being developed and tested experimentally as well as clinically. Some of these compounds, may not be translatable clinically but could help provide beneficial insights for future drug design (Figure 4.4). These include selexipag, which is a prodrug, non PGI_2 analogue and selective IP receptor agonist. Whilst selexipag is selective in its binding, it has not shown great efficacy in vasodilating pulmonary arteries. One reason for this may be the broad selectivity of other prostanoid therapies, which produce a dilatory effect, with a combination of pro-dilatory prostanoid receptors being stimulated. Currently selexipag is not approved for use in PAH therapy.

PDE inhibitors have proved useful in PAH therapy. Compounds such as 3 - isobutyl-1-methylxanthine (IBMX), targets multiple PDE's (PDE1-5, 7 and 11)' increasing intracellular levels of both cAMP and cGMP.

An alternative compound to riociguat could be forskolin, which instead of activating sGC, activates adenylyl cyclase (AC). Forskolin is used within traditional medicine for multiple diseases including cardiovascular, respiratory and neuronal, but is not approved clinically for use in the treatment of any condition (Henderson *et al.,* 2005).

Another experimental compound which may be of use is the compound ONO-RS-082, a reversible phospholipase A_2 (PLA_2) inhibitor. The use of PLA_2

inhibitors acts higher up the signalling pathway, than currently approved therapies, PLA_2 is an enzyme that generates arachidonic acid (AA), which is a precursor to PGI_2. Experimentally ONO-RS-082 has been shown to increase K^+ channel current, specifically Twik-Related Acid-Sensitive Channel 1 (TASK-1) current, which has been widely implicated in PAH pathogenesis.

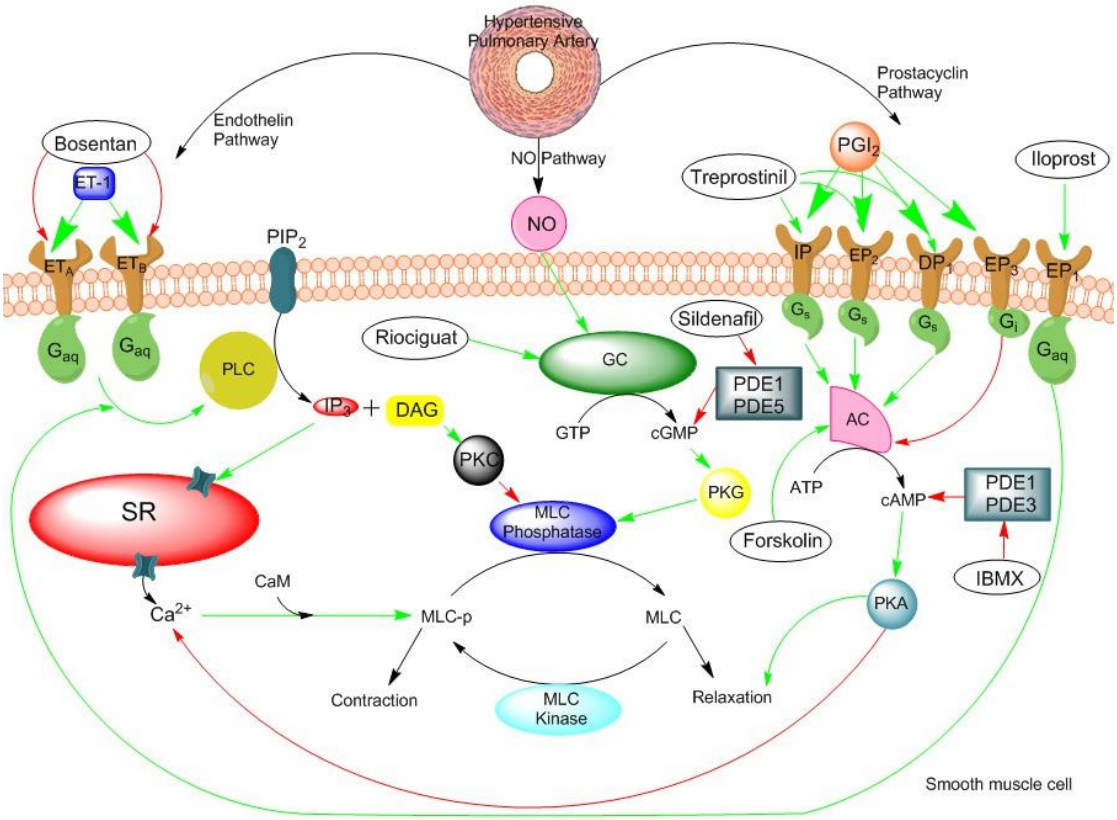

Figure 4.4 – Action of Drugs and Compounds on PAH pathways

Diagram shows where the approved therapies and experimental compounds play a role in PAH pathways. Note IBMX can also act to increase cGMP levels as well as cAMP levels.

4.1.4 Implications of the Two-Pore Domain K^+ Channel (TASK-1) in Pulmonary Arterial Hypertension

As previously mentioned, one major factor in the development of PAH are genetic predispositions. 80% of patients with hPAH carry a recognisable pathogenic mutation such as bone morphogenetic protein receptor type 2 (BMPR2), mothers against decapentaplegic homologue 1 (SMAD1), Neurogenic locus notch homolog protein 3 (NOTCH3) and two-pore domain K^+ channel subfamily member 3 (KCNK3; Navas *et al.,* 2016). KCNK3 gene encodes the TASK-1 potassium channel and there is now increasing evidence for a role of TASK-1 in PAH through the regulation of pulmonary vascular tone.

In early studies, TASK-1 channels were shown to be expressed within mammalian lungs although the specific cell type in which it is located was unclear. A few years later TASK-1 was then confirmed to play a major role in the resting potential of pulmonary arterial smooth muscle cells (PASMCs) within rabbits (Lesage and Lazdunski, 2000; Gurney *et al.,* 2003). Other concurrent work highlighted that the background current within PASMCs, shared properties of TASK-1 currents, such as a 50% inhibition of current at pH 7.3 and activation by halothane (Gurney *et al.,* 2003; Leonoudakis *et al.,* 1998). TASK-1 was identified as the potential O_2 sensor in PASMCs and further studies including siRNA silencing of TASK-1 channels confirmed its role in the regulation of PASMC membrane potential (Gurney and Joshi, 2006; Olschewski *et al.,* 2006).

An increase in PASMC proliferation and vasoconstriction was observed with reduced K^+ channel activity, particularly TASK-1 and Kv1.5 (KCNA5; Boucherat *et al.,* 2015). In regards to PAH, it has been shown that in human patients of PAH, TASK-1 expression is significantly reduced and TASK-1 inhibition lead to an increase in vasoconstriction, proliferation and inflammation (Antigny *et al.,* 2016). The same study also found that within experimental models of PAH, pharmacological activation of TASK-1 can relieve signs of PAH. The conclusion of this study was that TASK-1 channels and therefore loss of TASK-1 function or expression is a key event in PAH pathogenesis (Antigny *et al.,* 2016). Further work from the same group

identified that within rats, TASK-1 is expressed far more significantly in right ventricular (RV) cardiomyocytes compared to the left ventricle and there is a reduction in the TASK-1 function prior to the development of RV hypertrophy (Lambert *et al.,* 2018). PAH is proposed to arise through TASK-1 dysfunction/loss which results in PASMC membrane depolarisation, which in turn leads to constriction of the pulmonary artery. The pulmonary remodelling that occurs within PAH have been attributed to platelet-derived growth factor, which has been shown to have higher expression in PASMC, following TASK-1 inhibition (Humbert, 2013; Antigny *et al.,* 2016).

In combination with the experimental work implicating TASK-1 as a key mediator in PAH, genetic screening has advanced our understanding of the mechanisms underlying the disease. Using these screens, mutated genes are able to be analysed experimentally to determine their roles and potential therapeutic avenues. In TASK-1 channels, six heterozygous mutations were first indicated to play a role in PAH having been generated from hPAH and iPAH patients (Ma *et al.,* 2013). In this study they showed that mutations caused a loss of function, but using the phospholipase A2 inhibitor, ONO-RS-082, enabled limited recovery of current in homozygous mutant TASK-1 channels could be observed. This study highlighted a new target in the treatment of PAH as well as the first channelopathy within the disease (Girerd *et al.,* 2014). More recently, a brief report based on a Spanish cohort of patients revealed two novel mutations of TASK-1 present in an aggressive form of PAH, this time mutations were homozygous (Navas *et al.,* 2017). The two novel mutations are a glycine substituting an arginine at position 106 (G106R) and a leucine replacing an arginine at position 214 (L214R). Both mutations are located extracellularly, with G106R being located between the first pore (P) domain and the second transmembrane (TM) domain and L214R being located between the second P domain and fourth TM domain (Figure 4.5).

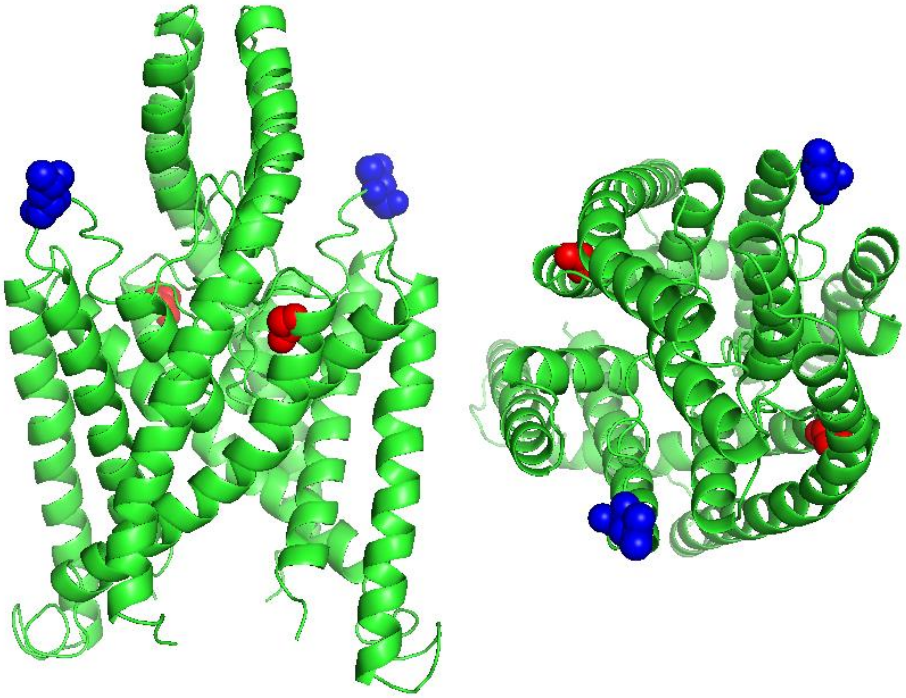

Figure 4.5 – Homology model of novel TASK-1 mutations

Homology TASK-1 model generated based on crystal structure of TRAAK (PDB ID 3UM7, Brohawn et al., 2012). G106R mutated amino acids are shown in red, L214R mutated amino acids are shown in blue. Left shows a side image of the channel, right shows a view from above the channel (Reproduced from Cunningham et al., 2018).

4.2 Objective

The objective for this set of experiments was to characterise the functional properties of the novel TASK-1 mutations, G106R and L214R, identified by *Navas et al.,* (2017). By generating electrophysiological profiles of the channels it was possible to analyse the effects of potential therapeutic options. Drugs and compounds used in this study were the phospholipase A2 inhibitor (ONO-RS-082), the PDE5 inhibitor (sildenafil), the non-selective PDE inhibitor (IBMX), the soluble guanylyl cyclase activator (Riociguat), the adenylyl cyclase activator (Forskolin) and the synthetic analogue of PGI_2 (Treprostinil). In addition to this, protein quantification studies and confocal imaging was conducted to determine whether the novel TASK-1 mutations are trafficked to the cell membrane as efficiently as WT TASK-1 channels. Finally, the effect of treprostinil on TWIK-related K^+ channel 1 (TREK-1) and 2 (TREK-2) was analysed to determine if these channels play a role in the site pain experienced by PAH patients, undergoing treprostinil therapy.

4.3 Results: Characterisation of Novel TASK-1 Mutations Implicated in PAH

4.3.1 Electrophysiological properties of TASK-1

hTASK-1 WT DNA was transiently transfected into tsA201 cells and used in whole-cell patch-clamp electrophysiological recordings. The application of the step-ramp voltage protocol (Figure 2.6) previously described ensured the generation of currents with TASK-1 electrophysiological characteristics (Figure 4.6). TASK-1_WT currents were measured as the current recorded at -40 mV.

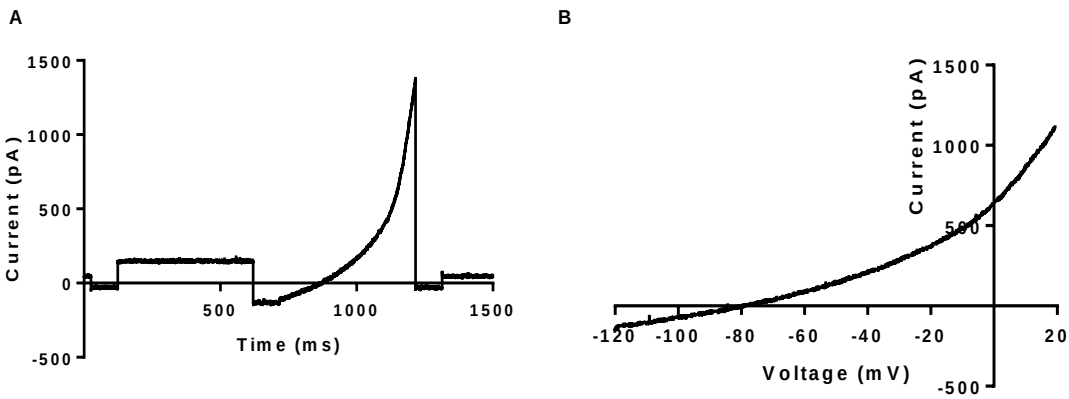

Figure 4.6 – TASK-1_WT electrophysiological profile.

A) Representative trace for TASK-1_WT channel in control conditions exposed to the step-ramp voltage protocol detailed in the methods. B) Current-voltage graph for TASK-1_WT in control conditions.

The electrophysiological profile for TASK-1_WT in extracellular solution (2.5 mM K^+, pH 7.4, see methods 2.3.3) yielded an average whole-cell current of 8 ± 1 pA/pF (n = 44) with an average reversal potential of -73 ± 2 mV (n = 13) close to the equilibrium potential for K^+ ions under these recording conditions based on the Nernst equation. TASK-1_WT has an outwardly rectifying current, as shown in the exemplar current-voltage graph (Figure 4.6B), at higher voltages the current increases significantly as seen from the steep curve, this is the activation of endogenous K_V channels within the tsA201 cells.

By measuring current at -40 mV it ensures any change in current seen is a change of TASK-1 current and not that of endogenous channels. This effect was present within TASK-3 currents however TASK-1 currents measured were far smaller displaying the effect of Kv activation as an exaggerated effect.

4.3.2 Electrophysiological properties of novel TASK-1 mutants

The channel functionality of the novel PAH mutants, G106R and L214R, were assessed using whole-cell patch-clamp techniques. TASK-1_G106R and TASK-1_L214R DNA was transiently expressed in tsA201 cells under experimental conditions (2.5 mM K^+, pH 7.4, see methods 2.3.3). The substitution of a glycine (G) residue with an arginine (R) at position 106 leads to the significant reduction ($p < 0.05$, one-way ANOVA with Dunnett's Multiple Comparisons test) in channel current (Figure 4.7A). The average whole-cell current measured at -40 mV for TASK-1_G106R was 2 ± 1 pA/pF ($n = 38$; $p < 0.05$) and an average reversal potential was also significantly changed with a value of -33 ± 8 ($n = 5$; $p < 0.05$; appendix 6.11 and 6.12). Similarly, L214R, a leucine (L) replaced with an arginine (R) at position 214 results in a significant reduction in channel current at -40 mV (Figure 4.7A). The average whole-cell current measured at -40 mV for TASK-1_L214R was 2 ± 1 pA ($n = 27$; $p < 0.05$) and average reversal potential was also significantly changed with a value of -19 ± 3 ($n = 5$; $p < 0.05$; appendix 6.11 and 6.12). Cells only transfected with GFP had a significantly smaller whole-cell current of 2 ± 1 pA ($n = 36$; $p < 0.05$; Figure 4.7A) with an average reversal potential of -32 ± 2 mV ($n = 13$; $p < 0.05$; appendix 6.11 and 6.12).

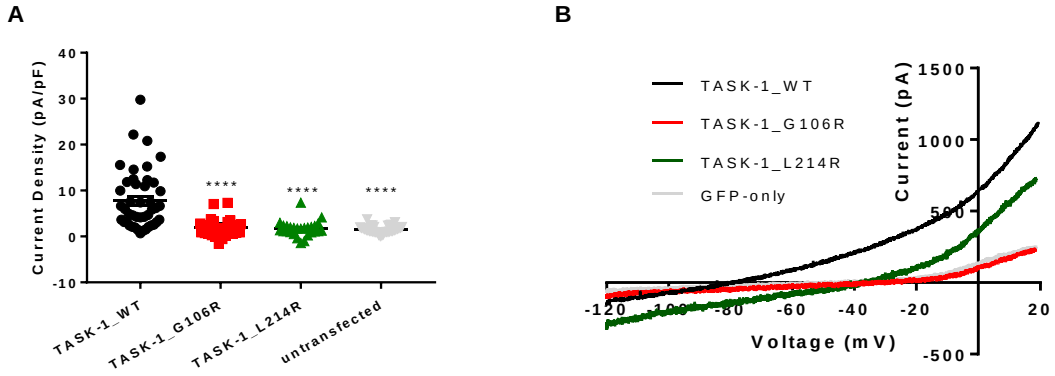

Figure 4.7 – Electrophysiological profile of novel TASK-1 mutants

A) Measurements of whole-cell current normalised against cell capacitance (pA/pF) at -40 mV for cells expressing TASK-1_WT, TASK-1_G106R, TASK-1_L214R or untransfected cells. Error bars represent the SEM. B) Current-voltage plot of TASK-1_WT, TASK-1_G106R, TASK-1_L214R and GFP only showing changes in currents over a voltage ramp from -120 mV to +20 mV.

4.3.3 Effect of TEA on TASK-1_WT and novel mutants

As there was substantial outward current seen at more positive potentials of the ramp within the step-ramp voltage protocol, tetraethylammonium chloride (TEA) was used to inhibit any background K_V current, which is found in the cells. K2P channels are insensitive to TEA, if current measured was due to the TASK-1 channel present then current should remain during the presence of TEA (10 mM; O'Connell *et al.,* 2002). Currents were measured at +20 mV as this was the highest voltage used in the step-ramp protocol, TASK-1_WT was not significantly affected by the use of TEA (10 mM) with values of 38 ± 4 pA/pF (n = 11) in control conditions and 36 ± 6 pA/pF (n = 8) in TEA (10mM; $p > 0.05$, Two-way ANOVA, Figure 4.8). Both currents within mutated channels were significantly reduced in the presence of TEA (10 mM) with TASK-1_G106R measured at 27 ± 5 pA/pF (n = 6) in control and 7 ± 1 pA/pF (n = 6) in TEA (10 mM). Whilst TASK-1_L214R had current of 22 ± 5 pA/pF (n = 6) in control and 8 ± 2 pA/pF (n = 6) in TEA (10 mM; $p < 0.05$, Two-way ANOVA, Figure 4.8). Cells transfected only with GFP were significantly reduced at +20 mV, from 21 ± 2 pA/pF (n = 6) in control conditions to 6 ± 1 pA/pF (n = 6) in

TEA (10 mM), suggesting endogenous K_V channels are present within the cells and represent the outward current seen with the novel mutations, at more positive voltages ($p < 0.05$, Two-way ANOVA, Figure 4.8).

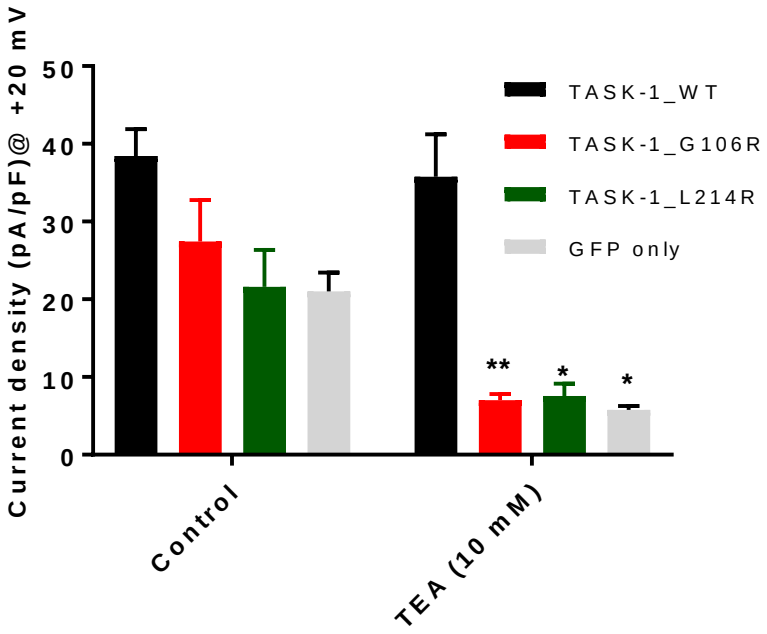

Figure 4.8 – Effect of TEA (10 mM) on TASK-1_WT and novel mutants

Measurements of whole-cell current normalised against cell capacitance (pA/pF) at +20 mV for cells expressing TASK-1_WT, TASK-1_G106R,TASK-1_L214R and GFP only in control conditions and TEA (10 mM)

4.3.4 Effect of alkalosis on the functionality of TASK-1 WT and novel mutants

After identifying the significantly attenuated current in the mutant channels as well as the change in reversal potentials compared to WT TASK-1 the next approach was to assess them under the effect of alkalosis. TASK-1 channels have a pK of 7.5 and as previously mentioned can therefore be inhibited or activated by acidosis and alkalosis respectively (Berg *et al.,* 2004). Our approach was to identify whether the mutant channels were still pH sensitive and determine if the reduced functionality of the mutant channels could be

rescued by an increase in extracellular pH from 7.4 to 8.4. In accordance with previous studies, TASK-1_WT current at -40 mV was significantly increased (paired *t*-test, $p < 0.05$) with outward currents enhancing from 11 ± 1 pA/pF (n = 17) at pH 7.4 to 27 ± 3 pA/pF (n = 17) at pH 8.4 (Figure 4.9). The increase in extracellular pH had no significant effect ($p > 0.05$) upon TASK-1_G106R current at -40 mV with outward current values of 1 ± 1 pA/pF (n = 12) at pH 7.4 to 3 ± 1 pA/pF (n = 12) at pH 8.4 (Figure 4.10). A similar result was recorded for the TASK-1_L214R mutation, with extracellular alkalosis having no significant effect ($p < 0.05$) on outward channel current at -40 mV, 1 ± 1 pA/pF (n = 5) at pH 7.4 to 1 ± 1 pA/pF (n = 5) at pH 8.4 (Figure 4.11).

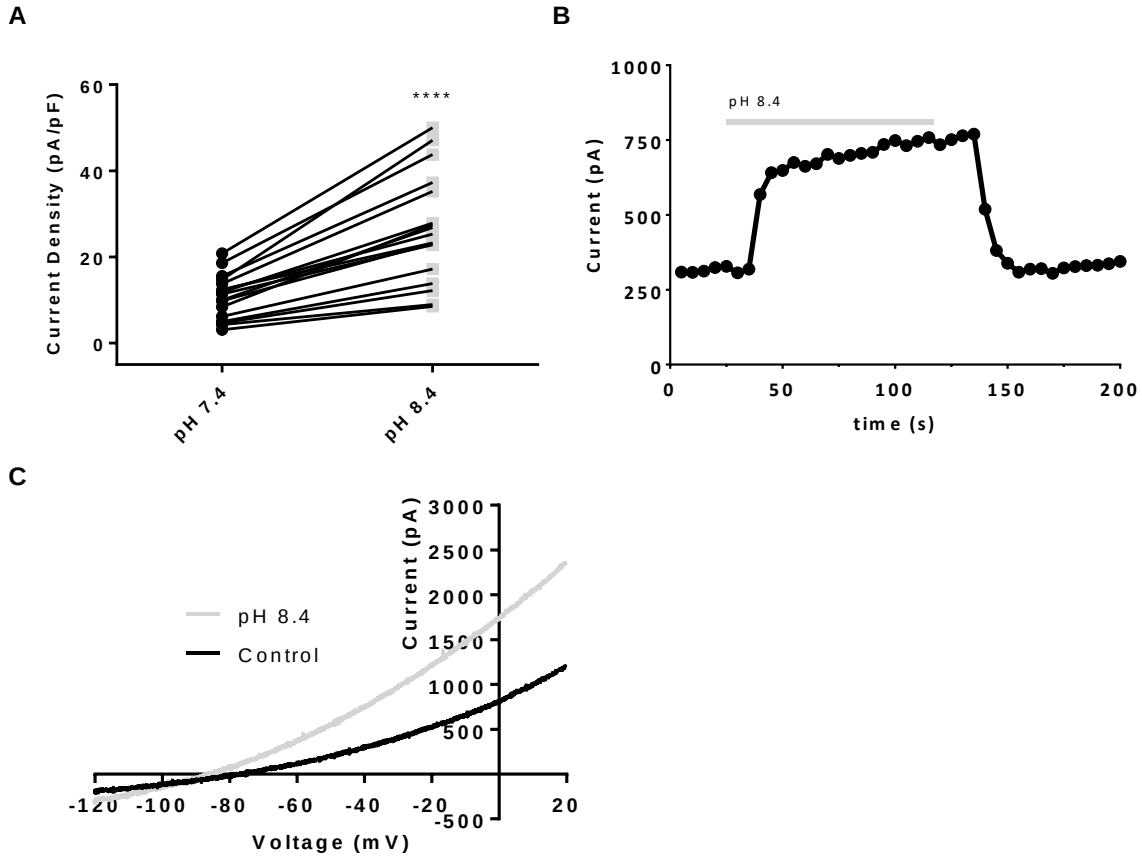

Figure 4.9 – Functional effects of extracellular alkalosis on TASK-1_WT

A) TASK-1_WT current values normalised to the cells capacitance (pA/pF) measured at -40 mV, recorded at extracellular pH 7.4 (black dots) or pH 8.4 (grey dots). Black line links the same cell in either condition. B) Time course graph showing TASK-1_WT outward current at -40 mV under the influence of pH 8.4. pH 8.4 application is represented at the grey bar, absence of the grey bar represents pH 7.4. C) Current-

voltage plot of TASK-1_WT in both pH 7.4 (black line) and pH 8.4 (grey line) recorded over a voltage ramp from -120 mV to +20 mV.

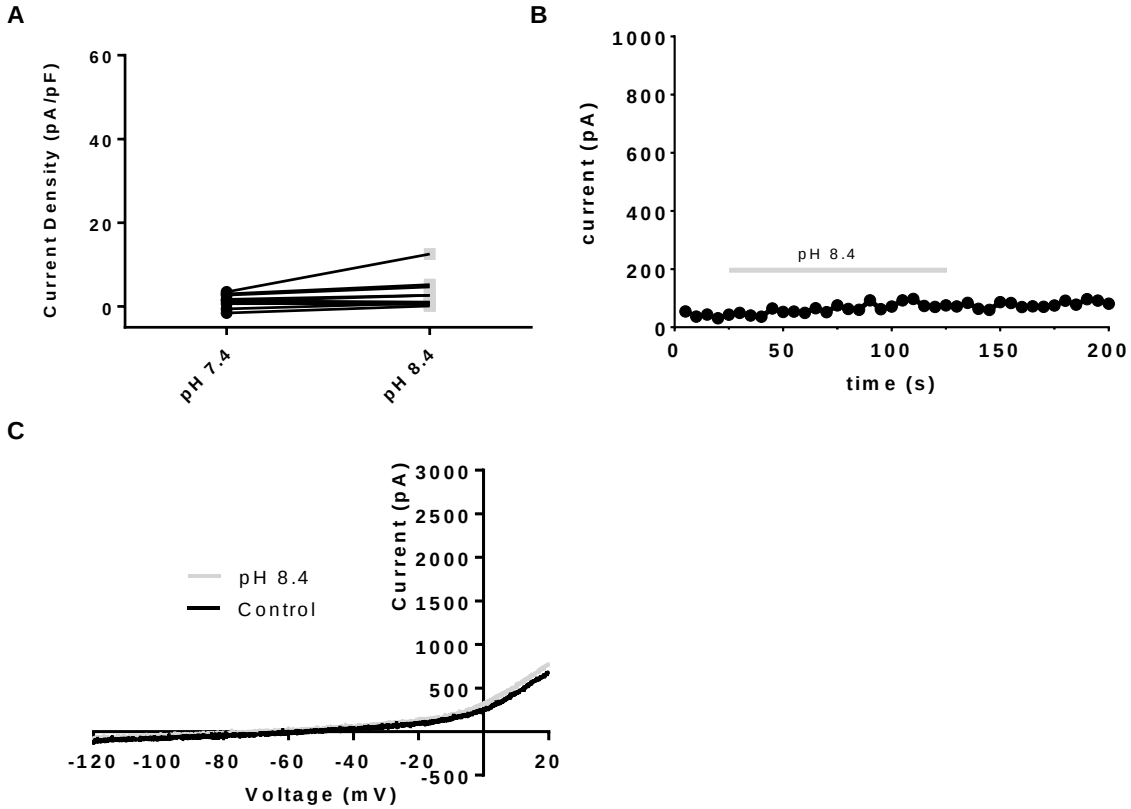

Figure 4.10 – Functional effects of extracellular alkalosis on TASK-1_G106R

A) TASK-1_G106R current values normalised to the cells capacitance (pA/pF) measured at -40 mV, recorded at extracellular pH 7.4 (black dots) or pH 8.4 (grey dots). Black line links the same cell in either condition. B) Time course graph showing TASK-1_G106R outward current at -40 mV under the influence of pH 8.4. pH 8.4 application is represented at the grey bar, absence of the grey bar represents pH 7.4. C) Current-voltage plot of TASK-1_G106R in both pH 7.4 (black line) and pH 8.4 (grey line) recorded over a voltage ramp from -120 mV to +20 mV.

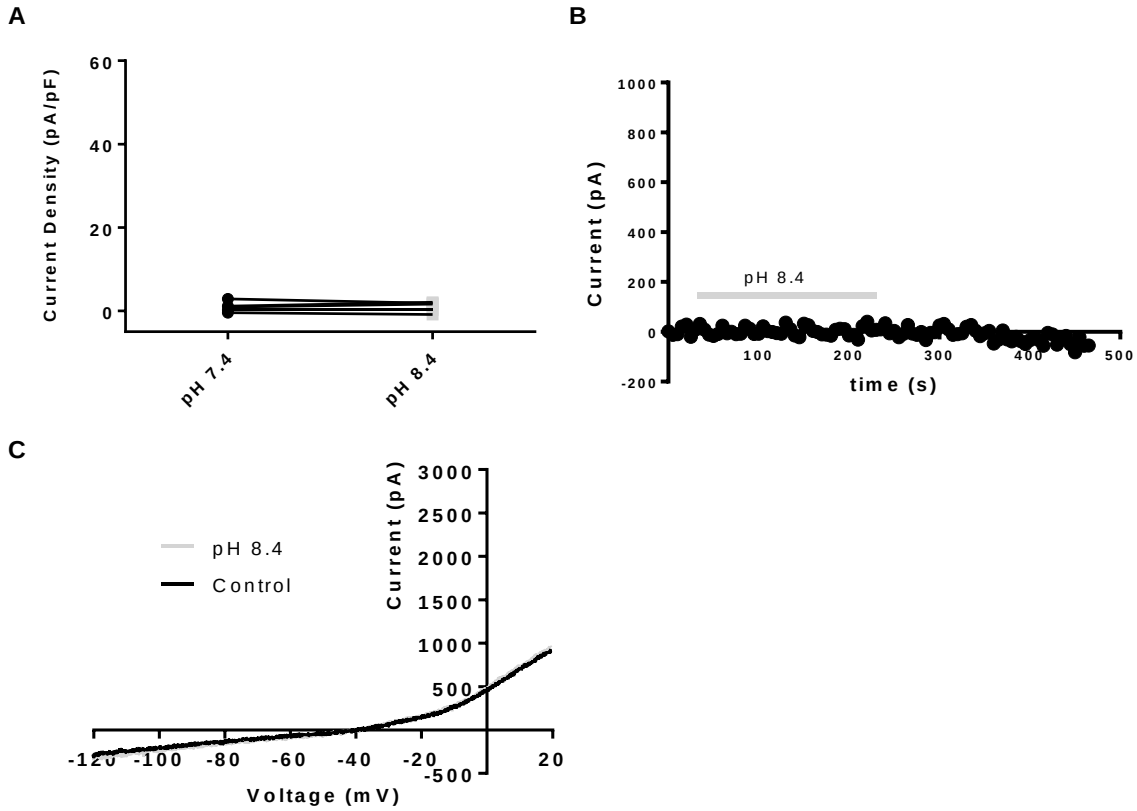

Figure 4.11 – Functional effects of extracellular alkalosis on TASK-1_L214R

A) TASK-1_L214R current values normalised to the cells capacitance (pA/pF) measured at -40 mV, recorded at extracellular pH 7.4 (black dots) or pH 8.4 (grey dots). Black line links the same cell in either condition. B) Time course graph showing TASK-1_L214R outward current at -40 mV under the influence of pH 8.4. pH 8.4 application is represented at the grey bar, absence of the grey bar represents pH 7.4. C) Current-voltage plot of TASK-1_L214R in both pH 7.4 (black line) and pH 8.4 (grey line) recorded over a voltage ramp from -120 mV to +20 mV.

4.3.5 Cellular localisation of TASK-1 WT and novel mutants

As a result of a reduced current observed in TASK-1_G106R and TASK-1_L214R mutant channels compared to TASK-1_WT, as well as a loss of pH sensitivity, it was appropriate to investigate whether these changes were due to cellular trafficking issues, which resulted in a reduction of channel expression at the plasma membrane. A combination of confocal microscopy and in/on cell assays were used to determine this. For confocal microscopy experiments the channels were tagged within a green fluorescent protein (GFP) at the C terminus of the channels and excited at 488 nm. The plasma membranes were stained with a membrane specific stain, CellMask™ Deep Red and excited at 561 nm. TASK-1_WT channels were shown to principally be expressed within the plasma membrane with both stains exhibiting similar profiles (Figure 4.12Ai and Aii, respectively) with an overlap image visually confirming this (Figure 4.12iii), along with a blue stained nuclei. To quantify the co-localisation of channel and membrane Pearson's correlation coefficient (PCC) was adopted, 12 individual cells were analysed originating from 8 separate plates and 4 different cultures. A PCC value of 0.65 ± 0.04 (n = 12) for TASK-1_WT was obtained indicating a strong correlation (PCC value of 1 = 100% correlation between channel and membrane) between TASK-1_WT channel and the plasma membrane (Figure 4.12D). For the two novel mutants the same analysis was conducted and both resulted in a similar profile to TASK-1_WT. For TASK-1_G106R and TASK-1_L214R, the channels were shown visually at the membrane and overlapped with the membrane stain (Figure 4.12Bi-iii and Ci-iii respectively). Quantification of TASK-1_G106R and TASK-1_L214R resulted in PCC values of 0.75 ± 0.03 (n = 12) and 0.72 ± 0.04 (n = 12) respectively and no significant difference was observed between TASK-1_WT and mutant channels ($p > 0.05$, one-way ANOVA). These findings suggest the trafficking to the plasma membrane and translation of mutant channels are equally as efficient as the TASK-1_WT channel under these experimental conditions.

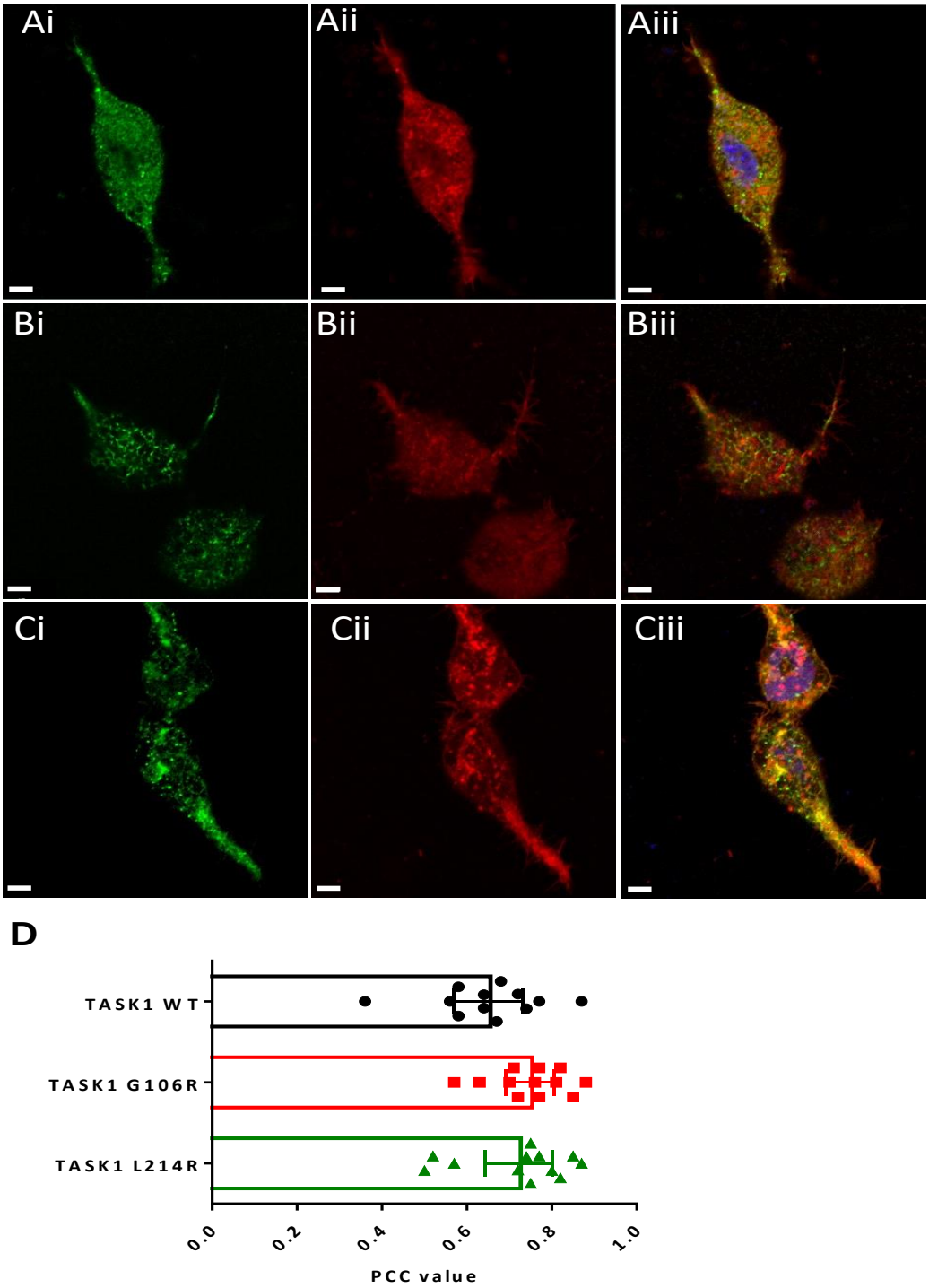

Figure 4.12 – Visualisation and quantification of cellular localisation of TASK-1 WT and mutant channels

Ai) Confocal microscope photomicrograph showing cellular localisation of TASK-1_WT channels tagged with GFP. Aii) Confocal microscope photomicrograph showing location of plasma membrane stained with CellMask deep red. Aiii) Is an overlay representation of (Ai) and (Aii) with overlap of channel and plasma membrane

appearing yellow. Nuclei were stained with Hoechst 33258 appearing blue. Bi, ii and iii) represents TASK-1_G106R as (Ai, ii and iii) does for TASK-1_WT respectively. Ci, ii and iii) represents TASK-1_L214R as (Ai, ii and iii) does for TASK-1_WT respectively. D) Bar chart depicting the quantification of co-localisation using PCC values of TASK-1_WT, TASK-1_G106R and TASK-1_L214R, PCC value of 1 signifies 100% correlation between membrane and channel. Each point represents PCC value for individual cell expressing the respective channel, error bars display SEM. Scale bars = 5 µM.

Whilst the Zeiss LSM880 microscope had an axial resolution of 400 nm, the cell thickness suggests confocal data alone cannot conclusively confirm the co-localisation of GFP-tagged channel and membrane. To further quantify the translation and trafficking of TASK-1_WT and mutant channels in-cell and on-cell assays were utilised. Channels were tagged using a human influenza hemagglutinin (HA) tag on the M1P1 loop. The M1P1 loop is an extracellular domain, that a primary antibody, anti-HA (mouse, H3663, Sigma Aldrich), can bind to and detect channels at the plasma membrane. To quantify the whole-cell channel expression, cell membranes were permeabilised using Triton X-100 and anti-HA was applied. A secondary antibody selective to the primary antibody and conjugated to a green dye (Goat anti-mouse IRDye 800CW, LiCOR) which is excited at 778 nm. DRAQ5 (ThermoFisher), a DNA stain was used to quantify the cell count to ensure equal cell numbers were present in each data set. Using DRAQ5 showed no difference in cell numbers between TASK-1_WT, TASK-1_G106R and TASK-1_L214R (Figure 4.13) with values of 408 ± 50 ($n = 9$), 341 ± 62 ($n = 9$) and 328 ± 65 ($n = 9$) respectively ($p > 0.05$). For TASK-1_WT, on-cell assay produced channel membrane expression values of 487 ± 69 ($n = 9$) and no significant difference was seen in TASK-1_G106R and TASK-1_L214R (Figure 4.13) with values of 443 ± 114 ($n = 9$) and 377 ± 27 ($n = 9$) respectively ($p > 0.05$, two-way ANOVA). Similarly, whole-cell channel expression was also not significantly different (Figure 4.13), between TASK-1_WT, TASK-1_G106R and TASK-1_L214R, with values of 1552 ± 313 ($n = 9$), 1892 ± 351 ($n = 9$) and 1219 ± 311 ($n = 9$) respectively ($p > 0.05$, two-way ANOVA). This data in combination with the

confocal imaging and electrophysiological data provides solid evidence that under these experimental conditions, the PAH mutations, TASK-1_G106R and TASK-1_L214R are trafficked and expressed, with similar efficiency to TASK-1_WT, but the mutations reduce channel functionality.

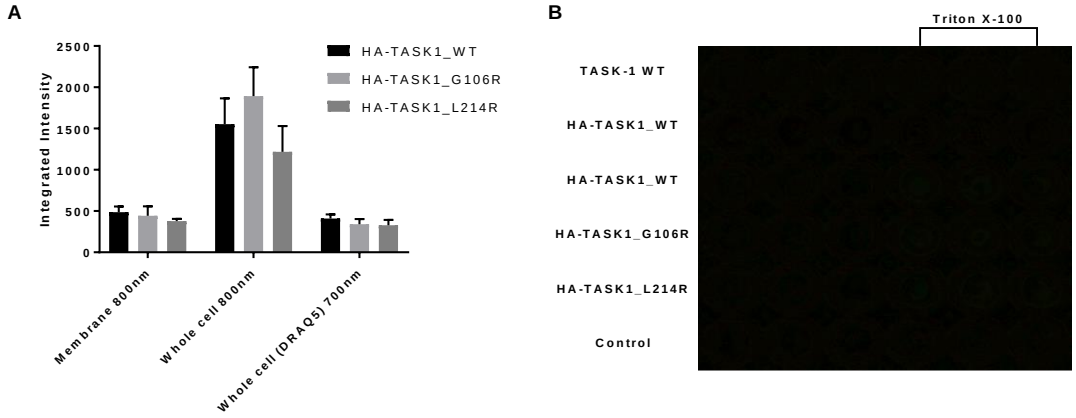

Figure 4.13 – Analysis of TASK-1_WT and mutant channels cellular localisation by in cell and on cell assays

A) Chart representing integrated intensity values of TASK-1_WT, TASK-1_G106R and TASK-1_L214R tagged with hemagglutinin (HA). Membrane values represent channels at the membrane of cell. Whole-cell 800 nm values represent total channel translation within the cell, generated by permeabilising cell membrane with Triton X-100 prior to anti-HA antibody binding. Whole-cell DRAQ5 700 nm represent total cell count. B) Image of plate wells used for in cell and on cell assays, each row identified with the DNA present, right half permeabilised with Triton X-100.

4.3.6 Effect of a TASK-1 activator, ONO-RS-082, on TASK-1 novel mutations

ONO-RS-082, a phospholipase A2 inhibitor, has been shown to activate TASK-1_WT current. More specifically it has been shown that heterozygous TASK-1 mutations found in PAH patients which express reduced channel current have been shown to have partial current rescued following the acute application of ONO-RS-082 (Ma *et al.,* 2013). As found by Ma *et al.,* 2013, TASK-1_WT outward current at -40 mV was significantly increased (Figure 4.14A) by ONO-RS-082 (10 µM) with values of 6 ± 2 pA/pF (n = 6) in control conditions and 14 ± 4 pA/pF (n = 6; $p < 0.05$, paired *t*-test) under ONO-RS-082 (10 µM). ONO-RS-082 was shown to be reversible and had an EC50 value of 2.94 µM (Figure 4.14B and D).

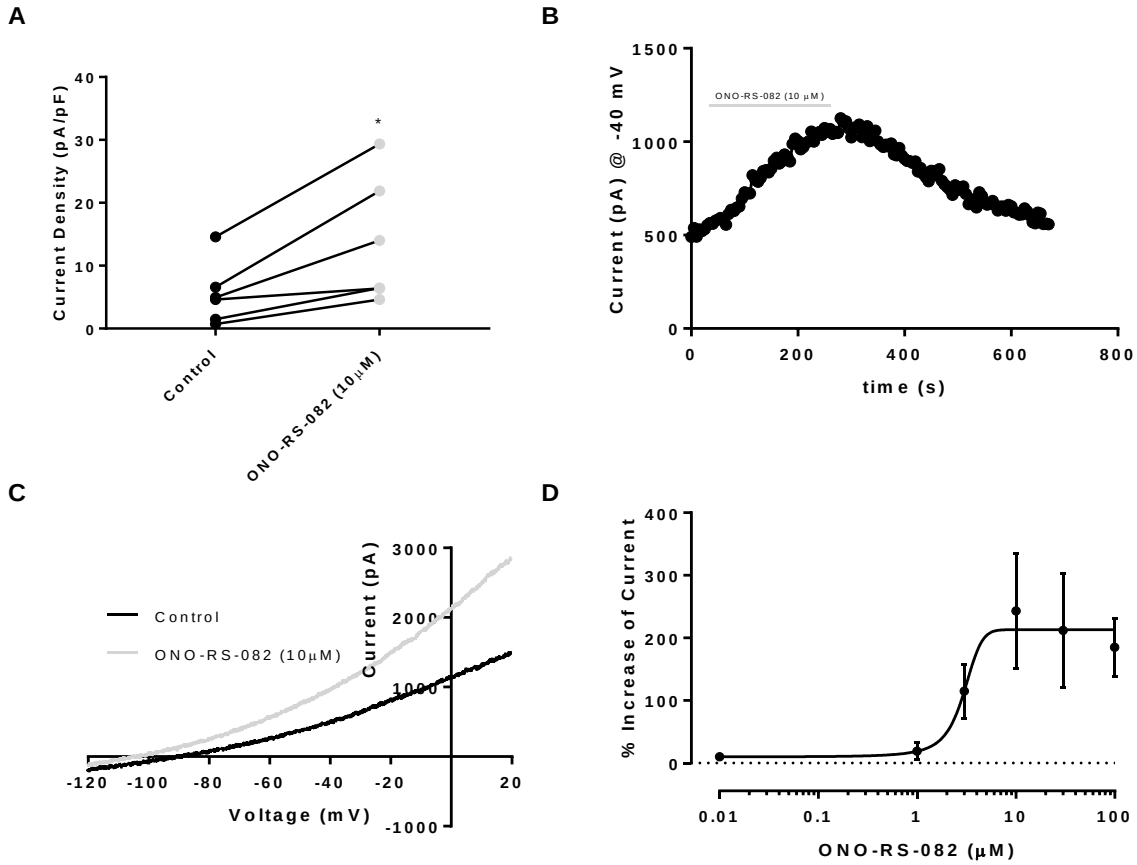

Figure 4.14 – Effect of ONO-RS-082 on TASK-1_WT

A) Effect of ONO-RS-082 (10 µM) on TASK-1_WT outward current measured at -40 mV. B) Time course graph showing TASK-1_WT outward current at -40 mV under the influence of ONO-RS-082 (10 µM). Application of ONO-RS-082 (10 µM) is represented with the grey bar, absence of the grey bar represents cell in control conditions. C) Current-voltage plot of TASK-1_WT in both pH 7.4 (black line) and ONO-RS-082 10 µM (grey line) recorded over a voltage ramp from -120 mV to +20 mV. D) Concentration response plot showing the effect of a range of ONO-RS-082 concentrations between 0.01 µM and 100 µM on TASK-1_WT outward current at -40 mV. Error bars represent SEM. Non-linear regression line fitted.

In contrast to TASK-1_WT and the two heterozygous mutations seen in Ma *et al.,* (2013), ONO-RS-082 (10 µM) has no significant effect on TASK-1_G106R (Figure 4.15, $p > 0.05$). TASK-1_G106R in control conditions had an outward current measured at -40 mV of 0.76 ± 0.3 pA/pF (n = 7) and under the acute application of ONO-RS-082 (10 µM) 0.66 ± 0.2 pA/pF (n = 7).

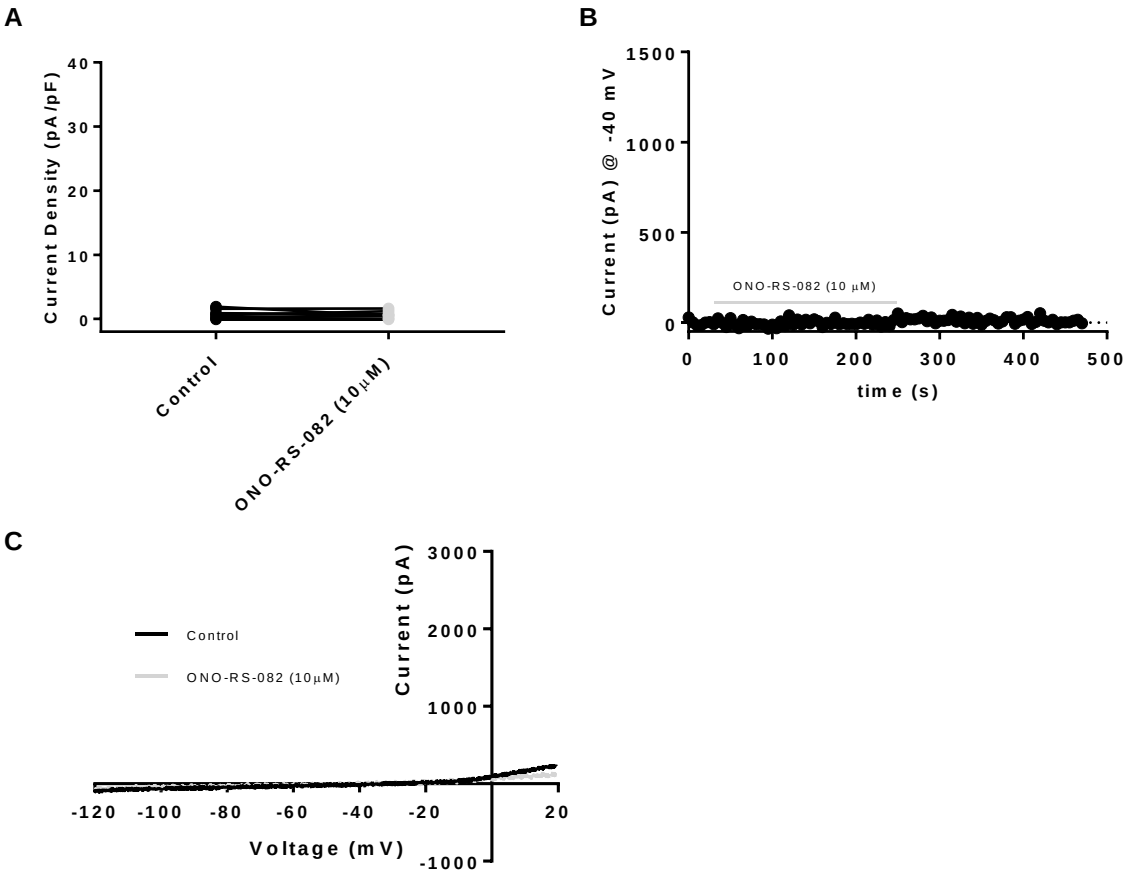

Figure 4.15 – Effect of ONO-RS-082 on TASK-1_G106R

A) Effect of ONO-RS-082 (10 µM) on TASK-1_G106R outward current measured at -40 mV. B) Time course graph showing TASK-1_G106R outward current at -40 mV under the influence of ONO-RS-082 (10 µM). Application of ONO-RS-082 (10 µM) is represented with the grey bar, absence of the grey bar represents cell in control conditions. C) Current-voltage plot of TASK-1_G106R in both pH 7.4 (black line) and ONO-RS-082 10 µM (grey line) recorded over a voltage ramp from -120 mV to +20 mV.

Similarly to TASK-1_G106R, ONO-RS-082 (10 µM) also did not have a significant effect upon TASK-1_L214R (Figure 4.16; $p > 0.05$)). In control conditions, TASK-1_L214R outward current at -40 mV was 2 ± 1 pA/pF (n = 7) and under the acute application of ONO-RS-082 (10 µM) was 1.8 ± 1 pA/pF (n = 7).

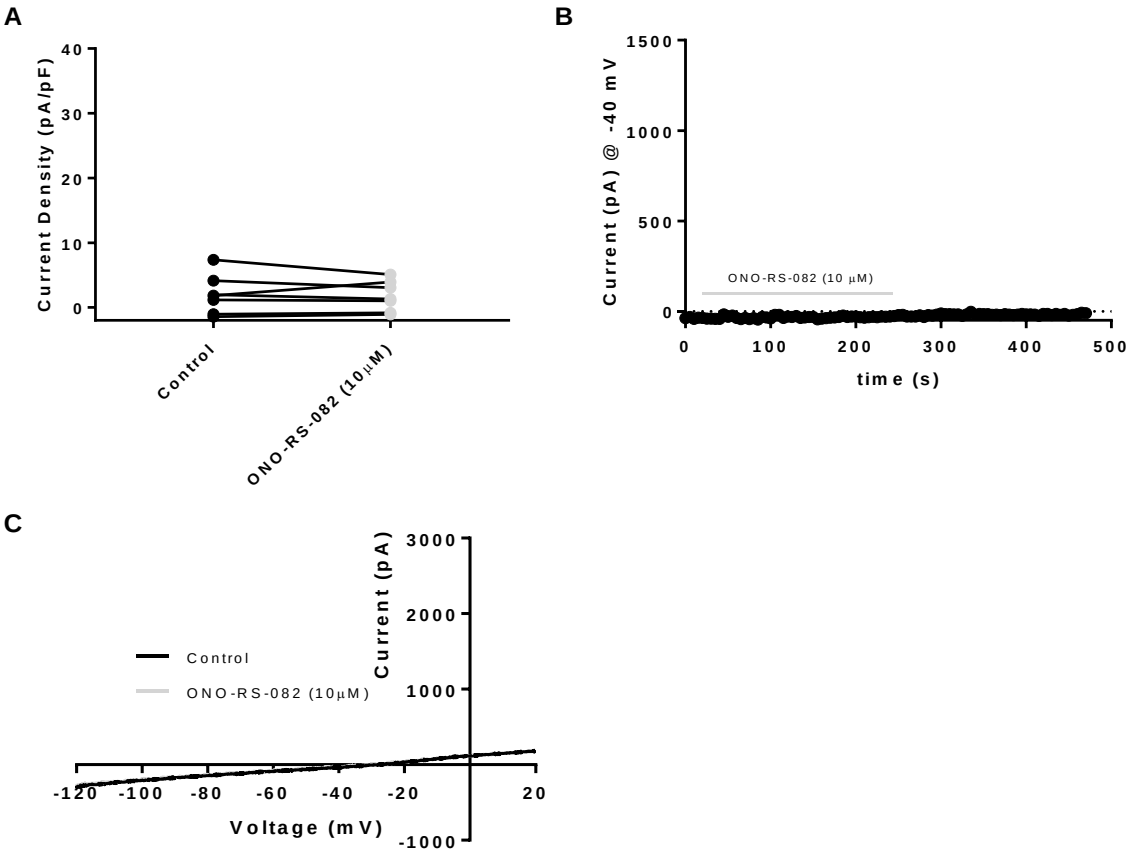

Figure 4.16 – Effect of ONO-RS-082 on TASK-1_L214R

A) Effect of ONO-RS-082 (10 µM) on TASK-1_L214R outward current measured at -40 mV. B) Time course graph showing TASK-1_L214R outward current at -40 mV under the influence of ONO-RS-082 (10 µM). Application of ONO-RS-082 (10 µM) is represented with the grey bar, absence of the grey bar represents cell in control conditions. C) Current-voltage plot of TASK-1_L214R in both pH 7.4 (black line) and ONO-RS-082 10 µM (grey line) recorded over a voltage ramp from -120 mV to +20 mV.

As ONO-RS-082 failed to enhance current of novel mutations, the next approach was to investigate a mutation (TASK-1_E182K) that has been reported to recover current under ONO-RS-082 (10 µM) application (Ma *et al.,* 2013). Compared to TASK-1_WT, TASK-1_E182K had a significantly reduced current in control conditions, 8 ± 1 pA/pF (n = 44) and 2 ± 1 pA/pF (n = 30) for TASK-1_WT and TASK-1_E182K respectively ($p < 0.05$, One-Way ANOVA with post-hoc Dunnett's, Figure 4.17A). In our hands, like the novel mutations (G106R and L214R) ONO-RS-082 (10 µM) failed to enhance TASK-1_E182K current with outward current measured at -40 mV (2 ± 1 pA/pF, n = 10 in control; 2 ± 1 pA/pF, n = 10 in ONO-RS-082 10 µM; $p > 0.05$, paired *t*-test, Figure 4.17B and C).

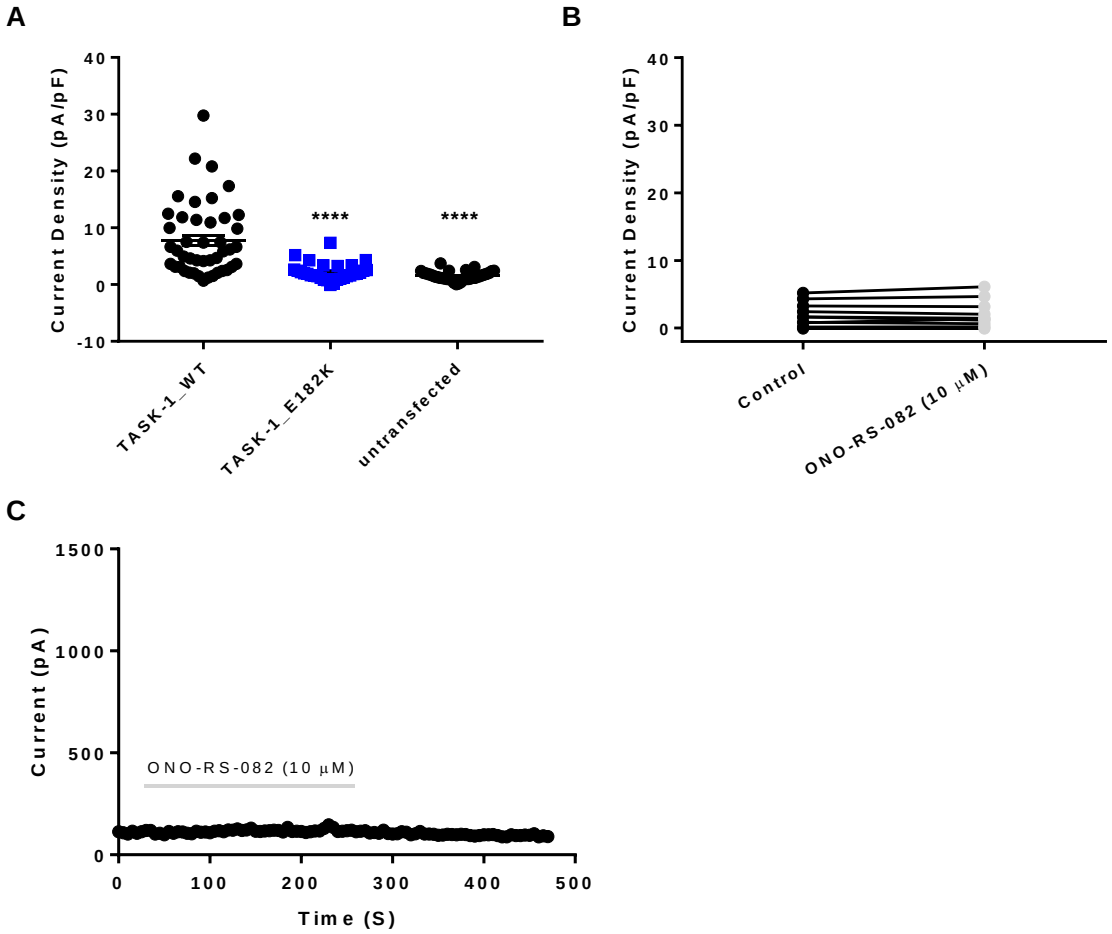

Figure 4.17 – Electrophysiological profile and response to ONO-RS-082 (10 µM) of TASK-1_E182K

A) Measurements of whole-cell current normalised against cell capacitance (pA/pF) at -40 mV for cells expressing TASK-1_WT and TASK-1_E182K. Error bars represent the SEM. B) Effect of ONO-RS-082 (10 µM) on TASK-1_E182K outward current measured at -40 mV. C) Time course graph showing TASK-1_E182K outward current at -40 mV under the influence of ONO-RS-082 (10 µM). Application of ONO-RS-082 (10 µM) is represented with the grey bar, absence of the grey bar represents cell in control conditions.

4.4 Results: Effect of Secondary Messenger Modulators on TASK-1 WT and Novel Mutations

Having shown that ONO-RS-082 failed to rescue current of the mutated channels G106R and L214R, and that the mutated channels were translated and trafficked to the plasma membrane as efficiently as the WT TASK-1 channel, it was decided to assess whether known PAH therapeutics could have an effect on TASK-1 and the novel mutations.

4.4.1 Effect of Sildenafil on TASK-1 WT and Novel Mutations

To assess the action of sildenafil (10 µM) upon TASK-1_WT and novel mutations in PAH patients, cells were incubated in either control conditions or extracellular solution containing sildenafil (10 µM) for 20 minutes prior to electrophysiological experiments. Incubation with sildenafil (10 µM) significantly enhanced the current of TASK-1_WT (Figure 4.18, $p < 0.05$, unpaired *t*-test). In control conditions the average TASK-1_WT outward current at -40 mV was 8 ± 1 pA/pF (n = 16) and after incubation 11 ± 1 pA/pF (n = 16). The average zero current potential was significantly hyperpolarised in the presence of sildenafil (10 µM) with values of -85 ± 2 mV (n = 16) in control conditions and -96 ± 2 mV (n = 16) under the influence of sildenafil (10 µM).

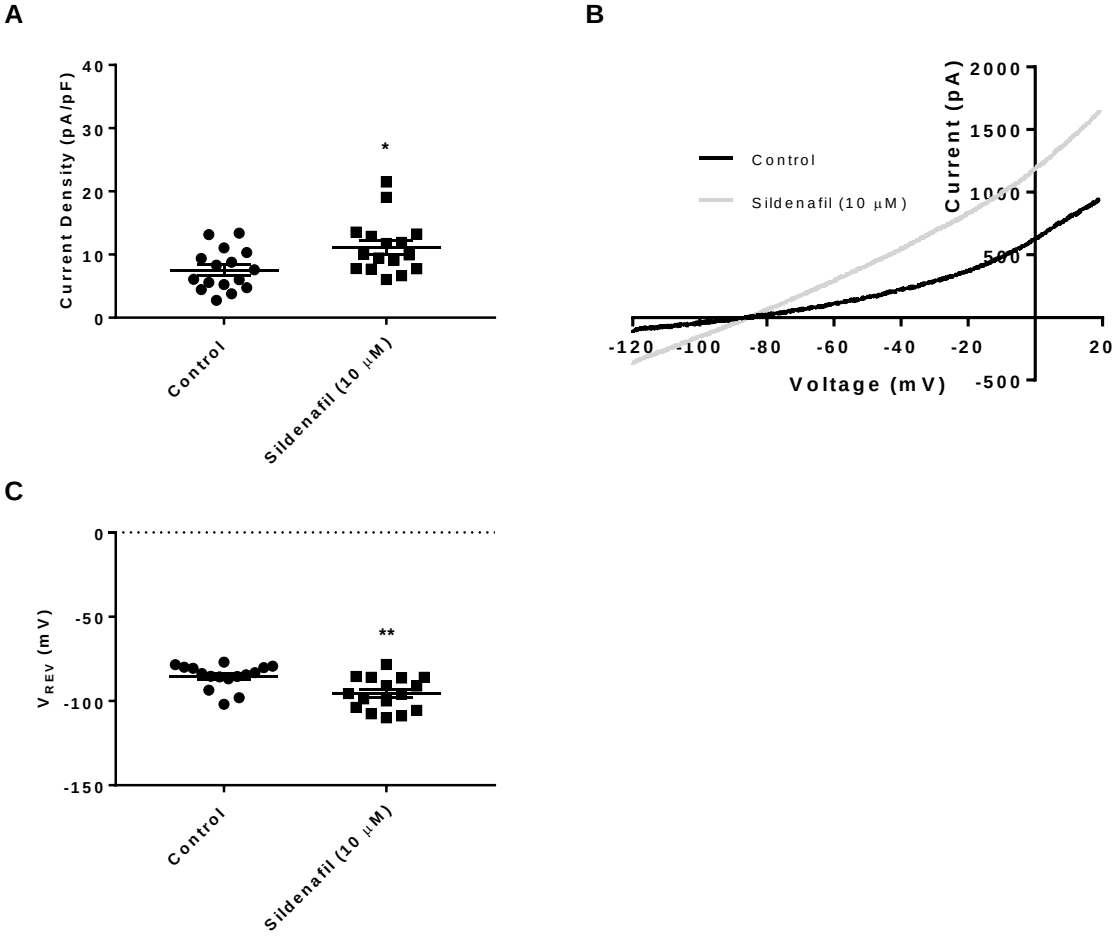

Figure 4.18 – Effect of Sildenafil (10 µM) on TASK-1_WT

A) Measurements of whole-cell current normalised against cell capacitance (pA/pF) at -40 mV for cells expressing TASK-1_WT in control conditions and sildenafil (10 µM). B) Current-voltage plot of TASK-1_WT in both control conditions (black line) and sildenafil (10 µM, grey line) recorded over a voltage ramp from -120 mV to +20 mV. C) Measurement of reversal potentials (mV) of cells expressing TASK-1_WT in control conditions and sildenafil (10 µM). Error bars represent SEM.

By contrast to TASK-1_WT, TASK-1_G106R outward current at -40 mV was not significantly affected by the incubation of sildenafil (10 µM, $p > 0.05$, unpaired *t*-test, Figure 4.19). TASK-1_G106R current in control conditions was measured as 1 ± 1 pA/pF (n = 6) and 2 ± 1 pA/pF (n = 6) in sildenafil (10 µM). Similarly to TASK-1_WT, the zero current potential of TASK-1_G106R was significantly hyperpolarised, however in this case closer to the equilibrium

potential for potassium ions under these recording conditions with values measured as -55 ± 2 mV (n = 6) in control conditions and -76 ± 9 mV (n = 6) in sildenafil (10 µM).

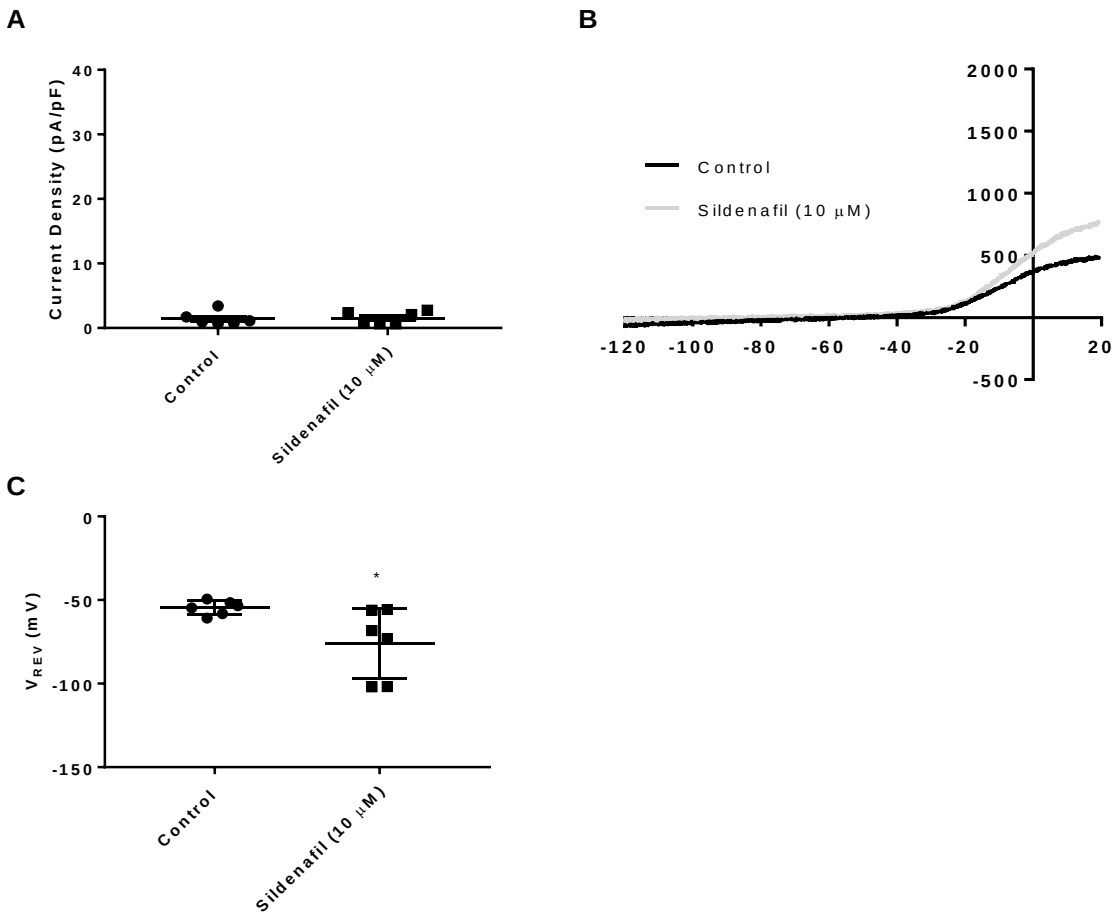

Figure 4.19 – Effect of Sildenafil (10 µM) on TASK-1_G106R

A) Measurements of whole-cell current normalised against cell capacitance (pA/pF) at -40 mV for cells expressing TASK-1_G106R in control conditions and sildenafil (10 µM). B) Current-voltage plot of TASK-1_G106R in both control conditions (black line) and sildenafil (10 µM, grey line) recorded over a voltage ramp from -120 mV to +20 mV. C) Measurement of reversal potentials (mV) of cells expressing TASK-1_G106R in control conditions and sildenafil (10 µM). Error bars represent SEM.

Similarly to TASK-1_G106R, sildenafil (10 µM) failed to increase TASK-1_L214R current (Figure 4.20). Outward TASK-1_L214R currents were

measured at -40 mV and in control conditions had values of 1 ± 1 pA/pF (n = 5) and in sildenafil (10 µM) 2 ± 1 pA/pF (n = 5). Unlike both TASK-1_WT and TASK-1_G106R, sildenafil (10 µM) had no effect on the zero current potential of TASK-1_L214R with -57 ± 4 mV (n = 5) in control conditions and -55 ± 2 mV (n = 5) under the influence of sildenafil (10 µM).

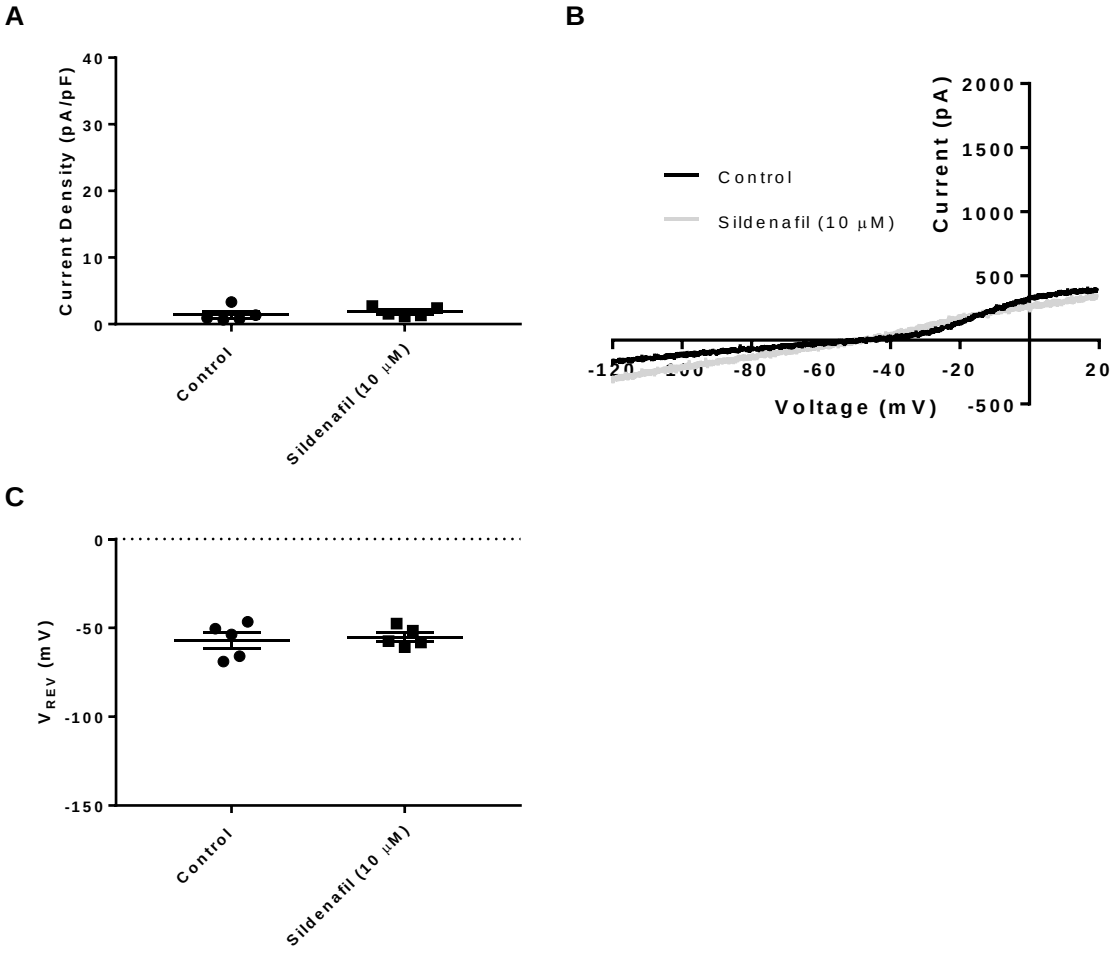

Figure 4.20 – Effect of Sildenafil (10 µM) on TASK-1_L214R

A) Measurements of whole-cell current normalised against cell capacitance (pA/pF) at -40 mV for cells expressing TASK-1_L214R in control conditions and sildenafil (10 µM). B) Current-voltage plot of TASK-1_L214R in both control conditions (black line) and sildenafil (10 µM, grey line) recorded over a voltage ramp from -120 mV to +20 mV. C) Measurement of reversal potentials (mV) of cells expressing TASK-1_L214R in control conditions and sildenafil (10 µM). Error bars represent SEM.

4.4.2 Effect of IBMX on TASK-1_WT

As the use of the selective PDE5 inhibitor enhanced WT TASK-1 current, it was decided to study a non-selective PDE inhibitor, IBMX. Unlike sildenafil, outward TASK-1_WT channel current incubated for 20 minutes with an extracellular solution containing IBMX (100 µM), did not significantly increase ($p > 0.05$, unpaired *t*-test, Figure 4.21). In control conditions at -40 mV, TASK-1_WT outward current measured was 7 ± 1 pA/pF (n = 17) and after incubation with IBMX (100 µM) was 9 ± 1 pA/pF (n = 16).

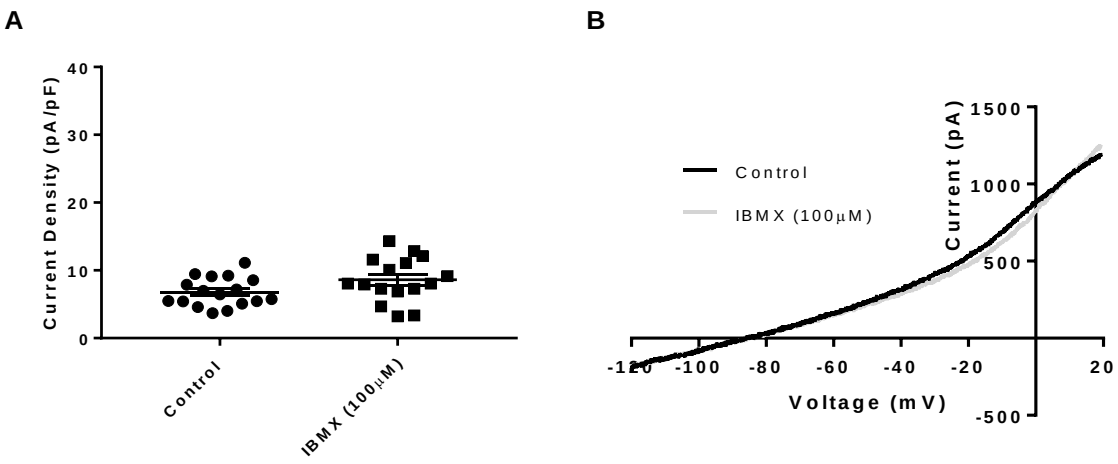

Figure 4.21 – Effect of IBMX (100 µM) on TASK-1_WT

A) Measurements of whole-cell current normalised against cell capacitance (pA/pF) at -40 mV for cells expressing TASK-1_WT in control conditions and IBMX (100 µM). B) Current-voltage plot of TASK-1_WT in both control conditions (black line) and IBMX (100 µM, grey line) recorded over a voltage ramp from -120 mV to +20 mV.

4.4.3 Effect of combining Sildenafil and IBMX on TASK-1_WT

As sildenafil (10 µM) significantly increased TASK-1_WT current whereas IBMX (100 µM) did not, investigating the combination of both compounds and its effect on TASK-1_WT was the next approach. The combination of the two compounds failed to significantly alter TASK-1_WT outward current at -40 mV

(p > 0.05, unpaired *t*-test, Figure 4.22). In control conditions at -40 mV, TASK-1_WT outward current measured was 7 ± 1 pA/pF (n = 16) and after incubation with sildenafil (10 µM) and IBMX (100 µM) was 8 ± 1 pA/pF (n = 17). Interestingly the addition of IBMX (100 µM) abolished the enhancing effects of sildenafil (10 µM) alone upon TASK-1_WT.

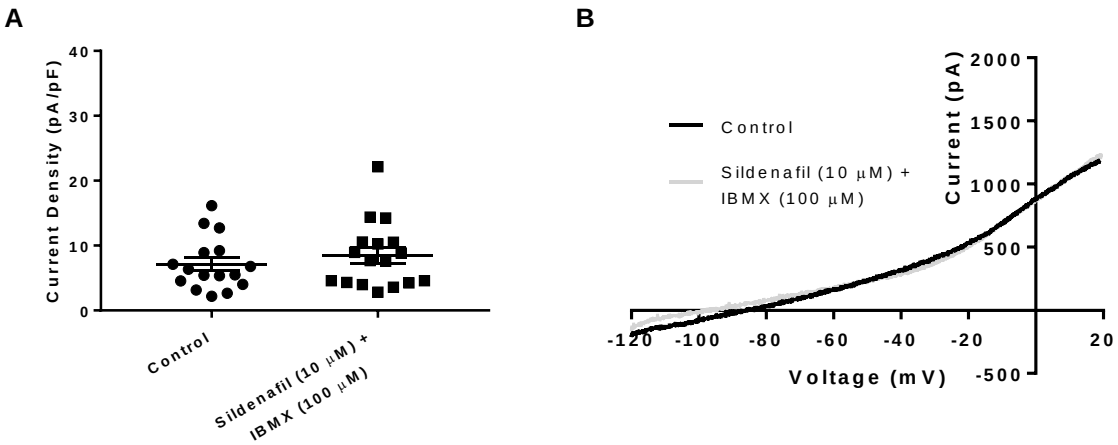

Figure 4.22 – Effect of Sildenafil (10 µM) + IBMX (100 µM) on TASK-1_WT

A) Measurements of whole-cell current normalised against cell capacitance (pA/pF) at -40 mV for cells expressing TASK-1_WT in control conditions and sildenafil (10 µM) + IBMX (100 µM). B) Current-voltage plot of TASK-1_WT in both control conditions (black line) and sildenafil (10 µM) + IBMX (100 µM, grey line) recorded over a voltage ramp from -120 mV to +20 mV.

4.4.4 Action of IBMX and Forskolin combination upon TASK-1_WT

Previous work conducted in our lab has shown that the combination of IBMX (100 µM) and forskolin (10 µM) on mouse concatamers of TASK-1 and TASK-3 has the ability to enhance outward current (appendix 6.10). In human TASK-1_WT channels the combination of IBMX (100 µM) and forskolin (10 µM) significantly enhanced TASK-1_WT current in a similar fashion to the mouse

concatamers ($p < 0.05$, unpaired *t*-test, Figure 4.23). After 20 minutes incubation with IBMX (100 µM) and forskolin (10 µM) TASK-1_WT outward currents at -40 mV were 14 ± 2 pA/pF (n = 21) compared to 6 ± 1 pA/pF (n = 21) in control conditions.

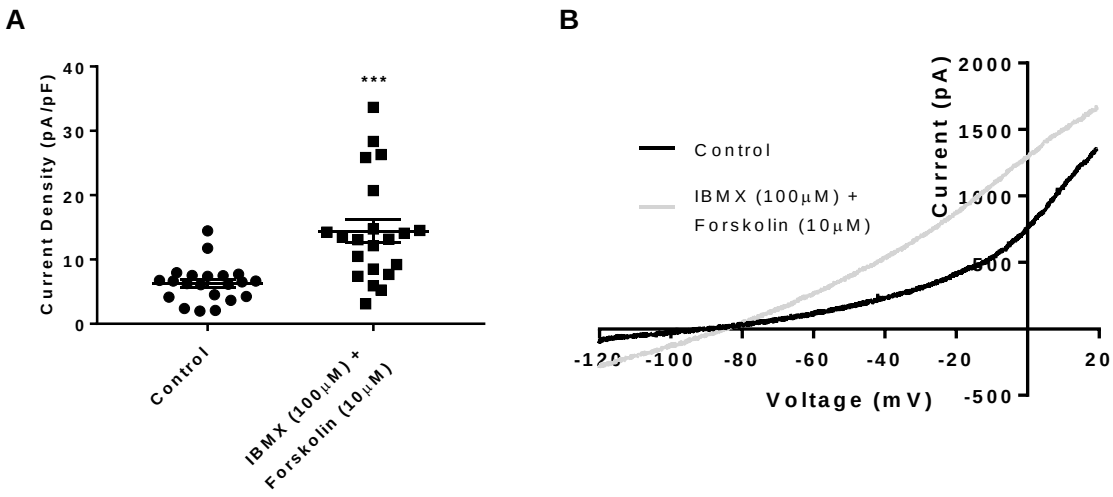

Figure 4.23 – Effect of IBMX (100 µM) + Forskolin (10 µM) on TASK-1_WT

A) Measurements of whole-cell current normalised against cell capacitance (pA/pF) at -40 mV for cells expressing TASK-1_WT in control conditions and IBMX (100 µM) + Forskolin (10 µM). B) Current-voltage plot of TASK-1_WT in both control conditions (black line) and IBMX (100 µM) + Forskolin (10 µM, grey line) recorded over a voltage ramp from -120 mV to +20 mV.

4.4.5 Effect of Riociguat on TASK-1 WT and Novel Mutations

Cells expressing TASK-1_WT were incubated in the soluble guanylyl cyclase stimulator, riociguat (10 µM), for 20 minutes prior to electrophysiological experiments. The incubation in riociguat (10 µM) significantly increased the outward current of TASK-1_WT measured at -40 mV, 11 ± 2 pA/pF (n = 17)

compared to 6 ± 1 pA/pF (n = 19) in control conditions ($p < 0.05$, unpaired *t*-test, Figure 4.24).

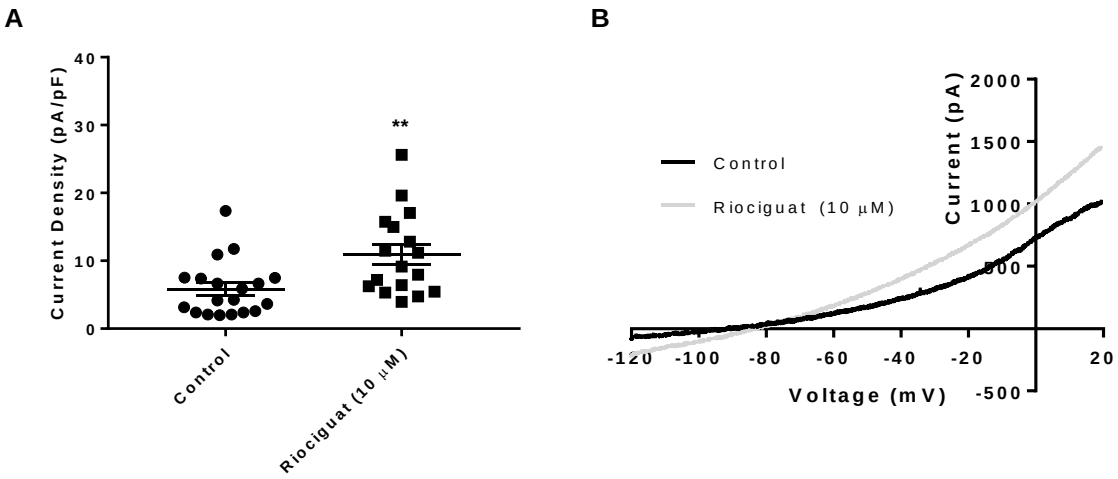

Figure 4.24 – Effect of Riociguat (10 µM) on TASK-1_WT

A) Measurements of whole-cell current normalised against cell capacitance (pA/pF) at -40 mV for cells expressing TASK-1_WT in control conditions and riociguat (10 µM). B) Current-voltage plot of TASK-1_WT in both control conditions (black line) and riociguat (10 µM, grey line) recorded over a voltage ramp from -120 mV to +20 mV.

The reduced outward current at -40 mV through TASK-1_G106R channels could not be significantly increased after incubation with riociguat (10 µM) with currents measured at 2 ± 1 pA/pF (n = 15) compared to 3 ± 1 pA/pF (n = 19) in control conditions ($p < 0.05$, unpaired *t*-test, Figure 4.25).

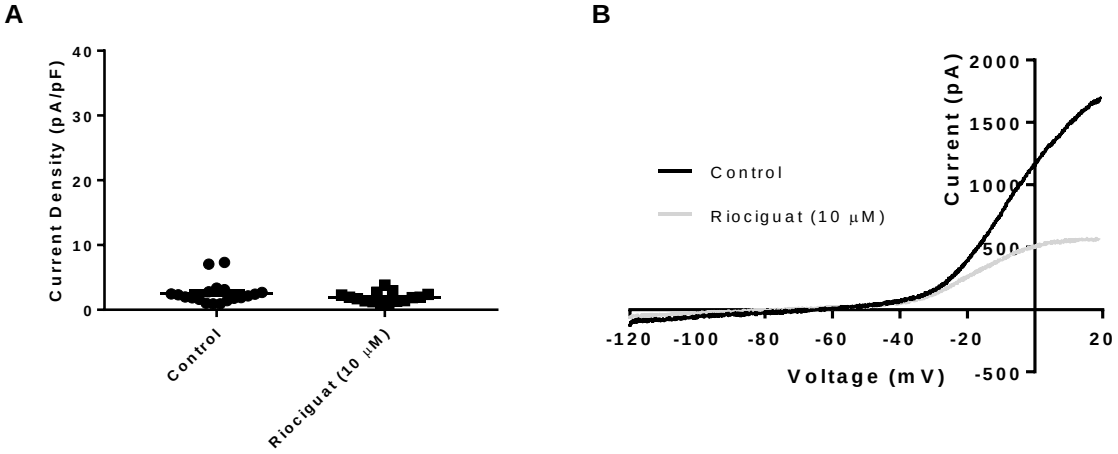

Figure 4.25 – Effect of Riociguat (10 µM) on TASK-1_G106R

A) Measurements of whole-cell current normalised against cell capacitance (pA/pF) at -40 mV for cells expressing TASK-1_G106R in control conditions and riociguat (10 µM). B) Current-voltage plot of TASK-1_G106R in both control conditions (black line) and riociguat (10 µM, grey line) recorded over a voltage ramp from -120 mV to +20 mV.

Similarly to TASK-1_G106R, TASK-1_L214R also had no significant outward current change at -40 mV after incubation with riociguat (10 µM, Figure 4.26). In control conditions, TASK-1_L214R outward currents at -40 mV were measured as 2 ± 1 pA/pF (n = 15) and 2 ± 1 pA/pF (n = 19).

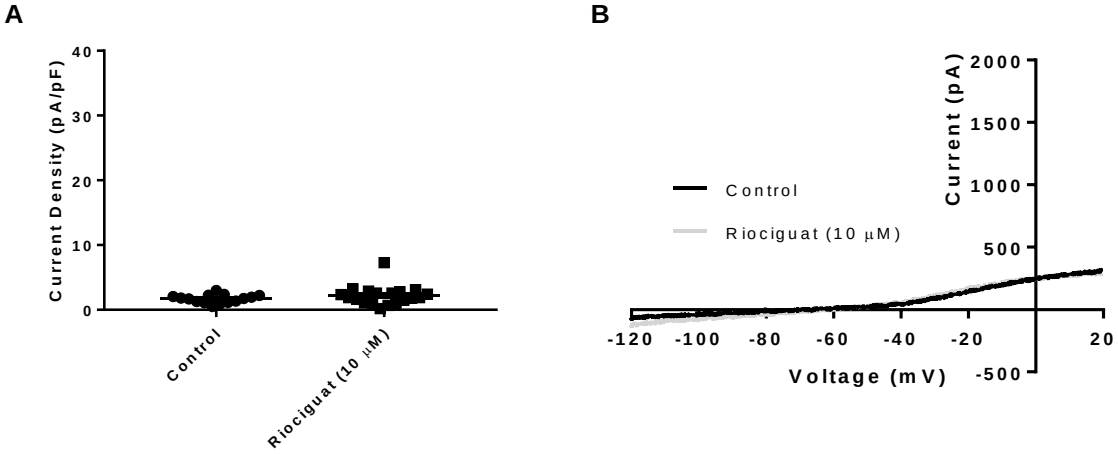

Figure 4.26 – Effect of Riociguat (10 µM) on TASK-1_L214R

A) Measurements of whole-cell current normalised against cell capacitance (pA/pF) at -40 mV for cells expressing TASK-1_L214R in control conditions and riociguat (10 µM). B) Current-voltage plot of TASK-1_L214R in both control conditions (black line) and riociguat (10 µM, grey line) recorded over a voltage ramp from -120 mV to +20 mV.

4.5 Results: Effect of Treprostinil on TASK-1, TREK-1 and TREK-2 K2P channels

Treprostinil, a synthetic prostacyclin analogue, targets a different pathway (the prostacyclin pathway) in PAH, compared to compounds previously explored within this study. Vasodilatory tests are used to determine how pulmonary blood vessels respond to treatments, it also helps with determining prognosis for patients. As treprostinil has been shown to exceed vasodilatory testing

predictions, it may have additional mechanisms of action, such as targeting and enhancing TASK-1 current (Clapp and Gurung, 2015).

4.5.1 Effect of Acute Application of Treprostinil on TASK-1_WT

To assess whether treprostinil has a direct effect on the TASK-1_WT channel, treprostinil (100 nM) was acutely applied and yielded no significant change in TASK-1_WT outward current when measured at -40 mV ($p > 0.05$, paired *t*-test, Figure 4.27). TASK-1_WT current at -40 mV in the presence of treprostinil (100 nM) was 8 ± 1 pA/pF (n = 7) compared to 7 ± 1 pA/pF (n = 7) in control conditions.

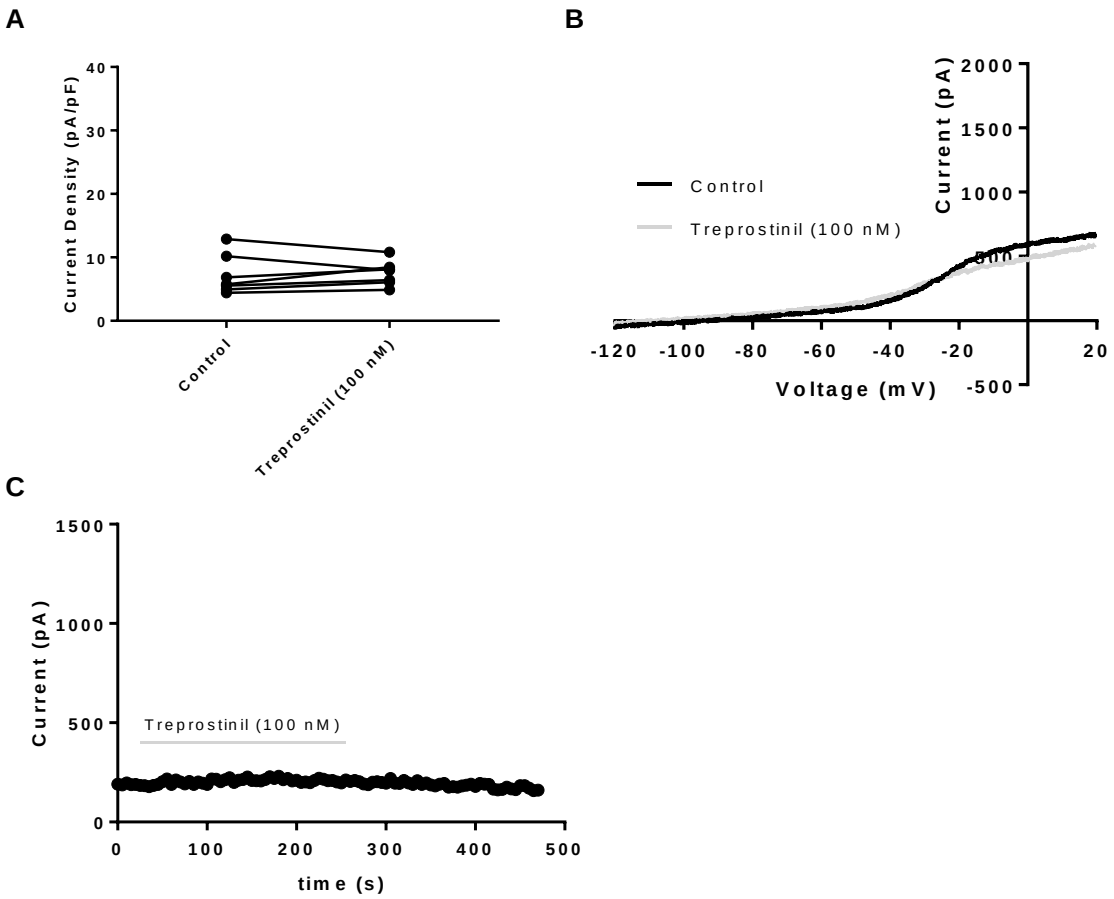

Figure 4.27 – Effect of Acutely Applied Treprostinil (100 nM) on TASK-1_WT

A) Measurements of whole-cell current normalised against cell capacitance (pA/pF) at -40 mV for cells expressing TASK-1_WT in control conditions and treprostinil (100 nM). B) Current-voltage plot of TASK-1_WT in both control conditions (black line) and treprostinil (100 nM, grey line) recorded over a voltage ramp from -120 mV to +20 mV. C) Time course graph showing TASK-1_WT outward current at -40 mV under the influence of treprostinil (100 nM). Treprostinil (100 nM) application is represented at the grey bar, absence of the grey bar represents control conditions.

A 10-fold increase in treprostinil concentration to 1 µM, also had no significant effect on TASK-1_WT outward current ($p > 0.05$, paired *t*-test, Figure 4.28). In control conditions TASK-1_WT currents were measured at 6 ± 2 pA/pF (n = 5) and after acute application of treprostinil (1 µM) at 6 ± 1 pA/pF (n = 5).

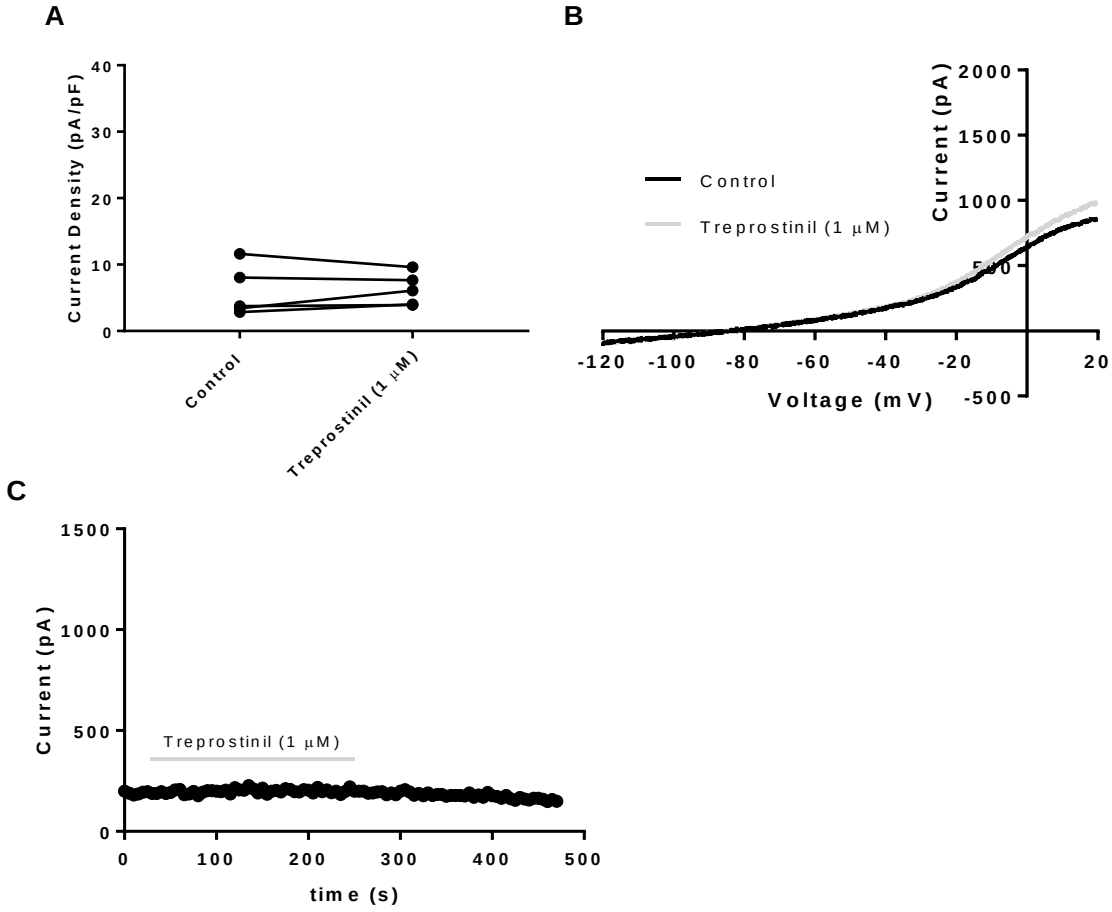

Figure 4.28 – Effect of Acutely Applied Treprostinil (1 μM) on TASK-1_WT

A) Measurements of whole-cell current normalised against cell capacitance (pA/pF) at -40 mV for cells expressing TASK-1_WT in control conditions and treprostinil (1 μM). B) Current-voltage plot of TASK-1_WT in both control conditions (black line) and treprostinil (1 μM, grey line) recorded over a voltage ramp from -120 mV to +20 mV. C) Time course graph showing TASK-1_WT outward current at -40 mV under the influence of treprostinil (1 μM). Treprostinil (1 μM) application is represented at the grey bar, absence of the grey bar represents control conditions.

A further 10-fold increase in treprostinil concentration to 10 μM also had no significant effect on TASK-1_WT outward current ($p > 0.05$, paired *t*-test, Figure 4.29). Under acute application with treprostinil (10 μM), TASK-1_WT outward current measured at -40 mV was 12 ± 2 pA/pF (n = 5) compared to 13 ± 3 pA/pF (n = 5) in control conditions.

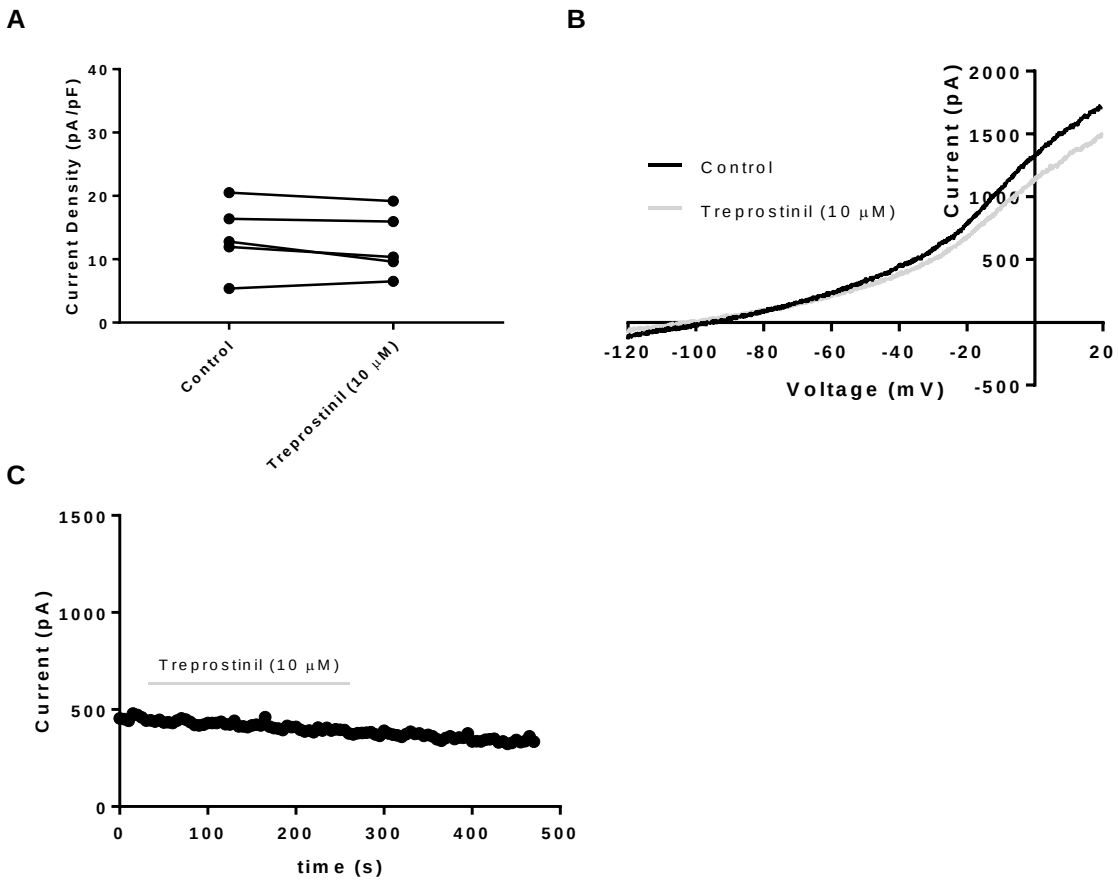

Figure 4.29 – Effect of Acutely Applied Treprostinil (10 µM) on TASK-1_WT

A) Measurements of whole-cell current normalised against cell capacitance (pA/pF) at -40 mV for cells expressing TASK-1_WT in control conditions and treprostinil (10 µM). B) Current-voltage plot of TASK-1_WT in both control conditions (black line) and treprostinil (10 µM, grey line) recorded over a voltage ramp from -120 mV to +20 mV. C) Time course graph showing TASK-1_WT outward current at -40 mV under the influence of treprostinil (10 µM). Treprostinil (10 µM) application is represented at the grey bar, absence of the grey bar represents control conditions.

4.5.2 Effect of Treprostinil Pre-Incubation on TASK-1_WT

As treprostinil appeared to have no direct action upon TASK-1_WT channels across a range of concentrations, investigation into whether treprostinil had an effect signalling pathways, which affect TASK-1_WT outward current was conducted by incubation with treprostinil. Incubation with treprostinil (1 µM), as described in the section 2.3.1, significantly enhanced outward TASK-1_WT

current at -40 mV being 11 ± 1 pA/pF (n = 15) compared to 7 ± 1 (n = 17) in control conditions ($p < 0.05$, unpaired *t*-test, Figure 4.30).

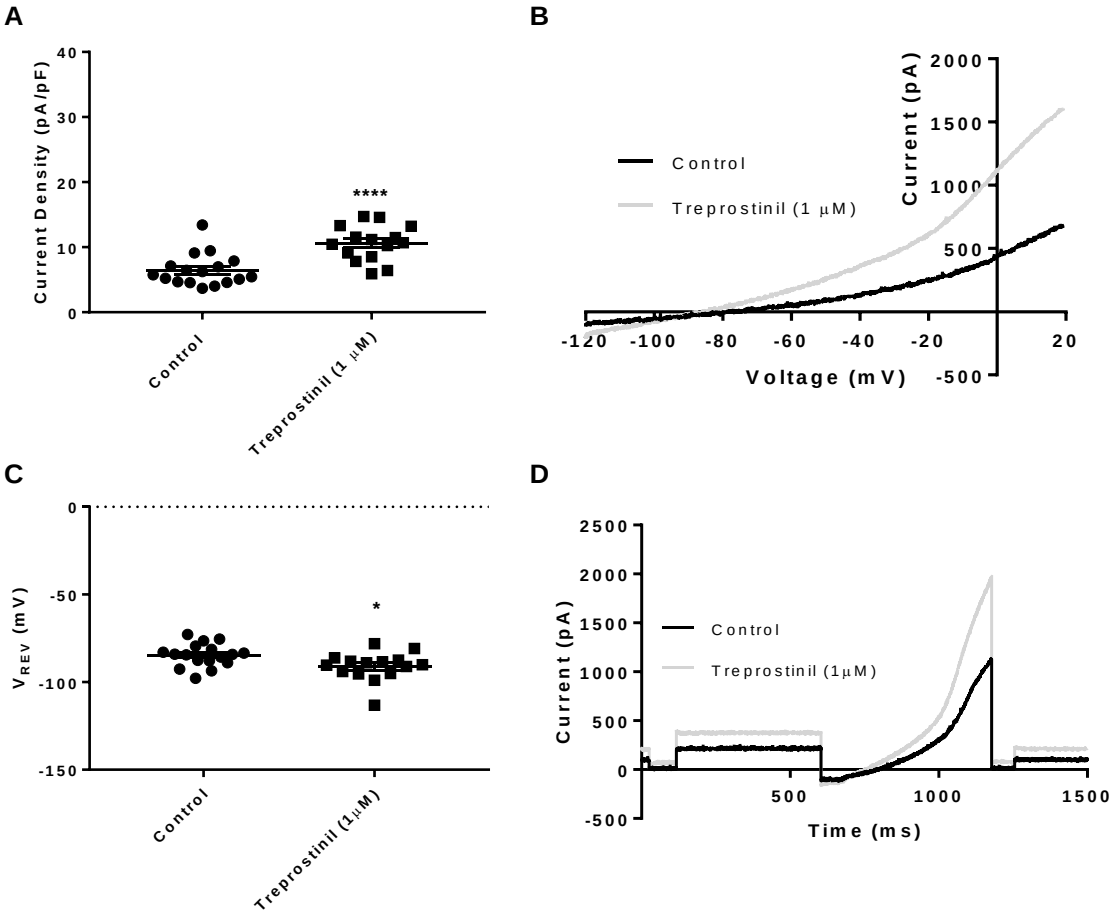

Figure 4.30 – Effect on TASK-1_WT due to incubation with Treprostinil (1 μM)

A) Measurements of whole-cell current normalised against cell capacitance (pA/pF) at -40 mV for cells expressing TASK-1_WT in control conditions and treprostinil (1 μM). B) Current-voltage plot of TASK-1_WT in both control conditions (black line) and treprostinil (1 μM, grey line) recorded over a voltage ramp from -120 mV to +20 mV. C) Measurement of reversal potentials (mV) of cells expressing TASK-1_WT in control conditions and treprostinil (1 μM). Error bars represent SEM. D) Representation of a raw data trace of TASK-1_WT in control conditions (black line) and treprostinil (1 μM, grey line) under the step-ramp voltage protocol.

4.5.3 Co-expression of TASK-1_WT with Prostanoid Receptors

As our data suggests that, treprostinil can activate TASK-1_WT is an undetermined manner, it would suggest that it acts through an alternative secondary messenger-mediated pathway. We investigated whether the expression of prostanoid receptors (DP_2, EP_2 and IP) has an effect on TASK-1_WT channel functionality and its response to treprostinil. When co-expressed with the prostanoid receptor DP_2, TASK-1_WT outward current was not significantly altered ($p > 0.05$, one-way ANOVA, Figure 4.31). TASK-1_WT only outward current at -40 mV was measured at 6 ± 1 pA/pF (n = 22) and co-expression with DP_2 did not significantly affect current at 11 ± 2 pA/pF (n = 11). In contrast, co-expression with the EP_2 receptor significantly increased TASK-1_WT outward current with values of 11 ± 1 pA/pF (n = 23; $p < 0.05$, one-way ANOVA, Figure 4.31). Similarly to DP_2, co-expression of TASK-1_WT with IP receptor did not yield a significant change in outward current at -40 mV, 8 ± 1 pA/pF (n = 22; $p > 0.05$, Figure 4.31).

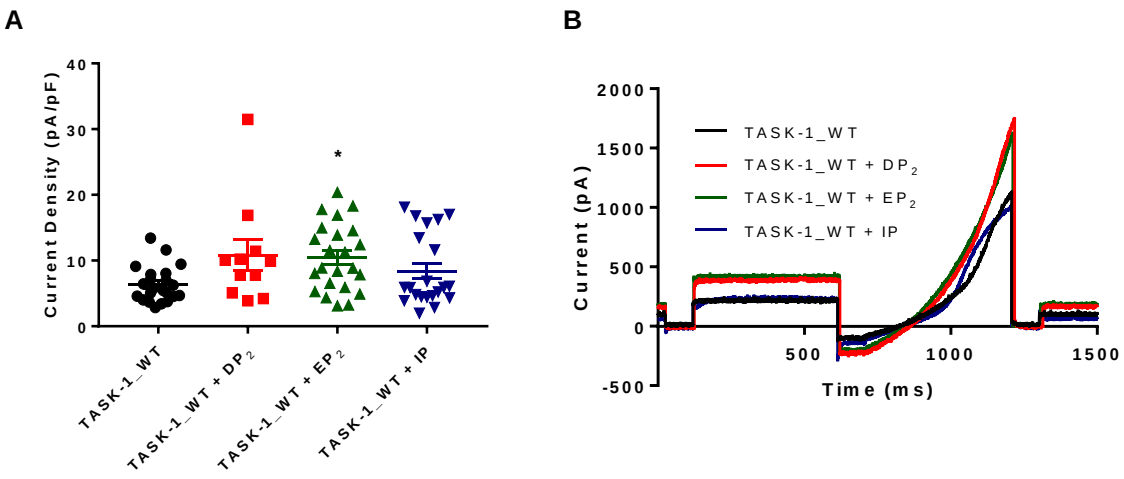

Figure 4.31 – Co-expression of prostanoid receptors DP_2, EP_2 and IP with TASK-1_WT

A) Measurements of whole-cell current normalised against cell capacitance (pA/pF) at -40 mV for cells expressing TASK-1_WT (black), TASK-1_WT + DP_2 (red), TASK-1_WT + EP_2 (green) or TASK-1_WT + IP (blue). Error bars represent the SEM. B)

Representation of a raw data trace of TASK-1_WT (black line), TASK-1_WT + DP_2 (red line), TASK-1_WT + EP_2 (green line) and TASK-1_WT + IP (blue line) under the step-ramp voltage protocol.

4.5.4 Effect of Treprostinil Pre-Incubation on TASK-1_WT Channels Co-expressed with Prostanoid Receptors

Pre-incubation of cells expressing TASK-1_WT only with treprostinil (1 µM) lead to a significant increase in outward current measured at -40 mV (Figure 4.30). With the co-expression of TASK-1_WT and DP_2, pre-incubating cells with 20 minutes incubation in treprostinil (1 µM) did not significantly alter outward current measured at -40 mV ($p > 0.05$, unpaired *t*-test, Figure 4.32). In control conditions outward current values were 12 ± 4 pA/pF (n = 6) and 16 ± 4 pA/pF (n = 6) after incubation with treprostinil (1 µM).

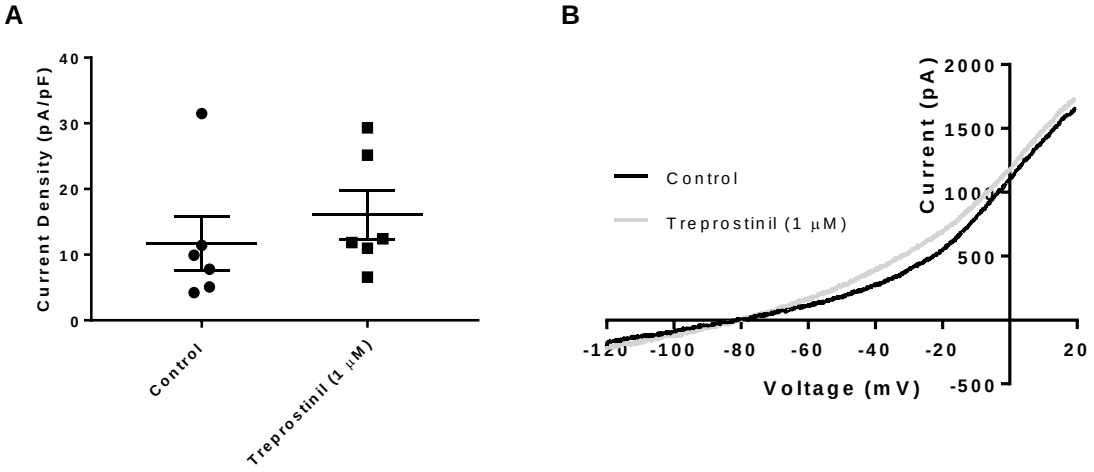

Figure 4.32 – Effect of Treprostinil (1 μM) Pre-incubation on Co-expressed TASK-1_WT and DP_2 receptor

A) Measurements of whole-cell current normalised against cell capacitance (pA/pF) at -40 mV for cells expressing TASK-1_WT and DP_2 receptor in control conditions and after 20 minutes incubation with treprostinil (1 μM). B) Current-voltage plot of TASK-1_WT and DP_2 in both control conditions (black line) and after 20 minutes incubation with treprostinil (1 μM, grey line) recorded over a voltage ramp from -120 mV to +20 mV.

Co-expression of TASK-1_WT and EP_2 receptor leads to an increase in TASK-1_WT current compared to cells expressing only TASK-1_WT (Figure 4.31). This increased current could not be further enhanced with the pre-incubation of cells with treprostinil (1 μM). In control conditions TASK-1_WT and EP_2 was measured at 12 ± 1 (n = 15) compared to 13 ± 2 (n = 16; $p > 0.05$, in treprostinil, unpaired *t*-test, Figure 4.33).

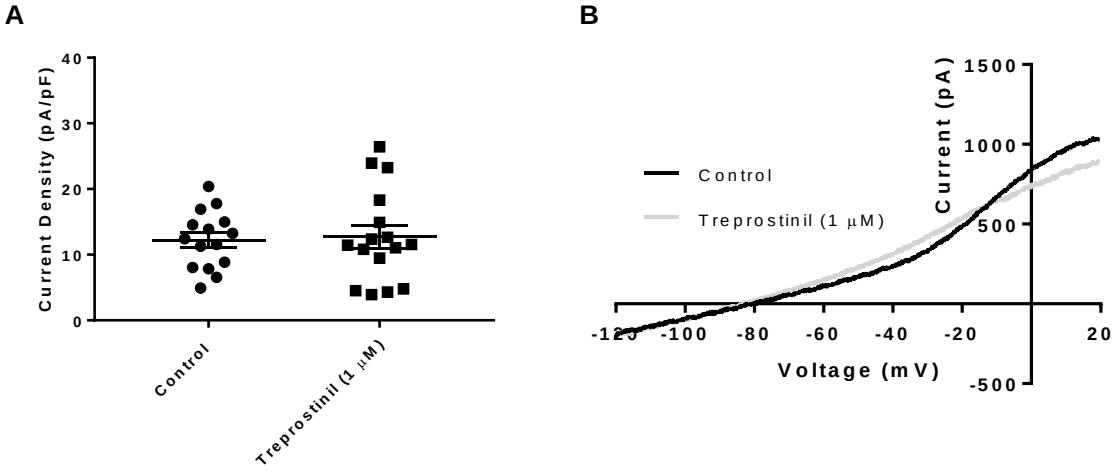

Figure 4.33 – Effect of Treprostinil (1 μM) Pre-incubation on Co-expressed TASK-1_WT and EP_2 receptor

A) Measurements of whole-cell current normalised against cell capacitance (pA/pF) at -40 mV for cells expressing TASK-1_WT and EP_2 receptor in control conditions and after 20 minutes incubation with treprostinil (1 μM). B) Current-voltage plot of TASK-1_WT and EP_2 in both control conditions (black line) and after 20 minutes incubation with treprostinil (1 μM, grey line) recorded over a voltage ramp from -120 mV to +20 mV.

Similarly to the co-expression of TASK-1_WT with DP_2 and EP_2, the co-expression of TASK-1_WT and IP receptor, could not be enhanced with pre-incubation of treprostinil (1 μM). In control conditions outward currents measured at -40 mV were 8 ± 1 pA/pF (n = 15) and 7 ± 2 pA/pF (n = 16) after treprostinil treatment ($p > 0.05$, unpaired *t*-test, Figure 4.34).

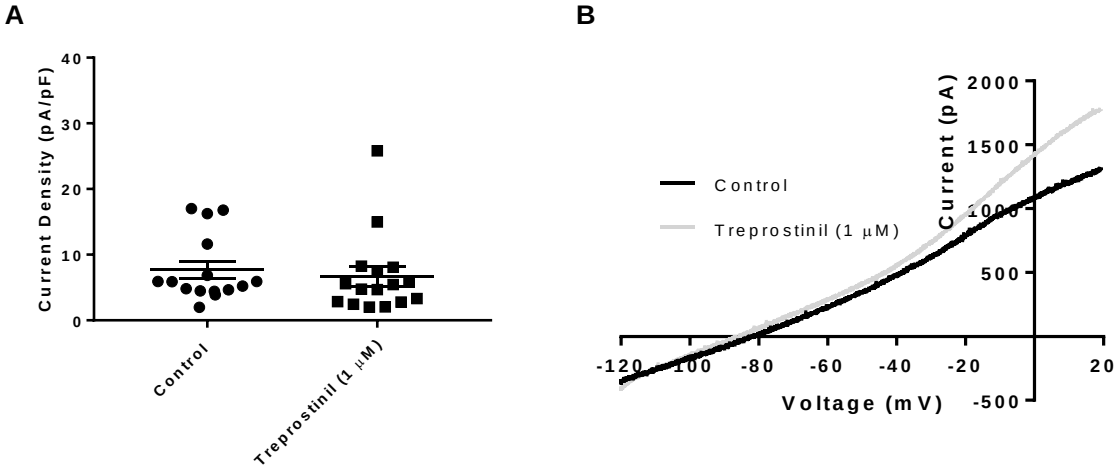

Figure 4.34 – Effect of Treprostinil (1 μM) Pre-incubation on Co-expressed TASK-1_WT and IP receptor

A) Measurements of whole-cell current normalised against cell capacitance (pA/pF) at -40 mV for cells expressing TASK-1_WT and IP receptor in control conditions and after 20 minutes incubation with treprostinil (1 μM). B) Current-voltage plot of TASK-1_WT and IP in both control conditions (black line) and after 20 minutes incubation with treprostinil (1 μM, grey line) recorded over a voltage ramp from -120 mV to +20 mV.

Analysis of co-expressed receptors with TASK-1_WT channels highlighted only a tonic increase in TASK-1_WT outward current when expressed with EP_2 receptor ($p < 0.05$, two-way ANOVA, Figure 4.35). Pre-incubation of cells with treprostinil (1 μM), failed to significantly enhance cells co-expressing the prostanoid receptors (DP_2, EP_2 or IP).

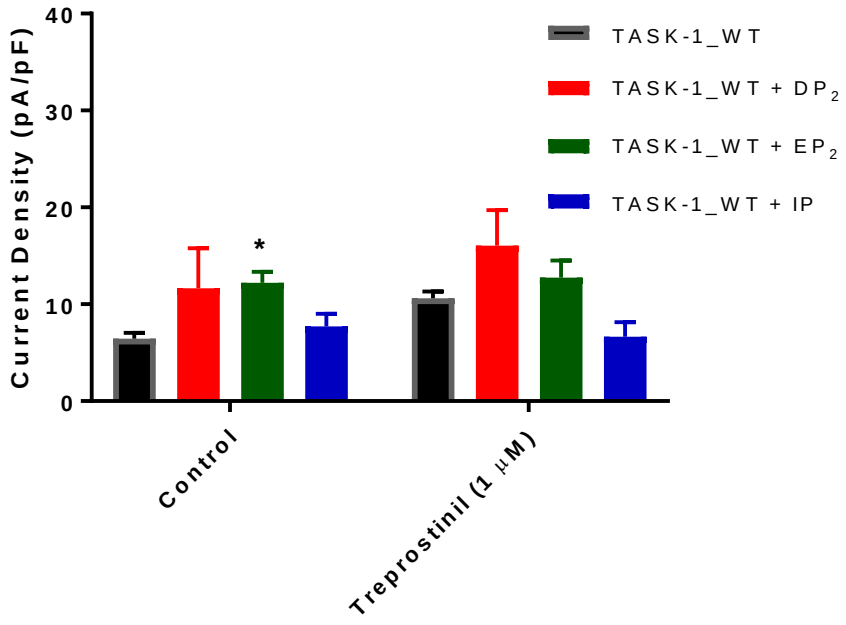

Figure 4.35 – Measurement of TASK-1_WT current of cells co-expressed with prostanoid receptors following incubation with treprostinil (1 µM)

A) Chart showing measurements of whole-cell current normalised against cell capacitance (pA/pF) at -40 mV for cells expressing TASK-1_WT either solo or with DP_2, EP_2 or IP receptor in control conditions and after 20 minutes incubation with treprostinil (1 µM). Error bars represent SEM.

4.5.5 Effect of Acute Application of Treprostinil on TASK-1_WT Channels Co-expressed with Prostanoid Receptors

The effect of treprostinil (1 µM) when applied acutely had no effect upon TASK-1_WT outward current measured at -40 mV (Figure 4.27-4.29). The co-expression of prostanoid receptors changed the response of treprostinil (1 µM)

acute application on TASK-1_WT current in a receptor dependent manner. The co-expression of TASK-1_WT and DP_2 receptor did not significantly alter outward current measured at -40 mV ($p > 0.05$, paired *t*-test, Figure 4.36). In control conditions, outward current was 10 ± 2 pA/pF (n = 5) and 10 ± 2 pA/pF (n = 5) after acute application of treprostinil (1 µM).

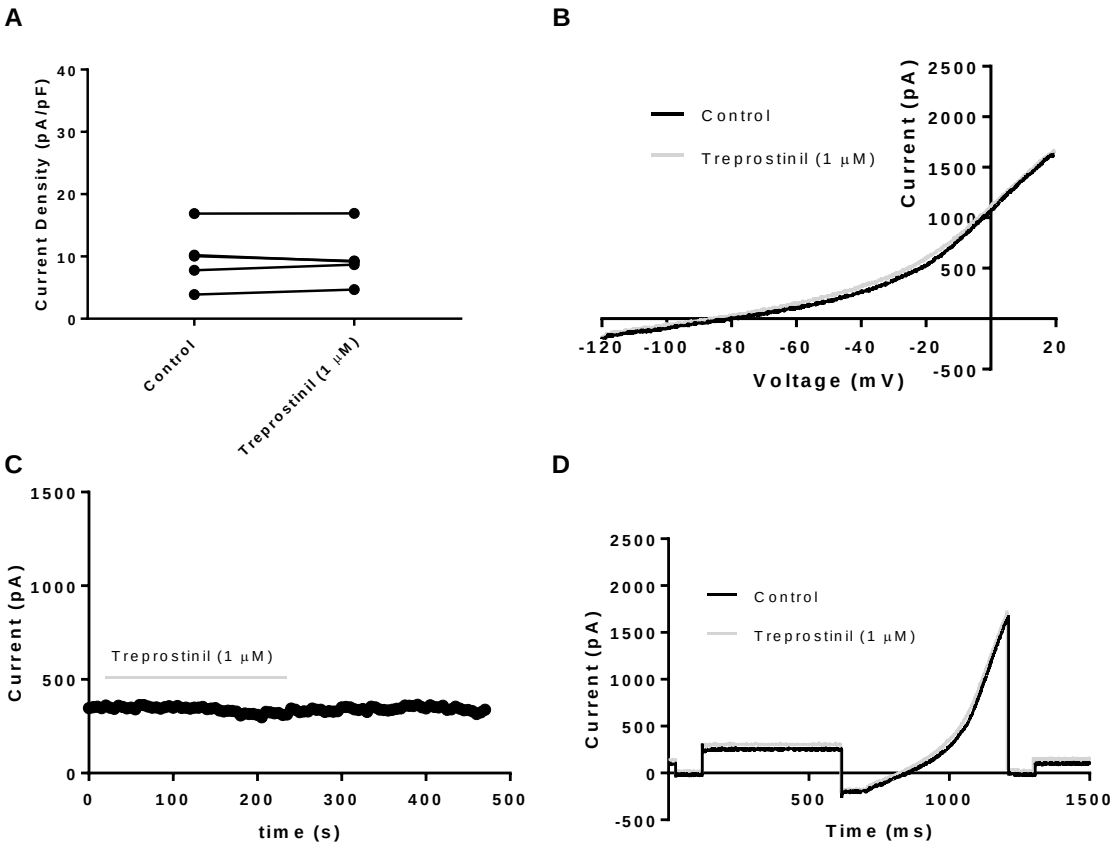

Figure 4.36 – Effect of Acute Application of Treprostinil (1 µM) on Co-expressed TASK-1_WT and DP_2 receptor

A) Measurements of whole-cell current normalised against cell capacitance (pA/pF) at -40 mV for cells expressing TASK-1_WT and DP_2 in control conditions and treprostinil (1 µM). B) Current-voltage plot of TASK-1_WT and DP_2 in both control conditions (black line) and treprostinil (1 µM, grey line) recorded over a voltage ramp

from -120 mV to +20 mV. C) Time course graph showing TASK-1_WT and DP_2 outward current at -40 mV under the influence of treprostinil (1 µM). Treprostinil (1 µM) application is represented at the grey bar, absence of the grey bar represents control conditions. D) Representation of a raw data trace of TASK-1_WT and DP_2 in both control conditions (black line) and treprostinil (1 µM, grey line) under the step-ramp voltage protocol.

Acute application of treprostinil (1 µM) significantly enhanced TASK-1_WT current when co-expressed with the EP_2 receptor ($p < 0.05$, paired *t*-test, Figure 4.37). In control conditions, outward current of TASK-1_WT channels in cells expressing TASK-1_WT + EP_2 was 7 ± 2 (n = 8) and after acute application of treprostinil (1 µM) was 9 ± 2 (n = 8).

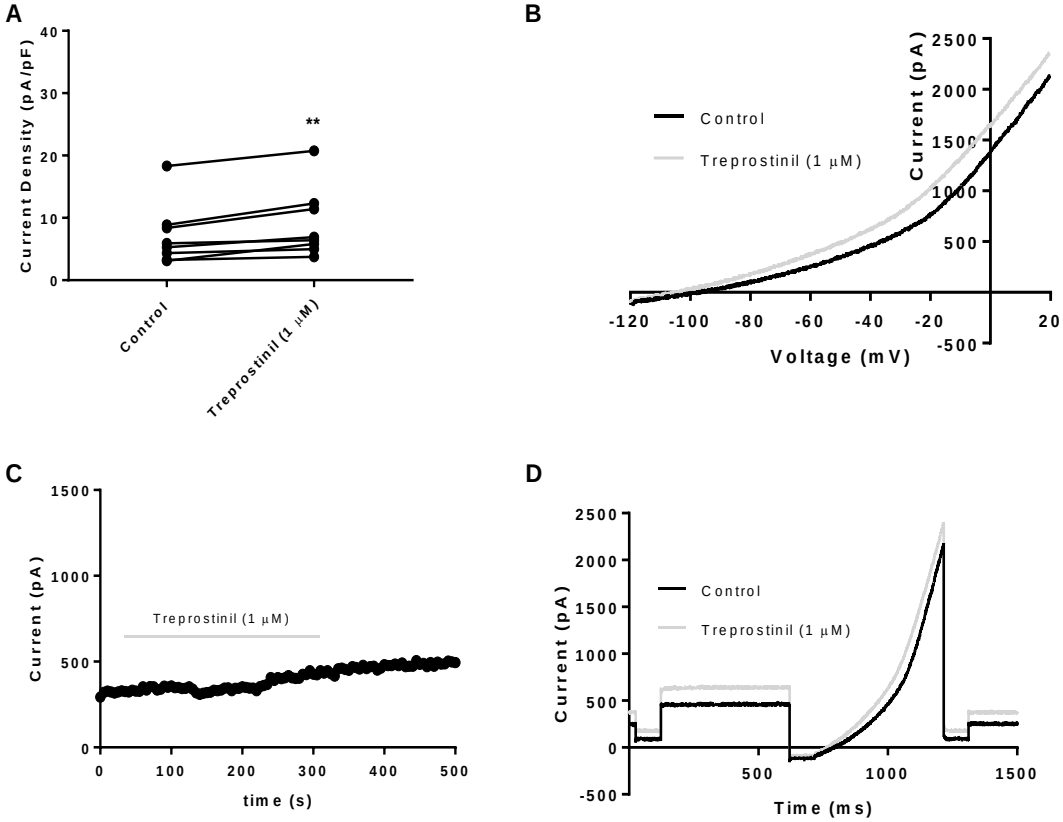

Figure 4.37 – Effect of Acute Application of Treprostinil (1 μM) on Co-expressed TASK-1_WT and EP_2 receptor

A) Measurements of whole-cell current normalised against cell capacitance (pA/pF) at -40 mV for cells expressing TASK-1_WT and EP_2 in control conditions and treprostinil (1 μM). B) Current-voltage plot of TASK-1_WT and EP_2 in both control conditions (black line) and treprostinil (1 μM, grey line) recorded over a voltage ramp from -120 mV to +20 mV. C) Time course graph showing TASK-1_WT and EP_2 outward current at -40 mV under the influence of treprostinil (1 μM). Treprostinil (1 μM) application is represented at the grey bar, absence of the grey bar represents control conditions. D) Representation of a raw data trace of TASK-1_WT and EP_2 in both control conditions (black line) and treprostinil (1 μM, grey line) under the step-ramp voltage protocol.

Interestingly, co-expression of TASK-1_WT and IP receptor had the opposite effect to EP_2 when exposed to acute application of treprostinil (1 μM) with a significant reduction in TASK-1_WT current ($p < 0.05$, paired *t*-test, Figure 4.38). In control conditions, outward current of TASK-1_WT channels in cells

expressing TASK-1_WT + IP was 10 ± 2.6 (n = 6) and after acute application of treprostinil (1 µM) was 5.4 ± 1.7 (n = 6).

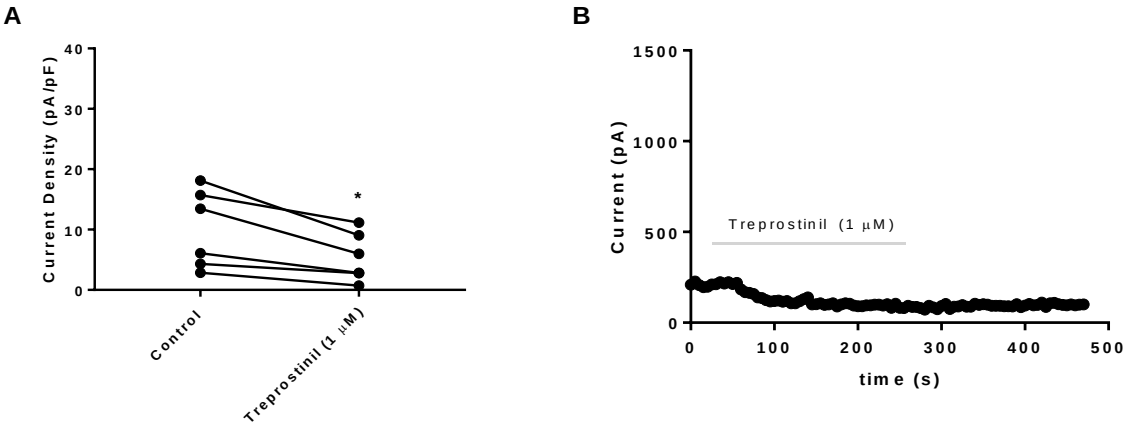

Figure 4.38 – Effect of Acute Application of Treprostinil (1 µM) on Co-expressed TASK-1_WT and IP receptor

A) Measurements of whole-cell current normalised against cell capacitance (pA/pF) at -40 mV for cells expressing TASK-1_WT and IP in control conditions and treprostinil (1 µM). B) Current-voltage plot of TASK-1_WT and IP in both control conditions (black line) and treprostinil (1 µM, grey line) recorded over a voltage ramp from -120 mV to +20 mV. C) Time course graph showing TASK-1_WT and IP outward current at -40 mV under the influence of treprostinil (1 µM). Treprostinil (1 µM) application is represented at the grey bar, absence of the grey bar represents control conditions. D) Representation of a raw data trace of TASK-1_WT and IP in both control conditions (black line) and treprostinil (1 µM, grey line) under the step-ramp voltage protocol.

4.5.6 Action of Treprostinil on TREK-1 and TREK-2

Patients undergoing treprostinil therapy often experience severe site pain at the infusion site. We investigated if TREK-1 and TREK-2 channels, which are capable of regulating sensory neuron excitability, are affected by treprostinil treatment.

4.5.6.1 Electrophysiological characterisation of TREK-1 WT

hTREK-1 WT DNA was transiently transfected in tsA201 cells and used for whole-cell patch-clamp recordings. The application of the step-ramp voltage protocol (Figure 2.6) previously described elicited TREK-1 electrophysiological characteristics (Figure 4.39). TREK-1_WT current was measured from the current values given when at -40 mV.

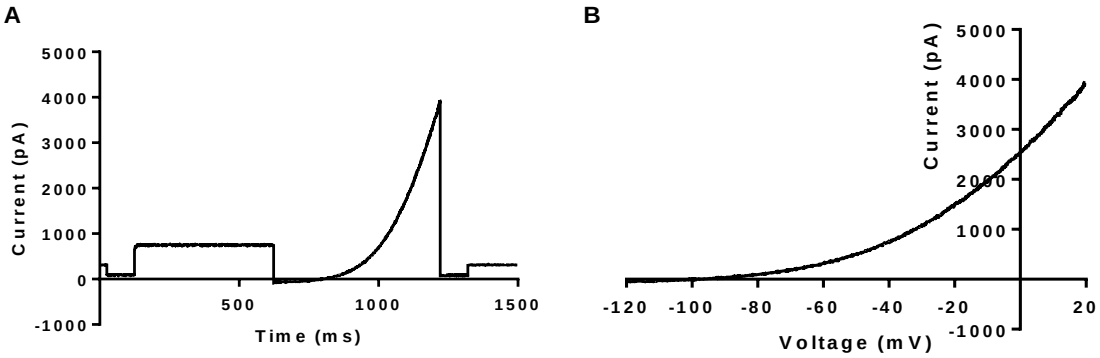

Figure 4.39 – TREK-1_WT electrophysiological profile.

A) Representative trace for TREK-1_WT channel in control conditions exposed to the step-ramp voltage protocol detailed in the methods. B) Current-voltage graph for TREK-1_WT in control conditions.

The electrophysiological profile for TREK-1_WT in extracellular solution (2.5 mM K^+, pH 7.4, see methods 2.3.3) yielded an average whole-cell current of 40 ± 4 pA/pF (n = 23) with an average reversal potential of -93 ± 1 mV (n = 23).

4.5.6.2 Acute Application of Treprostinil on TREK-1_WT

Acute application of treprostinil (1 µM) on cells expressing TREK-1_WT channels generated a reversible, potent inhibitory effect on TREK-1_WT outward current measured at -40 mV. TREK-1_WT current was significantly reduced from 33 ± 8 pA/pF (n = 5) in control conditions to 6 ± 3 pA/pF (n = 5) in treprostinil (1 µM; $p < 0.05$, paired *t*-test, Figure 4.40).

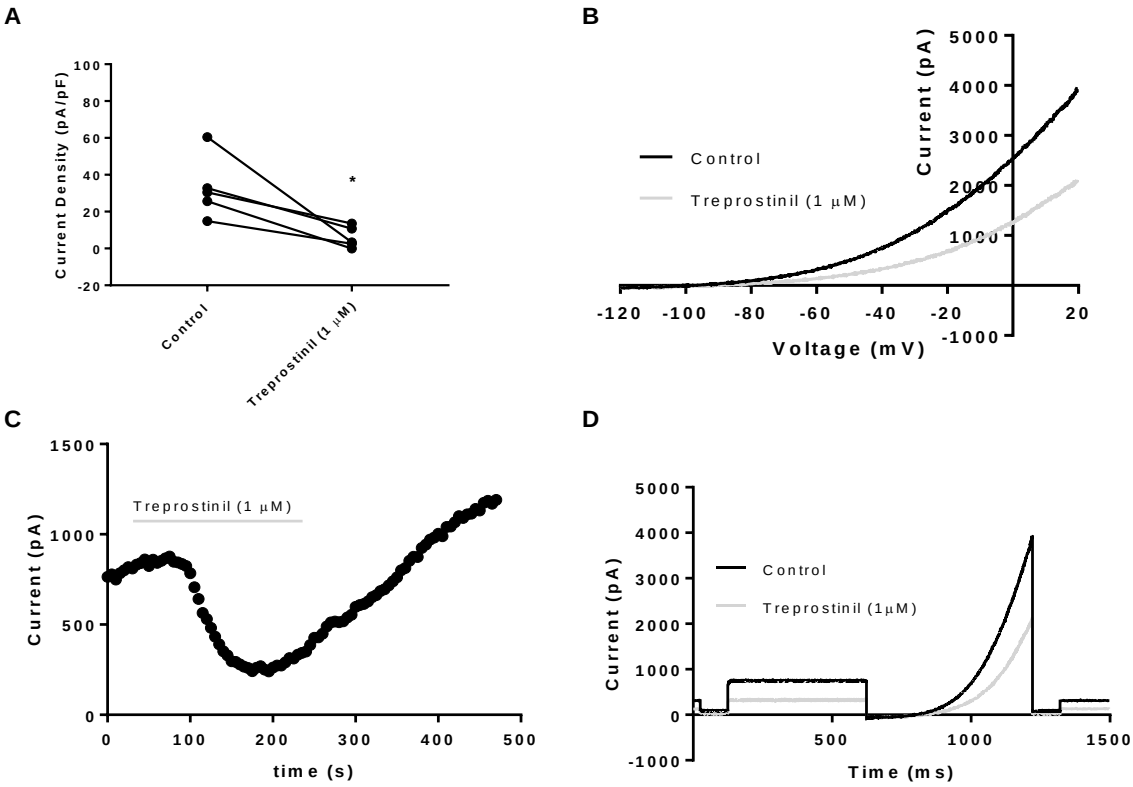

Figure 4.40 – Effect of Acute Application of Treprostinil (1 μM) TREK-1_WT

A) Measurements of whole-cell current normalised against cell capacitance (pA/pF) at -40 mV for cells expressing TREK-1_WT in control conditions and treprostinil (1 μM). B) Current-voltage plot of TREK-1_WT in both control conditions (black line) and treprostinil (1 μM, grey line) recorded over a voltage ramp from -120 mV to +20 mV. C) Time course graph showing TREK-1_WT outward current at -40 mV under the influence of treprostinil (1 μM). Treprostinil (1 μM) application is represented at the grey bar, absence of the grey bar represents control conditions. D) Representation of a raw data trace of TREK-1_WT in both control conditions (black line) and treprostinil (1 μM, grey line) under the step-ramp voltage protocol.

A 10-fold reduction in treprostinil to a concentration of 0.1 μM still resulted in a significant reversible, potent inhibition of TREK-1_WT current ($p < 0.05$, paired *t*-test, Figure 4.41). TREK-1_WT current was significantly reduced from 43 ± 5 pA/pF (n = 5) in control conditions to 13 ± 4 pA/pF (n = 5) in treprostinil (0.1 μM).

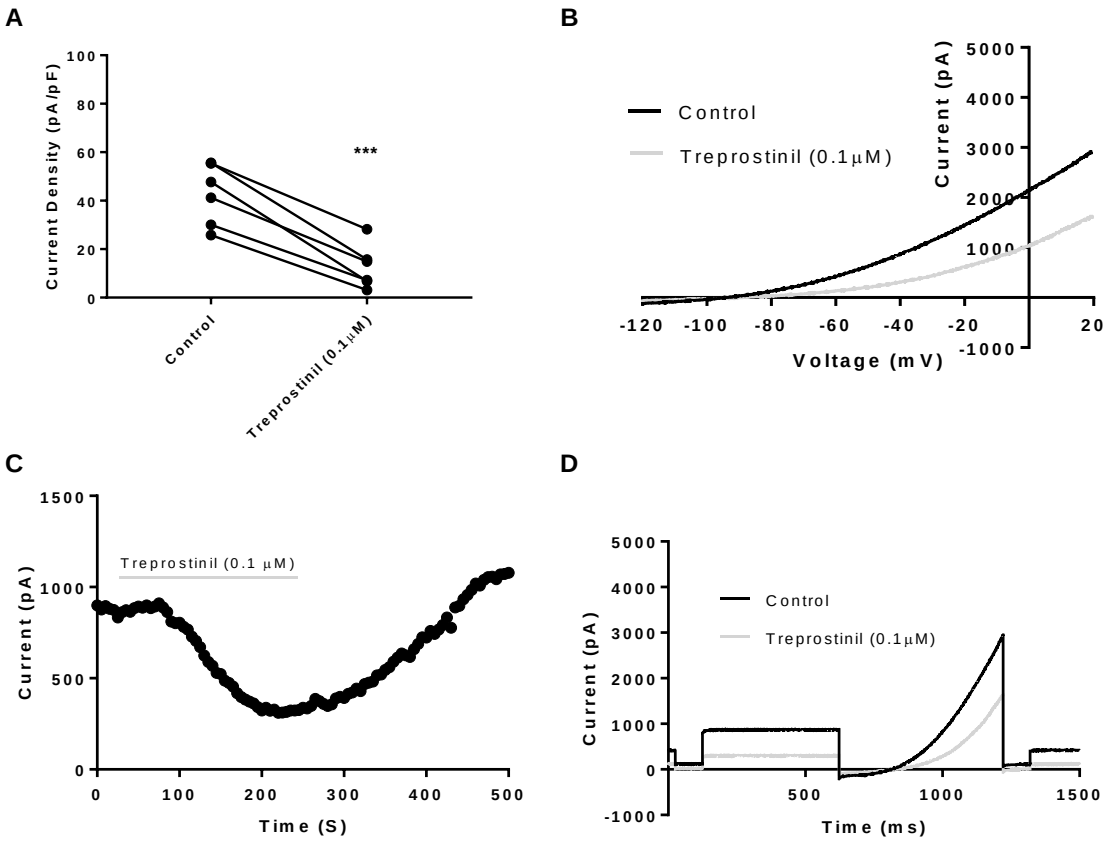

Figure 4.41 – Effect of Acute Application of Treprostinil (0.1 μM) TREK-1_WT

A) Measurements of whole-cell current normalised against cell capacitance (pA/pF) at -40 mV for cells expressing TREK-1_WT in control conditions and treprostinil (0.1 μM). B) Current-voltage plot of TREK-1_WT in both control conditions (black line) and treprostinil (0.1 μM, grey line) recorded over a voltage ramp from -120 mV to +20 mV. C) Time course graph showing TREK-1_WT outward current at -40 mV under the influence of treprostinil (0.1 μM). Treprostinil (1 μM) application is represented at the grey bar, absence of the grey bar represents control conditions. D) Representation of a raw data trace of TREK-1_WT in both control conditions (black line) and treprostinil (0.1 μM, grey line) under the step-ramp voltage protocol

Two further concentrations of treprostinil, 0.03 μM and 0.01 μM were investigated. Acute application of treprostinil (0.03 μM) significantly reduced TREK-1_WT current (control: 47 ± 11 pA/pF, n = 7 and treprostinil 0.03 μM: 31 ± 9, n = 7; $p < 0.05$, paired *t*-test, Figure 4.42A and B) whereas 0.01 μM failed to do so (control: 34 ± 6 pA/pF, n = 5 and treprostinil 0.01 μM: 32 ± 5, n = 5; $p > 0.05$, paired *t*-test, Figure 4.42 C and D). Concentration-response

curve was fitted revealing an IC50 value of 0.03 µM for treprostinil on TREK-1_WT current (Figure 4.42E).

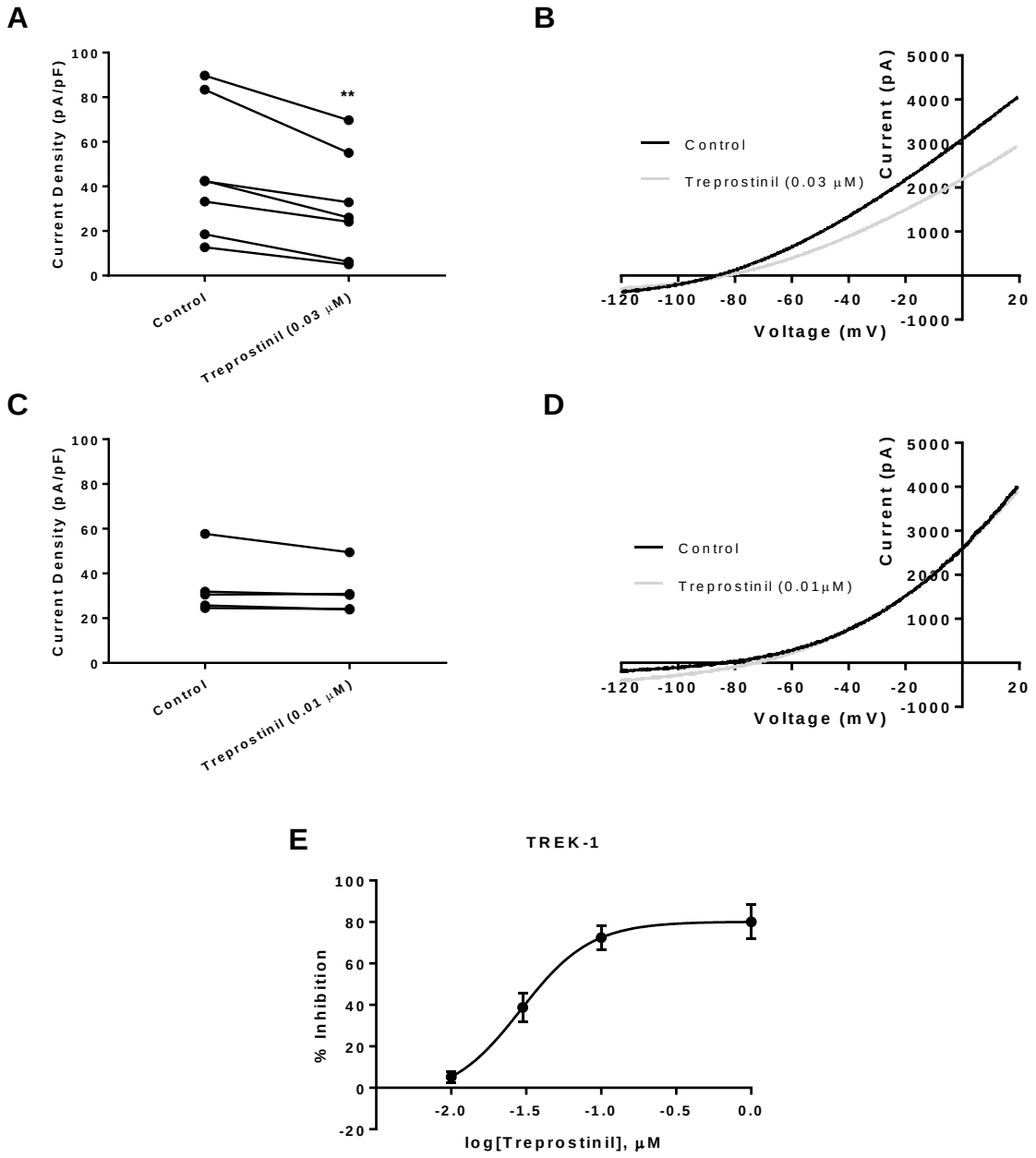

Figure 4.42 – Effect of Acute Application of Treprostinil on TREK-1_WT

A) Measurements of whole-cell current normalised against cell capacitance (pA/pF) at -40 mV for cells expressing TREK-1_WT in control conditions and treprostinil (0.03 µM). B) Current-voltage plot of TREK-1_WT in both control conditions (black line) and

treprostinil (0.03 µM, grey line) recorded over a voltage ramp from -120 mV to +20 mV. C) Measurements of whole-cell current normalised against cell capacitance (pA/pF) at -40 mV for cells expressing TREK-1_WT in control conditions and treprostinil (0.01 µM). D) Current-voltage plot of TREK-1_WT in both control conditions (black line) and treprostinil (0.01 µM, grey line) recorded over a voltage ramp from -120 mV to +20 mV. E) concentration-response plot for treprostinil inhibition on TREK-1_WT current. Error bars represent SEM.

4.5.6.3 Electrophysiological characterisation of TREK-2 WT

Like TREK-1 channels, TREK-2 channels have been shown to play a role in sensory neuron pain signalling, therefore we looked at treprostinil on TREK-2 channels. hTREK-2 WT DNA was transiently transfected in tsA201 cells and used for whole-cell patch-clamp recordings. The application of the step-ramp voltage protocol (Figure 2.6), previously described, generated TREK-2 electrophysiological characteristics (Figure 4.43). TREK-2_WT current was measured from the current values given when at -40 mV.

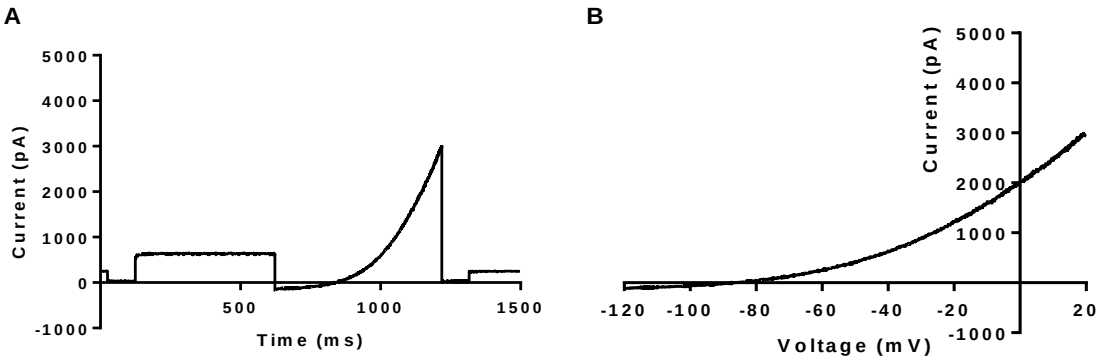

Figure 4.43 – TREK-2_WT electrophysiological profile.

A) Representative trace for TREK-2_WT channel in control conditions exposed to the step-ramp voltage protocol detailed in the methods. B) Current-voltage graph for TREK-2_WT in control conditions.

The electrophysiological profile for TREK-2_WT in extracellular solution (2.5 mM K^+, pH 7.4, see methods 2.3.3) yielded an average whole-cell current of

55 ± 10 pA/pF (n = 22) with an average reversal potential of -89 ± 1 mV (n = 22).

4.5.6.4 Acute Application of Treprostinil on TREK-2_WT

Acute application of treprostinil (1 µM) on cells expressing TREK-2_WT channels generated a reversible, potent inhibitory effect on TREK-2_WT outward current measured at -40 mV. TREK-2_WT current was significantly reduced from 38 ± 6 pA/pF (n = 5) in control conditions to 17 ± 5 pA/pF (n = 5) in treprostinil (1 µM; $p < 0.05$, paired *t*-test, Figure 4.44).

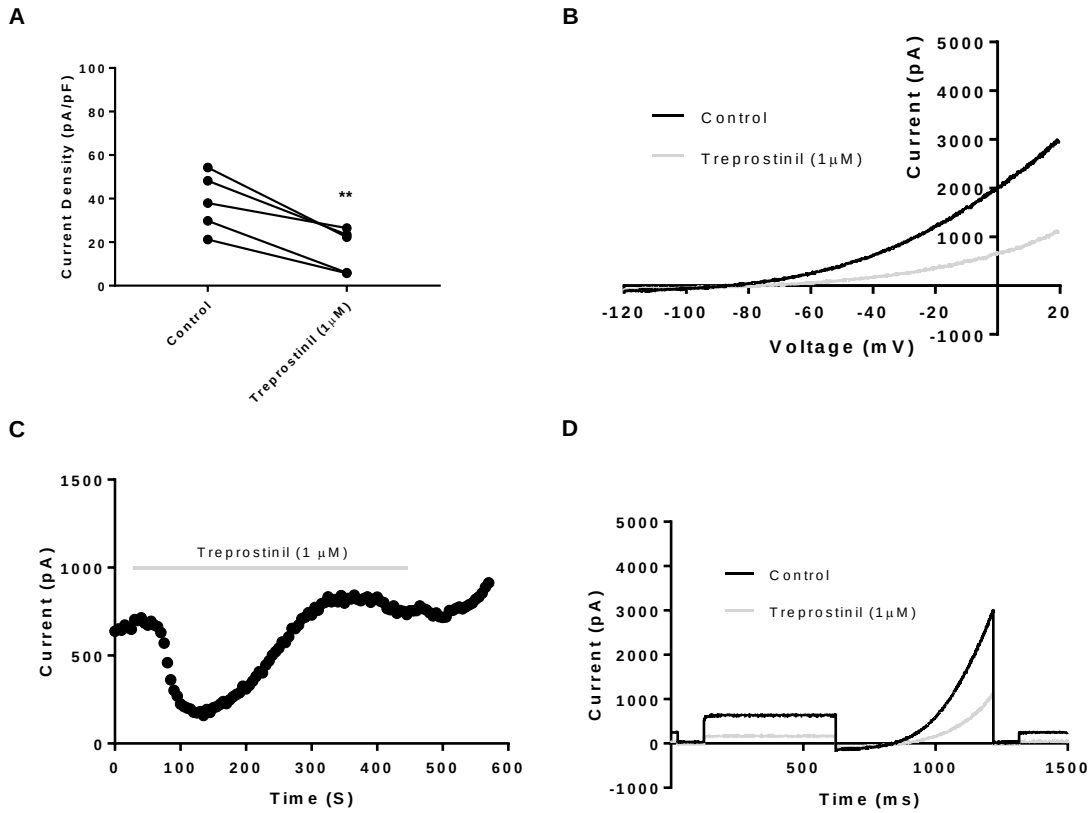

Figure 4.44 – Effect of Acute Application of Treprostinil (1 µM) TREK-2_WT

A) Measurements of whole-cell current normalised against cell capacitance (pA/pF) at -40 mV for cells expressing TREK-2_WT in control conditions and treprostinil (1 µM). B) Current-voltage plot of TREK-2_WT in both control conditions (black line) and treprostinil (1 µM, grey line) recorded over a voltage ramp from -120 mV to +20 mV. C) Time course graph showing TREK-2_WT outward current at -40 mV under the influence of treprostinil (1 µM). Treprostinil (1 µM) application is represented at the

grey bar, absence of the grey bar represents control conditions. D) Representation of a raw data trace of TREK-2_WT in both control conditions (black line) and treprostinil (1 µM, grey line) under the step-ramp voltage protocol.

A 10-fold reduction in treprostinil to a concentration of 0.1 µM still resulted in a significant reversible, potent inhibition of TREK-2_WT current ($p < 0.05$, paired *t*-test, Figure 4.45). TREK-2_WT current was significantly reduced from 88 ± 29 pA/pF (n = 5) in control conditions to 57 ± 25 pA/pF (n = 5) in treprostinil (0.1 µM).

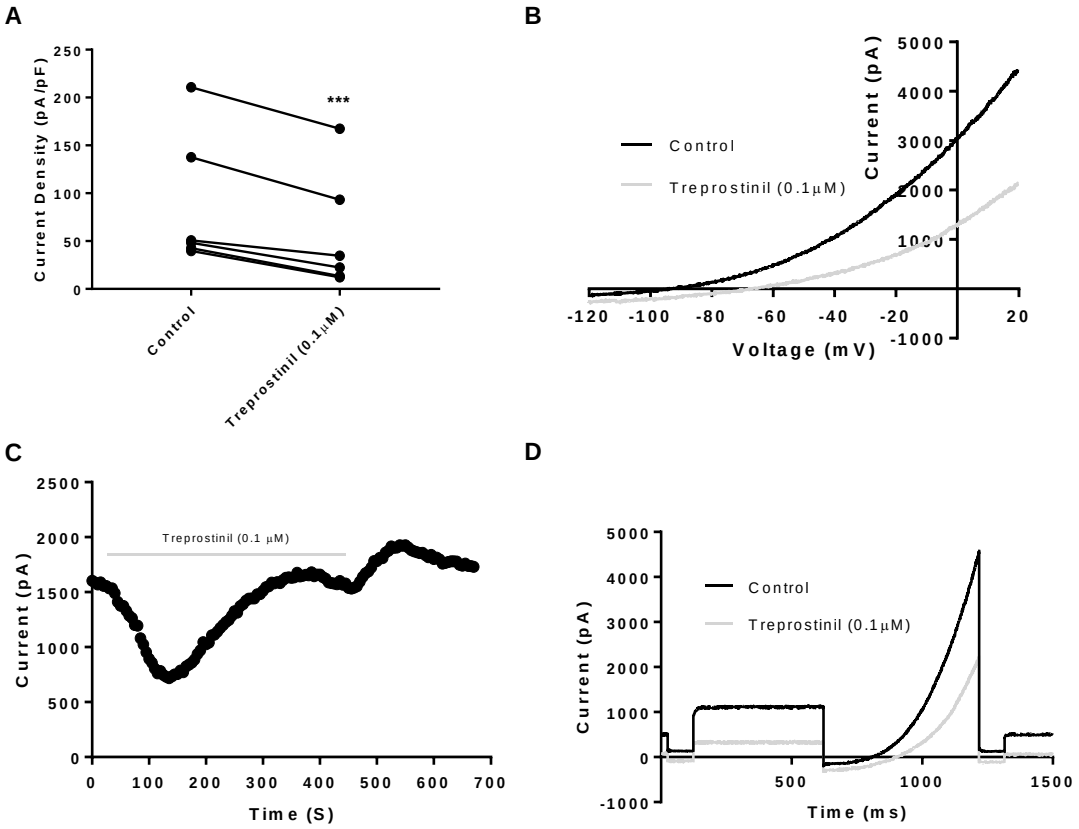

Figure 4.45 – Effect of Acute Application of Treprostinil (0.1 µM) TREK-2_WT

A) Measurements of whole-cell current normalised against cell capacitance (pA/pF) at -40 mV for cells expressing TREK-2_WT in control conditions and treprostinil (0.1 µM). B) Current-voltage plot of TREK-2_WT in both control conditions (black line) and treprostinil (0.1 µM, grey line) recorded over a voltage ramp from -120 mV to +20 mV. C) Time course graph showing TREK-2_WT outward current at -40 mV under the influence of treprostinil (0.1 µM). Treprostinil (1 µM) application is represented at the

grey bar, absence of the grey bar represents control conditions. D) Representation of a raw data trace of TREK-2_WT in both control conditions (black line) and treprostinil (0.1 µM, grey line) under the step-ramp voltage protocol.

Two further concentrations of treprostinil, 0.03 µM and 0.01 µM were investigated. Acute application of treprostinil (0.03 µM) significantly reduced TREK-2_WT current (control: 41 ± 14 pA/pF, n = 6 and treprostinil 0.03 µM: 34 ± 12, n = 6; $p < 0.05$, paired *t*-test, Figure 4.46A and B) whereas 0.01 µM failed to do so (control: 49 ± 11 pA/pF, n = 5 and treprostinil 0.01 µM: 43 ± 11, n = 5; $p > 0.05$, paired *t*-test, Figure 4.46 C and D). Concentration-response curve was fitted revealing an IC50 value of 0.04 µM for treprostinil on TREK-2_WT current (Figure 4.46E).

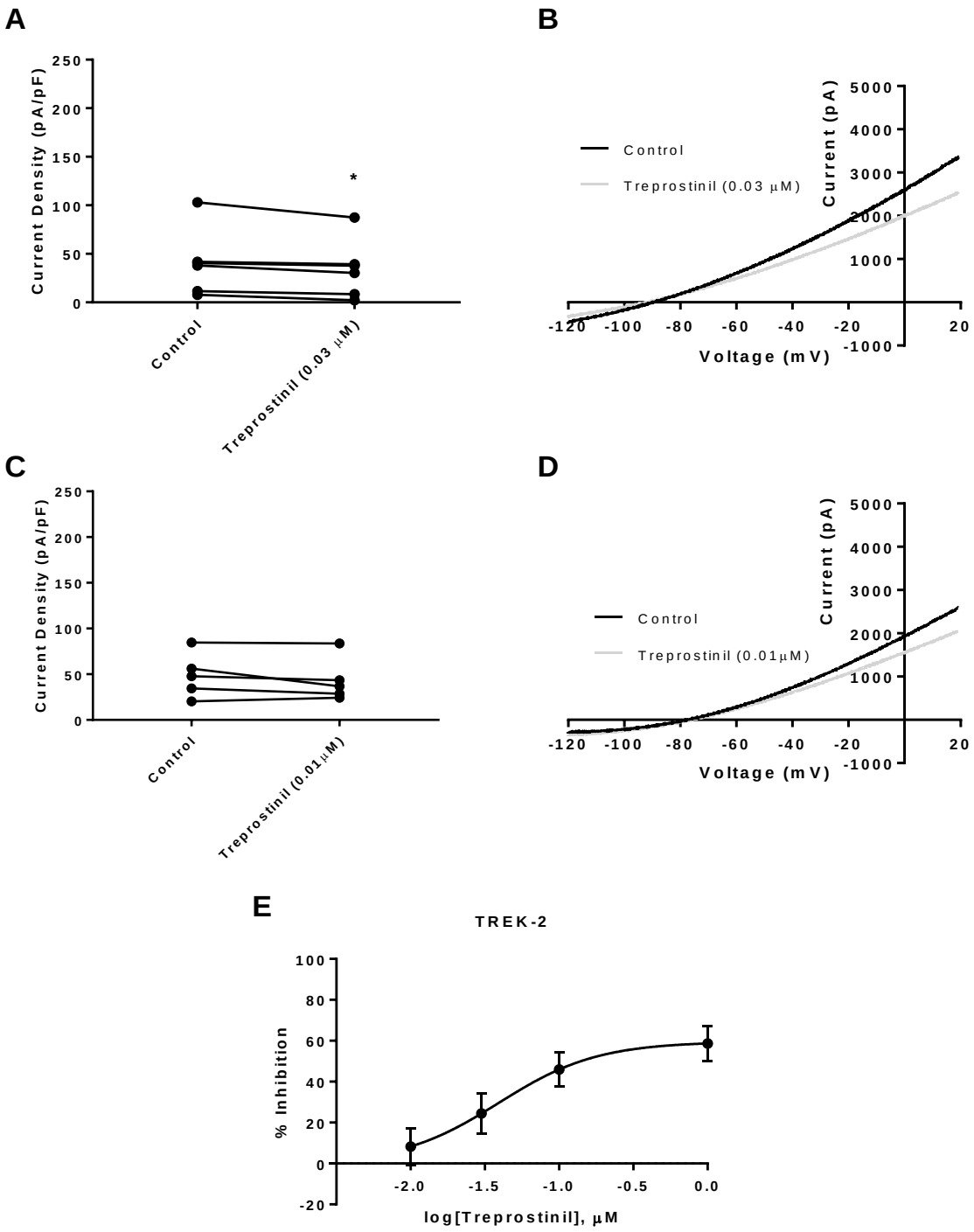

Figure 4.46 – Effect of Acute Application of Treprostinil on TREK-2_WT

A) Measurements of whole-cell current normalised against cell capacitance (pA/pF) at -40 mV for cells expressing TREK-2_WT in control conditions and treprostinil (0.03 μM). B) Current-voltage plot of TREK-2_WT in both control conditions (black line) and treprostinil (0.03 μM, grey line) recorded over a voltage ramp from -120 mV to +20 mV. C) Measurements of whole-cell current normalised against cell capacitance

(pA/pF) at -40 mV for cells expressing TREK-2_WT in control conditions and treprostinil (0.01 µM). D) Current-voltage plot of TREK-2_WT in both control conditions (black line) and treprostinil (0.01 µM, grey line) recorded over a voltage ramp from -120 mV to +20 mV. E) concentration-response plot for treprostinil inhibition on TREK-2_WT current. Error bars represent SEM.

4.5.6.5 Effect of Acute Application of Treprostinil on TREK-1_Δ1-41

To assess whether N-terminus plays a role in treprostinil inhibition we studied TREK-1_Δ1-41, where the first 41 amino acids of the N-terminus are removed. Similar to previous literature, TREK-1_Δ1-41 showed a significantly reduced current compared to TREK-1_WT ($p < 0.05$, unpaired *t*-test, Figure 4.47; Veale *et al.,* 2010). TREK-1_Δ1-41 had an outward current of 2.2 ± 0.7 pA/pF (n = 5) at -40 mV compared to 39.7 ± 4.2 pA/pF (n = 23) in TREK-1_WT.

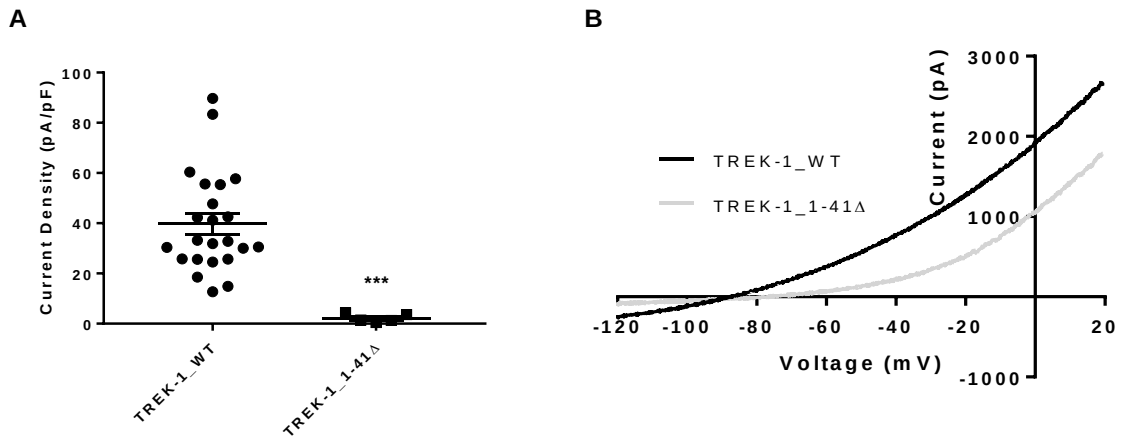

Figure 4.47 - TREK-1_Δ1-41 Electrophysiological Profile Compared to TREK-1_WT

A) Measurement of whole-cell current normalised against cell capacitance (pA/pF) at -40 mV for cells expressing TREK-1_WT or TREK-1_Δ1-41. B) Current-voltage plot of TREK-1_WT (black line) and TREK-1_Δ1-41 (grey line) in control conditions recorded over a voltage ramp from -120 mV to +20 mV.

As acute application of treprostinil (1 µM) potently inhibited TREK-1_WT, we investigated whether acute application of treprostinil (1 µM) had an inhibitory effect upon the already significantly reduced current of TREK-1_Δ1-41 channels. TREK-1_Δ1-41 current measured at -40 mV was significantly reduced in the presence of treprostinil (1 µM) with values of 2 ± 1 pA/pF (n = 5) compared to 0 ± 1 pA/pF (n = 5) in control conditions ($p < 0.05$, paired *t*-test, Figure 4.48).

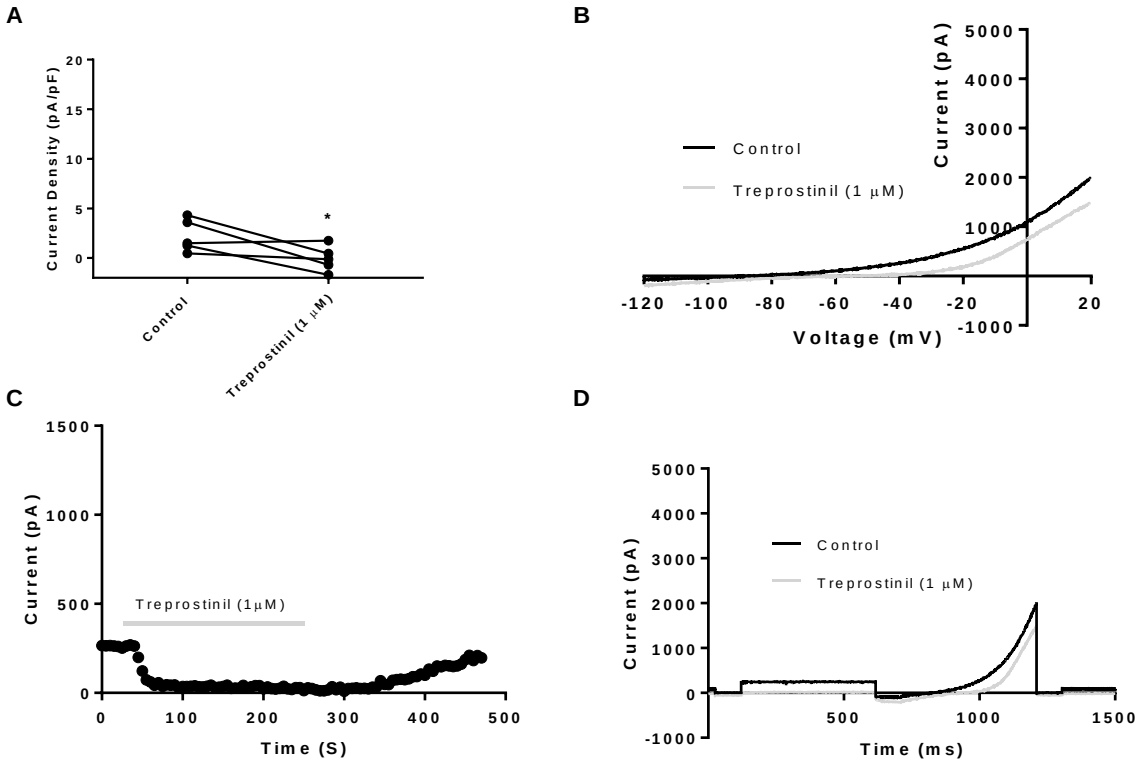

Figure 4.48 – Inhibitory Effect of Acute Application of Treprostinil (1 µM) on TREK-1_Δ1-41

A) Measurements of whole-cell current normalised against cell capacitance (pA/pF) at -40 mV for cells expressing TREK-1_Δ1-41 in control conditions and treprostinil (1 µM). B) Current-voltage plot of TREK-1_Δ1-41 in both control conditions (black line) and treprostinil (1 µM, grey line) recorded over a voltage ramp from -120 mV to +20 mV. C) Time course graph showing TREK-1_Δ1-41 outward current at -40 mV under the influence of treprostinil (1 µM). Treprostinil (1 µM) application is represented at the grey bar, absence of the grey bar represents control conditions. D) Representation of a raw data trace of TREK-1_Δ1-41 in both control conditions (black line) and treprostinil (1 µM, grey line) under the step-ramp voltage protocol.

4.6 Discussion

TASK-1 has been indicated as the major TASK channel present in human PASMCs and the main regulator of PASMCs excitability (Olschewski *et al.,* 2006). A reduction in TASK-1 expression and function has been suggested as a key event in the pathogenesis of PAH (Antigny *et al.,* 2016). The phospholipase A2 inhibitor, ONO-RS-082, has been shown to treat PAH in rat models by reversing inflammation, proliferation and vasoconstriction (Antigny *et al.,* 2016). In addition to this, two TASK-1 mutations (T8K and E182K) known to cause PAH were able to have channel current partially recovered with ONO-RS-082 treatment, further pinpointing TASK-1 importance in PAH in patients (Ma *et al.,* 2013). To address the role of TASK-1 in PAH it was essential to characterise the novel homozygous mutations (G106R and L214R) identified within patients of aggressive PAH.

In this study, it has been shown that the two novel mutations of TASK-1 produce a significant reduction in their outward currents, compared to the wild-type. The clear reduction in TASK-1 channel currents seen in the mutated channels were not found to be caused by trafficking or translation of the channel to the membrane, as imaging and quantification experiments showed equal distribution between mutant and WT channels at the membrane. This indicates the mutations affect the structural and functional properties of the TASK-1 channel to reduce current. Both pathogenic mutations are located extracellularly on the channel. G106R between the first pore and the second transmembrane domain and L214R being located between the second P domain and fourth transmembrane domain. In both cases an arginine substitution occurs, which is a large, positively charged, hydrophilic amino acid. In G106R, the glycine residue is a small, uncharged amino acid and in L214R the leucine is a small, hydrophobic amino acid. It has previously been suggested that within TASK-1 channels the arrangement of the histidine at amino acid 98 (H98) and the aspartic acid at 204 (D204) in both subunits is vital not only for pH sensing but for the channel to function as a selective K^+ channel (Yuill *et al.,* 2004). It is thought that D204 optimises TASK-1 sensitivity to pH changes by providing a more optimal conformation, within the selectivity

pathway opposed to a direct pH sensor as in the case of H98. The H98-D204-H98-D204 ring is situated at the mouth of the selectivity filter. Both G106R and L214R lie close to this ring and an arginine replacement may alter the optimal structure causing a blockade of the selectivity filter due to the increased residue size. It may be that the arginine substitution creates a structure that closes off the selectivity filter, preventing ion flow through the channel. As both H98 and D204 play a role in TASK-1 pH sensing, disruption to their structure through either the G106R or L214R mutation may explain the loss in sensitivity to alkalosis observed.

Enhancement of the current through the mutant channels, G106R and L214R, could not be achieved with ONO-RS-082 (10 µM) as seen in previous mutations (Ma *et al.,* 2013). This may be due to the closure of the selectivity filter, as previously suggested, meaning the enhancing effects of ONO-RS-082 does not alter channel structure sufficiently to open the selectivity filter in these mutations. It must be noted that not all mutations previously treated with ONO-RS-082 were able to be recovered such as the mutation G203D (Ma *et al.,* 2013). Furthermore, we were unable to replicate the enhancement seen for TASK-1_E182K with ONO-RS-082 (10 µM). This may be due to the current being measured at -40 mV, rather than +60 mV, as in Ma *et al.,* 2013. To investigate the current at more positive voltages, where you see a contribution from endogenous voltage-gated K_v channels, we used TEA, which K2P channels are insensitive to. Application of TEA (10 mM) abolished current at positive voltages and identified that this current was due to the presence of endogenous K_v channels present within the tsA201 cells (Jiang *et al.,* 2002). With our data despite a reduction in current seen at +20 mV with the novel mutations, with the cells expressing TASK-1_WT only no inhibition at +20 mV was observed, this may be due to the presence of TASK-1 dominating the +20 mV current and the Kv current change being too small in comparison. It could be suggested that the current seen in the previous study with TASK-1_E182K may be due to the endogenous channels within the cells, as the cell line used in the study, COS-7, cells have been shown to express endogenous potassium channels (Kang *et al.,* 2006). Also the reversal potentials of the mutations, T8K and E182K, were shifted close to 0 mV suggesting the where the channel does

not carry current, other non-selective leak currents dominate and shift the reversal potential towards 0 mV which could indicate the enhancement may be an enhancement of a non-potassium current, therefore ONO-RS-082 therapy may only exacerbate symptoms caused by the mutations in PAH patients (Ma *et al.,* 2013).

One key feature of the two novel mutations, G106R and L214R, were that both reversal potentials were significantly shifted towards 0 mV. This suggests that in patients this shift in reversal potentials could lead to a depolarisation of the pulmonary artery and resultant vasoconstriction. Depolarised membrane potentials has been observed in PASMCs of PAH rat models (Antigny *et al.,* 2016). The shift in reversal potential suggests a reduction in K^+ ion selectivity, of the channels however further experiments from within the lab indicated a reduction in permeability to a number of ions (Appendix 6.11 and 6.12). This reduction further suggests a structural block of the channel pore caused by these novel mutations.

Another possibility as to why ONO-RS-082 was effective on mutations seen previously but not in this study, may be due to the hetero or homogeneity of the mutation (Ma *et al.,* 2013). Both novel mutations G106R and L214R are homozygous and display a very aggressive form of PAH, the first to be reported within PAH patients (Navas *et al.,* 2017). It has been suggested that the dimerization of TASK channels leads to the lung-specific phenotypes observed within PAH patients with KCNK3 mutations (Bohnen *et al.,* 2017). TASK-3 is not expressed within human lung PASMC and a patient with heterozygous mutation of PAH will express a combination of three isoforms of TASK-1 within the lungs – TASK-1_WT/TASK-1_WT, TASK-1_mutated/TASK-1_WT and TASK-1_mutated/TASK-1_mutated. Whereas outside of the lungs where TASK-3 is expressed, TASK-1 can further dimerize with TASK-3 allowing two further TASK-1 dimers – TASK-1_WT/TASK-3_WT and TASK-1_mutated/TASK-3_WT. The increased diversity of TASK-1 outside of the lungs, in tissues such as carotid bodies and atrial cardiomyocytes may provide protection to TASK-1 dysfunction (Bohnen *et al.,*

2017; Kim *et al.,* 2009; Rinne *et al.,* 2015). With this in mind only homozygous mutated TASK-1 channels would be expressed within the lungs, but in other tissues, there could be heterozygous channel expression through heterodimerisation. This may explain the aggressive nature of the disease seen within homozygous carrying patients (Navas *et al.,* 2017). The initial study on TASK-1_E182K appears to present the heterozygous mutation as having the ability to recover current in the presence of ONO-RS-082 when expressed in a homozygous manner (Ma *et al.,* 2013). A further study from the same group provided supplementary data showing homozygous expression of TASK-1_E182K could not be enhanced by ONO-RS-082 however a forced concatamer expressing TASK-1_WT/TASK-1_E182K was able to be (Bohnen *et al.,* 2017). This indicates further that in the initial study it may not have been clear that they co-expressed TASK-1_WT cDNA and TASK-1_E182K with the action of ONO-RS-082 acting on the WT subunit of the channel (Ma *et al.,* 2013).

Sildenafil is a PDE5 inhibitor that promotes an increase in intracellular levels of cGMP. Originally developed to treat angina, it was noted to have a greater therapeutic effect in treating erectile dysfunction (Boolell *et al.,* 1996). The increase in cGMP levels leads to an increase in PKG activation which in turn acts to reduce intracellular Ca^{2+} levels and inhibit smooth muscle contraction (Ghofrani *et al.,* 2017). Activation of PKG has been previously described to upregulate TASK-1 channel activity within the brain by altering the K_d values required for protonation of the H98 residue (Toyoda *et al.,* 2010). As PDE5 levels are high within the lungs, almost equal to that in the penile corpus cavernosum, sildenafil was proposed as a possibly treatment for PAH (Corbin *et al.,* 2005). This study indicates for the first time that sildenafil enhances current through WT TASK-1 channels and this may contribute to the beneficial effects seen within PAH therapy. Sildenafil had no effect on the novel mutations, G106R and L214R, nor did it have an effect on TASK-1_E182K current. This may mean that sildenafil use could be strategized in PAH therapy. Despite this study showing it had no effect upon TASK-1_E182K it may be that sildenafil will still provide some therapeutic benefit through TASK-1 current activation when expressed in a heterozygous manner. Depending on

whether the primary therapeutic action of sildenafil is generated through the action of TASK-1 channels or whether TASK-1 activation is a beneficial secondary action of sildenafil, would be critical to strategizing sildenafil treatment. If TASK-1 current activation is the primary action of sildenafil it may be that alternative therapies would prove more beneficial to PAH patients carrying the G106R or L214R mutation.

Similarly to sildenafil this study shows that, for the first time that riociguat acts in the same manner, enhancing TASK-1_WT currents but failing to have an effect on the novel mutated channels. Riociguat acts along the same pathway as sildenafil by stimulating soluble guanylyl cyclase and promoting PKG activation through increased intracellular levels of cGMP and inhibiting smooth muscle cell contraction (Ghofrani *et al.,* 2017). Once again, it may be that riociguat could be tailored for patients as suggested above (with sildenafil) that if TASK-1 activation was the main source of therapeutic benefit, alternative therapies may provide a better outcome for PAH patients carrying the G106R or L214R mutation. A previous study looking into cGMP and TASK-1 activation has indicated TASK-1 is not activated by the NO/cGMP pathway. However, in that study the duration of 8-Br-cGMP application is not stated (Lloyd *et al.,* 2009). A more recent study has shown PKG-loaded HEK293 cells had enhanced TASK-1 WT current at pH 7.3, similarly to the application of riociguat and sildenafil in this study, further indicating a role of PKG in TASK-1 WT regulation (Toyoda *et al.,* 2010).

IBMX was used experimentally as it non-selectively targets multiple PDE's, IBMX failed to enhance WT TASK-1 current indicating that the wide range of PDE's IBMX targets, may reduce its efficacy on PDE's that affect TASK-1 channel current. IBMX has been shown to increase both cAMP and cGMP levels and activate PKA and PKG respectively (Yamaki *et al.,* 1992). Interestingly, combining IBMX with sildenafil abolished the enhancement seen with sildenafil treatment on its own. The eradication of sildenafil's effect on TASK-1_WT when combined with IBMX suggests the possibility that inhibition of an alternative PDE that IBMX inhibits may counteract the effect of sildenafil. Sildenafil has been shown to have an IC_{50} value of 3.6 nM on human PDE5 compared to IBMX with 5.7 µM (Wang *et al.,* 2001). Another possibility may

be that where sildenafil selectively targets PDE5, IBMX although a PDE inhibitor, may competitively block sildenafil on PDE5 and exert a less potent effect, reducing enhancement seen through sildenafil treatment alone.

Interestingly, IBMX combined with the adenylyl cyclase activator, Forskolin, increased TASK-1_WT current. Previous work within the lab showed that concatamers of mouse TASK-1_WT with TASK-3_WT varied the response of IBMX and Forskolin to channel current based on the orientation of the concatamer. Having the concatamer with the C-terminus of TASK-3 fused to TASK-1 at the N-terminus results in IBMX and Forskolin enhancing the channel current whereas the reverse formation leads to an inhibition of channel current (Appendix 6.10). Forskolin and IBMX applied individually had no effect on the construct with TASK-1 at the N-terminus (Appendix 6.9). This suggests the arrangement of heterodimers has a significant effect on the response of channels to compounds, this has been shown in previous work by Cotton *et al.,* 2006, where different arrangement of TASK-1 and TASK-3 have a varied response to doxapram inhibition and also in Blin *et al.,* 2016 with TREK-1 and TREK-2 heterodimers exhibiting different pharmacological properties. These differences generated by subunit arrangement highlights the importance of the C-terminus. In the forced concatamers the availability of one C-terminus may be lower due to the first having its C-terminus fused to the N-terminus of the second subunit. *In vivo,* heterodimers may act differently, as both C-termini should be available for interaction (Czirjak and Enyedi, 2002). In both TASK-1 and TASK-3, phosphorylation of serine residues (Serine 393 and Serine 373 for TASK-1 and TASK-3 respectively) in the 'trafficking control region' of the C-terminus is critical in determining the ability of channel to be transported to the cell surface (Kilisch *et al.,* 2016). Within the trafficking control region, the 14-3-3 binding domain and coat protein complex I (COPI) binding domain overlap. Binding of COPI to the COPI binding domain, within the C-terminus retains, TASK channels within the early secretory pathway (O'Kelly *et al.,* 2002). Phosphorylation of the serine residues prevents COPI binding to a specific domain on the C-terminus. This enables the binding domain of 14-3-3 proteins to remain available for binding. Bound 14-3-3 proteins facilitate the TASK-1 channels to leave the endoplasmic reticulum

(O'Kelly *et al.,* 2002; Zuzarte *et al.,* 2009). It has recently been identified that a second serine residue (S392) within the trafficking control region of TASK-1 may have effects on channel surface expression. Whilst phosphorylation of S393 has been identified as promoting 14-3-3 binding, promoting cell surface expression. Phosphorylation of S392 is inhibitory to 14-3-3 binding, preventing cell surface expression of TASK-1 (Kilisch *et al.,* 2016). TASK-1 C-terminus phosphorylation has been attributed to PKA, with both serine residues of the TASK-1 C-terminus having been shown to be phosphorylated by PKA *In vitro.* More recently, PKA has been shown to prevent COPI interaction even in the absence of 14-3-3, indicating its vital role in TASK-1 channel cell surface expression (Mant *et al.,* 2011; Kilisch *et al.,* 2016). It may be that the enhanced current seen in TASK-1_WT channels, after the application of IBMX and forskolin is due to an increase in channel surface expression following the activation of PKA.

As an enhancement of PKA through the use of a combination of IBMX and forskolin increased TASK-1_WT channel current, treprostinil, a synthetic prostacyclin analogue which has been shown to enhance TASK-1_WT current through PKA activation in human PASMCs was investigated (Olschewski *et al.,* 2006). I showed that acute application of treprostinil over a range of concentrations failed to enhance TASK-1_WT current, however incubation with treprostinil did enhance TASK-1_WT current. This difference in effect of treprostinil may be due to the incubation, enabling adequate time for PKA phosphorylation of TASK-1 to occur and a subsequent increase in cell surface expression of TASK-1 channels. A greater cell surface expression would result in higher current seen with electrophysiological experiments. This increase in channel surface expression may explain the improvements in PAH patients (Clapp and Gurung, 2015). The enhancement in TASK-1 cell surface expression will lead to an increase in the number of voltage-gated calcium channels being closed which reduces intracellular Ca^{2+} and promotes smooth muscle cell relaxation. This effect compliments the proposed main action of treprostinil to promote protein kinase A (PKA) activation, leading to an reduction of sarcoplasmic Ca^{2+} release (through RGS4 phosphorylation and $G_{\alpha q}$ inhibition) and ultimately a promotion in smooth muscle cell relaxation

(Olschewski *et al.,* 2006). This proposed main pathway of treprostinil action could thus occur through TASK-1 channels. The inhibition of $G_{\alpha q}$, results in an inhibition of phospholipase C (PLC) activity, which in turn reduces the production of the intracellular messengers diacylglycerol (DAG) and inositol triphosphate (IP_3). This PLC inhibition may be critical to TASK-1 enhancement as it has been shown that a change in intracellular levels of DAG (and not its metabolites) can directly regulate TASK-1 activity (Wilke *et al.,* 2014).

Prostaglandins are produced after phospholipase A_2 generates arachidonic acid from membrane phospholipids. Subsequent metabolism through cyclooxygenase (COX) synthases and prostaglandin synthases, results in the generation of prostaglandins (prostaglandin D_2, PGD_2; prostaglandin E_2, PGE_2; prostaglandin $F_{2\alpha}$, $PGF_{2\alpha}$ and prostacyclin, PGI_2). Prostaglandins are greatly increased after acute inflammation and in low levels within uninflamed tissues (Ricciotti and FitzGerald, 2011). Each prostaglandin can bind to prostaglandin receptors with different affinities and coupled with a variety of G-proteins that initiate different cellular pathways. Prostaglandin receptors present in vascular smooth muscle cells include DP_{1+2}, EP_{1-4} and IP receptors (Parameswaran *et al.,* 2007; Pluchart *et al.,* 2017). Interestingly DP_2 has an alternative name, CRTH2, as it belongs to another family of receptors (the chemoattractant receptors) and was first identified within T helper 2 cells hence CRTH2. Receptors analysed in this study were DP_2, EP_2 and IP, as mentioned previously prostaglandin receptors are coupled to different G-proteins, DP_2 is coupled to G_i proteins which decrease cAMP levels and promote intracellular Ca^{2+} levels. EP_2 is coupled with G_s proteins which promotes intracellular levels of cAMP which promotes smooth muscle cell relaxation through activation of PKA. IP receptors have been found to have multiple G-proteins coupled to the receptor. Prostacyclin analogues have been shown to promote relaxation by activating adenylyl cyclase through G_s proteins, in a dose-dependent manner. Whereas it would appear higher concentrations of IP ligands have the opposite effect, promoting smooth muscle contraction through PLC and G_q-coupled proteins (Smyth *et al.,* 2000; Bley *et al.,* 1998). PLC activation promotes increases in intracellular IP_3 and leads to an inhibition of myosin light chain (MLC) phosphatase and promotes

release of sarcoplasmic Ca^{2+}. In this study we showed that co-expression of TASK-1_WT with EP_2 receptor significantly enhanced baseline TASK-1_WT current. The increase in TASK-1_WT current suggests that the presence of the EP_2 receptor within the cells naturally activates PKA and its downstream effects of increased channel expression on the cell surface and reduction in DAG levels, as a result of RGS4 phosphorylation and $G_{\alpha q}$ inhibition. Co-expression of TASK-1_WT with IP or DP_2 receptors did not alter TASK-1_WT current significantly. After co-expression with any of prostaglandin receptors (DP_2, EP_2 and IP), further incubation with treprostinil failed to affect TASK-1_WT current any further. As DP_2 appeared to have a similar trend to EP_2, I conducted post-hoc power analysis of the data to determine the power of the study using power calculation software outlined in section 2.6. Data collected for DP_2 co-expression had a power of 0.31 and required an n = 41 (30 more repeats) to gain a power of 0.8. EP_2 co-expression had a 0.92 and only required an n = 16 to gain a power of 0.8 whereas IP co-expression required an n = 142 with a power of 0.20. Further experiments, particularly with DP_2 co-expression may help fully determine whether a significant difference is present opposed to a trend seen similar to that of EP_2.

Interestingly, I found that acute application of treprostinil altered TASK-1_WT current in a receptor dependent manner. Co-expression of TASK-1_WT and DP_2 did not respond to the acute application of treprostinil, treprostinil has yet to be shown to bind DP_2 receptors, but has high affinity for EP_2, DP_1 and IP (Clapp and Gurung, 2015). Acute application of treprostinil upon cells expressing both TASK-1_WT and EP_2 generated a significantly enhanced TASK-1_WT current. This enhancement, although significant is small and gradual indicating that it may be an increase in cell surface expression of TASK-1_WT, through PKA activation as described previously. Application of treprostinil on TASK-1_WT and IP generated a significant decrease in TASK-1_WT current. IP receptors are proposed to act as activators of adenylyl cyclase and PKA in a dose-dependent manner (Smyth *et al.,* 2000). At higher concentrations it has been proposed IP receptors can activate PLC. It may be that the inhibition seen for TASK-1_WT current during this acute application is due to the concentration of treprostinil activating PLC (and DAG as a result)

through G_q coupling and not the desired G_s proteins (Bley *et al.,* 1998). Further evidence for this has been shown from prostacyclin treatments that affect the pathway activated in HEK293 cells. A short, high dose PGI_2 treatment activated PKC whereas a long, low dose PGI_2 treatment, resulted in PKA activation (Moriyama *et al.,* 2005). With this in mind the pathways involved in PAH pathogenesis can be updated to indicate the biphasic effects of IP receptors (Figure 4.49). IP receptors have been shown to form heterodimers with thromboxane receptors (TP). TP receptors are $G_{\alpha q}$-coupled and activate PLC (and PKC downstream) which may provide insight to the inhibitory actions of IP receptors (Pluchart *et al.,* 2017). Another insight is the EC_{50} for treprostinil action upon IP receptors is 1.9 nM whereas the concentration used within these experiments was at 1 µM (Whittle *et al.,* 2012).

Compounds, analysed in this study suggest that their mechanism of action is primarily to act through G-coupled receptors and C-terminus phosphorylation. In regards to the therapy for patients expressing the novel mutations, G106R and L214R, it would appear that this therapeutic target would not be a prudent line of therapy. The novel mutations appear to block the selectivity filter through large changes in amino acid structure and charge. It is this block of the selectivity filter that needs to be addressed in order to alleviate non-functionality seen within the mutated TASK-1 channels as increasing cell surface expression of a non-functioning channel will not generate an increase in TASK-1 current. One possible approach to rectify this would be to use homology modelling to analyse the G106R and L214R areas and develop compounds that could structurally alter the channel to open the selectivity filter. Alternatively the rise of CRISPR-Cas9 and other gene-editing tools could hold promise to repairing disease-causing mutations in ion channels (Snowball, 2015). Finally stimulating alternative ion channels and pathways may compensate for loss of TASK-1 activity.

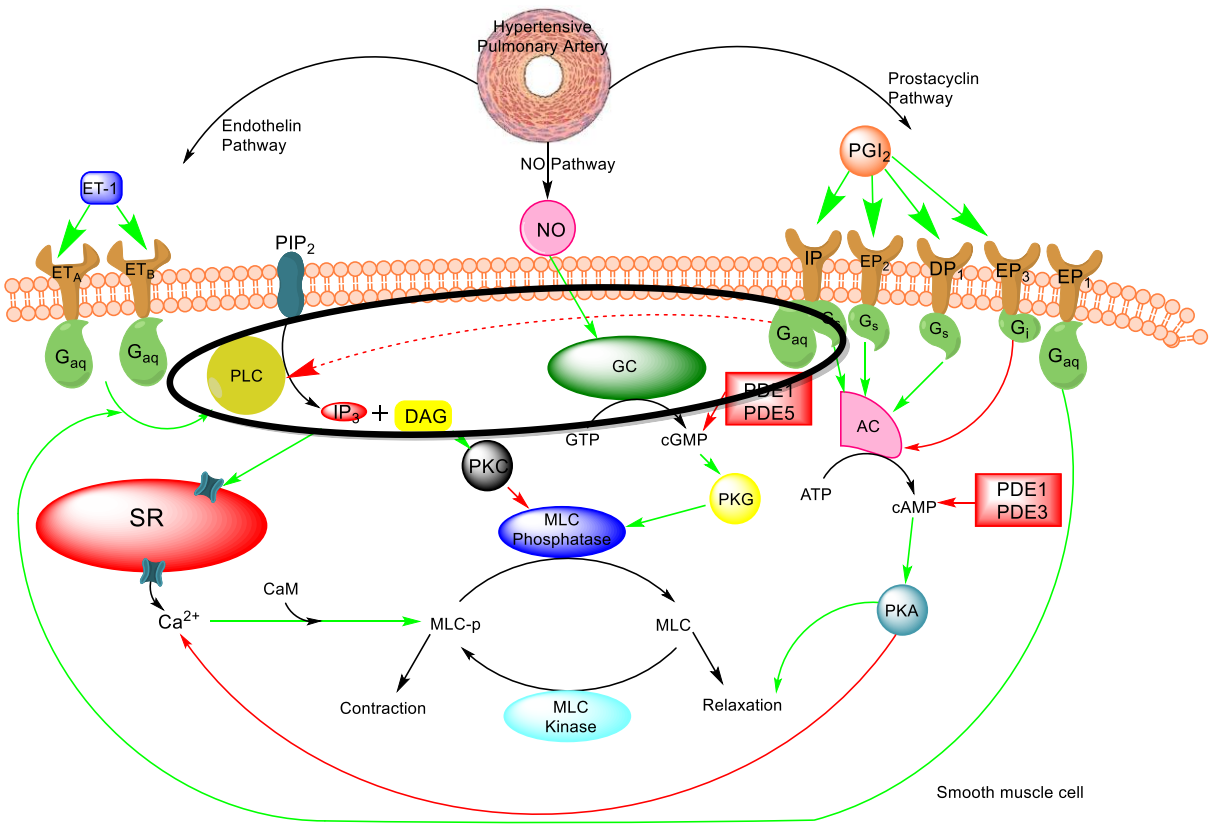

Figure 4.49 – Updated Key Pathways in Pulmonary Arterial Hypertension

Updated version of Figure 4.3, indicating the dual pathways of IP receptor upon PGI_2 binding. High concentrations of prostacyclin results in activation of $G_{\alpha q}$ couple proteins and the constrictive pathway whereas low concentrations activates G_s coupled proteins and relaxation pathway.

As treprostinil therapy causes severe site pain in 85% of patients undergoing subcutaneous infusion, causing 8% to withdraw from treatment, known K2P channels involved in pain signalling, were investigated for modulation by treprostinil (Simmonneau *et al.,* 2002). Current therapeutic strategies are to apply pain relief in the form of lidocaine, topically to the infusion site, however the pain is still experienced, which indicates lidocaine is not an adequate pain preventative approach. TREK-1 and TREK-2 have been implicated heavily in the pain signalling pathway and are expressed abundantly within nociceptors (Marsh *et al.,* 2012; Alloui *et al.,* 2006). Like TASK-1, TREK-1 and TREK-2 channels have been shown to be regulated by multiple G proteins (Mathie, 2007). In this study I have shown that acute application of treprostinil, potently and reversibly inhibits WT TREK-1 and TREK-2 currents. Some applications of treprostinil showed an over recovery of current following wash-off of

treprostinil, this is commonly seen with TREK inhibitors and current comes back down to baseline after a short period of time. The TREK-1 variant TREK1Δ1-41, has been shown previously to have reduced current levels, which can be recovered through histidine-modifying agents (Veale *et al.,* 2010). In this study we have shown that despite the reduced current of TREK-1Δ1-41, treprostinil still has a significant inhibition on whole-cell current. Whilst it appears the N-terminus influences functional and trafficking properties of the channel, the findings from this study indicating that the N-terminus does not play a role in treprostinil inhibition of TREK-1 (Thomas *et al.,* 2008; Simkin *et al.,* 2008; Veale *et al.,* 2010). As mentioned previously that S333 phosphorylation is crucial to the open probability of the channel and these findings further suggest that the inhibitory action of treprostinil on TREK channels occurs through PKA and S333 phosphorylation (Bockenhauer *et al.,* 2001).

Due to the speed of the effect seen by treprostinil it appears to have a direct action upon the channel. A secondary mechanism of action for treprostinil, may occur through the increase in cAMP levels and subsequent PKA activation. TREK channels are down-regulated by $G_{\alpha s}$ coupling as well as $G_{\alpha q}$ activation and subsequent PKC phosphorylation (Lesage *et al.,* 2000; Kang *et al.,* 2006; Murbartian *et al.,* 2005). Treprostinil acts primarily on IP receptors. Signalling pathways activated by treprostinil on IP receptors are dose-dependent. IP receptors couple with either $G_{\alpha s}$ or $G_{\alpha q}$ proteins both of which promote TREK channel inhibition. This provides a useful option for enhancing patient comfort during therapy. Application of a TREK activator at the site of administration may alleviate the pain experienced. Another possibility is to co-treat patients with a cAMP inhibitor, such as a topical cream localised to the site of infusion. It may be that the effect of treprostinil is an unfortunate, but necessary side effect, as an increase in cAMP levels is the desired effect to promote vasorelaxtion, anti-proliferation and anti-thrombotic effects. However possible pain-relieving sources should be explored providing they do not hinder the benefits of treprostinil.

5. Consolidation

5. Consolidation

Pulmonary disorders are a major cause of deaths within the United Kingdom with 20% of all deaths a consequence of a pulmonary disorder (British Lung Foundation, 2012). In this study multiple K2P channels have been investigated in their relation to pulmonary disorders. Doxapram, a ventilatory stimulant, is used in multiple pulmonary disorders including post-operative respiratory depression, acute respiratory failure chronic obstructive pulmonary disorder and apnoea (Yost *et al.*, 2008). We studied the effect of doxapram upon TASK-3 channels as well as any differences in action of the GAL-054, the eutomer of doxapram.

The second part of my study focused on pulmonary arterial hypertension (PAH) and how TASK-1 may play a role in the disease state. PAH is an incurable disease and current research indicates that three key pathways are involved in its pathogenesis – endothelin (ET), nitric oxide (NO) and prostacyclin (PGI_2). These pathways provide the major therapeutic targets in the treatment of PAH, which currently, are not sufficient for long-term patient survival. In chapter 4, novel genetic mutations of TASK-1 found in patients with an aggressive form of PAH, were characterised for the first time and known therapeutic compounds investigated to determine if that therapeutic effect occurs via the modulation of TASK-1 channels. Finally, I looked into whether a commonly used PAH therapeutic, treprostinil, had an effect upon known pain signalling K2P channels, TREK-1 and TREK-2.

5.1. Pharmacological action of doxapram on TASK-3 and future perspectives

TASK-3 channels are widely distributed but play a major role within the central nervous system (Goldstein *et al.,* 2005). The pharmacological action of doxapram is disputed with conflicting evidence between animal and human studies. Previous data obtained within the lab has shown that doxapram is equally potent on both human TASK-1 and human TASK-3 (Cunningham *et al.,* 2016). Furthermore it is suggested that putative site on TASK-3, previously

proposed on rat TASK-3 channels may be responsible for the action of doxapram. Two key mutations, L122D and L239D, suggest that a change within a 'hydrophobic cuff' of TASK-3 is responsible for preventing doxapram having its desired inhibitory effect. In addition to doxapram, we analysed GAL-054, an isolated eutomer of doxapram. Previous studies have indicated GAL-054 retains the therapeutic effects of doxapram with a reduction in adverse side effects (Golder *et al.,* 2012). Previous work within our lab showed that GAL-054 inhibited TASK-1 and TASK-3 channels equally (Appendix 6.5 and 6.6).

The M1P1 loop, a large extracellular pre-pore linker, has been widely implicated in K2P channel function as it lies close to the channel pore (Clarke *et al.,* 2008). It has also been shown to be vital for channel dimerization and certain residues have been found to be critical in channel regulation such as H98 in pH sensing (Lesage *et al.,* 1996; Morton *et al.,* 2002). We showed in this study that the M1P1 loop was critical to doxapram inhibition of TASK-3, by replacing the M1P1 loop with that of TASK-2, a similar but different K2P subfamily, the effect of doxapram was significantly reduced. I postulate that the structure of the TASK-3 M1P1 loop is vital to doxapram gaining access to a binding site on the channel and alteration of the loop results in a conformation that is non-conducive, to doxapram entry.

It would be insightful to look into the effects of doxapram on the heterodimeric channel TASK-1/TASK-3 and introduce the point mutations of the putative binding site. Currently very few studies have been conducted using GAL-054 to identify its full therapeutic profile. It is clear that TASK channels within the carotid bodies are a potential target for regulating ventilatory response, with new studies showing expression of TASK channels, enhanced following activation of pathways to increase oxygen supply, in response to hypoxic conditions (Yuan *et al.,* 2018).

5.2 TASK-1 involvement in pulmonary arterial hypertension

TASK-1 channels have been identified as the major contributor to pulmonary arterial smooth muscle cell (PASMC) resting membrane potential (Olschewski

et al., 2006). TASK-1 expression has been shown to be reduced with PAH and this has a vital role in the disease (Antigny *et al.,* 2016). Whole exome screening of patients with PAH have identified mutations residing on TASK-1 (Ma *et al.,* 2013). A parallel example of TASK channels in disease states is shown in TASK-3, where it has been found to play a key role in neuronal development (Bando *et al.,* 2012). Birk Barel mental retardation syndrome is caused by a single mutation (G236R) on the KCNK9 gene which is maternally transmitted and results in the developmental disorder observed in patients (Barel *et al.,* 2008). TASK-3_G236R currents are significantly smaller and inwardly rectifying compared to WT TASK-3 channels and can be partially recovered using pharmacological intervention (Veale *et al.,* 2014a).

With this in mind, studies have shown TASK-1 channels containing loss of function mutations, can also lead to PAH. It has been shown that the phospholipase A2 inhibitor, ONO-RS-082, can enhance TASK-1 channel activity and provide a potential avenue for PAH therapy (Ma *et al.,* 2013). In chapter 4, I characterised two novel mutations, G106R and L214R, found in patients with an aggressive form of PAH. These channels, appeared to be non-functional, however were translated and expressed with the same efficiency as TASK-1_WT at the membrane therefore it suggests that these channels are structurally closed, one possibility is that the selectivity filter has collapsed which prevents ion flow through the channel (See Appendix 6.11). As pharmacological recovery of these channels may be impossible, an alternative may be genome editing, such as CRISPR/CAS-9. Unfortunately, this still seems a long way from clinical use. One key aspect may be the hetero or homozygous nature of the mutation. Homozygous mutations are more aggressive and less susceptible to pharmacological regulation and further research will be required to improve therapeutic options for homozygous patients.

5.3 K2P involvement in PAH therapy

PAH therapeutics aim to promote the increase of intracellular secondary messengers, cAMP and cGMP, either through G-coupled receptors or direct

activation of a cyclase. It has been shown that cAMP and cGMP have vasodilatory and anti-proliferative effects (Stewart *et al.,* 1999; Fukumoto *et al.,* 2018; Buys *et al.,* 2018; Haynes Jr *et al.,* 1992). The action of secondary messengers on TASK-1 occurs through phosphorylation of the C-terminus. Phosphorylation of TASK-1 increases cell surface expression and would keep the pulmonary artery hyperpolarised. However in the case of G106R and L214R mutated TASK-1 channels, which sits at depolarised potentials, this is not a satisfactory therapeutic intervention. Increasing the amount of non-functioning channels expressed at the membrane will fail to create the normal negative membrane potential, meaning the cells will sit at a less polarised potential. TASK-1 is inhibited by $G_{\alpha q}$-coupled and activated by $G_{\alpha s}$-coupled receptors. In this study we show that activation of EP_2 receptors enhances TASK-1 current. However, IP receptor activation, can inhibit TASK-1, despite being $G_{\alpha s}$-coupled. This is probably due to IP receptors coupling also with $G_{\alpha q}$-proteins. Whilst treprostinil potently binds to EP_2 receptors, it also binds to IP receptors with high affinity (Clapp and Gurung, 2015; Patel *et al.,* 2018). Binding to IP receptors may hinder the maximum therapeutic effects of treprostinil, as IP receptors have been shown to form heterodimeric receptors with TP receptors, which are also $G_{\alpha q}$-coupled receptors (Pluchart *et al.,* 2017). In this study I also showed that co-expression with receptors has an inhibiting or enhancing effect on baseline TASK-1 current. This may occur through natural elevation of cAMP. It has been identified that within cAMP production, receptor expression is the main limiting factor in the cAMP production pathway (Alousi *et al.,* 1991).

I show that treprostinil has a direct and potent action upon TREK channels. TREK channels have implicated in pain signalling, having been identified in nociceptors (Alloui *et al.,* 2006). Patients undergoing treprostinil therapy experience severe site pain at the site of infusion, causing them to withdraw from therapy. Finding a therapeutic intervention to combat this pain is vital, in order to allow patients to comply with treatment. Whilst the experimental work shown in this study is at an early stage, the results presented and previous studies in TREK channels highlight a promising area of exploration. Patient comfort is a key area within drug delivery. Alleviating pain suffered by patients

would be a big step particularly in a disease with very few effective treatment options.

5.4 Future Experiments

With the work in this study being conducted in heterologous mammalian cell cultures, the next step would be to conduct testing within isolated human and/or animal tissues or animal models. To date, there is already a substantial amount of work conducted on the role of TASK-1 within the PASMCs of different species. Whilst TASK-1 properties have shown similarities in human, rabbit and rat PASMCs there are differences revealed in mice (Olschewski *et al.,* 2006; Gurney *et al.,* 2003; Antigny *et al.,* 2016; Manoury *et al.,* 2011). Mice with the TASK-1 gene knocked out do not show phenotypic signs of PAH and the cardiovascular phenotype observed is due to hyperaldosteronism, rather than vascular impairment (Manoury *et al.,* 2011; Heitzmann *et al.,* 2008). Therefore when selecting appropriate models of PAH and TASK-1, mice models/PASMCs would not be a prudent choice to translate the results in regard to human PAH and pulmonary physiology. Mice TASK-1 channels appear to act in a different way to those of rats, rabbits and humans. Species differences were also seen by Manoury *et al.,* 2013, with regard to doxapram as binding shown in Chapter 3.

5.5 Concluding remarks

PAH is a progressive and ultimately fatal disease, establishing effective therapeutic interventions remains paramount for future research. To summarise this study, with the use of electrophysiological and imaging techniques, I have characterised two novel mutations of TASK-1 present in PAH patients. The mutations cause a non-functioning channel which could not be recovered with current pharmacological tools and is, likely to play a role in the pathogenesis of the disease. I show that therapeutic compounds such as sildenafil and riociguat enhance TASK-1_WT current, but fail to recover current through disease causing mutations suggesting, they may not be useful therapies for these particular PAH patients. Increasing cell surface expression of TASK-1 channels, may prove helpful for low-functioning channels, but has

little benefit in non-functional channels such as G106R and L214R. Further work is required on the precise action of PAH therapeutics on TASK-1 channels. TASK-1 and its regulation appears to be receptor dependent in its response to treprostinil. Further work to clarify prostanoid receptor interaction with TASK-1 is required, also, further research into TREK channel involvement in the local site pain experienced during treprostinil therapy will need to be conducted however this study has indicated a possible cause and therefore treatment option for the pain. The use of a TREK channel activator, such as an anaesthetic, could alleviate the pain experienced during treprostinil therapy.

6. Appendix

6. Appendix

6.1 Human TASK-1 amino acid sequence

```
        10         20         30         40         50
MKRQNVRTLA LIVCTFTYLL VGAAVFDALE SEPELIERQR LELRQQELRA
        60         70         80         90        100
RYNLSQGGYE ELERVVLRLK PHKAGVQWRF AGSFYFAITV ITTIGYGHAA
       110        120        130        140        150
PSTDGGKVFC MFYALLGIPL TLVMFQSLGE RINTLVRYLL HRAKKGLGMR
       160        170        180        190        200
RADVSMANMV LIGFFSCIST LCIGAAAFSH YEHWTFFQAY YYCFITLTTI
       210        220        230        240        250
GFGDYVALQK DQALQTQPQY VAFSFVYILT GLTVIGAFLN LVVLRFMTMN
       260        270        280        290        300
AEDEKRDAEH RALLTRNGQA GGGGGGGSAH TTDTASSTAA AGGGGFRNVY
       310        320        330        340        350
AEVLHFQSMC SCLWYKSREK LQYSIPMIIP RDLSTSDTCV EQSHSSPGGG
       360        370        380        390
GRYSDTPSRR CLCSGAPRSA ISSVSTGLHS LSTFRGLMKR RSSV
```

Figure 6.1 – Human TASK-1 amino acid sequence

Uniprot entry ID: O14649, Length: 394 amino acids, molecular weight: 43.5 kDa

6.2 Human TASK-3 amino acid sequence

```
        10         20         30         40         50
MKRQNVRTLS LIVCTFTYLL VGAAVFDALE SDHEMREEEK LKAEEIRIKG
        60         70         80         90        100
KYNISSEDYR QLELVILQSE PHRAGVQWKF AGSFYFAITV ITTIGYGHAA
       110        120        130        140        150
PGTDAGKAFC MFYAVLGIPL TLVMFQSLGE RMNTFVRYLL KRIKKCCGMR
       160        170        180        190        200
NTDVSMENMV TVGFFSCMGT LCIGAAAFSQ CEEWSFFHAY YYCFITLTTI
       210        220        230        240        250
GFGDYVALQT KGALQKKPLY VAFSFMYILV GLTVIGAFLN LVVLRFLTMN
       260        270        280        290        300
SEDERRDAEE RASLAGNRNS MVIHIPEEPR PSRPRYKADV PDLQSVCSCT
       310        320        330        340        350
CYRSQDYGGR SVAPQNSFSA KLAPHYFHSI SYKIEEISPS TLKNSLFPSP
       360        370
ISSISPGLHS FTDHQRLMKR RKSV
```

Figure 6.2 – Human TASK-3 amino acid sequence

Uniprot entry ID: Q9NPC2, length: 374 amino acids, molecular weight: 42.3 kDa

6.3 Human TREK-1 amino acid sequence

```
        10         20         30         40         50
MLPSASRERP GYRAGVAAPD LLDPKSAAQN SKPRLSFSTK PTVLASRVES
        60         70         80         90        100
DTTINVMKWK TVSTIFLVVV LYLIIGATVF KALEQPHEIS QRTTIVIQKQ
       110        120        130        140        150
TFISQHSCVN STELDELIQQ IVAAINAGII PLGNTSNQIS HWDLGSSFFF
       160        170        180        190        200
AGTVITTIGF GNISPRTEGG KIFCIIYALL GIPLFGFLLA GVGDQLGTIF
       210        220        230        240        250
GKGIAKVEDT FIKWNVSQTK IRIISTIIFI LFGCVLFVAL PAIIFKHIEG
       260        270        280        290        300
WSALDAIYFV VITLTTIGFG DYVAGGSDIE YLDFYKPVVW FWILVGLAYF
       310        320        330        340        350
AAVLSMIGDW LRVISKKTKE EVGEFRAHAA EWTANVTAEF KETRRRLSVE
       360        370        380        390        400
IYDKFQRATS IKRKLSAELA GNHNQELTPC RRTLSVNHLT SERDVLPPLL
       410        420
KTESIYLNGL TPHCAGEEIA VIENIK
```

Figure 6.3 – Human TREK-1 amino acid sequence

Uniprot entry ID: O95069, length: 426 amino acids, molecular weight: 47.1 kDa

6.4 Human TREK-2 amino acid sequence

```
        10         20         30         40         50
MFFLYTDFFL SLVAVPAAAP VCQPKSATNG QPPAPAPTPT PRLSISSRAT
        60         70         80         90        100
VVARMEGTSQ GGLQTVMKWK TVVAIFVVVV VYLVTGGLVF RALEQPFESS
       110        120        130        140        150
QKNTIALEKA EFLRDHVCVS PQELETLIQH ALDADNAGVS PIGNSSNNSS
       160        170        180        190        200
HWDLGSAFFF AGTVITTIGY GNIAPSTEGG KIFCILYAIF GIPLFGFLLA
       210        220        230        240        250
GIGDQLGTIF GKSIARVEKV FRKKQVSQTK IRVISTILFI LAGCIVFVTI
       260        270        280        290        300
PAVIFKYIEG WTALESIYFV VVTLTTVGFG DFVAGGNAGI NYREWYKPLV
       310        320        330        340        350
WFWILVGLAY FAAVLSMIGD WLRVLSKKTK EEVGEIKAHA AEWKANVTAE
       360        370        380        390        400
FRETRRRLSV EIHDKLQRAA TIRSMERRRL GLDQRAHSLD MLSPEKRSVF
       410        420        430        440        450
AALDTGRFKA SSQESINNRP NNLRLKGPEQ LNKHGQGASE DNIINKFGST
       460        470        480        490        500
SRLTKRKNKD LKKTLPEDVQ KIYKTFRNYS LDEEKKEEET EKMCNSDNSS
       510        520        530
TAMLTDCIQQ HAELENGMIP TDTKDREPEN NSLLEDRN
```

Figure 6.4 – Human TREK-2 amino acid sequence

Uniprot entry ID: P57789, length: 538 amino acids, molecular weight: 59.8 kDa

6.5 Effect of Doxapram and its enantiomers (GAL-053 & -054) on human TASK-1

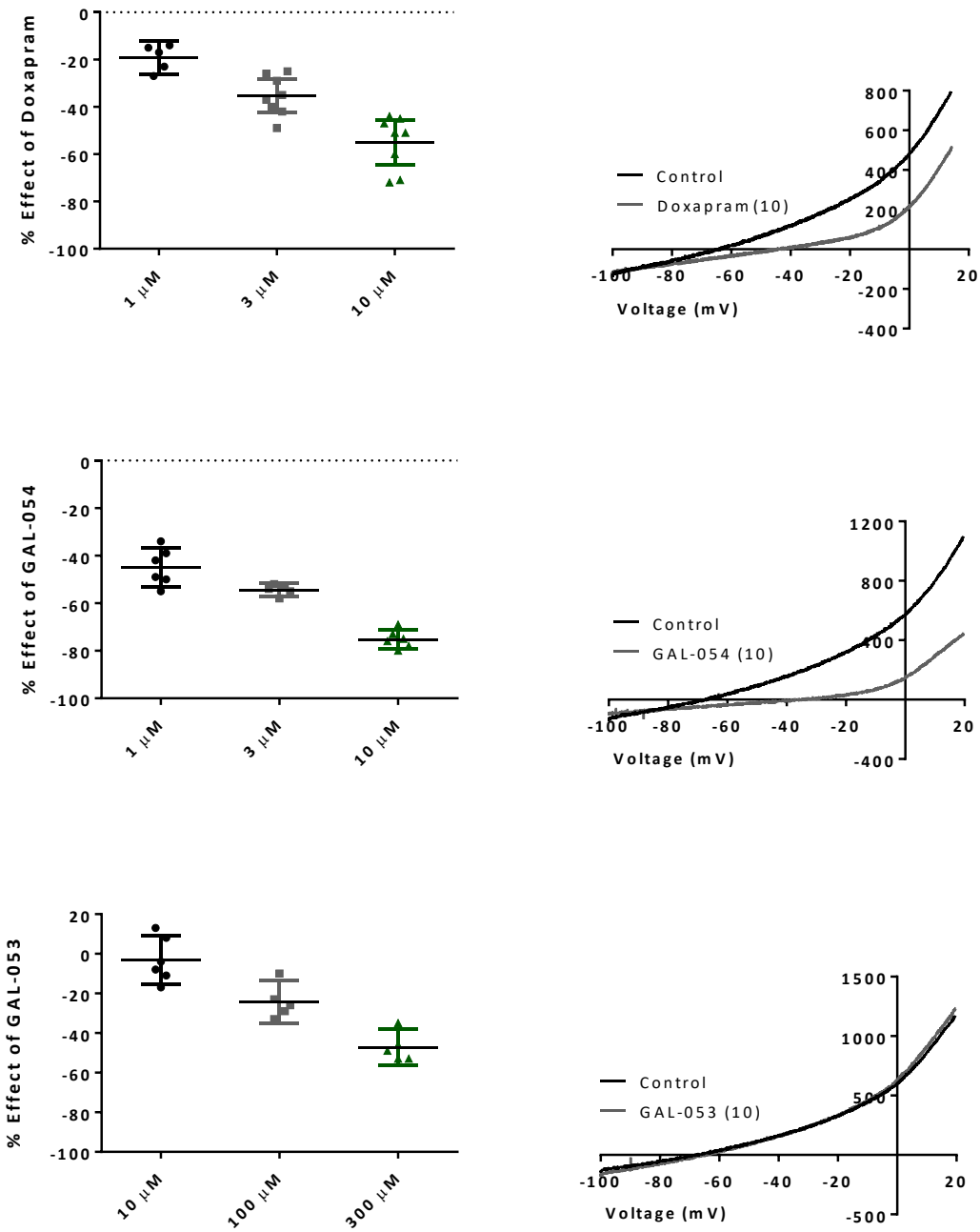

Figure 6.5 – Effect of doxapram, GAL-053 and GAL-054 on human TASK-1_WT channels

6.6 Effect of Doxapram and its enantiomers (GAL-053 & -054) on human TASK-3

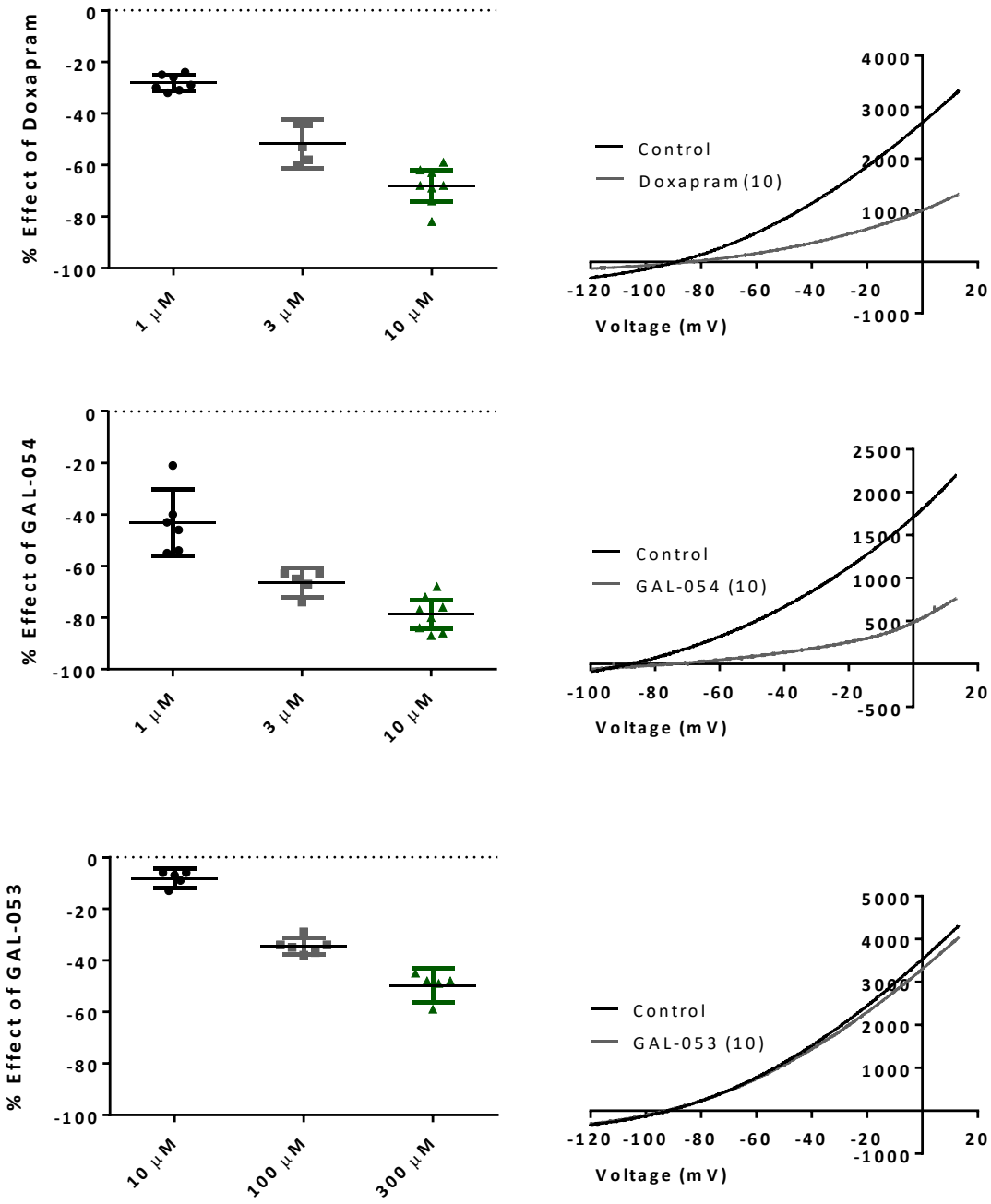

Figure 6.6 - Effect of doxapram, GAL-053 and GAL-054 on human TASK-3_WT channels

6.7 Doxapram Inhibition of Human TASK-1/TASK-3 Heterodimers

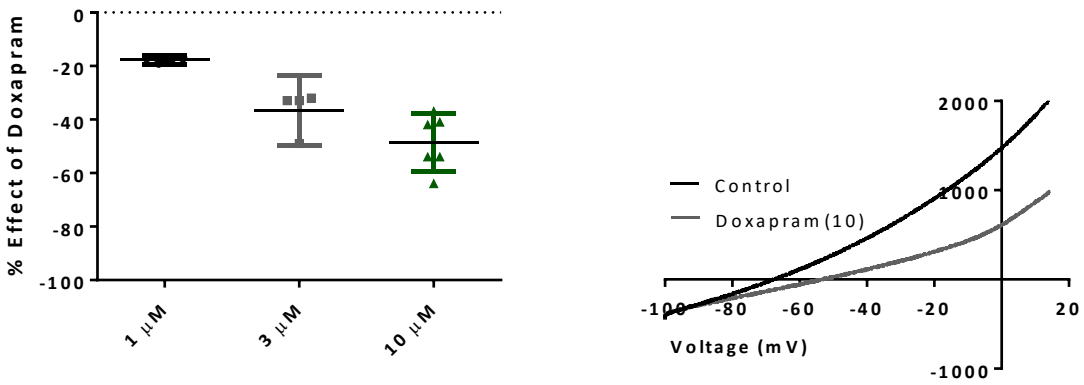

Figure 6.7 – Effect of Doxapram on TASK-1/TASK-3 Heterodimeric channels

6.8 Doxapram Inhibition of Mouse TASK-1 and TASK-3

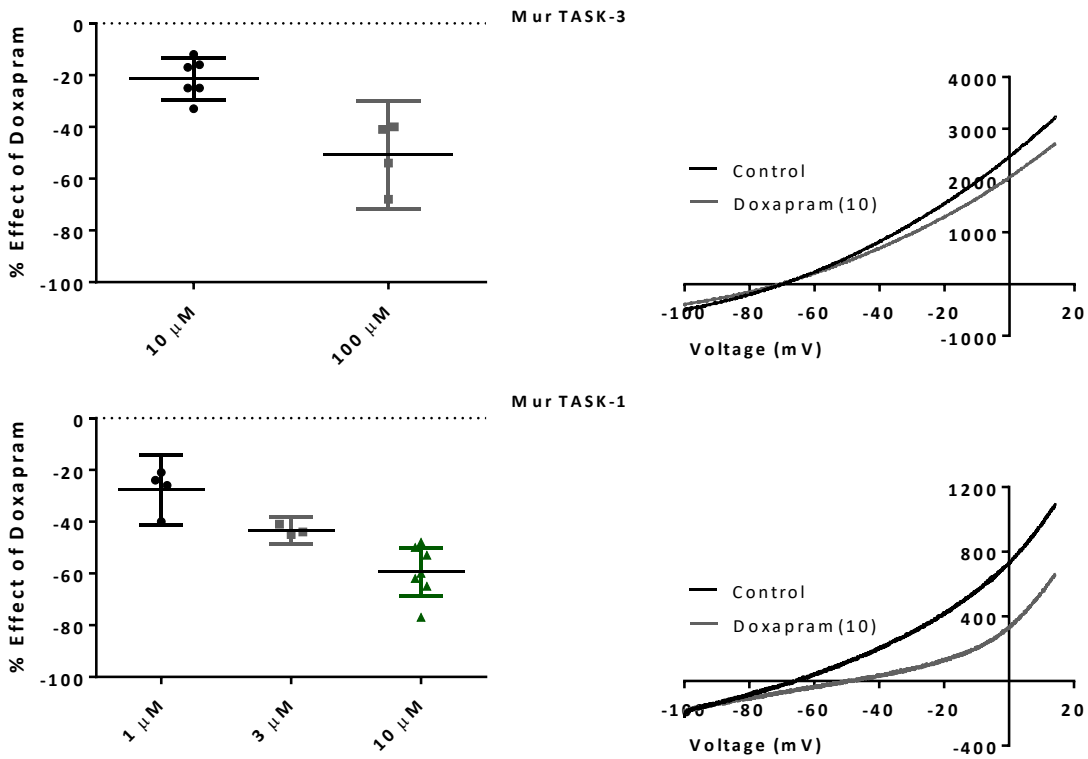

Figure 6.8 – Effect of Doxapram on mouse TASK-1 and TASK-3 channels

6.9 Effect of Forskolin and IBMX on Mouse TASK-3/TASK-1

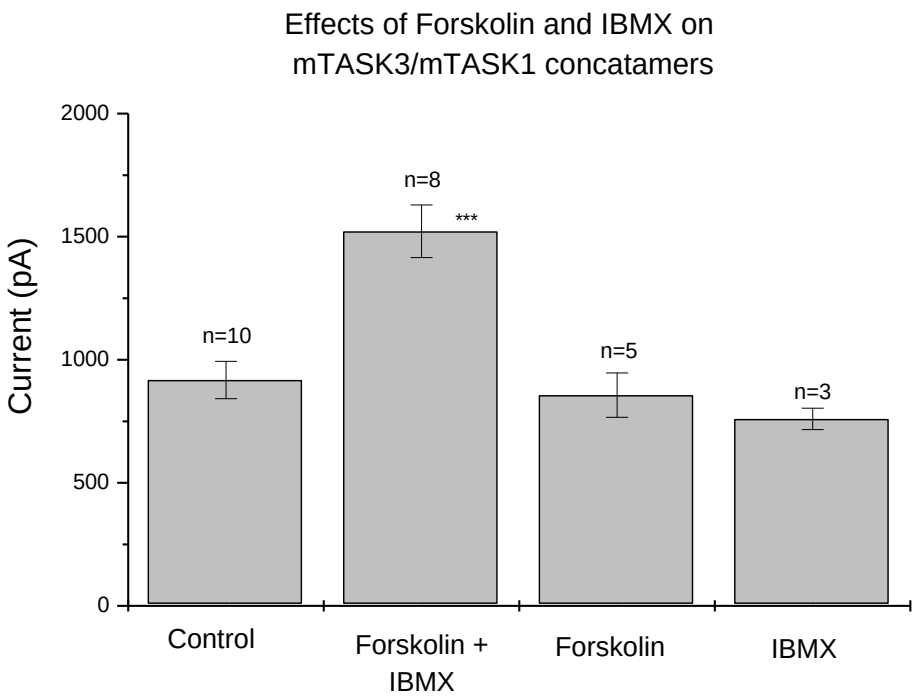

Figure 6.9 – Effect of Forskolin and IBMX on Mouse TASK-3/TASK-1

Unpublished work conducted within the lab.

6.10 Effect of Concatamer Arrangment on Forskolin and IBMX Action

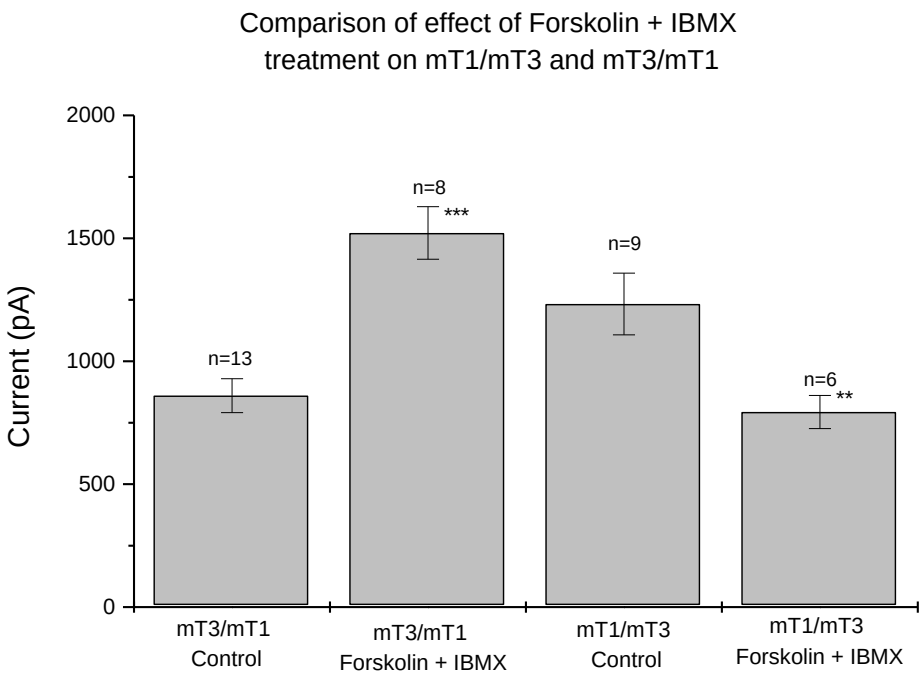

Figure 6.10 – Effect of Concatamer Arrangment on Forskolin and IBMX Action

Arrangement of TASK-1/TASK-3 alters the effect of forskolin and IBMX, TASK-1 n terminus results in enhancement of channel current whereas TASK-3 n terminus results in inhibition of channel current. Unpublished work conducted within the lab.

6.11 Permeability of TASK-1 WT and Novel Mutants

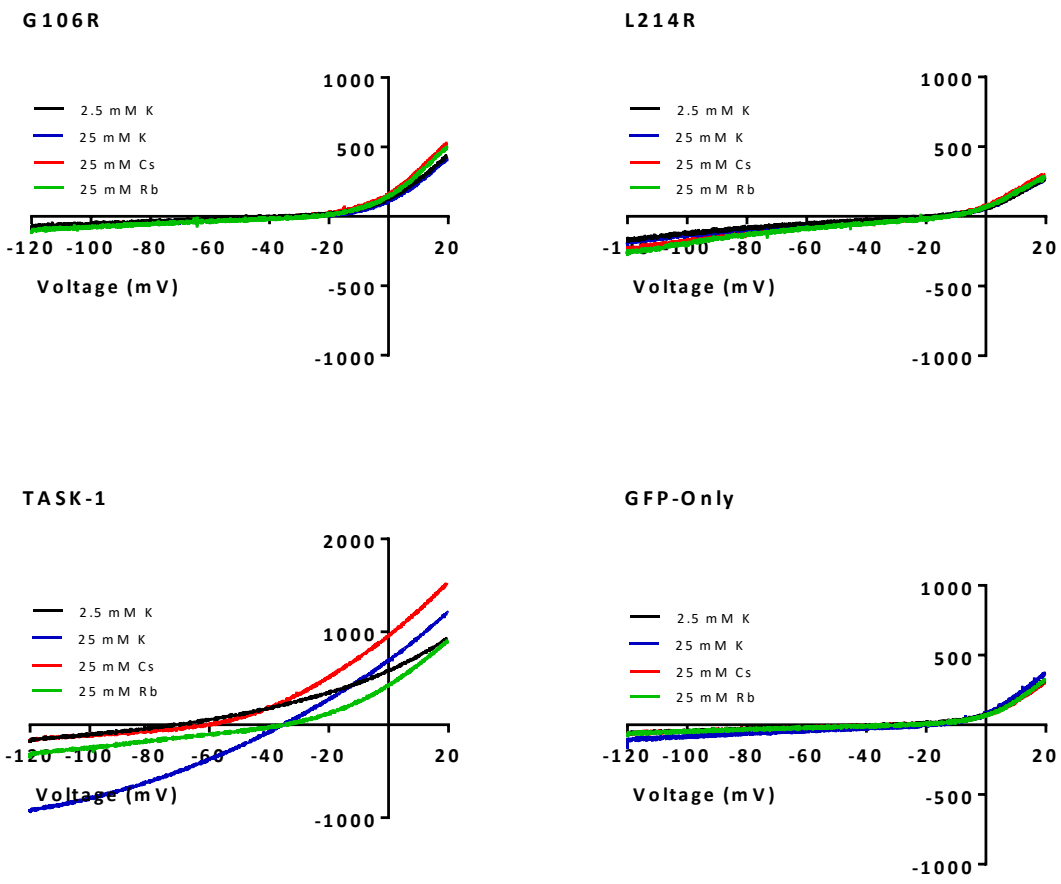

Figure 6.11 – Permeability of TASK-1_WT and Novel Mutant channels

Permeability of cells expressing either TASK-1_WT, TASK-1_G106R, TASK-1_L214R or GFP to 2.5 mM K^+ (black line), 25 mM K^+ (blue line), 25 mM Cs (red line) and 25 mM Rb (green line). Permeability of channels are recorded over voltages ranging from -120 mV to +20 mV.

6.12 Effect of permeating ion on TASK-1 channel current reversal potential

	2.5 mM K	**25 mM K**	**25 mM Cs**	**25 mM Rb**
TASK-1	-73 ± 2 (n = 13)	-38 ± 1 (n = 10)	-64 ± 2 (n = 8)	-41 ± 3 (n = 7)
TASK-1_G106R	-33 ± 8 (n = 5)	-28 ± 4 (n = 5)	-29 ± 5 (n = 5)	-25 ± 3 (n = 5)
TASK-1_L214R	-19 ± 3 (n = 5)	-17 ± 2 (n = 5)	-18 ± 4 (n = 5)	-15 ± 3 (n = 5)
GFP alone	-32 ± 2 (n =13)	-25 ± 3 (n = 6)	-31 ± 4 (n = 5)	-27 ± 3 (n = 5)

Figure 6.12 – Effect of Permeating Ion on TASK-1 Channel Current

Reversal potentials (in mV) obtained for TASK-1, TASK-1_G106R, TASK-1_L214R and GFP alone transfected cells when the external solution contained 2.5 mM K, 25 mM K, 25 mM Cs, or 25 mM Rb.

7. References

Acosta, C., Djouhri, L., Watkins, R., Berry, C., Bromage, K. and Lawson, S.N. (2014). 'TREK2 expressed selectively in IB4-binding C-fiber nociceptors hyperpolarizes their membrane potentials and limits spontaneous pain.' *The Journal of Neuroscience*, 34 (4): 1494 – 1509.

Alexander, S.P.H., Peters, J.A., Kelly, E., Marrion, N., Benson, H.E., Faccenda, E., Pawson, A.J., Sharman, J.L., Southan, C., Davies, J.A., *et al.* (2015). 'The Concise Guide to PHARMACOLOGY 2015/16: Ligand-gated ion channels.' *British Journal of Pharmacology – The Concise Guide to Pharmacology 2015/16,* 172 (24).

Alloui, A., Zimmermann, K., Mamet, J., Duprat, F., Noël, J., Chemin, J., Guy, N., Blondeau, N., Voilley, N., Rubat-Coudert, C., Borsotto, M., Romey, G., Heurteaux, C., Reeh, P., Eschalier, A. and Lazdunski, M. (2006). 'TREK-1, a K^+ channel involved in polymodal pain perception.' *EMBO J,* 25: 2368 – 2376.

Alousi, A.A., Jasper, J.R., Insel, P.A. and Motulsky, H.J. (1991). 'Stoichiometry of receptor-Gs-adenylate cyclase interactions.' *FASEB J,* 5 (9): 2300 – 2303.

Anderson-Beck, R., Wilson, L., Brazier, S., Hughes, I.E. and Peers, C. (1995). 'Doxapram stimulates dopamine release from the intact rat carotid body in vitro.' *Neuroscience Letters,* 187 (1): 25 – 28.

Anichkov, S. and Belen'kii, M. (1963). 'Pharmacology of the Carotid Body Chemoreceptors.' *Pergamon Press, Oxford, England*.

Antigny, F., Hautefort, A., Meloche, J., Belacel-Ouari, M., Manoury, B., Rucker-Martin, C., Péchoux, C., Potus, F., Nadeau, V., Tremblay, E., Ruffenach, G., Bourgeois, A., Dorfmüller, P., Breuils-Bonnet, S., Fadel, E., Ranchoux, B., Jourdon, P., Girerd, B., Montani, D., Provencher, S., Bonnet, S., Simonneau, G., Humbert, M. and Perros, F. (2016). 'Potassium Channel Subfamily K Member 3 (KCNK3) Contributes to the Development of Pulmonary Arterial Hypertension.' *Circulation,* 133 (4): 1371-1385.

Arrighi, I., Lesage, F., Scimeca, J.C., Carle, G.F. and Barhanin, J. (1998). 'Structure, chromosome localization, and tissue distribution of the mouse twik K^+ channel gene.' *FEBS Letters,* 425 (2): 310-316.

Aryal, P., Jarerattanachat, V., Clausen, M.V., Schewe, M., McClenaghan, C., Argent, L., Conrad, L.J., Dong, Y.Y., Pike, A.C.W., Carpenter, E.P., Baukrowitz, T., Sansom, M.S.P. and Tucker, S.J. (2017). 'Bilayer-Mediated Structural Transitions Control Mechanosensitivity of the TREK-2 K2P Channel.' *Structure,* 25 (5): 708 – 718.

Bagriantsev, S.N., Ang, K.H., Gallardo-Godoy, A., Clark, K.A., Arkin, M.R., Renslo, A.R. and Minor Jr, D.L. (2013). 'A high-throughput functional screen identifies small molecule regulators of temperature- and mechano-sensitive K2P channels.' ACS Chemical Biology, 8 (8): 1841 – 1851.

Bal, R., Ozturk, G., Etem, E.O., Him, A., Cengiz, N., Kuloglu, T., Tuzcu, M., Yildirim, C. and Tektemur, A. (2018). 'Modulation of excitability of stellate neurons in the ventral cochlear nucleus of mice by ATP-sensitive potassium channels.' *Journal of Membrane Biology,* 251 (1): 163-178.

Bando, Y., Hirano, T. and Tagawa, Y. (2014). 'Dysfunction of KCNK Potassium Channels Impairs Neuronal Migration in the Developing Mouse Cerebral Cortex.' *Cerebral Cortex,* 24 (4): 1017-1029.

Barberà, J.A., Román, A., Gómez-Sánchez, M.A., Blanco, I., Otero, R., López-Reyes, R., Otero, I., Pérez-Peñate, G., Sala, E. and Escribano, P. (2018). 'Guidelines on the Diagnosis and Treatment of Pulmonary Hypertension: Summary of Recommendations.' *Archivos de Bronconeumología,* 54 (4): 205-215.

Bardou, O., Trinh, N.T.N and Brochiero, E. (2009). 'Molecular diversity and function of K^+ channels in airway and alveolar epithelial cells.' *American Journal of Physiology – Lung Cellular and Molecular Physiology,* 296 (2): L145-L155.

Barel, O., Shalev, S.A., Ofir, R., Cohen, A., Zlotogora, J., Shorer, Z., Mazor, G., Finer, G., Khateeb, S., Zilberberg, N. and Birk, O.S. (2008). 'Maternally Inherited Birk Barel Mental Retardation Dysmorphism Syndrome Caused by a Mutation in the Genomically Imprinted Potassium Channel *KCNK9.*' *The American Journal of Human Genetics,* 83 (2): 193-199.

Barst, R. (2010). 'How has epoprostenol changed the outcome for patients with pulmonary arterial hypertension?' *The International Journal of Clinical Practice,* 64 (s168): 23-32.

Batard, P., Jordan, M. and Wurm, F. (2001) 'Transfer of high copy number plasmid into mammalian cells by calcium phosphate transfection', *Gene*, 270 (1–2): 61 – 68. doi: 10.1016/S0378-1119(01)00467-X.

Bautista, D.M., Sigal, Y., Milstein, A.D., Garrison, J.L., Zorn, J.A., Tsuruda, P.R., Nicoll, R.A. and Julius, D. (2008). 'Pungent agents from Szechuan peppers excite sensory neurons by inhibiting two-pore potassium channels.' *Nature Neuroscience,* 11 (7): 772 – 779.

Bayliss, D.A., Sirois, J.E. and Talley, E.M. (2003). 'The TASK Family: Two-pore domain background K^+ channels.' *Molecular Interventions,* 3 (4): 205-219.

Bayliss, D.A. and Barrett, P.Q. (2008). 'Emerging roles for two-pore-domain potassium channels and their potential therapeutic impact.' *Trends in Pharmacological Sciences,* 29 (11): 566-575.

Bayliss, D.A., Barhanin, J., Gestreau, C. and Guyenet, P.G. (2015). 'The role of pH-sensitive TASK channels in central respiratory chemoreception.' *Pflugers Archiv: European Journal of Physiology,* 467 (5): 917 – 929.

Belknap, J.K., Orton, E.C., Ensley, B., Tucker, A. and Stenmark, K.R. (1997). 'Hypoxia increases bromodeoxyuridine labeling indices in bovine neonatal pulmonary arteries.' *American Journal of Respiratory Cell and Molecular Biology,* 16 (4): 366-371.

Berg, A.P., Talley, E.M., Manger, J.P. and Bayliss, D.A. (2004). 'Motoneurons Express Heteromeric TWIK-Related Acid-Sensitive K^+ (TASK) Channels Containing TASK-1 (KCNK3) and TASK-3 (KCNK9) Subunits.' *The Journal of Neuroscience,* 24 (30): 6693-6702.

Bernstein J. (1902a) Untersuchungen zur Thermodynamik der bioelektrischen Ströme: Erster Theil. Pflügers Arch., 92: 521-562.

Bernstein J. and Tschermak A. (1902b). Ueber die Beziehung der negativen Schwankung des Muskelstromes zur Arbeitsleistung des Muskels. Pflügers Arch., 89: 289-333.

Bernstein J. (1912). Elektrobiologie. Die Lehre von den elektrischen Vorgangen in Organismus, auf moderner Grundlage dargestellt. Braunschweig, Vieweg.

Biggin, P.C., Roosild, T. and Choe, S. (2000). 'Potassium channel structure: domain by domain.' *Current Opinion in Structural Biology,* 10 (4): 456-461.

Bittner, S., Ruck, T., Schuhmann, M.K., Herrmann, A.M., Moha ou Maati, H., Bobak, N., Göbel, K., Langhauser, F., Stegner, D., Ehling, P., Borsotto, M., Pape, H.C., Nieswandt, B., Kleinschnitz, C., Heurteaux, C., Galla, H.J., Budde, T., Wiendl, H. and Meuth, S.G. (2013). 'Endothelial TWIK-related potassium channel-1 (TREK1) regulates immune-cell trafficking into the CNS.' *Nature Medicine,* 19 (9): 1161-1165.

Bley, K.R., Hunter, J.C., Eglen, R.M. and Smith, J.A.M. (1998). 'The role of IP prostanoid receptors in inflammatory pain.' *Trends in Pharmacological Sciences,* 19 (4): 141 – 147.

Blin, S., Chatelain, F.C., Feliciangeli, S., Kang, D., Lesage, F. and Bichet, D. (2014). 'Tandem Pore Domain Halothane-inhibited K+ Channel Subunits THIK1 and THIK2 Assemble and Form Active Channels.' *Journal of Biological Chemistry,* 289: 28202 – 28212.

Blin, S., Soussia, I.B., Kim, E.J., Brau, F., Kang, D., Lesage, F. and Bichet, D. (2016). 'Mixing and matching TREK/TRAAK subunits generate heterodimeric K2P channels with unique properties.' *Proceedings of the National Academy of Sciences of the United States of America,* 113 (15): 4200 – 4205.

Bockenhauer, D., Zilberberg, N. and Goldstein, S.A. (2001). 'KCNK2: reversible conversion of a hippocampal potassium leak into a voltage-dependent channel.' *Nature Neuroscience,* 4 (5): 486 – 491.

Bohnen, M.S., Roman-Campos, D., Terrenoire, C., Jnani, J., Sampson, K.J., Chung, W.K. and Kass, R.S. (2017). 'The Impact of Heterozygous KCNK3

Mutations Associated With Pulmonary Arterial Hypertension on Channel Function and Pharmacological Recovery.' *Journal of American Heart Association,* 6 (9): e006465.

Boolell, M., Allen, M.J., Ballard, S.A. (1996). 'Sildenafil: an orally active type 5 cyclic GMP-specific phosphodiesterase inhibitor for the treatment of penile erectile dysfunction.' *International Journal of Impotence Research,* 8 (2): 47-52.

Boucherat, O., Chabot, S., Antigny, F., Perros, F., Provencher, S. and Bonnet, S. (2015). Potassium channels in pulmonary arterial hypertension. *European Respiratory Journal,* 46 (4): 1167-1177

British Lung Foundation. (2012). 'Lung disease in the UK – big picture statistics'. Accessed on: 13/08/2018. [https://statistics.blf.org.uk/lung-disease-uk-big-picture].

Browhan, S.G., del Mármol, J. and MacKinnon, R. (2012). 'Crystal structure of the human K2P TRAAK, a lipid- and mechano-sensitive K+ ion channel.' *Science,* 335 (6067): 436-441.

Brohawn, S. G., Su, Z. and MacKinnon, R. (2014). 'Mechanosensitivity is mediated directly by the lipid membrane in TRAAK and TREK1 K + channels.' *Proceedings of the National Academy of Sciences*, 111 (9): 3614–3619.

Buckler, K.J. (1997). 'A novel oxygen-sensitive potassium current in rat carotid body type I cells.' *The Journal of Physiology,* 498 (Pt 3): 649 – 662.

Buckler, K.J., Williams, B.A. and Honore, E. (2000). 'An oxygen-, acid, and anaesthetic-sensitive TASK-like background potassium channel in rat arterial chemoreceptor cells. *The Journal of Physiology,* 525 (1): 135-142.

Buckler, K.J. (2007). 'TASK-like potassium channels and oxygen sensing in the carotid body.' *Respiratory Physiology & Neurobiology,* 157 (1): 55 – 64.

Buckler, K. J. (2015). 'TASK channels in arterial chemoreceptors and their role in oxygen and acid sensing', *Pflugers Archiv European Journal of Physiology*, 467 (5): 1013–1025.

Bushell, T., Clarke, C., Mathie, A. and Robertson, B. (2002). 'Pharmacological characterization of a non-inactivating outward current observed in mouse cerebellar Purkinje neurones.' *British Journal of Pharmacology,* 135: 705-712.

Buxton, I.L., Singer, C.A. and Tichenor, J.N. (2010). 'Expression of stretch-activated two-pore potassium channels in human myometrium in pregnancy and labor.' *PLoS One,* 5 (8): e12372.

Buys, E.S., Zimmer, D.P., Chickering, J., Graul, R., Chien, Y.T., Profy, A., Hadcock, J.R., Masferrer, J.L. and Milne, G.T. (2018). 'Discovery and development of next generation sGC stimulators with diverse multidimensional pharmacology and broad therapeutic potential.' *Nitric Oxide,* 78 (1): 72 – 80.

Chazova, I., Loyd, J.E., Zhdanov, V.S., Newman, J.H., Belenkov, Y. and Meyrick, B. (1995). 'Pulmonary artery adventitial changes and venous involvement in primary pulmonary hypertension.' *The American Journal of Pathology,* 146 (2): 389-97.

Chemin, J., Patel, A.J., Duprat, F., Lauritzen, I., Lazdunski, M. and Honoré, E. (2005). 'A phospholipid sensor controls mechanogating of the K^+ channel TREK-1.' *EMBO J,* 24 (1): 44 – 53.

Chemin, J, Patel, A.J, Duprat, F., Sachs, F., Lazdunski, M. and Honoré, E. (2007). 'Up- and down-regulation of the mechano-gated K(2P) channel TREK-1 by PIP (2) and other membrane phospholipids.' *European Journal of Physiology,* 455 (1): 97 – 103.

Chen, C. and Okayama, H. (1987) 'High-efficiency transformation of mammalian cells by plasmid DNA.', *Molecular and cellular biology*, 7 (8): 2745 – 2752. doi: 10.1128/MCB.7.8.2745.

Chen, X., Talley, E.M., Patel, N., Gomis, A., McIntire, W.E., Dong, B., Viana, F., Garrison, J.C. and Bayliss, D.A. (2006). 'Inhibition of a background potassium channel by Gq protein α-subunits.' *PNAS,* 103 (9): 3422-3427.

Chen, H., Chatelain, F.C. and Lesage, F. (2014). 'Altered and dynamic ion selectivity of K+ channels in cell development and excitability.' *Trends in Pharmacological Sciences,* 35 (9): 461 – 469.

Chen, Y., Zeng, X., Huang, X., Serag, S., Woolf, C.J. and Spiegelman, B.M. (2017). ‘Crosstalk between KCNK3-Mediated Ion Current and Adrenergic Signaling Regulates Adipose Thermogenesis and Obesity.’ *Cell,* 171 (4): 836-848.

Cheng, P.M. and Donnelly, D.F. (1995). 'Relationship between changes of glomus cell current and neural response of rat carotid body.' *The Journal of Neurophysiology,* 74 (5): 2077 - 2086.

Chester, A.H and Yacoub, M.H. (2014). ‘The role of endothelin-1 in pulmonary arterial hypertension.’ *Global Cardiology Science and Practice,* 29: 63-78.

Choe, S. (2002). ‘Potassium Channel Structures.’ *Nature Reviews,* 3 (2): 115-121.

Chokshi, R.H., Larsen, A.T., Bhayana, B. and Cotton, J.F. (2015). 'Breathing stimulant compounds inhibit TASK-3 potassium channel function likely by binding at a common site in the channel pore', *Molecular Pharmacology,* 88: 926-934.

Clapp, L. and Gurung, R. (2015). ‘The mechanistic basis of prostacyclin and its stable analogues in pulmonary arterial hypertension: Role of membrane versus nuclear receptors.’ *Prostaglandins and Other Lipid Mediators,* 120: 56-71.

Clarke, C.E., Veale, E.L., Green, P.J., Meadows, H.J. and Mathie, A. (2004). 'Selective block of the human 2-P domain potassium channel, TASK-3, and the native leak potassium current, IK_{SO}, by zinc.' *The Journal of Physiology,* 560 (1): 51 - 62.

Clarke, C.E., Veale, E.L., Wyse, K., Vandenberg, J.I. and Mathie, A. (2008). 'The M1P1 Loop of TASK3 K2P channels Apposes the Selectivity Filter and Influences Channel Function', *The Journal of Biological Chemistry,* 283: 16985 - 16992.

Cohen, A., Sargon, R., Somech, E., Segal-Hayoun, Y. and Zilberberg, N. (2009). ‘Pain-associated signals, acidosis and lysophosphatidic acid,

modulate the neuronal K(2P)2.1 channel.' Molecular and Cellular Neuroscience, 40 (3): 382 – 389.

Cole, K.S. (1949). Dynamic Electrical Characteristics of the Squid Axon Membrane. *Archives des Sciences Physiologiques,* 3: 253-258.

Cole, K.S. and Curtis, H.J. (1939). Electric Impedance of the Squid Giant Axon during Activity. *Journal of General Physiology.* 22: 649-670.

Conway, K.E. and Cotton, J.F. (2012). 'Covalent modification of a volatile anesthetic regulatory site activates TASK-3 (KCNK9) tandem-pore potassium channels.' *Molecular Pharmacology,* 81 (3): 393 - 400.

Cotten, J.F., Keshavaprasad, B., Laster, M.J., Eger, E.L. and Yost, C.S. (2006). 'The ventilatory stimulant doxapram inhibits TASK tandem pore (K2P) potassium channel function but does not affect minimum alveolar anesthetic concentration', *Anesthesia and Analgesia*, 102 (3): 779–785.

Cunningham, K.P., MacIntyre, D.E., Mathie, A. and Veale, E.L. (2016). 'The ventilatory stimulant, doxapram, is an equally potent inhibitor of the human two-pore domain potassium (K2P) channels, TASK-3 (KCNK9) and TASK-1 (KCNK3)', *pA2 online, British Pharmacological Society Meeting: Pharmacology 2016*, 16 (1): 83p

Cunningham, K.P., Cogolludo, A., Escribano, M., Veale, E.L. and Mathie, A. (2018). 'Characterisation and regulation of wild type and mutant TASK-1 two pore domain potassium channels indicated in Pulmonary Arterial Hypertension.' *Journal of Physiology* (Under Review).

Czirjak, G., Petheo, G.L., Spat, A. and Enyedi, P. (2001). 'Inhibition of TASK-1 potassium channel by phospholipase C.' *American Journal of Physiology Cell Physiology,* 281 (2): C700 – C708.

Czirjak, G. and Enyedi, P. (2002). 'Formation of functional heterodimers between the TASK-1 and TASK-3 two-pore domain potassium channel subunits.' *The Journal of Biological Chemistry,* 277 (7): 5426–5432.

D'Alonzo, G.E., Barst, R.J., Ayres, S.M., Bergofsky, E.H., Brundage, B.H., Detre, K.M., Fishman, A.P., Goldring, R.M., Groves, B.M, Kernis, J.T. *et al.*

(1991). ‘Survival in patients with primary pulmonary hypertension. Results from a national prospective registry.’ *Ann Inter Med,* 115: 343-349.

Davies, L.A., Hu, C., Guagliardo, N.A., Sen, N., Chen, X., Talley, E.M., Carey, R.M., Bayliss, D.A. and Barrett, P.Q. (2008). ‘TASK channel deletion in mice causes primary hyperaldosteronism.’ *PNAS*, 105: 2203-2208.

Decher, N., Maier, M., Dittrich, W., Gassenhuber, J., Brüggemann, A., Busch, A.E. and Steinmeyer, K. (2001). ‘Characterization of TASK-4, a novelmember of the pH-sensitive, two-pore domain potassium channel family.’ *FEBS Letters,* 492: 84-89.

Dedman, A., Sharif-Naeini, R., Folgering, J.H.A., Duprat, F., Patel, A. and Honoré, E. (2009). ‘The mechano-gated K2P channel TREK-1.’ *European Biophysics Journal,* 38 (3): 293 – 303.

Dobler, T., Springauf, A., Tovornik, S., Weber, M., Schmitt, A., Sedlmeier, R., Wischmeyer, E. and Döring, F. (2007). ‘TRESK two-pore-domain K+ channels constitute a significant component of background potassium currents in murine dorsal root ganglion neurones.’ *Journal of Physiology,* 3 (15): 867 – 879.

Dong, Y.Y., Pike, A.C.W., Mackenzie, A., McClenaghan, C., Aryal, P., Dong, L., Quigley, A., Grieben, M., Goubin, S., Mukhopadhyay, S., Ruda, G.F., *et al.* (2015). 'K2P channel gating mechanisms revealed by structures of TREK-2 and a complex with Prozac.' *Science,* 347 (6227): 1256 - 1259.

Döring, F., Scholz, H., Kühnlein, R.P., Karschin, A. and Wischmeyer, E. (2006). 'Novel *Drosophila* two-pore domain K^+ channels: rescue of channel function by heteromeric assembly', *European Journal of Neuroscience,* 24 (8): 2264-2274.

Doyle, D.A., Morais, C.J., Pfuetzner, R.A., Kuo, A., Gulbis, J.M., Cohen, S.L., Chait, B.T. and MacKinnon, R. (1998). ‘The structure of the potassium channel: molecular basis of K^+ conduction and selectivity. *Science,* 280 (5360): 69-77.

Doyle, T.P. and Donnelly, D.F. (1994). 'Effect of Na+ and K+ channel blockade

on baseline and anoxia-induced catecholamine release from rat carotid body.' *The Journal of Applied Physiology,* 77 (6): 2606 - 2611.

Duprat, F., Lesage, F., Patel, A.J., Fink, M., Romey, G. and Lazdunski, M. (2000). 'The neuroprotective agent riluzole activates the two P domain K(+) channels TREK1 and TRAAK.' *Molecular Pharmacology,* 57 (5): 906 – 912.

Dupuis, J., Jasmin, J.F., Prié, S. and Cernacek, P. (2000). 'Importance of local production of endothelin-1 and of the ET(B)Receptor in the regulation of pulmonary vascular tone.' *Pulmonary Pharmacology and Therapeutics,* 13 (3): 135-140.

Dupuis, J. and Hoeper, M.M. (2008). 'Endothelin receptor antagonists in pulmonary arterial hypertension.' *European Respiratory Journal,* 31 (2): 407-415.

Enyedi, P. and Czirjak, G. (2010). 'Molecular Background of Leak K^+ Currents: Two-Pore Domain Potassium Channels.' *Physiological Reviews,* 90 (2): 559-605.

Enyedi, P., Braun, G. and Czirjak, G. (2012). 'TRESK: The lone ranger of two-pore domain potassium channels.' *Molecular and Cellular Endocrinology,* 353 (1-2): 75-81.

Etter, E.F., Eto, M., Wardle, R.L., Brautigan, D.L. and Murphy, R.A. (2001). 'Activation of Myosin Light Chain Phosphatase in Intact Arterial Smooth Muscle During Nitric Oxide-induced relaxation.' *The Journal of Biological Chemistry,* 276 (37): 34681-34685.

Eyzaguirre, C. (2007). 'Electric synapses in the carotid body-nerve complex.' *Respiratory Physiology and Neurobiology,* 157 (1): 116 - 122.

Feliciangeli, S., Chatelain, F.C., Bichet, D. and Lesage, F. (2015). 'The family of K2P channels: salient structural and functional properties.' *The Journal of Physiology*, 593 (12): 2587-2603.

Fernandez, R.A., Sundivakkam, P., Smith, K.A., Zeifman, A.S., Drennan, A.R. and Yuan, J.X.J. (2012). 'Pathogenic Role of Store-Operated and Receptor-

Operated Ca^{2+} Channels in Pulmonary Arterial Hypertension.' *Journal of Signal Transduction,* Article ID 951497: 1-16.

Fink, M., Duprat, F., Lesage, F., Reyes, R., Romey, G., Heurteaux, C. and Lazdunski, M. (1996). 'Cloning, functional expression and brain localization of a novel unconventional outward rectifier K+ channel.' *The EMBO Journal*, 15(24): 6854–6862.

Fink, M., Lesage, F., Duprat, F., Heurteaux, C., Reyes, R., Fosset, M. and Lazdunski, M. (1998). 'A neuronal two P domain K+ channel stimulated by arachidonic acid and polyunsaturated fatty acids'. *EMBO Journal*, 17 (12): 3297–3308.

Finkelstein, G. (2015). 'Mechanical neuroscience: Emil du Bois-Reymond's innovations in theory and practice'. *Frontiers in Systems Neuroscience*, 9(September), pp. 1–4. doi: 10.3389/fnsys.2015.00133.

Fukumoto, S., Koyama, H., Hosoi, M., Yamakawa, K., Tanaka, S., Morii, H. and Nishizawa, Y. (2018). 'Distinct Role of cAMP and cGMP in the Cell Cycle Control of Vascular Smooth Muscle Cells.' *Circulation Research,* 85 (11): 985 – 991.

Galiè, N., Manes, A. and Branzi, A. (2004). 'The endothelin system in pulmonary arterial hypertension.' *Cardiovascular Research,* 61 (2): 227-237.

Galiè, N., Rubin, L.J., Hoeper, M., Jansa, P., Al-Hiti, H., Meyer, G., Chiossi, E., Kusic-Pajic, A. and Simonneau, G. (2008). 'Treatment of patients with mildly symptomatic pulmonary arterial hypertension with bosentan (EARLY study): a double-blind, randomised controlled trial.' *Lancet,* 371 (9630): 2093-2100.

Galiè, N., Palazzini, M. and Manes, A. (2010). 'Pulmonary arterial hypertension: from the kingdom of the near-dead to multiple clinical trial meta-analyses.' *European Heart Journal,* 31 (17): 2080-2086.

Galiè, N., Humbert, M., Vachiery, J.L., Gibbs, S., Lang, I., Torbicki, A., Simonneau, G., Peacock, A., Vonk Noordegraaf, A., Beghetti, M., Ghofrani, A., Gomez Sanchez, M.A., Hansmann, G., Klepetko, W., Lancellotti, P.,

Matucci, M., McDonagh, T., Pierard, L.A., Trindade, P.T., Zompatori, M. and Hoeper, M. (2015a). ‘ESC/ERS Guidelines for the diagnosis and treatment of pulmonary hypertension: The Joint Task Force for the Diagnosis and Treatment of Pulmonary Hypertension of the European Society of Cardiology (ESC) and the European Respiratory Society (ERS): Endorsed by: association for European Paediatric and Congenital Cardiology (AEPC), International Society for Heart and Lung Transplantation (ISHLT).’ *European Heart Journal,* 37 (1): 67-119.

Galiè, N., Müller, K., Scalise, A.V. and Grünig, E. (2015b). ‘PATENT PLUS: a blinded, randomised and extension study of riociguat plus sildenafil in pulmonary arterial hypertension.’ *The European Respiratory Journal,* 45 (5): 1314-1322.

Ghofrani, H.A, Humbert, M., Langleben, D., Schermuly, R., Stasch, J.P., Wilkins, M.R. and Klinger, J.R. (2017). ‘Riociguat: Mode of Action and Clinical Development in Pulmonary Hypertension.’ *Chest,* 151 (2): 468-480.

Girard, C., Duprat, F., Terrenoire, C., Tinel, N., Fosset, M., Romey, G., Lazdunski, M. and Lesage, F. (2001). 'Genomic and Functional Characteristics of Novel Human Pancreatic 2P Domain K^+ Channels.' *Biochemical and Biophysical Research Communications,* 282: 249-256.

Girerd, B., Perros, F., Antigny, F., Humbert, M. and Montani, D. (2014). ‘KCNK3: new gene target for pulmonary hypertension?’ *Expert Review of Respiratory Medicine,* 8 (4): 385-387.

Gögelein, H., Brendel, J., Steinmeyer, K., Strübing, C., Picard, N., Rampe, D., Kopp, K., Busch, A.E. and Bleich, M. (2004). 'Effects of the atrial antiarrhythmic drug AVE0118 on cardiac ion channels.' *Naunyn-Schmiedebergs Archives of Pharmacology,* 370 (3): 183 -192.

Golder, F.J., Gruber, R.B., Baby, S.M., Puskovic, V., Ideo, C.M., Peng, S., Dax, S.L., MacIntyre, E.D. and Mannion, J.C. (2012). 'Enantiomeric separation of doxapram reveals a superior respiratory stimulant, GAL-054', *The FASEB Journal,* 26 (1): S894.22

Golder, F.J., Hewitt, M.M. and McLeod, J.F. (2013). 'Respiratory stimulant

drugs in the post-operative setting.' *Respiratory Physiology & Neurobiology,* 189 (2): 395-402.

Goldstein, S.A.N., Wang, K.W., Ilan, N. and Pausch, M.H. (1998). 'Sequence and function of the two P domain potassium channels: implications of an emerging superfamily.' *Journal of Molecular Medicine,* 76: 13-20.

Gomez-Niño, A., Obeso, A., Baranda, J.A., Santo-Domingo, J., Lopez-Lopez, J.R. and Gonzalez, C. (2009). 'MaxiK potassium channels in the function of chemoreceptor cells of the rat carotid body.' *American Journal of Physiology - Cell Physiology,* 297 (3): C715 - C722.

Gonzalez, C., Almaraz, L., Obeso, A. and Rigual, R. (1992). 'Oxygen and acid chemoreception in the carotid body chemoreceptors.' *Trends in Neurosciences,* 15 (4): 146 - 153.

Gonzalez, C., Almaraz, L., Obeso, A. and Rigual, R. (1994). 'Carotid body chemoreceptors: from natural stimuli to sensory discharges.' *Physiological Reviews,* 74 (4): 829 - 898.

González, W., Zúñiga, L., Cid, L.P., Arévalo, B. Niemeyer, M.I. and Sepúlveda, F.V. (2013). 'An extracellular ion pathway plays a central role in the cooperative gating of a K2P K^+ Channel by extracellular pH.' *The Journal of Biological Chemistry,* 288 (8): 5984-5991.

Guide, T. A. (2008) *THE AXON GUIDE A Guide to Electrophysiology & Biophysics Laboratory Techniques*, *In Vitro*. doi: citeulike-article-id:960830.

Gurney, A.M., Osipenko, O.N., MacMillan, D., McFarlane, K.M., Tate, R.J. and Kempsill, F.E. (2003). ‘Two-Pore Domain K Channel, TASK-1, in Pulmonary Artery Smooth Muscle Cells.’ *Circulation Research,* 93 (10): 957 – 964.

Gurney, A.M. and Joshi, S. (2006). ‘The role of twin pore domain and other K+ channels in hypoxic pulmonary vasoconstriction.’ *Novartis Foundation Symposium,* 272: 218 – 228.

Haynes Jr, J., Robinson, J., Saunders, L., Taylor, A.E. and Strada, S.J. (1992). ‘Role of cAMP-dependent protein kinase in cAMP-mediated vasodilation.’

American Journal of Physiology – Heart and Circulatory Phsyiology, 262 (2): H511 – H516.

Heitzmann, D., Derand, R., Jungbauer, S., Bandulik, S., Sterner, C., Schweda, F., El Wakil, A., Lalli, E., Guy, N., Mengual, R., Reichold, M., Tegtmeier, I., Bendahhou, S., Gomez-Sanchez, C.E., Aller, M.I., Wisden, W., Weber, A., Lesage, F., Warth, R. and Barhanin, J. (2008). 'Invalidation of TASK1 potassium channels disrupts adrenal gland zonation and mineralocorticoid homeostasis.' *EMBO J,* 27: 179–187.

Hemnes, A.R. (2014). 'Pulmonary Arterial Hypertension Treatment Guidelines.' *Chest,* 146 (2): 239 – 241.

Hemnes, A.R. and Humbert, M. (2017). 'Pathobiology of pulmonary arterial hypertension: understanding roads less travelled.' *European Respiratory Review,* 246 (146): 170093.

Henderson, S., Magu, B., Rasmussen, C., Lancaster, S., Kerksick, C., Smith, P., Melton, C., Cowan, P., Greenwood, M., Earnest, C., Almada, A., *et al.* (2005). 'Effects of Coleus Forskohlii Supplementation on Body Composition and Hematological Profiles in Mildly Overweight Women.' *Journal of International Society of Sports Nutrition,* 2 (2): 54 – 62.

Hernandez, C.C., Zaika, O., Tolstykh, G.P. and Shapiro, M.S. (2008). 'Regulation of neural KCNQ channels: signalling pathways, structural motifs and functional implications.' *Journal of Physiology,* 586 (Pt 7): 1811-1821.

Heurteaux, C., Lucas, G., Guy, N., El Yacoubi, M., Thümmler, S., Peng, X.D., Noble, F., Blondeau, N., Widmann, C., Borsotto, M., Gobbi, G., Vaugeois, J.M., Debonnel, G. and Lazdunski, M. (2006). 'Deletion of the background potassium channel TREK-1 results in a depression-resistant phenotype.' *Nature Neuroscience,* 9 (9): 1134-1141.

Hibino, H., Inanobe, A., Furutani, K., Murakami, S., Findlay, I. and Kurachi, Y. (2010). 'Inwardly Rectifying Potassium Channels: Their Structure, Function, and Physiological Roles.' *Physiological Reviews,* 90 (1): 291:336.

Hille, B. (2001). Ion channels of excitable membranes. 1st ed. Sunderland, Mass.: Sinauer.

Hisatsune, C., Nakamura, K., Kuroda, Y., Nakamura, T. and Mikoshiba, K. (2005). ‘Amplification of Ca^{2+} Signaling by Diacylglycerol-mediated Inositol 1,4,5-Trisphosphate Production.’ *Journal of Biological Chemistry,* 280 (12): 11723 – 11730.

Hodgkin, A.L. (1937). Evidence for Electrical Transmission in Never Pat I & II. *Journal of Physiology,* 90 (2): 183-210 & 211-232.

Hodgkin, A.L and Huxley, A.F. (1939). Action Potentials Recorded from Inside a Nerve Fibre. *Nature,* 144: 710-711

Hodgkin, A.L and Huxley, A.F. (1945). Resting and Action Potentials in Single Nerve Fibres. *Journal of Physiology,* 104 (2): 176-195.

Hodgkin, A.L and Huxley, A.F. (1952). 'A quantitative description of membrane current and its application to conduction and excitation in nerve.' *Journal of Physiology,* 117 (4): 500-544.

Hodgkin, A.L. and Katz, B. (1949). The Effect of Sodium Ions on the Electrical Activity of the Giant Axon of the Squid. *Journal of Physiology,* 108: 37-77.

Hoggart, C.J., Venturini, G., Mangino, M., Gomez, F., Ascari, G., Zhao, J.H., Teumer, A., Winkler, T.W., Tšernikova, N., Luan, J., Mihailov, E., *et al.* (2014). 'Novel Approach Identifies SNPs in SLC2A10 and KCNK9 with Evidence for Parent-of-Origin Effect on Body Mass Index.' *PLOS Genetics,* 10 (7): e1004508.

Honoré, E. (2007). 'The neuronal background K2P channels: focus on TREK1.' *Nature Reviews Neuroscience,* 8: 251-261.

Huang, D.Y., Yu, B.W. and Fan, Q.W. (2008). ‘Roles of TRESK, a novel two-pore domain K^+ channel, in pain pathway and general anesthesia.’ *Neuroscience Bulletin,* 24: 166.

Humbert, M., Segal, E.S., Kiely, D.G., Carlsen, J., Schwierin, B. and Hoeper, M.M. (2007). ‘Results of European post-marketing surveillance of bosentan in pulmonary hypertension.’ *The European Respiratory Journal,* 30 (2): 338-344.

Humbert, M. (2013). ‘Impression, Sunset.’ *Circulation,* 127 (10): 1098 – 1100.

Humbert, M., Lau, E.M., Montani, D., Jaïs, X., Sitbon, O. and Simonneau, G. (2014). ‘Advances in therapeutic interventions for patients with pulmonary arterial hypertension.’ *Circulation,* 130 (24): 2189-2208.

Humbert, M. and Ghofrani, H.A. (2016). ‘The molecular targets of approved treatments for pulmonary arterial hypertension.’ *Thorax,* 71: 73-83.

Huxley, A.F. (2002). Classical Perspectives: Hodgkin and the action potential 1935-1952. *Journal of Physiology,* 538: p2.

Iglarz, M. and Clozel, M. (2010). ‘At the heart of tissue: endothelin system and end-organ damage.’ *Clinical Science,* 119 (11): 453-463.

Jasińska-Stroschein, M. and Orszulak-Michalak, D. (2014). ‘The current approach into signalling pathways in pulmonary arterial hypertension and their implication in novel therapeutic strategies.’ *Pharmacological Reports,* 66 (4): 552-564.

Jiang, B., Sun, X., Cao, K. and Wang, R. (2002). Endogenous Kv channels in human embryonic kidney (HEK-293) cells. *Molecular and Cellular Biochemistry,* 238: 69-79.

Jing, Z.C., Parikh, K., Pulido, T., Jerjes-Sanchez, C., White, R.J., Allen, R., Torbicki, A., Xu, K.F., Yehle, D., Laliberte, K., Arneson, C. and Rubin, L.J. (2013). ‘Efficacy and safety of oral treprostinil monotherapy for the treatment of pulmonary arterial hypertension: a randomized, controlled trial.’ *Circulation,* 127 (5): 624-633.

Kang, D. and Kim, D. (2004). 'Single-channel properties and pH sensitivity of two-pore domain K^+ channels of the TALK family.' *Biochemical and Biophysical Research Communications,* 315: 836-844.

Kang, D., Mariash, E. and Kim, D. (2004). 'Functional expression of TRESK-2, a new member of the tandem-pore K + channel family.' *Journal of Biological Chemistry,* 27 (2): 28063 - 28070.

Kang, D., La, J.H., Kim, E.J., Park, J.Y., Hong, S.G. and Han, J. (2006). An endogenous acid-sensitive K+ channel expressed in COS-7 cells. *Biochemical and Biophysical Research Communications,* 341 (4): 1231-1236.

Kedzierski, R.M. and Yanagisawa, M. (2001). ‘Endothelin System: The Double-Edged Sword in Health and Disease.’ *Annual Review of Pharmacology and Toxicology,* 41 (1): 851-876.

Kemp, P.J., Peers, C., Lewis, A. and Miller, P. (2004). 'Regulation of recombinant human brain tandem P domain K^+ channels by hypoxia: a role for O_2 in the control of neuronal excitability?' *Journal of Cellular and Molecular Medicine,* 8: 38-44.

Ketchum, K.A., Joiner, W.J., Sellers, A.J., Kaczmarek, L.K. and Goldstein, S.A.N. (1995). 'A new family of outwardly rectifying potassium channel proteins with two pore domains in tandem.' *Nature,* 376: 690-695.

Kilisch, M., Lytovchenko, O., Schwappach, B., Renigunta, V. and Daut, J. (2015). 'The role of protein–protein interactions in the intracellular traffic of the potassium channels TASK-1 and TASK-3.' *European Journal of Physiology,* 467 (5): 1105 - 1120.

Kilisch, M., Lytovchenko, O., Arakel, E.C., Bertinetti, D. and Schwappach, B. (2016). ‘A dual phosphorylation switch controls 14-3-3-dependent cell surface expression of TASK-1.’ *Journal of Cell Science,* 129 (4): 831 – 842.

Kim, D., Cavanaugh, E.J., Kim, I. and Carroll, J.L. (2009). ‘Heteromeric TASK-1/TASK-3 is the major oxygen-sensitive background K+ channel in rat carotid body glomus cells.’ *The Journal of Physiology,* 587 (Pt 12): 2963 – 2975.

Kiper, A.K., Rinné, S., Rolfes, C., Ramírez, D., Seebohm, G., Netter, M.F., González, W. and Decher, N. (2015). 'Kv1.5 blockers preferentially inhibit TASK-1 channels: TASK-1 as a target against atrial fibrillation and obstructive sleep apnea?' *European Journal of Physiology,* 467 (5): 1081 - 1090.

Kiss, L. and Korn, S.J. (1998). ‘Modulation of C-Type Inactivation by K+ at the Potassium Channel Selectivity Filter.’ *Biophysical Journal,* 74 (4): 1840 – 1849.

Kozak, M. (2005). ‘Regulation of translation via mRNA structure in prokaryotes and eukaryotes.' *Gene*, 361 (1–2): 13–37.

Labro, A.J. and Snyders, D.J. (2012). 'Being flexible: the voltage-controllable activation gate of Kv channels.' *Frontiers in Pharmacology,* 3 (168): 1-12.

Lafreniere, R.G., Cader, M.Z., Poulin, J.F., Andres-Enguix, I., Simoneau, M., Gupta, N., Boisvert, K., Lafrenière, F., McLaughlan, S., Dubé, M.P., Marcinkiewicz, M.M., *et al.* (2010). 'A dominant-negative mutation in the TRESK potassium channel is linked to familial migraine with aura.' *Nature Medicine,* 16 (10): 1157-1160.

Lambert, M., Boet, A., Rucker-Martin, C., Mendes-Ferreira, P., Capuano, V., Hatem, S., Adão, R., Brás-Silva, C., Hautefort, A., Michel, J.B., Dorfmuller, P., *et al.* (2018). ‘Loss of KCNK3 is a hallmark of RV hypertrophy/dysfunction associated with pulmonary hypertension.’ *Cardiovascular Research,* 114 (6): 880-893.

Lazarenko, R.M., Fortuna, M.G., Shi, Y., Mulkey, D.K., Takakura, A.C., Moreira, T.S., Guyenet, P.G. and Bayliss, D.A. (2010). 'Anesthetic activation of central respiratory chemoreceptor neurons involves inhibition of a THIK-1-like background K(+) current.' *The Journal of Neuroscience,* 30 (27): 9324 - 9334.

Lee, K.J., Czech, L., Waypa, G.B. and Farrow, K.N. (2013). ‘Isolation of Pulmonary Artery Smooth Muscle Cells from Neonatal Mice’, *Journal of Visualized Experiments*, (80): 1 – 8. doi: 10.3791/50889.

Leonard, E.M., Salman, S. and Nurse, C.A. (2018). 'Sensory processing and intergration at the carotid body tripartite synapse: neurotransmitter functions and effects of chronic hypoxia.' *Frontiers in Physiology.* DOI: 10.3389/fphys.2018.00225

Leonoudakis, D., Gray, A.T., Winegar, B.D., Kindler, C.H., Harada, M., Taylor, D.M., Chavez, R.A., Forsayeth, J.R. and Yost, C.S. (1998). ‘An open rectifier potassium channel with two pore domains in tandem cloned from rat cerebellum.’ *The Journal of Neuroscience,* 18 (3): 868 – 877.

Lesage, F., Reyes, R., Fink, M., Duprat, F., Guillemare, E. and Lazdunski, M. (1996a). 'Dimerization of TWIK-1 K+ channel subunits via a disulfide bridge', *EMBO J,* 15 (23): 6400-6407.

Lesage, F., Guillemare, E., Fink, M. Duprat, F., Lazdunski, M., Romey, G. and Barhanin, J. (1996b). 'TWIK-1, a ubiquitous human weakly inward rectifying K^+ channel with a novel structure.' *EMBO J,* 15: 1004-1011.

Lesage, F. and Lazdunski, M. (2000). 'Molecular and functional properties of two-pore-domain potassium channels.' *American Journal of Physiology – Renal Physiology,* 279 (5): F793-F801.

Lesage, F., Terrenoire, C., Romey, G. and Lazdunski, M. (2000). 'Human TREK2, a 2P domain mechano-sensitive K+ channel with multiple regulations by polyunsaturated fatty acids, lysophospholipids, and Gs, Gi, and Gq protein-coupled receptors.' *The Journal of Biological Chemistry,* 275 (37): 28398 – 28405.

Leuthy, A., Boghosian, J.D., Srikantha, R. and Cotten, J.F. (2017). ' Halogenated Ether, Alcohol, and Alkane Anesthetics Activate TASK-3 Tandem Pore Potassium Channels Likely through a Common Mechanism.' *Molecular Pharmacology,* 91: 620-629.

Levitz, J., Royal, P., Comoglio, Y., Wdziekonski, B., Schaub, S., Clemens, D.M., Isacoff, E.Y. and Sandoz, G. (2016). 'Heterodimerization within the TREK channel subfamily produces a diverse of highly regulated potassium channels.' *PNAS,* 113 (15): 4194-4199.

Li, X.T., Dyachenko, V., Zuzarte, M., Putzke, C., Preisig-Müller, R., Isenberg, G. and Daut, J. (2006). 'The stretch-activated potassium channel TREK-1 in rat cardiac ventricular muscle.' *Cardiovascular Research,* 69 (1): 86-97.

Limberg, S.H., Netter, MF., Rolfes, C., Rinné, S., Schlichthörl, G., Zuzarte, M., Vassiliou, T., Moosdorf, R., Wulf, H., Daut, J., Sachse, F.B. and Decher, N. (2011). 'TASK-1 channels may modulate action potential duration of human atrial cardiomyocytes.' *Cell physiology and Biochemistry,* 28 (4): 613 - 624.

Linden, A.M., Sadu, C., Aller, M.I., Vekovischeva, O.Y., Rosenberg, P.H.,

Wisden, W. and Korpi, E.R. (2007). 'TASK-3 knockout mice exhibit exaggerated nocturnal activity, impairments in cognitive functions, and reduced sensitivity to inhalation anesthetics.' *Journal of Pharmacology and Experimental Therapeutics,* 323: 924-934

Lloyd, E.E., Marelli, S.P. and Bryan Jr, R.M. (2009). ‘cGMP does not activate two-pore domain K^+ channels in cerebrovascular smooth muscle.’ *American Journal of Physiology: Heart and Circulatory Physiology,* 296 (6): H1774 – H1780.

Lolicato, M., Arrigoni, C., Mori, T., Sekioka, Y., Bryant, C., Clark, K.A. and Minor Jr, D.L. (2017). 'K2P2.1 (TREK-1)-activator complexes reveal a cryptic selectivity filter binding site.' *Nature,* 547 (7663): 364 - 368.

Lopes C.M., Rohacs T., Czirjak G., Balla, T., Enyedi, P. and Logothetis, D.E. (2005). ‘PIP2 hydrolysis underlies agonist-induced inhibition and regulates voltage gating of two-pore domain K+ channels.’ *The Journal of Physiology,* 564 (Pt 1): 117 – 129.

López-Barneo, J., López- López, J.R., Ureña, J. and González, C. (1988). 'Chemotransduction in the carotid body: K+ current modulated by PO2 in type I chemoreceptor cells.' *Science,* 241 (4865): 580 - 582.

López-Izquierdo, A., Aréchiga-Figueroa, I.A, Moreno-Galindo, E.G., Ponce-Balbuena, D., Rodríguez-Martínez, M., Ferrer-Villada, T., Rodríguez-Menchaca, A.A., van der Heyden, M.A. and Sánchez-Chapula, J.A. (2011). 'Mechanisms for Kir channel inhibition by quinacrine: acute pore block of $K_{ir2.x}$ channels and interference in PIP_2 interaction with $K_{ir2.x}$ and $K_{ir6.2}$ channels.' *Pflügers Archiv - European Journal of Physiology,* 462 (4): 505-517.

Loucif, A.J.C., Saintot, P.P., Liu, J., Antonio, B.M., Zellmer, S.G., Yoger, K., Veale, E.L., Wilbrey, A., Omoto, K., Cao, L., Gutteridge, A., Castle, N.A., Stevens, E.B., Mathie, A. (2018). 'GI-530159, a novel, selective, mechanosensitive two-pore-domain potassium (K2P) channel opener, reduces rat dorsal root ganglion neuron excitability.' *British Journal of Pharmacology,* 175 (12): 2272 - 2283.

Lunsford, C.D., Cale Jr, A.D., Ward, J.W., Franko, B.V. and Jenkins, H. (1964).

'4-(β-Substituted ethyl)-3,3-diphenyl-2-pyrrolidinones. A New Series of CNS Stimulants.' *Journal of Medicinal Chemistry,* 7 (3): 302 - 310.

Ma, L., Roman-Campos, D., Austin, E.D., Eyries, M., Sampson, K.S., Soubrier, F., Germain, M., Trégouët, D.A., Borczuk, A., Rosenzweig, E.B., Girerd, B., *et al.* (2013). 'A Novel Channelopathy in Pulmonary Arterial Hypertension.' *The New England Journal of Medicine,* 369 (4): 351-361.

MacKinnon, R. (2004). 'Potassium Channels and the Atomic Basis of Selective Ion Conduction (Nobel Lecture).' *Angewandte Chemie,* 43 (33): 4265-4277.

Madonna, R., Cocco, N. and De Caterina, R. (2015). 'Pathways and Drugs in Pulmonary Arterial Hypertension – Focus on the Role of Endothelin Receptor Antagonists.' *Cadiovascular Drugs and Therapy,* 29 (5): 469-479.

Maingret, F., Lauritzen, I., Patel, A.J., Heurteaux, C., Reyes, R., Lesage, F., Lazdunski, M. and Honoré, E. (2000). 'TREK1 is a heat-activated background K(+) channel.' *EMBO,* 19 (11): 2483 -2491.

Maingret, F., Patel, A.J., Lazdunski, M. and Honore, E. (2001). 'The endocannabinoid anandamide is a direct and selective blocker of the background K^+ channel TASK-1.' *EMBO J,* 20 (1-2): 47-54.

Manoury, B., Lamalle, C., Oliveira, R., Reid, J. and Gurney, A.M. (2011). 'Contractile and electrophysiological properties of pulmonary artery smooth muscle are not altered in TASK-1 knockout mice.' *The Journal of Physiology,* 589 (13): 3231 – 3246.

Mant, A., Elliot, D., Eyers, P.A. and O'Kelly, I.M. (2011). 'Protein Kinase A Is Central for Forward Transport of Two-pore Domain Potassium Channels $K_{2P}3.1$ and $K_{2P}9.1$.' *The Journal of Biological Chemistry,* 286 (16): 14110 – 14119.

Marsh, B., Acosta, C., Djouhri, L. and Lawson, S.N. (2012). 'Leak K^+ channel mRNAs in dorsal root ganglia: relation to inflammation and spontaneous pain behaviour.' *Molecular and Cellular Neuroscience,* 49 (3): 375 – 386.

Mathie, A. (2007). ‘Neuronal two-pore-domain potassium channels and their regulation by G protein-coupled receptors.’ *The Journal of Physiology,* 578 (Pt2): 377 – 385.

Mathie, A. (2010). ‘Ion channels as novel therapeutic targets in treatment of pain.’ *Journal of Pharmacy and Pharmacology,* 62 (9): 1089 – 1095.

Mathie, A. and Veale, E.L. (2007). 'Therapeutic potential of neuronal two-pore domain potassium-channel modulators.' *Current Opinion in Investigational Drugs,* 8 (7): 555-562.

Mathie, A., Al-Moubarak, E. and Veale, E.L. (2010a). 'Gating of two pore domain potassium channels.' *Journal of Physiology,* 588 (17): 3149-3156.

Mathie, A., Rees, K.A., Hachmane, M.F.E. and Veale, E.L. (2010b). 'Trafficking of Neuronal Two Pore Domain Potassium Channels.' *Current Neuropharmacology,* 8 (3): 276 - 286.

Mathie, A. and Veale, E.L. (2015). ‘Two-pore domain potassium channels: Potential therapeutic targets for the treatment of pain.’ *European Journal of Physiology,* 467 (5): 931 – 943.

McDonald, D.M. (1981). 'Peripheral chemoreceptors: structure–function relationships of the carotid body.' *In: Hornbein TF, Lenfant C, editors. Regulation of Breathing,* 17: 105 - 320.

McLaughlin, V.V., Benza, R.L., Rubin, L.J., Channick, R.N., Voswinckel, R., Tapson, V.F., Robbins, I.M., Olschewski, H., Rubenfire, M. and Seeger, W. (2010). ‘Addition of inhaled treprostinil to oral therapy for pulmonary arterial hypertension: a randomized controlled clinical trial.’ *Journal of the American College of Cardiology,* 55 (18): 1915-1922.

Miller, C. (2000). 'An overview of the potassium channel family.' *Genome Biology,* 1 (4): 4.1-4.5.

Mirkovic, K. and Wickman, K. (2011). ‘Identification and characterization of alternative splice variants of the mouse Trek2/Kcnk10 gene.’ *Neuroscience*, 194 (October 2009): 11–18.

Mitchell, R.A. and Herbert, D.A. (1975). 'Potencies of Doxapram and Hypoxia

in Stimulating Carotid-body Chemoreceptors and Ventilation in Anesthetized Cats.' *Anesthesiology,* 42 (5): 559 - 566.

Montoro, R.J., Ureña, J., Fernández-Chaćon, R., Alvarez de Toledo, G. and López-Barneo, J. (1996). 'Oxygen sensing by ion channels and chemotransduction in single glomus cells.' *Journal of General Physiology,* 107 (1): 133 - 143.

Moonen, A., Garsia, R., Youssef, P., Torzillo, P., Corte, T., Boehm, C., Cordina, R., Celermajer, D. and Lau, E. (2017). 'Outcomes of pulmonary arterial hypertension therapy in Australia: is monotherapy adequate?' *Internal Medical Journal,* 47 (10): 1124-1128.

Morais-Cabral, J.H., Zhou, Y. and MacKinnon, R. (2001). 'Energetic optimization of ion conduction rate by the K^+ selectivity filter.' *Nature,* 414: 37-42.

Moriyama, T., Higashi, T., Toagshi, K., Iida, T., Segi, E., Sugimoto, Y., Tominaga, T., Narumiya, S. and Tominaga, M. (2005). 'Sensitization of TRPV1 by EP1 and IP reveals peripheral nociceptive mechanism of prostaglandins.' *Molecular Pain,* 1 (3): 1 – 13.

Morton, M.J., O'Connell, A.D., Sivaprasadarao, A. and Hunter, M. (2002). 'Determinants of pH sensing in the two-pore domain K^+channels TASK-1 and -2.' *European Journal of Physiology,* 445 (5): 577 – 583.

Mu, D., Chen, L., Zhang, X., See, L.H., Koch, C.M., Yen, C., Tong, J.J., Spiegel, L., Nguyen, K.C., Servoss, A., Peng, Y., *et al.* (2003). 'Genomic amplification and oncogenic properties of the KCNK9 potassium channel gene.' *Cancer Cell,* 3 (3): 297-302.

Mulligan, E. and Lahiri, S. (1982). 'Separation of carotid body chemoreceptor responses to O_2 and CO_2 by oligomycin and by antimycin A.' *American Journal of Physiology - Cell Physiology,* 11 (2): C200 - C206.

Murbartian, J., Lei, Q., Sando, J.J. and Bayliss, D.A. (2005). 'Sequential phosphorylation mediates receptor- and kinase-induced inhibition of TREK-1

background potassium channels.' *The Journal of Biological Chemistry,* 280 (34): 30175 – 30184.

Murthy, K.S. (2006). 'Signaling for contraction and relaxation in smooth muscle of the gut.' *Annual Review of Physiology,* 68: 345 – 374.

Navas, P., Tenorio, J., Palmonio, J., Arias, P., Gordo, G., López, M., Román, A., Lapunzina, P. and Escribano, P. (2017). 'An homozygous mutation in KCNK3 is associated with an aggressive form of hereditary pulmonary arterial hypertension.' *Clinical Genetics,* 91 (3): 453-457.

Navas, P., Tenorio, J., Quezada, C.A., Barrios, E., Gordo, G., Arias, P., López, M., Santos-Lozano, A., Palomino, J., Lapunzina, P. and Escribano, P. (2016). 'Molecular Analysis of *BMPR2*, *TBX4*, and *KCNK3* and Genotype-Phenotype Correlations in Spanish Patients and Families With Idiopathic and Hereditary Pulmonary Arterial Hypertension.' *Rev Esp Cardiol (Engl Ed),* 69 (11): 1011-1019.

Neher, E. and Sakmann, B. (1976). Single-channel currents recorded from membrane of denervated frog muscle fibres. *Nature,* 260: 799-802.

Niemeyer, M.I., Cid, L.P., Valenzuela, X., Paeile, V. and Sepúlveda, F.V. (2003). 'Extracellular conserved cysteine forms an intersubunit disulphide bridge in the KCNK5 (TASK-2) K+ channel without having an essential effect upon activity.' *Molecular Membrane Biology,* 20 (2): 185-191.

Niemeyer, M.I., Cid, P.L., González, W. and Sepúlveda, F.V. (2016). 'Gating, Regulation, and Structure in K2P K^+ channels: *In Varietate Concordia?'. Molecular Pharmacology,* 90 (3): 309-317

Nishino, T., Mokashi, A. and Lahiri, S. (1982). 'Stimulation of carotid chemoreceptors and ventilation by doxapram in the cat.' *Journal of Applied Physiology,* 52 (5): 1261-1265.

Noda, M., Takahashi, H., Tanabe, T., Toyosato, M., Furutani, Y., Hirose, T., Asai, M., Inayama, S., Miyata, T. and Numa, S. (1982). Primary structure of α-subunit precursor of Torpedo californica acetylcholine receptor deduced from cDNA sequence. *Nature,* 299 (5886): 793-797.

Noda, M., Shimizu, S., Tanabe, T., Takai, T., Kayano, T., Ikeda, T., Takahashi, H., Nakayama, H., Kanaoka, Y., Minamino, N., *et al.* (1984). Primary structure of Electrophorus electricus sodium channel deduced from cDNA sequence. *Nature,* 312 (5990): 121-127.

Noël, J., Sandoz, G. and Lesage, F. (2011) 'Molecular regulations governing TREK and TRAAK channel functions.' *Channels (Austin, Tex.)*, 5 (5): 402–409.

Nurse, C.A. (2005). 'Neurotransmission and neuromodulation in the chemosensory carotid body.' *Autonomic Neuroscience: Basic and Clinical,* 120 (1-2): 1 - 9.

Nurse, C.A. (2014). 'Synaptic and paracrine mechanisms at carotid body arterial chemoreceptors.' *The Journal of Physiology,* 592 (16): 3419 - 3426.

O'Connel, A.D., Morton, M.J. and Hunter, M. (2002). 'Two-pore domain K+ channels—molecular sensors.' *Biochimica et Biophysica Acta (BBA) – Biomembranes,* 1566 (1-2): 152 – 161.

O'Kelly, I., Butler, M.H., Zilberberg, N. and Goldstein, S.A. (2002). 'Forward transport. 14-3-3 binding overcomes retention in endoplasmic reticulum by dibasic signals.' *Cell,* 111 (4): 577 – 588.

Olschewski, A., Li, Y., Tang, B., Hanze, J., Eul, B., Bohle, R.M., Wilhelm, J., Morty, R.E., Brau, M.E., Weir, E.K., Kwapiszewska, G., *et al.* (2006). 'Impact of TASK-1 in Human Pulmonary Artery Smooth Muscle Cells.' *Circulation Research,* 98 (8): 1072-1080.

Olschewski, A., Veale, E.L., Nagy, B.M., Nagaraj, C., Kwapiszewska, G., Antigny, F., Lambert, M., Humbert, M., Czirják, G., Enyedi, P. and Mathie, A. (2017). 'TASK-1 (KCNK3) channels in the lung: from cell biology to clinical implications.' *European Respiratory Journal,* 50 (5): 1700754.

Ortega-Sáenz, P., Pascual, A., Gómez-Díaz, R. and Lopez-Barneo, J. (2006). 'Acute oxygen sensing in heme oxygenase-2 null mice.' *Journal of General Physiology,* 128 (4): 405 - 411.

Overton, E. (1902). Beiträge zur allgemeinen Muskel- und Nervenphysiologie,

II. Mittheilung: Ueber die Unentbehrlichkeit von Natrium- (oder Lithium-) Ionen für den Contractionsact des Muskels. *Pflugers Archive,* 92: 346-386.

Parameswaran, K., Radford, K., Fanat, A., Stephen, J., Bonnans, C., Levy, B.D., Janssen, L.J. and Cox, P.G. (2007). ‘Modulation of Human Airway Smooth Muscle Migration by Lipid Mediators and Th-2 Cytokines.’ *American Journal of Respiratory Cell and Molecular Biology,* 37 (2): 240 – 247.

Pardal, R., Ludewig, U, Garcia-Hirschfeld, J. and Lopez-Barneo, J. (2000). 'Secretory responses of intact glomus cells in thin slices of rat carotid body to hypoxia and tetraethylammonium.' *PNAS,* 97 (5): 2361 - 2366.

Patel, A.J., Honoré, E., Maingret, F., Lesage, F., Fink, M., Duprat, F. and Lazdunski, M. (1998). 'A mammalian two pore domain mechano-gated S-like K+ channel.' *EMBO J,* 17 (15): 4283-4290.

Patel, J.A., Shen, L., Hall, S.M., Benyahia, C., Norel, X., McAnulty, R.J., Moledina, S., Silverstein, A.M., Whittle, B.J. and Clapp, L.H. (2018). ‘Prostanoid EP_2 Receptors Are Up-Regulated in Human Pulmonary Arterial Hypertension: A Key Anti-Proliferative Target for Treprostinil in Smooth Muscle Cells.’ *Internation Journal of Molecular Science,* 19 (8): E2372.

Peers, C. (1990). 'Hypoxic suppression of K^+ currents in type I carotid body cells: selective effect on the $Ca^{2(+)}$-activated K^+ current.' *Neuroscience Letters,* 119 (2): 253 - 256.

Peers, C. and Buckler, K.J. (1995). 'Transduction of chemostimuli by the type I carotid body cell.' *Journal of Membrane Biology,* 144 (1): 1 - 9.

Peers, C. and Green, F.K. (1991). 'Inhibition of Ca(2+)-activated K+ currents by intracellular acidosis in isolated type I cells of the neonatal rat carotid body.' *The Journal of Physiology,* 437 (1): 589 - 602.

Peers, C. and Kemp, P. (2001). 'Acute oxygen sensing: diverse but convergent mechanisms in airway and arterial chemoreceptors.' *Respiratory Research,* 2 (3): 145 - 149.

Peers, C. and O'Donnell, J. (1990). 'Potassium currents recorded in type I carotid body cells from the neonatal rat and their modulation by

chemoexcitatory agents.' *Brain Research,* 522 (2): 259 - 266.

Pera M. (1992). The Ambiguous Frog: The Galvani-Volta Controversy on Animal Electricity, tr. Jonathan Mandelbaum. *Princeton: Princeton University Press.*

Perry, J.R.B., Day, F., Elks, C.E., Sulem, P., Thompson, D.J., Ferreira, T., He, C., Chasman, D.I., Esko, T., Thorleifsson, G., Albrecht, E., *et al.* (2014). 'Parent-of-origin specific allelic associations among 106 genomic loci for age at menarche.' *Nature,* 514 (7520): 92 - 97.

Piccolino, M. (2008) 'Visual images in Luigi Galvani's path to animal electricity', *Journal of the History of the Neurosciences*, 17(3), pp. 335–348. doi: 10.1080/09647040701420198.

Plant, L.D., Zuniga, L., Araki, D., Marks, J.D. and Goldstein, S.A. (2012). 'SUMOylation Silences Heterodimeric TASK Potassium Channels Containing K2P1 Subunits in Cerebellar Granule Neurons.' *Science Signaling,* 5 (251): ra84.

Pluchart, H., Khouri, C., Blaise, S., Roustit, M. and Cracowski, J.L. (2017). 'Targeting the Prostacyclin Pathway: Beyond Pulmonary Arterial Hypertension.' *Trends in Pharmacological Science,* 38 (6): 512 – 523.

Pongs, O., Kecskemethy, N., Müller, R., Krah-Jentgens, I., Baumann, A., Kiltz, H.H., Canal, I., Llamazares, S. and Ferrus, A. (1988). 'Shaker encodes a family of putative potassium channel proteins in the nervous system of Drosophila.' *EMBO J,* 7: 1087-1096.

Prentice, P. and Viner, R.M. (2013). 'Pubertal timing and adult obesity and cardiometabolic risk in women and men: a systematic review and meta-analysis.' *International Journal of Obesity,* 37: 1036 - 1043.

Pulido, T., Adzerikho, I., Channick, R.N., Delcroix, M., Galiè, N., Ghofrani, H.A., Jansa, P., Jing, Z.C., Le Brun, F.O., Mehta, S. and Mittelholzer, C.M. (2013). 'Macitentan and morbidity and mortality in pulmonary arterial hypertension.' *The New England Journal of Medicine,* 369 (9): 809-818.

Popa, A. (2002). ‘Bosentan (Tracleer™), a New Agent for the Treatment of Pulmonary Arterial Hypertension.’ *Pharmacotherapy Update,* V (2).

Rajan, S., Wischmeyer, E., Liu, G.X., Preisig-Muller, R., Daut, J., Karschin, A. and Derst, C. (2000). 'TASK-3 a novel tandem pore domain acid sensitive potassium channel. An extracellular histidine as a pH sensor. *Journal of Biological Chemistry,* 275: 16650-16657.

Rajan, S., Wischmeyer, E., Karschin, C., Preisig-Müller, R., Grzeschik, K.H., Daut, J., Karschin, A. and Derst, C. (2001). 'THIK-1 and THIK-2, a novel subfamily of tandem pore domain K^+ channels.' *Journal of Biological Chemistry,* 276: 7302-7311.

Rasband, M.N. (2010). 'Ion Channels and Excitable Cells.' *Nature Education,* 3 (9): 41.

Renigunta, V., Yuan, H., Zuzarte, M., Rinné, S., Koch, A., Wischmeyer, E., Schlichthörl, G., Gao, Y., Karschin, A., Jacob, R., Schwappach, B., Daut, J. and Preisig-Müller, R. (2006). 'The retention factor p11 confers an endoplasmic reticulum-localization signal to the potassium channel TASK-1.' *Traffic,* 7 (2): 168 - 181.

Renigunta, V., Zou X., Kling, S., Schlichthörl, G. and Daut, J. (2014a). 'Breaking the silence: functional expression of the two-pore-domain potassium channel THIK-2.' *European Journal of Physiology,* 466 (9): 1735 - 1745.

Reningunta, V., Fischer, T., Zuzarte, M., Kling, S., Zou, X., Siebert, K., Limberg, M.M., Rinné, S., Decher, N., Schlichthörl, G. and Daut, J. (2014b). 'Cooperative endocytosis of the endosomal SNARE protein syntaxin-8 and the potassium channel TASK-1.' *Molecular Biology of the Cell,* 25 (12): 1877 - 1891.

Reyes, R., Duprat, F., Lesage, F., Fink, M., Salinas, M., Farman, N. and Lazdunski, M. (1998). 'Cloning and expression of a novel pH-sensitive two pore domain K^+ channel from human kidney.' *Journal of Biological Chemistry,* 273: 30863-30869

Ricciotti, E. and FitzGerald, G.A. (2011). 'Prostaglandins and Inflammation.' *Arteriosclerosis, Thrombosis, and Vascular Biology,* 31 (5): 986 – 1000.

Ringer, S. (1882a) 'Concerning the Influence exerted by each of the Constituents of the Blood on the Contraction of the Ventricle', *The Journal of Physiology*, 3(5–6).

Ringer, S. (1882b) 'Regarding the Action of Hydrate of Soda, Hydrate of Ammonia, and Hydrate of Potash on the Ventricle of the Frog's Heart', *The Journal of Physiology*, 3(3–4), pp. 195–202.

Ringer, S. (1883a) 'A further Contribution regarding the influence of the different Constituents of the Blood on the Contraction of the Heart', *The Journal of Physiology*, 4(1), pp. 29–42.

Ringer, S. (1883b) 'A third contribution regarding the Influence of the Inorganic Constituents of the Blood on the Ventricular Contraction', *The Journal of Physiology*, 4(2–3), pp. 222–225.

Ringer, S. (1884) 'An Investigation regarding the Action of Rubidium and Cæsium Salts compared with the Action of Potassium Salts on the Ventricle of the Frog's Heart', *The Journal of Physiology*, 4(6), pp. 370–386.

Ringer, S. (1885) 'Regarding the influence of the Organic Constituents of the blood on the Contractility of the Ventricle', *The Journal of Physiology*, 6(6), pp. 361–463.

Ringer, S. (1887) 'Upon the Similarity and Dissimilarity of the behaviour of Cardiac and Skeletal Muscle when brought into relation with Solutions containing Sodium, Calcium and Potassium Salts', *The Journal of Physiology*, 8(5), pp. 288–295.

Rinné, S., Kiper, A.K., Schlichthörl, G., Dittmann, S., Netter, M,F., Limberg, S.H., Silbernagel, N., Zuzarte, M., Moosdorf, R., Wulf, H., Schulze-Bahr, E., Rolfes, C. and Decher, N. (2015). 'TASK-1 and TASK-3 may form heterodimers in human atrial cardiomyocytes.' *Journal of Molecular and Cellular Cardiology,* 81: 71 – 80.

Robson, R.H. and Prescott, L.F. (1978). ‘A PHARMACOKINETIC STUDY OF DOXAPRAM IN PATIENTS AND VOLUNTEERS.’ *British Journal of Clinical Pharmacology,* 7: 81 – 87.

Rocher, A., Geijo-Barrientos, E., Cáceres, A.I., Rigual, R., González, C. and Almaraz, L. (2005). 'Role of voltage-dependent calcium channels in stimulus-secretion coupling in rabbit carotid body chemoreceptor cells.' *Journal of Physiology,* 562 (2): 407 - 420.

Rubin, L.J., Badesch, D.B., Fleming, T.R., Galiè, N., Simonneau, G., Ghofrani, H.A., Oakes, M., Layton, G., Serdarevic-Pehar, M., McLaughlin, V.V., Barst, R.J., *et al.* (2011). ‘Long-term treatment with sildenafil citrate in pulmonary arterial hypertension: the SUPER-2 study.’ *Chest,* 140 (5): 1274-1283.

Salinas, M., Reyes, R., Lesage, F., Fosset, M., Heurteaux, C., Romey, G. and Lazdunski, M. (1999). 'Cloning of a new mouse two-P domain channel subunit and a human homologue with a unique pore structure.' *Journal of Biological Chemistry,* 274: 11751-11760.

Sandoz, G., Thümmler, S., Duprat, F., Feliciangeli, S., Vinh, J., Escoubas, P., Guy, N., Lazdunski, M. and Lesage, F. (2006). 'AKAP150, a switch to convert mechano-, pH- and arachidonic acid-sensitive TREK K+ channels into open leak channels.' *EMBO J,* 25 (24): 5864 - 5872.

Sandoz, G., Tardy, M.P., Thümmler, S., Feliciangeli, S., Lazdunski, M. and Lesage, F. (2008). 'Mtap2 Is a Constituent of the Protein Network That Regulates Twik-Related K+ Channel Expression and Trafficking.' *Journal of Neuroscience,* 28 (34): 8545 - 8552.

Sandoz, G., Douguet, D., Chatelain, F., Lazdunski, M. and Lesage, F. (2009). ‘Extracellular acidification exerts opposite actions on TREK1 and TREK2 potassium channels via a single conserved histidine residue.’ Proceedings of the National Academy of Sciences of the United States of America, 106 (34): 14628 – 14633.

Sano, Y., Inamura, K., Miyake, A., Mochizuki, S., Kitada, C., Yokoi, H., Nozawa, K., Okada, H., Matsushime, H. and Furuichi, K. (2003). 'A novel two-pore domain K+ channel, TRESK, is localized in the spinal cord.' *Journal of*

Biological Chemistry, 30 (25): 27406 - 27412.

Sauvageau, S., Thorin, E., Caron, A. and Dupuis, J. (2007). ‘Endothelin-1-induced pulmonary vasoreactivity is regulated by ET(A) and ET(B) receptor interactions.’ *Journal of Vascular Research,* 44 (5): 375-381.

Schermuly, R.T., Pullamsetti, S.S., Kwapiszewska, G., Dumitrascu, R., Tian, X., Weissmann, N., Ghofrani, H.A., Kaulen, C., Dunkern, T., Schudt, C., Voswinckel, R., *et al.* (2007). ‘Phosphodiesterase 1 upregulation in pulmonary arterial hypertension. Target for reverse-remodeling therapy.’ *Circulation,* 115: 2331-2339.

Schewe, M., Nematian-Ardestani, E., Sun, H., Musinszki, M., Cordeiro, S., Bucci, G., de Groot, B.L., Tucker, S.J., Rapedius, M. and Baukrowitz, T. (2016). 'A Non-canonical Voltage-Sensing Mechanism Controls Gating in K2P K+ Channels.' *Cell,* 164 (5): 937 - 949.

Schmidt, C., Wiedmann, F., Langer, C., Tristram, F., Anand, P., Wenzel, W., Lugenbiel, P., Schweizer, P.A., Katus, H.A. and Thomas, D. (2014). 'Cloning, functional characterization, and remodeling of K2P3.1 (TASK-1) potassium channels in a porcine model of atrial fibrillation and heart failure.' *Heart Rhythm,* 11 (10): 1798 - 1805.

Shiekel, J., Lindner, M., Hetzel, A., Wemhöner, K., Renigunta, V., Schlichthörl, G., Decher, N., Oliver, D. and Daut, J. (2013). 'The inhibition of the potassium channel TASK-1 in rat cardiac muscle by endothelin-1 is mediated by phospholipase C.' *Cardiovascular Research,* 97: 97-105.

Sibton, O. and Morrell, N.W. (2012). ‘Pathways in pulmonary arterial hypertension: the future is here.’ *European Respiratory Review,* 21 (126): 321-327.

Simkin, D., Cavanaugh, E.J. and Kim, D. (2008). ‘Control of the single channel conductance of K2P10.1 (TREK-2) by the amino-terminus: role of alternative translation initiation.’ *The Journal of Physiology,* 586 (23): 5651 – 5663.

Simonneau, G., Barst, R.J., Galiè, N., Naeije, R., Rich, S., Bourge, R.C., Keogh, A., Oudiz, R., Frost, A., Blackburn, S.D., Crow, J.W., Rubin, L.J., *et al.*

(2002). ‘Continuous subcutaneous infusion of treprostinil, a prostacyclin analogue, in patients with pulmonary arterial hypertension: a double-blind, randomized, placebo-controlled trial.’ *American Journal of Respiratory and Critical Care Medicine,* 165 (6): 800-804.

Simonneau, G., Gatzoulis, M.A., Adatia, I., Celermajer, D., Denton, C., Ghofrani, A., Gomez Sanchez, M.A., Krishna Kumar, R., Landzberg, M., Machado, R.F., Olschewski, H., Robbins, I.M. and Souza, R. (2013). ‘Updated Clinical Classification of Pulmonary Hypertension.’ *Journal of the American College of Cardiology,* 65 (25): D34-D41.

Smyth, E.M., Austin, S.C., Reilly, M.P. and FitzGerald, G.A. (2000). ‘Internalisation and sequestration of the human prostacyclin receptor.’ *The Journal of Biological Chemistry,* 275 (41): 32037 – 32045.

Snowball, A. (2015). ‘Changing channels in pain and epilepsy: Exploiting ion channel gene therapy for disorders of neuronal hyperexcitability.’ *FEBS letters,* 589 (14): 1620 – 1634.

Statista. (2018). ‘Worldwide revenue of Pfizer's Viagra from 2003 to 2017 (in million U.S. dollars).’ Viewed on 06/07/18,[https://www.statista.com/statistics/264827/pfizers-worldwide-viagra-revenue-since-2003/]

Stenmark, K.R., Nozik-Grayck, E., Gerasimovskaya, E., Anwar, A., Li, M., Riddle, S. and Frid, M. (2011). ‘The Adventitia: Essential Role in Pulmonary Vascular Remodeling.’ *Compr Physiol,* 1 (1): 141-161.

Stenmark, K.R., Frid, M.G., Yeager, M., Li, M., Riddle, S., McKinsey, T. and El Kasmi, K.C. (2012). ‘Targeting the adventitial microenvironment in pulmonary hypertension: A potential approach to therapy that considers epigenetic change.’ *Pulmonary Circulation,* 2 (1): 3 – 14.

Stewart, A.G., Harris, T., Fernandes, D.J., Schachte, L.C., Koutsoubos, V., Guida, E., Ravenhall, C.E., Vadiveloo, P. and Wilson, J.W. (1999). ‘Beta2-adrenergic receptor agonists and cAMP arrest human cultured airway smooth muscle cells in the G(1) phase of the cell cycle: role of proteasome degradation of cyclin D1.’ *Molecular Pharmacology,* 56 (5): 1079 – 1086.

Streit, A.K., Netter, M.F., Kempf, F., Walecki, M., Rinné, S., Bollepalli, M.K., Preisig-Müller, R., Renigunta, V., Daut, J., Baukrowitz, T., Sansom, M.S., Stansfeld, P.J. and Decher, N. (2011). 'A specific two-pore domain potassium channel blocker defines the structure of the TASK-1 open pore.' *Journal of Biological Chemsitry,* 286 (16): 13977 - 13984.

Sun, H., Luo, L., Lal, B., Ma, X., Chen, L., Hann, C.L., Fulton, A.M., Leahy, D.M., Laterra, J. and Li, M. (2016). 'A monoclonal antibody against KCNK9 K(+) channel extracellular domain inhibits tumour growth and metastasis.' *Nature Communications,* 4 (7): 10339.

Talley, E.M., Lei, Q., Sirois, J.E. and Bayliss, D.A. (2001). 'CNS distribution of members of the two-pore-domain (KCNK) potassium channel family.' *Journal of Neuroscience,* 21: 7491-7505.

Tang, H., Desai, A.A. and Yuan, J.X. (2016). 'Genetic Insights into Pulmonary Arterial Hypertension. Application of Whole-Exome Sequencing to the Study of Pathogenic Mechanism. *American Journal of Respiratory and Critical Care Medicine,* 194 (4): 393-397.

Thomas, P. and Smart, T.G. (2005). 'HEK293 cell line: a vehicle for the expression of recombinant proteins.' *Journal of Pharmacological and Toxicological Methods,* 51 (3): 187 - 200.

Thomas, D., Plant, L.D., Wilkens, C.M., McCrossan, Z.A. and Goldstein, S.A. (2008). 'Alternative translation initiation in rat brain yields K2P2.1 potassium channels permeable to sodium.' *Neuron,* 58 (6): 859 – 870.

Toncheva, D., Mihailova-Hirstova, M., Vazharova, R., Staneva, R., Karachanak, S., Dimitrov, P., Simeonov, V., Ivanov, S., Balabanski, L., Serbezov, D., Malinov, M., *et al.* (2014). 'NGS Nominated CELA1, HSPG2, and KCNK5 as Candidate Genes for Predisposition to Balkan Endemic Nephropathy.' *BioMed Research International,* 2014: 920723.

Townsley, M.I. (2013). 'Structure and composition of pulmonary arteries, capillaries and veins.' *Compr Physiol,* 2: 675-709.

Toyoda, H., Saito, M., Okazawa, M., Hirao, K., Sato, H., Abe, H., Takada, K., Funabiki, K., Takada, M., Kaneko, T. and Kang Y. (2010). ‘Protein Kinase G Dynamically Modulates TASK1-Mediated Leak K^+ Currents in Cholinergic Neurons of the Basal Forebrain.’ *Journal of Neuroscience,* 30 (16): 5677 – 5689.

Tsunozaki, M. and Bautista, D.M. (2009). ‘Mammalian somatosensory mechanotransduction.’ *Current Opinion in Neurobiology,* 19 (4): 362 – 369.

Turner, P.J. and Buckler, K.J. (2013). 'Oxygen and mitochondrial inhibitors modulate both monomeric and heteromeric TASK-1 and TASK-3 channels in mouse carotid body type-1 cells.' *The Journal of Physiology,* 591 (23): 5977 - 5998.

Veale, E.L., Clarke, C.E. and Mathie, A. (2005). 'A key glutamate residue (E30), conserved in many K channels, regulates the gating of TASK3 two pore domain potassium channels.' *The Journal of Physiology,* 567P: PC196.

Veale, E.L., Rees, K., Mathie, A. and Trapp, S. (2010). ‘Dominant Negative effects of a Non-conducting TREK1 Splice Variant Expressed in Brain.’ *The Journal of Biological Chemistry,* 285 (35): 29295 – 29304.

Veale, E.L., Hassan, M., Walsh, Y., Al-Moubarak, E. and Mathie, A. (2014a). 'Recovery of Current through Mutated TASK3 Potassium Channels Underlying Birk Barel Syndrome.' *Molecular Pharmacology,* 85 (3): 397-407.

Veale, E.L., Al-Moubarak, E., Bajaria, N., Omoto, K., Cao, L., Tucker, S.J., Stevens, E.B. and Mathie, A. (2014b). 'Influence of the N terminus on the biophysical properties and pharmacology of TREK1 potassium channels.' *Molecular Pharmacology,* 85 (5): 971 - 981.

Veale, E.L. and Mathie, A. (2016). 'Aristolochic acid, a plant extract used in the treatment of pain and linked to Balkan endemic nephropathy, is a regulator of K2P channels.' *British Journal of Pharmacology,* 173 (10): 1639 - 1652.

Vliegenthart, R.J.S., ten Hove, C.H., Onland, W. and van Kaam, A.H.L.C. (2017). 'Doxapram Treatment for Apnea of Prematurity: A Systematic Review.' *Neonatology,* 111 (2): 162 - 171.

Voloshyna, I., Besana, A., Castillo, M., Matos, T., Weinstein, I.B., Mansukhani, M., Robinson, R.B., Cordon-Cardo, C. and Feinmark, S.J. (2008). 'TREK-1 is a novel molecular target in prostate cancer.' *Cancer Research,* 68 (4): 1197 - 1203.

Wang, W. and MacKinnon, R. (2017). 'Cryo-EM Structure of the Open Human *ether-à-go-go*-related K^+ Channel hERG.' *Cell,* 169 (3): 422-430.

Wang, C.L., Tsai, M.L. and Wu, S.N. (2012). Evidence for mitoxantrone-induced block of inwardly rectifying K channels expressed in the osteoclast precursor RAW 264.7 cells differentiated with lipopolysaccharide.' *Cellular Physiology and Biochemistry,* 30 (3): 687-701.

Wang, P., Wu, P., Myers, J.G., Stamford, A., Egan, R.W. and Billah, M.M. (2001). ‘Characterization of human, dog and rabbit corpus cavernosum type 5 phosphodiesterases.’ *Life Sciences,* 68 (17): 1977 – 1987.

Ward, J.P.T., Knock, G.A., Snetkov, V.A. and Aaronson, P.I. (2004). ‘Protein kinases in vascular smooth muscle tone—role in the pulmonary vasculature and hypoxic pulmonary vasoconstriction.’ *Pharmacology & Therapeutics,* 104 (3): 207-231.

Warner, W.A., Sanchez, R., Dawoodian, A., Li, E. and Momand, J. (2012). 'Identification of FDA-approved Drugs that Computationally Bind to MDM2. *Chem Biol Drug Des,* 80: 631-637.

Waxman, S.G. and Zamponi, G.W. (2014). ‘Regulating excitability of peripheral afferents: emerging ion channel targets.’ *Nature Neuroscience,* 17 (2): 153 – 163.

Whittle, B.J., Silverstein, A.M., Mottola, D.M. and Clapp, L.H. (2012). ‘Binding and activity of the prostacyclin receptor (IP) agonists, treprostinil and iloprost, at human prostanoid receptors: treprostinil is a potent DP1 and EP2 agonist.’ *Biochemical Pharmacology,* 84 (1): 68-75.

Wilke, B.U., Lindner, M., Greifenberg, L., Albus, A., Kronimus, Y., Bünemann, M., Leitner, M.G. and Oliver, D. (2014). ‘Diacylglycerol mediates regulation of

TASK potassium channels by Gq-couple receptors.' *Nature Communications,* 5: 5540.

Woodward, D.F., Jones, R.L. and Narumiya, S. (2011). 'International union of basic and clinical pharmacology. LXXXIII: Classification of prostanoid receptors, updating 15 years of progress.' *Pharmacological Reviews,* 63 (3): 471 538.

Woolf, C.J. and Ma, Q. (2007). 'Nociceptors – Noxious Stimulus Detectors.' *Neuron,* 55 (3): 353 – 364.

Wright, P.D., Veale, E.L., McCoull, D., Tickle, D.C., Large, J.M., Ococks, E., Gothard, G., Kettleborough, C., Mathie, A. and Jerman, J. (2017). 'Terbinafine is a novel and selective activator of the two-pore domain potassium channel TASK3.' *Biochemical and Biphysical Research Communications,* 493 (1): 444-450.

Yamaki, M., McIntyre, S., Rassier, M.E., Schwartz, J.H. and Dousa, T.P. (1992). 'Cyclic 3',5'-nucleotide diesterases in dynamics of cAMP and cGMP in rat collecting duct cells.' *American Journal of Physiology – Renal Fluid and Electrolyte Physiology,* 262 (6): F957 – F964.

Yamamoto, Y., Kummer, W., Atoji, Y. and Suzuki, Y. (2002). 'TASK-1, TASK-2, TASK-3 and TRAAK immunoreactivities in the rat carotid body.' *Brain Research,* 950 (1-2): 304-307.

Yost, C.S., Oh, I., Efer, E.I. and Sonner, J.M. (2008). 'Knockout of the gene encoding the K2Pchannel KCNK7 does not alter volatile anesthetic sensitivity', *Behavioural Brain Research*, 193 (2): 192–196.

Yu, F.H. and Catterall, W.A. (2004). 'The VGL-Chanome: A protein superfamily specialised for electrical signaling and iconic homeostasis', *Science STKE,* 2004 (253): re15.

Yuan, F., Wang, H., Feng, J., Wei, Z., Yu, H., Zhang, X., Zhang, Y. and Wang, S. (2018). 'Leptin Signaling in the Carotid Body Regulates a Hypoxic Ventilatory Response Through Altering TASK Channel Expression.' *Frontiers in Physiology,* 9: 249.

Yuill, K., Ashmole, I. and Stanfield, P.R. (2004). ‘The selectivity filter of the tandem pore potassium channel TASK-1 and its pH-sensitivity and ion selectivity.’ *Pflügers Archiv,* 444 (1): 63 – 69.

Yuill, K.H., Stansfeld, P.J., Ashmore, I., Sutcliffe, M.J. and Stanfield, P.R. (2007). 'The selectivity, voltage-dependence and acid sensitivity of the tandem pore potassium channel TASK-1, contributions of the pore domains.' *Pflugers Arch,* 455: 333-348.

Zhou, Y.F., Morais-Cabral, J.H., Kaufman, A. and MacKinnon, R. (2001). ‘Chemistry of ion coordination and hydration revealed by a K+ channel–Fab complex at 2.0 Å resolution.’ *Nature,* 414: 43 – 48.

Zuzarte, M., Heusser, K., Renigunta, V., Schlichthörl, G., Rinné, S., Wischmeyer, E., Daut, J., Schwappach, B. and Preisig-Müller, R. (2009). ‘Intracellular traffic of the K^+ channels TASK-1 and TASK-3: role of N- and C-terminal sorting signals and interaction with 14-3-3 proteins.’ *The Journal of Physiology,* 587 (5): 929 – 952.